

# The Development of Electrochemical Sensors and their Application in Real Biological Environments

**Simon Peter Whelan**

March 28, 2023

Copyright: The Author, Simon P. Whelan, 2023.



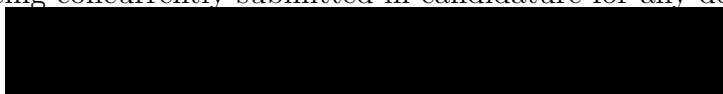
**Prifysgol Abertawe  
Swansea University**

## Declarations and statements

### Declaration

This work has not previously been accepted in substance for any degree and is not being concurrently submitted in candidature for any degree.

Signed:...

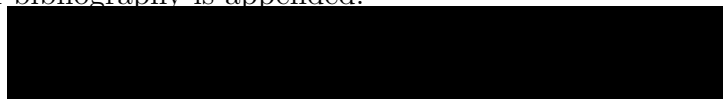


Date: 22<sup>nd</sup> March 2023 .....

### Statement 1

This thesis is the result of my own investigations, except where otherwise stated. Other sources are acknowledged by footnotes giving explicit references. A bibliography is appended.

Signed:...




Date: 22<sup>nd</sup> March 2023 .....

### Statement 2

I hereby give consent for my thesis, if accepted, to be available for photocopying and for inter-library loans after expiry of a bar on access approved by the University.

Signed:...



Date: 22<sup>nd</sup> March 2023 .....



### **Statement 3**

The University's ethical procedures have been followed and, where appropriate, that ethical approval has been granted.

Signed:...



Date: 22<sup>nd</sup> March 2023 .....



Ysgoloriaethau Sgiliau Economi Gwybodaeth  
Knowledge Economy Skills Scholarships



Ysgoloriaeth Sgiliau Economi Gwybodaeth (KESS) yn Gymru gyfan sgiliau lefel uwch yn fenter a arweinir gan Brifysgol Bangor ar ran y sector AU yng Nghymru. Fe'i cyllidir yn rhannol gan Gronfeydd Cymdeithasol Ewropeaidd (ESF) cydgyfeirio ar gyfer Gorllewin Cymru a'r Cymoedd.

Knowledge Economy Skills Scholarships (KESS) is a pan-Wales higher level skills initiative led by Bangor University on behalf of the HE sector in Wales. It is part funded by the Welsh Government's European Social Fund (ESF) convergence programme for West Wales and the Valleys.

**This work is part funded by the Welsh Government's European Social Fund (ESF) convergence programme for West Wales and the Valleys.**

## Abstract

Screen printed sensors and applications have been developed that utilise carbon/graphite working and counter electrodes and silver reference electrodes. The first sensor produced is a pH sensor where the working electrode has been functionalised by spin coating a layer of DMSO-melanin which enables it to become sensitive to changes in pH. This pH sensor was initially tested in reference buffer solutions where the sensitivity to pH was  $-49.79\text{mV/pH} \pm 8.93$  over a range of pH4 to pH10. Further testing showed an improved sensitivity of  $-63\text{mV/pH} \pm 4.79$  over a range of pH5 to pH8 which is a biologically relevant range. The DMSO-melanin pH sensor was tested in culturing media that had been inoculated and live bacteria were present where it was demonstrated to maintain sensitivity to pH in the presence of bacteria suggesting that it is suitable for the use in bacterial culturing applications. It was observed that signal measured depends on the type of culturing media used so therefore the type of culturing media must be known in advance of testing and a standard curve for each type of media being tested must be established before testing. Testing the DMSO-melanin pH sensors with blood samples in a preclinical model revealed challenges in obtaining repeatable results in blood samples. Subsequent investigation into this indicated that substances within the blood interfere with the signal that is measured by the sensor, in particular NaCl, KCl and  $\text{MgCl}_2$ . This work also produced a nonfunctionalised carbon/graphite screen printed electrode that was able to accurately measure the concentration of *Lactobacillus casei* bacteria in culturing media solutions using square wave voltammetry. The shape of the voltammograms measured was different when cultures of *Escherichia coli* and *Saccharomyces*

*cerevisiae* were tested suggesting that there might be potential useful applications involving this technique to identify characteristics of microbiota (such as domain, species, Gram type and quantity) based on the measured voltammograms. However further research on an expanded number of different prokaryotic and eukaryotic microorganisms is needed to confirm whether such applications are possible.

## **Acknowledgements**

The author would like to thank his supervisory team Dr Zari Tehrani, Professor David Gethin and Dr Martin Peacock for their support and guidance.

The author would also like to thank Professor Owen Guy who whilst not a member of the supervisory team has also contributed to the support and guidance of the author over the course of the project as well as Zimmer & Peacock and KESS2 for project funding.

The author would like to thank friends and family including Shirin Naserikarimvand, Peter, Kim and Liam Whelan as well as colleagues at the Centre for Nanohealth.

Lastly the author would like to thank Dr Peter Coussons and Dr Don Keiller for inspiring him to pursue a career in research during his undergraduate days many years ago.

# Contents

<b>List of Figures</b>	<b>ix</b>
<b>List of Tables</b>	<b>xxiii</b>
<b>1 Background</b>	<b>1</b>
1.1 Thesis structure . . . . .	1
1.2 Background and motivation . . . . .	2
1.2.1 The importance of pH measurements . . . . .	3
1.2.2 Potential advantages of a screen printed sensor . . . . .	4
1.2.3 The importance of microbial quantification . . . . .	5
1.2.4 Microbial identification . . . . .	6
1.2.5 Point of care testing . . . . .	7
1.2.6 Summary of importance . . . . .	7
<b>2 Literature review</b>	<b>9</b>
2.1 Carbons . . . . .	9
2.2 Carbon sensors . . . . .	11
2.2.1 Electrochemical sensor . . . . .	11
2.2.2 Biomarker detection and functionalisation . . . . .	12
2.3 Principles and applications of biosensors . . . . .	13
2.3.1 Biosensors for pathogen detection . . . . .	13

2.3.2	Biomarker biosensors . . . . .	14
2.4	Systems of pH measurement . . . . .	15
2.4.1	Potential for printed implementation of pH measurement	16
2.5	pH sensors . . . . .	16
2.6	Materials used in semiconductor pH sensors . . . . .	17
2.7	Graphene based pH sensors . . . . .	19
2.8	Additional studies investigating graphene and pH . . . . .	20
2.9	Materials considered for pH sensitivity element . . . . .	23
2.9.1	DMSO-melanin . . . . .	23
2.9.2	Polyalanine . . . . .	24
2.9.3	Aluminium oxide . . . . .	25
2.9.4	Screen printing and pH sensors . . . . .	25
2.10	Biomaterials . . . . .	26
2.11	Melanin . . . . .	26
2.11.1	Natural sources of melanin . . . . .	27
2.11.2	Microbiological melanin . . . . .	28
2.11.3	Melanin precursors . . . . .	28
2.11.4	Chemical synthesis of melanin . . . . .	29
2.11.5	Synthesising melanin using DMSO . . . . .	29
2.12	The potential useful application involving a pH sensor in a lactic acid bioreactor . . . . .	30
2.12.1	Proposed mechanism of action for DMSO-melanin pH sensitivity . . . . .	31
2.12.2	Overview of lactic acid bacteria . . . . .	33
2.12.3	Industrial uses . . . . .	34
2.12.4	The importance of pH in healthcare . . . . .	35
2.13	Current gaps in research . . . . .	35

<b>3</b>	<b>Sensor fabrication and characterisation</b>	<b>38</b>
3.1	Introduction . . . . .	38
3.1.1	Principles of screen printing . . . . .	39
3.1.2	SPE designs . . . . .	40
3.2	SPE fabrication . . . . .	44
3.2.1	Screen printer operation . . . . .	44
3.2.2	Printing settings . . . . .	47
3.3	Characterisation techniques . . . . .	48
3.3.1	Scanning electron microscopy . . . . .	49
3.3.2	Surface roughness and thickness of the printed working electrodes . . . . .	51
3.3.3	Raman spectroscopy . . . . .	53
3.3.4	Fourier-transform infrared spectroscopy . . . . .	54
3.3.5	Resistance of the printed carbon working electrodes . .	55
3.4	Testing consistency between printed electrodes . . . . .	59
3.4.1	Electrode surface . . . . .	65
3.5	Summary . . . . .	66
<b>4</b>	<b>Electrochemistry</b>	<b>67</b>
4.0.1	Overview and theory . . . . .	67
4.0.2	The Nernst equation and pH . . . . .	67
4.0.3	Open circuit potentiometry . . . . .	69
4.0.4	Electrochemical impedance spectroscopy . . . . .	70
4.0.5	Relationship between $Z'$ and $Z''$ . . . . .	71
4.0.6	Fitting Nyquist plots to an equivalent circuit . . . . .	71
4.0.7	Equivalent circuit elements . . . . .	72
4.0.8	Cyclic voltammetry . . . . .	75
4.1	Square wave voltammetry . . . . .	78



4.2	Summary . . . . .	80
<b>5</b>	<b>Development and fabrication of a pH sensor utilising DMSO-melanin</b>	<b>81</b>
5.1	Introduction . . . . .	81
5.2	DMSO-melanin synthesis . . . . .	82
5.2.1	Application of DMSO-melanin to working electrode . .	83
5.3	Response of sensors to reference buffer solutions . . . . .	83
5.4	Sensor recovery and reusability . . . . .	90
5.5	Comparison with pH sensors reported in the literature . . . .	91
5.6	Characterisation studies . . . . .	93
5.6.1	Contact resistance . . . . .	94
5.6.2	Raman spectroscopy . . . . .	96
5.6.3	Scanning electron microscopy . . . . .	98
5.6.4	X-ray photoelectron spectroscopy . . . . .	104
5.6.5	Fourier-transform infrared spectroscopy . . . . .	105
5.6.6	Atomic force microscopy . . . . .	108
5.6.7	Thickness and roughness of the DMSO-melanin pH sensor . . . . .	109
5.7	Discussion . . . . .	109
5.8	Summary . . . . .	110
<b>6</b>	<b>Suitability of the DMSO-melanin pH sensor for pH monitoring of bacterial cultures</b>	<b>112</b>
6.1	Introduction . . . . .	112
6.2	Methods . . . . .	114
6.3	Testing the DMSO-melanin pH sensors with media and bacteria	116
6.3.1	Calibrating sterile media . . . . .	116

6.3.2	Testing in inoculated media . . . . .	119
6.4	Discussion . . . . .	122
6.5	Summary . . . . .	123
<b>7</b>	<b>Potential clinical appliaations for the pH sensor.</b>	<b>124</b>
7.1	Rationale . . . . .	124
7.2	Point of care testing . . . . .	125
7.2.1	Background . . . . .	125
7.2.2	Carbon based point of care devices . . . . .	126
7.2.3	Point of care tests for sepsis . . . . .	127
7.3	Lactic acidosis . . . . .	128
7.3.1	Lactic acidosis and sepsis . . . . .	129
7.3.2	Lactate directed therapy . . . . .	129
7.4	Materials and methods . . . . .	130
7.5	Results . . . . .	131
7.5.1	Initial sensitivity testing . . . . .	131
7.5.2	Investigation into alternative anticoagulants . . . . .	132
7.5.3	Initial testing on blood . . . . .	135
7.5.4	Expected pH change . . . . .	136
7.5.5	Comparison with sensors in the literature . . . . .	137
7.5.6	Initial testing of the DMSO-melanin pH sensors with plasma . . . . .	138
7.6	Investigation into alternative inks for the reference electrode .	139
7.7	Investigation into interfering substances . . . . .	142
7.7.1	Spiked pH7 buffer . . . . .	142
7.7.2	Clinical intravenous solutions . . . . .	145
7.7.3	Gold ink reference electrode . . . . .	148
7.7.4	Results . . . . .	151

7.8	Discussion . . . . .	154
7.8.1	Potential solutions and future work . . . . .	155
7.9	Summary . . . . .	156
<b>8</b>	<b>Investigation into using electrochemical techniques to assess microbial growth</b>	<b>158</b>
8.1	Introduction . . . . .	158
8.2	Culturing microorganisms . . . . .	159
8.2.1	Monitoring bacterial growth . . . . .	159
8.2.2	Growth curves . . . . .	159
8.2.3	Applications . . . . .	160
8.3	Electrochemical experimentation using screen printed electrodes and bacterial cultures . . . . .	164
8.3.1	Initial testing . . . . .	164
8.3.2	Square wave voltammetry . . . . .	164
8.4	Suitability of SPEs for taking repeat measurements . . . . .	171
8.5	Investigation into effect of different culturing media on the signal generated . . . . .	176
8.5.1	Media tested . . . . .	176
8.6	Testing with different species of microorganisms . . . . .	179
8.7	Discussion . . . . .	181
8.8	Summary . . . . .	182
<b>9</b>	<b>Conclusion and future work</b>	<b>184</b>
9.1	Novelty . . . . .	184
9.2	Conclusion . . . . .	185
9.2.1	Future work . . . . .	188
9.2.2	Research goals outcome . . . . .	189

<b>References</b>	<b>191</b>
<b>Appendix</b>	<b>243</b>
<b>A Microfluidic sample delivery system</b>	<b>244</b>
A.1 Dimensions . . . . .	244
<b>B Accompanying software application for pH sensor</b>	<b>248</b>
B.1 Interface and example usage . . . . .	249

# List of Figures

2.1	Skeletal diagram representing the structure of a graphene sheet (left) and graphene oxide (right). . . . .	11
2.2	Hydrogen acceptor sites on the DMSO-melanin molecule allow interactions to take place between the DMSO-melanin and the charged hydronium ( $\text{H}_3\text{O}^+$ ) and hydroxyl ( $\text{OH}^-$ ) molecules. Image produced using MarvinJS. . . . .	32
3.1	Diagram overviewing the general process of screen printing. . .	40
3.2	Designs for each layer of the screen printed electrode shown in purple in the order that they were printed. A. Silver or silver/silver chloride ink conductive tracks and reference electrode. B. Carbon/graphene working electrode. C. Insulator layer. . . . .	41
3.3	Side view showing the layers of a SPE that has been functionalised with DMSO-melanin. . . . .	41
3.4	Photographs of the screens that were used in the fabrication of the SPEs. A. Silver or silver/silver chloride connection tracks/reference electrode. B. Carbon/graphene working and counter electrodes. C. Insulating layer. These screens are capable of producing a total of 24 SPEs. . . . .	42

3.5	The pressure pump must be activated prior to operating the screen printer as the machine runs on compressed air. . . . .	45
3.6	The main menu screen that is displayed to users when opening the “Shuttle29” software that drives the screen printer. The frame must be removed from the screen printer so that the screen can be loaded onto it. To do this the “release stencil” button should be pressed. . . . .	45
3.7	The screen must be fixed securely in place using screws and washers. Once in place it is important to ensure that the screen is level before printing. . . . .	46
3.8	Menu displaying the various settings that can be edited, only options 1 to 4 were edited. . . . .	46
3.9	Menus displaying the print limits (A), the contact pressure of the table to the screen (B) and the pressure calibration settings for the squeegees (C). . . . .	47
3.10	An example of an image produced using SEM of a carbon/graphene working electrode from an SPE. . . . .	50
3.11	Example of the graphical output produced by WLI of printed carbon ink on a PET substrate. The left image shows a top down image of the surface where the height is represented by a colour spectrum ranging from blue (lowest) to red (highest). The right image shows a three dimensional representation of the measured surface. . . . .	52

3.12	Raman spectra obtained from a sample of molybdenum disulfide. The peaks in the spectra correspond with the absorption of infra red light at various different wavelengths. These provide a fingerprint that is associated with groups of atoms or functional groups thereby elucidating the chemical structure of the material that is undergoing analysis. . . . .	54
3.13	Layout of probe position for testing the working electrode of the SPEs for four point IV testing. This setup was maintained and applied to different areas on the working electrode in order to measure the consistency of resistance across the electrode surface. . . . .	57
3.14	Contact resistance for the working electrode measured using four point IV in the configuration shown in Figure 3.13. The error bars represent the standard error times 1.96 of the resistance that was measured on each sensor (n=5). The distance between the probes was kept constant between measurements. These results indicate that the sensors are consistent as there is little variation between the measured resistance. . . . .	58
3.15	A: Photograph showing a completed sheet of SPEs that are ready to be cut into individual units. B: Identification of each sensor on the sheet for use in subsequent testing. . . . .	60
3.16	Square wave voltammetry carried out on screen printed electrodes from positions along A: a row of the printed sheet and B: Across the rows of the printed sheet. From sheet number 22. The consistency appears to be greater within a row and less consistent between the different rows. This could possibly due to the age and condition of the screen printer. . . . .	61

3.17	Impedance spectroscopy of the different screen printed electrodes from sheet number 3. The impedance measured from the SPEs taken from different locations on the sheet is similar indicating that the electrodes are consistent. . . . .	62
3.18	A. Image of the silver track under white light interferometry and B. the associated graph measuring the thickness. . . . .	63
3.19	A. The thickness of the silver ink screen printed onto the PET substrate that composes the conductive tracks and the reference electrode of the sensor. B. The thickness of the working electrode printed with the carbon/carbon graphite ink measured with white light interferometry as described in section 3.3.2.2. The average thickness of the silver reference electrode is 10.63 with a standard deviation of 0.86 and the average thickness of the carbon working electrode is 8.61 with a standard deviation of 0.87 indicating that the thickness of both electrodes is consistent. . . . .	64
3.20	The working electrode of the sensor through a light microscope. A. Boundary where working electrode (black) and insulator layer (blue) meet. B. Working electrode. . . . .	65
3.21	SEM images of the printed working electrode of the sensor. . .	66
4.1	Nyquist plot generated by performing EIS on a SPE using the raw data output by the Metrohm Autolab potentiostat and K3/K4 solution. . . . .	72
4.2	Electrical symbol that represents a resistor. . . . .	73
4.3	Electrical symbol that represents a capacitor. . . . .	73
4.4	Electrical symbol that represents a CPE. . . . .	74
4.5	Electrical symbol that represents an inductor. . . . .	74



4.6	Equivalent circuit generated from the Nyquist plot shown in Figure 4.1. $R_1=36.1\Omega$ , $R_2=1.95\text{ k}\Omega$ , CPE: $Y_0 = 1.0026\times 10^{-6}$ , $n = 0.998$ . . . . .	75
4.7	A. Example of a classically shaped cyclic voltammetry plot with the oxidation, reduction and reverse potentials annotated. B. Schematic representing a triangular potential wave as it is used in CV. . . . .	77
4.8	A. Example of the shape of the potential waveform of the staircase. B. Plot representing a single potential cycle that takes place at each step of the staircase ramp. . . . .	79
5.1	Potential measured using the PANI coated electrodes over a 10 minute period in reference buffer solutions of known pH where red = pH4, green = pH4 and blue = pH10. A, B and C are replicates. While the signal that is measured appears to be stable across the replicates there is variability between them.	85
5.2	Potential measured using $\text{Al}_2\text{O}_3$ coated sensors in solutions of known pH for 10 minutes. Red = pH4, green = pH7 and blue = pH10. A, B, C and D are replicates. . . . .	86
5.3	Potential voltage measured using DMSO-melanin coated sensors in solutions of known pH for 10 minutes. Red = pH4, green = pH7 and blue = pH10. A, B, and C are replicates. . .	87
5.4	The mean signal that was measured using the sensors over a 10 minute period in reference buffer solutions at known pH levels (pH4, pH7 and pH10). PANI ( $n=3$ ), $\text{Al}_2\text{O}_3$ ( $n=4$ ), DMSO-melanin ( $n=3$ ). Error bars represent the standard error times 1.96. . . . .	89

5.5	Potential recorded using both DMSO-melanin (left) and PANI (right) functionalised sensors in buffer solutions of known pH. While both types of sensor showed a strong sensitivity to pH as they were exposed to buffers of increasing pH, the PANI based sensor was unable to recover after being exposed to a high pH buffer. . . . .	91
5.6	Average resistance that was measured with a two probe IV test (n=5). . . . .	95
5.7	The resistance that was measured using four point IV testing for the working electrode surface of both a blank SPE and one that had been coated with DMSO-melanin. Five sensors were tested for both sets, and each sensor was tested five times with the probes in different positions on the electrode surface. The error bars represent the standard error times 1.96 of the resistance that was measured on each sensor (n=5). The distance between the probes was kept constant between measurements.	96
5.8	Raman spectra measured before (red) and after (blue) the graphene electrode had been coated with DMSO-melanin. . . .	97
5.9	Raman spectra of bulk graphite and graphene . . . . .	98
5.10	SEM image of the surface of the working electrode of a DMSO-melanin pH sensor, at this magnification the surface of the electrode appears relatively rough. . . . .	99
5.11	Higher magnification SEM images of the working electrode of a DMSO-melanin pH sensor. These images were taken at different positions on the surface of the working electrode showing that it is consistent. . . . .	101

5.12	SEM at further magnifications reveal that the surface of the DMSO-melanin working electrode is not simply rough, there are two distinct surface morphologies here, graphite appears as smooth flakes of as well carbon black which appears as clumps. The DMSO-melanin is not visible under SEM. . . . .	102
5.13	Comparison of SEM images of carbon black and graphite . . .	103
5.14	XPS spectra where the DMSO-melanin coated electrode contains peaks that match with both DMSO-melanin alone and an uncoated electrode indicating that the DMSO-melanin coat has been successfully applied to the working electrode of the pH sensor. The melanin ink is shown in red, the carbon/graphene electrode is shown in blue and the carbon/graphene electrode coated in DMSO-melanin is shown in green. . . . .	105
5.15	Basic monomer proposed for DMSO-melanin. . . . .	106
5.16	Annotated FTIR spectra of a working electrode that had been coated with DMSO-melanin and an electrode that had not. Clear differences in the spectra are present with the presence of additional peaks in the spectra from the melanin coated electrode that are consistent with the elemental bonds that are present in the proposed structure of DMSO-melanin, with the addition of a C=O bond. . . . .	107
5.17	(A) Morphology of the surface of the working electrode before and after (B) the layer of DMSO-melanin has been applied. . .	109
6.1	The conversion of glucose-6-phosphate to 6-phosphogluconolactone in the Entner–Doudoroff pathway - an important metabolic pathway for bacteria for the metabolism of glucose. . . . .	114

6.2	Another step in the Entner-Doudoroff pathway where $H^+$ is released is during the conversion of glyceraldehyde 3-phosphate to 1,3-Bisphosphoglyceric acid. . . . .	114
6.3	Voltage measured in the four different solutions tested with the DMSO melanin pH sensor. (A) reference buffer, (B) lysogeny broth, (C) brain heart infusion broth, (D) nutrient broth. In addition to measuring the stability of the signal, the mean value from these measurements was taken to produce a calibration curve that was used to estimate changes in pH to each media sample following bacterial inoculation. . . . .	117
6.4	The slopes calculated from the data shown in Figure 6.3 showing the relationship between the pH of each solution to the voltage that was recorded during OCP measurements that were carried out using each pH sensor. The gradient of each slope suggests that the relationship between voltage and pH is a similar sensitivity across all of the solutions that were tested, the absolute voltage signal that was measured is variable. The slopes were generated by weighted least squares regression with error bars representing the standard error of the mean multiplied by two (n=5). . . . .	118
6.5	The lysogeny broth (LB) calibration curve was used to predict the pH of the serial dilutions of cultured <i>L. casei</i> in LB. The inset shows the same graph zoomed in on the region where the dilutions are. . . . .	121

7.1	(A) Potential measured in modified reference buffers that had a clinically relevant pH range (7.3 - 7.4) for the detection of acidosis. (B) Potential plotted against pH. Error bars represent the standard error multiplied by two (n=3). . . . .	132
7.2	Signal measured by a DMSO-melanin pH sensor in a citrated blood sample. As with the plasma sample there was a sharp drop in the potential that was measured at the start of the test. Each line represents the potential measured in a replicate.	134
7.3	Signal measured in blood where lithium heparin has been used as the anticoagulative agent. Each line represents the potential measured in a replicate. . . . .	135
7.4	Average signal taken from the final 100 seconds of a 10 minute measurement of citrated blood samples (n=5) that had been spiked with 10µl lactic acid in order to alter their pH. A gradual decrease in pH upon further additions of lactic acid in increments of 0.01mmol/l was observed as expected however it was slightly greater than what was predicted theoretically in Section 7.5.4. The pH of the samples were confirmed using a glass electrode pH meter. This was repeated across two different samples where the relationship between the pH and the signal varied between the different samples. . . . .	137
7.5	The potential measured using 5 DMSO-melanin pH sensors over a 20 minute period. The sensor took almost 10 minutes for the signal to become stable. Once stable the measured potential was not consistent enough between the sensors to indicate that they are repeatable enough to detect lactic acidosis in a clinical setting. . . . .	139

7.6	Signal measured in blood samples using DMSO-melanin pH sensors that utilised different inks for the reference electrode. Both sensors with the silver and silver silver chloride reference electrodes showed a similar decay in signal over time. This was not the case in the sensors that utilised a carbon/graphene reference electrode however the measurements did not show good repeatability. . . . .	141
7.7	pH7 reference buffer that had been spiked with clinically relevant concentrations of substances present in blood which may interfere with the signal including (A) BSA (as a substitute for human albumin), (B) glucose and (C) sodium chloride. (D) Shows all of these signals plotted together on the same axis showing clearly that sodium chloride has the greatest effect on the signal measured. . . . .	144
7.8	Signal measured using DMSO-melanin sensors in the two IV solutions provided by Morriston where red = saline and blue = Ringer's. Each line represents the signal recorded by a previously unused pH sensor (n=10). . . . .	146
7.9	pH sensor exposed to increasing concentrations of NaCl over 10 minute periods. . . . .	147
7.10	pH sensor exposed to increasing concentrations of Sodium and Chloride solutions over 10 minute periods. . . . .	148

7.11	The designs for the individual layers to be cut using the stencil cutter to compose the sensor. The primary difference between this design and that which was used for the screen printed electrodes is that the silver tracks and reference electrode layer has been split into two layers in order to facilitate having a separate gold reference electrode. (A) silver layer (B) gold layer (C) carbon/graphene layer. Designs were created using the Asymptote vector graphics language. . . . .	150
7.12	The stencil design layers from Figure 7.11 combined to show the full sensor design. . . . .	151
7.13	The final sensors that were produced using bar coating and the silver, gold and carbon/graphene ink. . . . .	151
7.14	Prototype DMSO-melanin pH sensors utilising a gold reference electrode were tested with reference buffers of a known pH (red = pH4, green = pH7, blue = pH10) in order to ensure that they were sensitive to difference pH levels. . . . .	152
7.15	The prototype pH sensors were run with a blood sample to see whether the same problems involving repeatability and signal decay were present as they were with the silver reference electrode. . . . .	153
7.16	A DropSens brand SPE produced by Metrohm that contains 8 working electrodes. This SPE or a similar design that incorporates multiple working electrodes could be used to measure an average signal in blood which might improve signal consistency.	156

8.1	An example of a typical bacterial growth curve which is composed of a lag phase immediately after inoculation has taken place followed by exponential growth over the course of the log phase before a growth plateau is reached at the stationary phase. . . . .	161
8.2	Square wave voltammogram of sterile and inoculated culturing media using screen printed electrodes with reference electrodes composed of either silver, silver/silver chloride or carbon/graphene ink. . . . .	166
8.3	Square wave voltammogram obtained from each of the serially diluted culture media samples ranging from $2^{-1}$ to $2^{-9}$ . A fresh (previously unused) sensor was used for each measurement. . .	168
8.4	Individual peaks calculated for each of the serial dilutions. The maxima are shown in red and the minima are shown in blue. The difference between the peaks correlates with the concentration of <i>L. casei</i> in the media. . . . .	169
8.5	Maximum and minimum peaks plotted against bacterial dilution in media ranging from the media containing full growth to $2^{-4}$ . Error bars represent the standard error times two. The predicted signal was obtained via polynomial regression. The $R^2$ values for the first maximum peak, minimum peak and second maximum peak are 0.9599, 0.9964 and 0.9983 respectively.	170
8.6	Absorbance of each <i>L. casei</i> serial dilution in LB measured using UV spectroscopy using a wavelength of 600nm. — represents sterile broth and + represents the undiluted bacterial culture. The inset graph shows the $\log_{10}$ of the absorbance plotted against the dilution number. The $R^2$ value is 0.9902. .	171



8.7	Square wave voltammogram from each of the serially diluted media run with reused sensors from negative to positive to simulate bacterial growth over time. . . . .	172
8.8	Voltammogram from a sensor that was used to measure five consecutive sterile media samples. . . . .	174
8.9	Voltammogram from a sensor that was used to measure five consecutive media samples that contained bacterial cultures that had reached the stationary phase of growth. . . . .	175
8.10	Voltammogram measured from square wave voltammetry applied to the SPE in different types of sterile (has not been inoculated) media. . . . .	178
8.11	Different media types were inoculated with <i>L. casei</i> bacteria, the morphology of the voltammogram appears to be influenced by the type of media that the bacteria were grown in. This is possibly due to the media being composed of different substances as shown in Table 8.1. . . . .	179
8.12	Square wave voltagram of sterile LB media and media that has various microbial cultures growing in it. . . . .	180
A.1	Design of protective case for SPEs with a microfluidic sample delivery system that consists of two parts. A top section which contains the microfluidic capillary as well as a chamber where the sample is able to pool above the sensor and a bottom section which contains a groove that keeps the sensor in the correct position underneath the sample pooling chamber of the top section. . . . .	245
A.2	Top and bottom sections of the protective case following 3D printing. . . . .	246

A.3	The protective case assembled and glued together with an SPE.	246
A.4	The pH sensor sealed inside the microfluidic protective case as shown in Figure A.3 was tested with the standard pH4, pH7 and pH10 reference buffer solutions in order to determine whether sealing it inside the microfluidic system had any impact upon the functionality of the sensor. . . . .	247
B.1	The initial interface presented by the pH calculator. . . . .	249
B.2	pH calculator example selection. . . . .	249
B.3	File selection menu of the pH calculator . . . . .	250
B.4	Example prediction using the “Lysogeny broth” slope . . . . .	250

# List of Tables

2.1	Commonly used applications and products that are produced using lactic acid bacteria. . . . .	31
2.2	Genera of lactic acid bacteria. . . . .	33
3.1	Printing parameters that were used during the fabrication of the screen printed electrodes. . . . .	48
3.2	Scanning electron microscopy settings used when visualising the electrode surface. . . . .	51
3.3	Settings used on the Keithley multimeter for resistance/conductivity measurements. . . . .	56
5.1	pH sensors that have been reported in the literature, along with the pH range of solutions that they have each been tested with along with their observed sensitivity. . . . .	93
6.1	Various species of microorganisms and the pH level that is optimal for culturing. . . . .	113
6.2	The types of culturing media that were tested in this study and their components. . . . .	115

6.3	The culturing media pH calculated from the OCP signal that was measured in the DMSO-melanin based pH sensor following <i>L. casei</i> inoculation and incubation to stationary phase. The accuracy of this predicted value was verified by measuring the pH of each sample using a standard commercial glass electrode pH meter which confirmed that accuracy of the sensor is good enough for laboratory practice. . . . .	119
6.4	The predicted pH values according to where the measured OCP values correlate with the LB calibration curve as shown in Figure 6.5 compared to the pH measured using a standard glass electrode pH meter. . . . .	121
7.1	Examples of improved clinical outcomes that arise when POC testing is used. . . . .	125
7.2	Substances were tested at both the top and bottom ends of the clinical reference ranges. Sodium and chloride reference ranges were added together for a NaCl solution as working individually with sodium and chlorine is difficult. These substances were selected for investigation as they are typical components of blood and understanding which (if any) of these substances interferes with the sensor may lead to a better understanding of how to fix or compensate for the interference in future work.	143
7.3	Composition of the solutions that were tested. . . . .	145
8.1	The components that make up LB, 2YT and BHI culturing media. . . . .	177

# Glossary

**AFM** atomic force microscopy. 49, 51, 58, 93, 107, 109, 185

**BHI** brain heart infusion. 113, 118, 175

**BSA** bovine serum albumin. 141

**CPE** constant phase element. 73, 74

**CV** cyclic voltammetry. 12, 74, 75, 79, 81, 169

**DHI** 5,6-dihydroxyindole. 27, 29

**DHICA** 5,6-dihydroxyindole-2-carboxylic acid. 27, 29

**DMSO** dimethyl sulphoxide. 23, 29, 30, 32, 35–38, 66, 79, 81, 82, 87, 89–93, 95, 97–99, 103, 105, 107–109, 111, 113, 115, 118, 119, 121, 122, 129, 132, 141, 150, 151, 153, 163, 183–188, 243, 247

**EIS** electrochemical impedance spectroscopy. 12, 59, 70, 71, 79, 184

**FET** field effect transistor. 11, 25

**FTIR** Fourier-transform infrared spectroscopy. 54, 55, 93, 109, 185

**GO** graphene oxide. 19–21

**ICU** intensive care unit. 128

**LAB** lactic acid bacteria. 33, 34

**LB** lysogeny broth. xvi, 113, 118–120, 175, 186

**LHD** lactate dehydrogenase. 127

**NAD** nicotinamide adenine dinucleotide. 127

**NB** nutrient broth. 113, 118

**OCP** open circuit potentiometry. 25, 69, 79, 81, 82, 115, 118, 119, 130, 141

**PANI** polyaniline. 23, 24, 80, 82, 87, 89, 91, 184, 185

**PCR** polymerase chain reaction. 6, 125, 126

**PET** polyetheylene. 91

**POC** point of care. 7, 124–126

**RBC** red blood cells. 127

**rGO** reduced graphene oxide. 19, 20

**SEM** scanning electron microscopy. 49, 50, 65, 93, 97, 99, 184, 185

**SNP** single nucleotide polymorphism. 125

**SPE** screen printed electrode. 2, 37, 38, 40, 47, 48, 66, 80, 82, 92, 108, 109, 136, 152, 154, 157, 163, 169, 180–182, 184–187, 189

**SWV** square wave voltammetry. 12, 59, 77, 79, 81, 157, 184, 186, 188

**WLI** white light interferometry. 49, 51, 52, 59, 93, 97, 108, 109, 184

**XPS** X-ray photoelectron spectroscopy. 93, 103, 109

## Publications

**Simon Peter Whelan**, Zari Tehrani, Martin Peacock, Joao Vitor Paulin, Owen Guy, David Gethin. Investigation into the suitability of screen printed graphene-melanin pH sensors for use in bacterial culturing applications *Journal of Electroanalytical Chemistry* page 115868 (2021). doi:<https://doi.org/10.1016/j.jelechem.2021.115868>.

Zari Tehrani **Simon Peter Whelan**, Matthew Lawrence, Suresh Pillai, Phillip Adrian Evans, Martin Peacock, David Gethin, Owen Guy. A new and accurate low-cost printable pH sensor tested in a preclinical model for detecting changed in metabolic acidosis *Critical Care* page 282 24 (Suppl 1), 87 (2020). doi:<https://doi.org/10.1186/s13054-020-2772-3>.

Zari Tehrani **Simon Peter Whelan** Bernard Mostert, Joao Vitor Paulin, Muhhamad Ali, Esanah Daghigh Ahmadi, Carlos Graeff, Owen Guy, David Gethin. Printable and flexible graphene H sensors utilising thin film melanin for physiological applications *2D materials* page 024008 (2020). doi:<https://doi.org/10.1088/2053-1583/ab72d5>.



# Chapter 1

## Background

### 1.1 Thesis structure

**Chapter 1** provides a general introduction to the thesis covering the background and motivation for carrying out the work and how the thesis is going to be structured. An overview of the applications that the sensors were developed for and their importance is also included here.

**Chapter 2** is a literature review that details carbon nanoparticles and their properties that are relevant to this work. This chapter discusses screen printed electrodes and the underlying technology that the sensors rely on.

**Chapter 3** describes how the sensors were fabricated and covers what was done to characterise and assess the quality of the sensors.

**Chapter 4** is a theoretical chapter that covers the electrochemical techniques that have been used throughout this research to characterise and

test the sensors.

**Chapter 5** details the development and testing of a pH sensor. Candidate materials with sensitivity to pH were selected and tested as a means to functionalise the working electrode of the screen printed electrode (SPE). The material that performed best was taken forward for further development where it was characterised and tested in various applications including monitoring the pH of bacterial culturing media, food spoilage and medical where it was tested in a preclinical model for lactic acidosis in **Chapter 6** and **Chapter 7** respectively.

**Chapter 8** covers the establishment of using electrochemical techniques with SPEs that have not been functionalised in order to measure the quantity of bacteria in a culturing media solution. This chapter also covers how the same electrochemical technique can be used to differentiate between different microorganisms.

**Chapter 9** provides a conclusion summarising what has been covered in the thesis and details what future work is necessary to further advance what has been described in this thesis.

## 1.2 Background and motivation

This research aims to develop sensors that utilise carbon for a number of applications such as monitoring conditions within a bioreactor and point of care diagnostics. Due to its electrical properties, carbon is a suitable material for sensor development. In addition to developing sensors this research also

focuses on the investigation of real world applications for these sensors in a variety of different fields and industries including food production, biotechnology and healthcare. This research also investigates how microfluidics can be used in combination with carbon sensors in order to create a fully integrated and working system.

The types of sensors can be split into two broad categories. The first of these types being laboratory machines that are sophisticated and are capable of rapid high throughput measurements of complex biological components and the second type being portable easy to use devices that are intended to be used by non specialists outside of a laboratory setting [1]. Electrochemical sensors have applications in a diverse range of industries [2]. Such applications include the analysis of food to detect food spoilage, assessment of drinking water quality and the screening of medical samples in point of care settings [3].

### **1.2.1 The importance of pH measurements**

The ability to determine the pH of a solution is an important process across a wide range of various disciplines [4, 5, 6, 7]. This stems from pH being an essential factor in chemical and biological processes due to reactions being dependent upon being within a specific local pH range. In biological systems, molecules such as enzymes are only able to function within a narrow pH range, this leads to accurate pH measurement being important in the biological, biomedical and environmental science. In chemistry and biology laboratories, pH has been measured for decades using the classical glass electrode pH meter system [8]. While this system is accurate provided that good laboratory procedures are followed, it suffers from the drawbacks of being fragile, expensive and in need of constant calibration to account for signal

drift. In medicine blood pH is an important diagnostic biomarker. In cases of sepsis and stroke the pH of the blood drops resulting in clinical acidosis [9]. Acidosis is not diagnosed using a glass electrode pH meter, rather it is determined by running the sample through a blood gas analyser [10] which is an expensive piece of equipment, it is also large and therefore not portable. Environmental pH is typically measured using a portable glass electrode similar to those that are used in laboratories.

Using a glass electrode to measure pH is not always desirable, for example in cell culture the pH of the media is monitored colourmetrically where the media contains a pH sensitive dye. Colour changes in the solution correspond to changes in pH which are linked to metabolites produced by the cells or due to the growth of contamination [11]. Glass electrodes are not useful here due to the need for sterility as well as the cost of the electrodes as typically many flasks are cultured simultaneously.

### **1.2.2 Potential advantages of a screen printed sensor**

The drawbacks that are associated with the glass electrode may be overcome by instead using a screen printed pH sensor. Screen printing is a traditional and simple technique that allows for a large number of sensors to be produced quickly. The mass production of such sensors should allow them to be affordable for use in a disposable manner as they already are for blood sugar, for example [12]. Potential usages for such sensors includes use in culturing, where incorporating sterile sensors into the structure of the flask would allow for the continuous monitoring of the pH levels of the media as well as allowing for the monitoring to be logged and viewed remotely and developing alerts that notify staff should the pH level drift outside of a defined range so that action can be taken against contamination more quickly. Another area

where a disposable screen printed pH sensor may yield benefits is the field of medicine. A disposable screen printed pH sensor that is able to accurately measure the pH of blood may be a useful point of care test, for use in doctors surgeries or carried by paramedics in order to get a rapid indication of whether a patients pH level has changed therefore informing treatment options more quickly which preferable especially in the serious conditions that are associated with acidosis. Such a sensor may also be useful in smart bandages for monitoring how wound healing is progressing and alerting hospital staff to any changes in pH that are associated with infection onset [13].

### **1.2.3 The importance of microbial quantification**

The quantification of microorganisms within a solution is desirable across various different disciplines [14, 15]. An important example is in antimicrobial sensitivity testing where microorganisms that have been sampled from patient swabs are cultured in the presence of various antimicrobial compounds in order to assess the microbes sensitivity and resistance to these various compounds. The basic principle of this relies on the fact that the microbes that are sensitive will grow in the presence of the antimicrobial compound with little to no inhibition if they are resistant to it and they will fail to grow if they are sensitive. This is an important clinical diagnostic test that is routinely carried out especially since the number of antibiotic resistant species is increasing, the World Health Organisation predicts that antibiotic resistance will be the leading cause of death by the year 2050 [16]. Currently the most popular methods for determining antimicrobial sensitivity involve spreading the cultured microbes across an agar plate and applying discs infused with antibiotics to the plate and measuring the distance at which the bacterial lawn grows in relation to the disc. This process is laborious and

requires trained staff to perform the procedure. Electrochemical sensors that are capable of measuring culture yield could provide a simpler method for determining the sensitivity profile. Furthermore due to the nature of these sensors being electronic the signal that they measure could be automatically saved and processed leading to efficiency improvements in the diagnostic process. Staff would also require less training aiding in a reduction in personnel costs. Another area where a sensor able to quantify microbial yield is within a bioreactor where the microbial concentration needs to be kept at a level that is suitable for optimal bioreactor activity.

#### **1.2.4 Microbial identification**

There are techniques for identifying the species of microbes such as DNA sequencing these are dependent on trained staff, a well equipped and sufficiently funded laboratory and laborious time consuming preparation procedures such as overnight culture preparation, DNA extraction and polymerase chain reaction (PCR). While it is useful to know the exact species and strain of microorganism present depending on the application it is not always necessary and a sensor that is capable of providing less detailed information at a more rapid rate may be more appropriate depending on the setting. An example of where a broader, quicker approach to microbe identification can be more useful is in a clinical setting with regards to treatment selection. A classical technique for the broad differentiation of bacteria is the Gram stain. This is a laborious and complicated technique which relies on human interpretation of microscopic images [17]. Techniques such as the Gram stain are ideal candidates to be replaced by electrochemical sensors as they offer inherent advantages such as being electronic in nature they produce a digital signal which can be automatically recorded and this also removes the risk of

human error or the variation associated with how different people interpret the microscopy. Such a sensor has the potential to increase accuracy and repeatability while also producing a result more quickly and reducing costs (staining reagents, need for trained staff).

### **1.2.5 Point of care testing**

Point of care (POC) offers advantages over centralised laboratory based testing such as a shorter turnaround time [18] and a reduced requirement for sample volume [19]. POC testing is also attractive for use in developing countries where resource limitations limit access to centralised laboratory services [20]. Screen printed carbon based sensors such as those developed in this research are interesting candidates for use in a POC setting as they can be produced at a high volume with low cost [19]. Furthermore the carbon electrode has the potential to be functionalised in a variety of ways that cause it to become sensitive to various different substances meaning that the same base sensor design has the potential to be used to detect different biomarkers for a variety of POC applications depending on how the electrode was functionalised [21]. The applications discussed above are potentially useful in a POC setting particularly in wound infection management as the colonisation of a wound with infectious microbes leads to changes in pH [22, 23] which could potentially be monitored using a disposable carbon based pH sensor could be used to help identify what the infectious agent is.

### **1.2.6 Summary of importance**

This work has highlighted sensors that have potential applications in a variety of different industries and settings where they may increase production output for example by being used within a bioreactor or detect food spoilage

leading to waste reduction. There are also potential applications for such sensors in healthcare where they may reduce the cost of healthcare while facilitating near patient point of care testing. These sensors are able to be used in challenging scenarios where confounding factors prevent traditional approaches that depend on expensive specialist laboratory equipment from being used.

The next chapter will present a review of the most relevant literature concerned with design and application of sensors that are relevant to the applications presented in the preceding sections.



# Chapter 2

## Literature review

This chapter is a review of the literature that provides the scientific background to the work. Carbon in the form of graphite/graphene are an fundamental part of this work as carbon paste is used for the fabrication of the sensors. As such nanoparticles are introduced and their properties that are relevant to this work are described. Electrochemical sensors are introduced and described along with their underlying principles and applications. The molecule melanin is covered as melanin plays an important role in how the pH sensor developed in this project functions, other pH sensors that utilise different functional materials are also discussed. This chapter also highlights where there are gaps in the current research that this work is aiming to address.

### 2.1 Carbons

This work makes extensive use of carbon as the sensors described are fabricated using carbon ink for the working and counter electrodes. Carbons such as graphene have been identified as having many interesting properties that

relate to potential applications within a wide range of fields. A general introduction of graphene as well as its properties that are relevant to producing sensors is discussed here.

First identified in 2004 [24, 25] graphene is a carbon allotrope that is composed of a single layer of atoms that are arranged in a hexagonal lattice structure that resembles a honeycomb (Figure 2.1). Multiple layers of this structure form graphite which is another carbon allotrope [26].

Each carbon atom within graphene is bonded to three other carbon atoms via a strong covalent  $\sigma$  bond within a single lattice. These atoms are in a  $sp^2$  hybridised state between two  $p$  orbitals and one  $s$  orbital which allows the support of both  $\sigma$  and  $\pi$  bonds [27]. The  $\sigma$  bonds are responsible for the strong mechanical and thermal properties of graphene which allow it to exist in a suspended form [28]. The  $\pi$  bonds are formed by the remaining electrons from each carbon atom in  $p$ -orbitals that are perpendicular to the graphene plane [29]. These  $\pi$  bonds are primarily responsible for providing a weak bond between multiple graphene sheets and do not provide much structural support within a single graphene plane as they are weaker than the in plane  $\sigma$  bonds. This weak  $\pi$  bond allows for the easy separation of graphene sheets [30]. The unit cell (smallest number of atoms necessary to produce the lattice structure) of graphene consists of two  $\pi$  bands. The bonding  $\pi$  band is in the lower energy valence band and the anti-bonding  $\pi$  band is in the higher energy conduction band. These two bands come into contact at the corners of the Brillouin zone (the area inside the lattice ring) and these are known as K points or Dirac points [31].

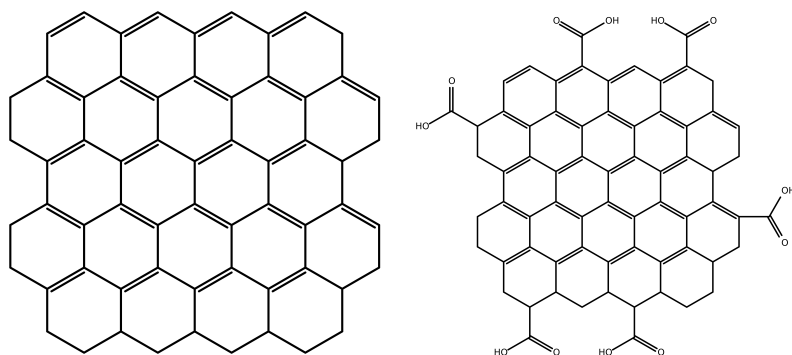


Figure 2.1: Skeletal diagram representing the structure of a graphene sheet (left) and graphene oxide (right).

## 2.2 Carbon sensors

The characteristic properties of carbon in the form of graphite make it suitable for use in sensors, this is because the high surface area to volume ratio and strong electrical conductivity allow for the detection of small changes. How carbon is used in sensors varies. Carbon can be used in electrochemical sensors as the working and/or counter electrode as well as being used as the conductive channel in measurements based on field effect transistor (FET).

### 2.2.1 Electrochemical sensor

Electrochemical carbon sensors generally function by utilising the carbon as the working electrode and also sometimes the counter electrode. This arrangement involves a three electrode system where electrons are transferred between the working electrode and the counter electrode that occurs as a result of events that take place on the surface of the working electrode [32]. The three electrode system also contains a reference electrode that should have a constant stable potential that can be used to measure changes in the

potential of the working and counter electrodes. Electrochemical sensors can be divided into two categories, these are potentiometric sensors and voltametric/amperometric sensors [3]. Potentiometric sensors measure a change in potential in the sensor which occurs in relation to the concentration of the analyte [33]. In the case of voltametric or amperometric sensors an oxidation-reduction reaction occurs at the working electrode that is relative to the analytes concentration [34]. The material used for the working electrode in electrochemical sensors is diverse with carbon, gold, platinum and silver electrodes being used for electrochemical sensor fabrication [35]. An important advantage of carbon over these other materials is cost as they are inexpensive [3] which makes carbon an attractive choice of material for the fabrication of disposable electrochemical sensors such as those described in this work. Electrochemical sensors and biosensors have applications in a diverse range of industries [2]. Such applications include the analysis of food to detect food spoilage, assessment of drinking water quality and the screening of medical samples in point of care settings [3]. Such applications are enabled by the sensors being sensitive to bacteria [36, 37] and biomarkers [38].

### **2.2.2 Biomarker detection and functionalisation**

Carbon sensors can be functionalised in order to induce sensitivity to biological molecules via chemically modifying the carbon surface with a bioreceptor [39]. This results in the formation of a biosensor that is able to detect target molecules with a high degree of specificity so long as the bioreceptor only binds to the target molecule. Electrochemical oxidation and reduction of the electrodes can be used to measure analytes by using various techniques such as electrochemical impedance spectroscopy (EIS), cyclic voltammetry (CV), square wave voltammetry (SWV) and chronoamperometry [40, 41].

## 2.3 Principles and applications of biosensors

Biosensors have been developed that are specific for a variety of different targets for a range of different use cases. Here some existing biosensors and their applications are described along with biosensor principles. There are three generations of biosensors. First generation biosensors detect the target analyte by signals that are generated from biocomponents that are bound to a membrane. Second generation biosensors utilise biocomponents that are bound to the surface of the working electrode where these biocomponents function as mediators and the signal is generated via electron transfer between these mediators and the working electrode. Having the biocomponents attached to the working electrode reduces the need for required reagents. Third generation biosensors function by immobilisation of receptors on the surface of the sensor and signal is generated by direct electron transfer as they lack a mediator [42].

### 2.3.1 Biosensors for pathogen detection

An example of a pathogen is the bacterial species *Escherichia coli*. It is often harmless and resides within the digestive system as part of the commensal flora without causing disease [43]. However there are strains of *E. coli* that are virulent pathogens the most notorious being *E. coli* strain O157 [44] which produces the Shiga toxin although other strains of Shiga producing *E. coli* do exist [45].

The current standard of techniques that are used to determine what a pathogen is are DNA based assays and immunoassays. The type of test used is based on factors such as the stage of infection and whether there are antibodies present at sufficient levels for detection.

While these techniques are accurate and reliable they have drawbacks associated with them such as needing to be performed by trained individuals in an appropriate laboratory setting that involves the use of consumables and reagents as well as expensive laboratory equipment that must be regularly calibrated and maintained in order to ensure that the results that are being generated are accurate and precise. These drawbacks create an opportunity that biosensors are well placed to solve due to their nature of being inexpensive to produce and that they can be used outside of a laboratory environment. In order to maximise their usefulness a biosensor should be a self contained unit that is able to provide quantitative or semi-quantitative data without prior processing or the need for additional reagents. This has been achieved and biosensors that are able to detect pathogens in various different environments have been reported [46, 47, 48, 49, 50].

### **2.3.2 Biomarker biosensors**

Biomarkers refer to molecules or characteristics that are components of a biological system the presence of which are associated with specific biological or clinical features [51]. Biomarkers are molecules of interest and have been investigated for their association with different prognostic outcomes in a variety of different and unrelated conditions including ischemic stroke [52], psychiatric disorders [53] and cancer [54, 55]. These characteristics of biomarkers make them attractive targets for detection and quantification using biosensors. Utilising biosensors that target biomarkers could lead to the generation of low cost devices that are able to be easily used in the diagnostics or progression monitoring of different disease states [56] that would be useful in a point of care setting [57]. The pH of biological fluids is a biomarker, for example blood pH is a biomarker for acidosis [58, 59] and salivary pH is a

biomarker indicating the seriousness of periodontal disease [60].

## 2.4 Systems of pH measurement

The determination of a solutions pH is important across many different industries and fields [61, 62, 63, 64, 65]. There are two methods that are used for measuring pH, electrochemical and colorimetric. Colorimetric pH determination relies upon colour changes that correlate with changes in pH however as they are not related to this work they are not discussed here. Electrochemical methods for pH measurement relies on electrodes within an electrochemical cell where the potential of the working electrode changes with pH and the reference electrode does not. The classic glass electrode used for pH measurements is composed of a glass bulb that contains a solution where the pH is constant. The reference electrode is located in this solution. The glass electrode pH meter contains a pH sensitive tip where  $H^+$  ions are exchanged leading to a measurable change in voltage due to the positive charge of the hydrogen.

The glass electrode pH meter has been used in a variety of laboratory and industrial environments. Limitations associated with it are related to the fragility of the glass electrode and the size of the electrode. Improvements on the technology have been developed that use the same principle such as the blood gas analyser that is used in the routine testing of blood samples in clinical settings. The blood gas analyser is a large machine that consists of several different electrodes that are used to measure the various components of blood including pH. The pH electrode within the blood gas analyser is essentially the same as the glass electrode pH meter [66].

### **2.4.1 Potential for printed implementation of pH measurement**

A printed implementation for the electrochemical determination of pH based on the same principles as the glass electrode pH meter has the potential to be useful in the production of inexpensive disposable pH sensors that may be useful in situations where it is not practical to use a glass electrode system. The underlying principle of determining pH by measuring the difference between the working and reference electrodes of an electrochemical cell should translate across to a screen printed sensor with electrodes that have been fabricated with conductive ink by functionalising the working electrode by coating it with a substance that is sensitive to pH and then measuring the difference in voltage between the pH sensitive working electrode and the pH insensitive reference electrode. This should theoretically produce a system that is sensitive to pH as it relies upon the same principles as the well established glass electrode pH meter.

## **2.5 pH sensors**

pH is measured currently using a variety of different techniques including the standard glass electrode pH meter, colourimetric systems based on pH sensitive dyes and systems based on spectrometers such as NMR spectroscopy [67]. The most frequent applications for pH determination are based on potentiometry, usually using a glass electrode [68, 69]. Film electrodes and ion selective membranes are also used to measure pH potentiometrically as are ion selective field effect transistors [70, 71]. pH may also be measured using a variety of ductometric [72] and optical [73] methods. This implies that there should be a wide variety of different commercial applications for



robust, screen printed pH sensors.

## 2.6 Materials used in semiconductor pH sensors

Ion sensitive field-effect transistor (ISFET)s are solid state electronic devices that are capable of sensing ion concentrations in a solution, this allows them to function as pH meters by sensing  $H^+$  ions. The ISFET pH sensing mechanism is built on a metal-oxide semiconductor field effect transistor (MOSFET). Its sensitivity to specific ions within a solution is due to the replacement of the metallic gate present in a MOSFET with a structure of membranes. The first material that was used as a pH sensitive membrane was  $SiO_2$ .

Silicon nitride  $Si_3N_4$  is a popular material for producing the membrane as it is easy to fabricate and is suitable for CMOS integration. However silicon nitride membranes typically show unstable properties regarding threshold voltage due to the conversion of silicon nitride film to a hydrated silicon dioxide  $SiO_2$  or a layer of oxynitride while in contact with an aqueous solution [74].

In the 1980s an investigation was carried out looking at electronically conducting metal oxides as pH sensors reporting that the following were suitable for measuring pH:  $PtO_2$ ,  $IrO_2$ ,  $RuO_2$ ,  $OsO_2$ ,  $Ta_2O_5$  and  $TiO_2$  [75].

Iridium oxide has been used to develop a flexible pH sensor, these sensors have been reported as having repeatable and reversible sensitivity between -51.1mV/pH and -51.7mV/pH in the range between pH 1.5 and 12 at 25 °C and a drift of 3-10mV over 300 seconds. The fabrication processes involved in producing this sensor are sol-gel deposition, thermal oxidation and AgCl

electro-plating on polymeric substrates [76].

An EIS device with a samarium oxide  $\text{Sm}_2\text{O}_3$  sensing membrane was developed for pH sensing. The sensing membrane was fabricated by reactive sputtering and post deposition annealing treatment was performed at  $700^\circ\text{C}$ . This device had a detection sensitivity of  $56.2\text{mV/pH}$  and a drift rate of  $1.29\text{mV/h}$  [74].

An array of pH sensors fabricated on a polymer-coated paper was developed with the intention of measuring the pH of chronic wound sites. The sensor is composed of two screen printed electrodes, a carbon electrode that has been coated with conductive proton selective polymeric membrane (polyaniline, PANI) and a Ag/AgCl reference electrode. This sensor is reported as having a sensitivity averaging at  $-50\text{mV/pH}$  and a drift of  $0.5\text{mV/h}$  operating between a range of pH4 and pH10 [77].

Thick film pH sensors intended for use in water pollution monitoring have been developed based upon the nanostructured  $\text{RuO}_2\text{--SnO}_2$  system and analysed using potentiometric and electrochemical impedance spectroscopic methods. The authors report that this sensor has a sensitivity of  $56.5\text{mV/pH}$  in the range of pH2 to pH12 [78]. The authors claim that this sensor does not have any drift in potential however the timespan of the measurements that they report is short - between 2 and 4 minutes at each pH level.

An investigation was carried out into the suitability of different metal oxides(MOx) coating SUS304 electrodes (SUS). (  $\text{M} = \text{Sc, Ti, V, Cr, Mn, Fe, Co, Ni, Cu, and Zn}$ ) for their pH sensing capabilities. The authors report

that all of the MOx/SUS electrodes showed a more rapid initial response time when measuring pH compared to a commercial glass electrode. They note that in particular, Co<sub>3</sub>O<sub>4</sub>/SUS and CuO/SUS electrodes had favourable pH activity and were considered candidates for needle type pH electrodes, disposable pH electrodes and pH microelectrodes [79].

## 2.7 Graphene based pH sensors

A pH sensor using graphene oxide (GO) as the pH sensitive layer has been reported in 2016. The pH sensitive layer is described as have being obtained via a 5µl drop casting of GO onto the working electrode of a screen printed sensor. The reported sensitivity was 31.8mV/pH with an accuracy of 0.3 unit of pH. The reliability of the sensor was tested via comparison to a traditional glass pH electrode where the greatest differences between the two were below 0.09 pH. Measurements were performed over a four day period [80].

A nanohybrid pH sensor composed of iridium oxide and reduced graphene oxide (rGO) has been produced on a thin film. Graphene oxide was reduced via repetitive cathodic potential cycling which can completely remove electrochemically unstable oxygenated groups while generating a homogenous film of graphene that is without defects. The sensor was reported as having slightly super Nernstian responses from pH 2-12 with good linearity and reproducibility. The authors also report that the results generated with this sensor were consistent with those that were produced with a commercially available glass electrode pH meter [61].

A pH sensor has been developed using three dimensional liquid gated graphene transistors. The sensor was composed of a suspended network of graphene that had been coated with a thin layer of hafnium oxide ( $\text{HfO}_2$ ). This sensor is described by the authors as being highly sensitive being capable of sensing beyond the Debye screening limit. The sensitivity of the sensor is reported as being  $71 \pm 7\text{mV/pH}$  in high ionic strength media where molarities are as high as  $289 \pm 1\text{mM}$ . The high sensitivity of the device is attributed to the three dimensional structure of graphene and electrolyte allowing an all round liquid gating of the graphene resulting in a higher electrostatic coupling efficiency of the electrolyte to the channel as well as increased gating control of the transistor channel by ions present in the electrolyte. The  $\text{HfO}_2$  film that coats the graphene provides binding sites for  $\text{H}^+$ , which also increases the sensitivity [81].

The development of a temperature and pH sensor has been reported, the temperature sensor was based on a layer of rGO, the electrical resistivity of this layer changed with temperature. The pH sensor was based on GO and had a sensitivity of  $40 \pm 4\text{mM/pH}$  in the range between pH 4 and pH 10 [82].

## **2.8 Additional studies investigating graphene and pH**

Beyond the above there are some addition studies that do not fall naturally into the previous sections and these are mentioned here for completeness. A study investigating the optical response of GO to pH reported that the visible and near-infrared fluorescence of GO nanosheets showed a sensitive

but reversible response to pH and ionic strength [83].

A composite hydrogel containing GO and poly vinyl alcohol has been developed. This hydrogel has pH sensitive properties, forming a gel while under acidic conditions and undergoing a gel-sol transition in alkaline conditions [84].

Solution gated epitaxial graphene has been reported as having pH sensing properties [85]. Triple layer graphene sheets were used in solution gate FETs using Ag/AgCl as the gate electrode [85, 86]. When the pH value of the buffer solution increased from 2 to 12, a positive shift of the transfer curve was found (drain to source current vs solution-gate potential) [86]. The sensing mechanism is based on the change of  $\text{OH}^-$  and  $\text{H}_3\text{O}^+$  ions adsorbed on the surface of the graphene at a different pH value, which changes the electrochemical double layer at the graphene solution interface.

Electrolyte-gate graphene field effect transistors (GFETs) were investigated and found to be highly sensitive electrical sensors for detecting pH and determining concentrations of biomolecules [87]. There has been a large variation in the reported sensitivities of GFETS, low values of 12mV/pH have been reported as well as a high value of 99 mV/pH. Some of the high values reported exceed the Nernst value of 60mV/pH which is the maximal shift that is thermodynamically allowed [88]. The reason behind this variation was investigated in 2011, where the authors found that the transfer characteristic of monolayer graphene shifts weakly ( $6\pm\text{mV/pH}$ ) when the buffer pH changed [88]. When a thin layer of aluminium oxide was added to the graphene the pH induced gate shift is reported to increase to  $17\pm 2$

mv/pH [88]. The authors suggest that the clean graphene does not expose terminal OH groups to the electrolyte and is therefore unable to sense the chemical potential of the protons, instead sensing the solutions electrostatic potential [88]. The authors continue by suggesting that the wide range of pH gate shifts involving graphene sensors reported in the literature reflects the quality of the graphene used. Where low quality graphene exhibits a large shift in response to pH due to the free bonds that are present on the surface, whereas high quality graphene does not have such bonds and shows no shift to pH [88].

An investigation into combining Graphene and poly(*N*-isopropylacrylamide) (PNIPAM) hydrogel was conducted in 2011. Graphene oxide covalently bonded to PNIPAM-*co*-AA microgels were shown to exhibit a reversible dual thermal and pH response [89].

In 2011 a study was conducted investigating the pH dependent behaviour of GO in aqueous solutions. The authors report that at a low pH, carboxyl groups are protonated causing the GO sheets to be less hydrophilic leading them to form aggregates. These aggregates were reported as being surface active and not exhibiting characteristic features of surfactant micelles. Based on MD simulations, it was suggested that the aggregates form a sandwich structure with water which prevents them from forming precipitate. At a pH the carboxyl groups are deprotonated and hydrophilic causing the GO sheets to disperse in water. The authors conclude by stating that GO does not behave like conventional surfactants in pH 1 and pH 14 aqueous solutions [90].

## 2.9 Materials considered for pH sensitivity element

As graphene is not sensitive to changes in pH alone, the working electrode of the sensor must be functionalised in order to gain pH sensitivity. Three materials were considered for this role. These included dimethyl sulphoxide (DMSO)-melanin - a derivative of standard melanin which is a well known naturally occurring biological pigment. A conductive polymer polyaniline (PANI), and  $\text{Al}_2\text{O}_3$  a ceramic semiconductor.

### 2.9.1 DMSO-melanin

Melanin will be discussed more fully in Section 2.11. The structure of melanin is believed to be composed of macromolecules of 5,6-dihydroxyindol-quinone (DHI) and 5,6-dihydroxyindole-2-carboxylic acid (DHICA) [91, 92, 93, 94, 95]. This structure features properties that may be useful as a pH sensitive layer. The hydroxyl groups of the quinone imine, the aromatic ring and the hydroxyl group of DHICA contain a large number of potential binding sites for  $\text{H}^+$  ions [96]. Melanin films have been demonstrated to have semiconductor properties that are dependent on water content [97]. DMSO is used to dissolve the melanin [98].

The use of melanin films in as the active layer in a pH sensing extended gate field effect transistor (EGFET) has been investigated. The melanin was described as having good sensitivity, with higher surface roughness providing larger effective sensing areas. The substrate used contributed to the sensitivity of the melanin, with a gold substrate producing a higher sensitivity to pH than indium tin oxide [91].

This study will explore the possibility of using melanin as the pH sensitive medium functionalising the carbon/graphene working electrode of SPEs. Melanins are a class of conjugated biomacromolecule. In nature melanin has many biological functions including photoprotection and photosensitisation, neuroprotection, metal ion chelation, free radical scavenging and structural colouration, [99, 100, 101, 102, 103, 104]. They are commonly present in biological systems and they can also be produced synthetically [91, 92]. Both naturally occurring and synthetic melanins have recently been receiving attention as versatile biomolecules with the potential for various biomedical applications [105, 106, 107].

### 2.9.2 Polyaniline

A promising candidate for further development is the pH sensor that was developed for wound monitoring using PANI coated carbon [77]. Their sensor was designed as a  $3 \times 3$  array of pH sensors on a paper substrate. Each pH sensor was composed of a reference electrode of AG/AgCl and a carbon electrode that had been coated with polyaniline (PANI), a conductive proton selective polymer. The pH sensors were based on the protonation and deprotonation of nitrogen atoms in PANI. While PANI is under acidic conditions it is doped with  $H^+$  ions creating the emeraldine salt form of PANI which has a high electrical conductivity. This results in an increase in the electrical potential of the sensing electrode relative to the reference electrode [77]. While under alkaline conditions the PANI enters its emeraldine base form, the captured  $H^+$  ions are neutralised which decreases the surface charge and potential of the PANI, rendering it not electronically conductive.

The electrochemical equilibrium between the emeraldine salt and emeraldine base forms of PANI is pH dependent and results in an inverse relationship



between the electrochemical potential of the sensing electrode and the environmental pH [77]. Measurements were performed by immersing the sensor for two minutes, and recording the potential between the reference and working electrodes.

### **2.9.3 Aluminium oxide**

Aluminium oxide ( $\text{Al}_2\text{O}_3$ ) is an ion sensitive metal oxide that is sensitive to changes in pH [108]. As such  $\text{Al}_2\text{O}_3$  has been reported as having being used successfully as the pH sensitive part of a FET based biosensor however it has not been reported as having been used in any pH sensitive device that relies on open circuit potentiometry (OCP) as the sensing mechanism. The low cost and easily available nature of  $\text{Al}_2\text{O}_3$  make it an interesting candidate for a pH sensitive medium. The pH sensitive properties of  $\text{Al}_2\text{O}_3$  are likely to be a result of the three hydrogen acceptor sites that are present on each molecule of  $\text{Al}_2\text{O}_3$ . The hydrogen acceptor sites allow for the molecule to form hydrogen bonds with hydroxide and hydronium which are responsible for the pH level of the solution.

### **2.9.4 Screen printing and pH sensors**

Screen printing is an attractive technique for the production of such sensors because the technology is well established and allows for the rapid production of sensors. Screen printing is often used for the fabrication of electrodes due to the low cost and simplicity of the technique [109, 110]. Screen printing is also scalable and compatible with low temperature processing and the fast high throughput fabrication of printed electronics suitable for manufacturing [111, 112]. Materials based on carbon have been extensively studied and are

often used in electrochemistry due to their electrical conductivity properties, as well as low density and low thermal expansion [113].

## **2.10 Biomaterials**

As the research and development of new electrical based pharmaceutical devices such as sensors increases in order to meet the requirements of advanced health informatics - one of the grand challenges that has been issued by the United States Academy of Engineering [114] where concern has been raised with regards to an increased generation of potentially harmful electronic waste [115]. The incorporation of biomaterials as functional components of such electronic pharmaceutical devices as an alternative to metals is an attractive potential solution in the attempt to mitigate some of the environmental pollution that occurs as a result of this industry. There are materials that exist within nature that have the potential to be applied in such uses [116].

## **2.11 Melanin**

Melanin is a naturally occurring biological pigment molecule that is a species of the polyindolequinone class of molecules. As a natural biological molecule with conductive properties melanin is a potentially interesting material to incorporate into the development of biosensors. Melanin pigments are present in many different organisms including humans as well as more ancient and lower order species [117]. Melanin pigments are diverse in structure and are divided into three primary groups. These include eumelanins which are a black to brown insoluble subgroup that are derived from L-dopa oxidative

polymerisation via 5,6-dihydroxyindole (DHI) intermediates [117]. Pheomelanin pigments are yellow to reddish brown and soluble in alkalis. They contain sulphur and are derived from the oxidation of cysteinyl-dopa precursors via intermediates of benzothiazole and benzothiazine [117]. Neuromelanins are dark pigments that are produced as a result of dopamine oxidation and other catecholamine precursors within neurons [117], they contain a mixture of eumelanin and pheomelanin [118].

The most well researched form of melanin is eumelanin. Eumelanin is synthesised from the 5,6-dihydroxyindole (DHI) and dihydroxyindole-2-carboxylic acid (DHICA) monomers and their redox forms. The redox properties of eumelanins monomer units cause eumelanin to be able to oxidise or reduce other molecules. Another feature that is characteristic to eumelanins is their ability to bind to various metal ions [119]. Melanin is one of the few biological macromolecules that displays conductive properties [120].

### **2.11.1 Natural sources of melanin**

Due to its abundance in nature there exist natural sources from which melanin can be extracted from and purified. A widely researched and accessible eumelanin source is the ink from cephalopods such as cuttlefish and squid. Melanin from cephalopod ink is a copolymer of tyrosine derived DHI and 5,6-dihydroxyindole-2-carboxylic acid (DHICA) moieties [121]. Cephalopods are an environmentally interesting source of melanin since they are frequently harvested for food however their ink sacs are rarely used despite being edible and generally discarded so utilising cephalopod melanin reduces resource waste while being readily available and inexpensive [122]. Due to the insolubility of melanin in water that is only able to be dissolved in alkaline solutions [123] it may be extracted from the ink using methods such as water

extraction or acidolysis and enzymolysis. Of these methods water extraction is the most capable of preserving the complete melanin structure whereas acidolysis and enzymolysis have a destructive effect [122]. Another natural source of melanin is hair. Melanin from hair should be extracted from fresh samples as structural modifications to the melanin takes place as the hair undergoes photoaging [117]. The melanin can be extracted by using a sequence of enzymes to degrade external proteins while preserving the melanosome [124, 125]. Other reported examples of melanin being extracted successfully from natural sources include mouse melanoma [126], feathers [127] and microbes [128].

### 2.11.2 Microbiological melanin

As well as animals, birds, reptiles and plants melanin pigments are also present in bacteria and fungi. In the case of fungi melanins are common however melanogenesis only occurs in specific developmental stages of mycelium or reactions to wounding or sporulation. Fungal melanin is primarily located within the cell wall. Fungi generally produce melanin via the secretion of precursors that are oxidised outside the cell wall [129]. Melanin is also commonly found in bacteria. Some bacterial species such as *Bacillus thuringiensis* and *Marinomonas mediterranea* [130, 131] contain active tyrosinase enzymes which oxidise the melanin precursor tyrosine causing them to become heavily pigmented in tyrosine rich environments [118].

### 2.11.3 Melanin precursors

Eumelanin and phomelanin are both derived from dopaquinone - a common precursor which is formed via the oxidation of either dopa or tyrosine. Eumelanin is subsequently formed by the cyclisation of dopaquinone to cyclodopa

which is in turn oxidised to dopachrome. Dopachrome is then converted into both DHI and DHICA. These units undergo oxidative polymerisation which results in the formation of eumelanin. Dopachrome is converted into 2-S-cysteinyl-dopa and 5-S-cysteinyl-dopa which are oxidised into 2-S and 5-S-cysteinyl-dopaquinone respectively.

#### **2.11.4 Chemical synthesis of melanin**

In addition to extracting melanin from a wide range of natural sources it is also possible to synthesise melanin in a laboratory setting. The most frequently synthesised melanins are dopamine-melanin and dopa-melanin which are produced via the chemical oxidation of dopa or dopamine. This can be achieved by using hydrogen peroxide in an alkali solution or atmospheric oxygen [132, 133]. An advantage to producing synthetic melanin is that they will not contain any protein or carryover cellular component from the extraction process which may occur when extracting melanin from natural sources. Synthetic melanin polymers that have been formed using the precursor DHI or dopa are similar to the black naturally occurring eumelanin whereas using dopamine produces polydopamine [105].

#### **2.11.5 Synthesising melanin using DMSO**

The insolubility of melanin in water causes problems in the synthesis of melanin by causing the reaction to be uncontrollably interrupted which leads to the material obtained being highly inhomogeneous [134]. Melanin synthesis can be improved by using a good solvent throughout the synthesis process [134]. DMSO is a well established solvent that is liquid over a wide range of temperatures [135]. The utilisation of DMSO in the synthesis of synthetic melanin was pioneered in 2004 [136]. Initial characterisation of melanin syn-

thesised using DMSO revealed that it was similar to melanin made using water with increased thermal stability. DMSO-melanin has improved solubility in DMSO which is relevant for processing purposes [137] Further research into DMSO-melanin suggest that sulphonate groups are incorporated into melanin from the oxidation of DMSO. These groups protect the phenolic hydroxyl group within its structure and are responsible for the solubility of DMSO-melanin in DMSO [138].

## **2.12 The potential useful application involving a pH sensor in a lactic acid bioreactor**

An example of a potentially useful application for a pH sensor is in a bioreactor containing lactic acid bacteria because these bacteria are sensitive to pH with optimal levels required for growth [139, 140]. This section describes their importance by providing background on lactic acid bacteria and their industrial uses. The various applications and products that lactic acid bacteria are used for are listed on Table 2.1.

Table 2.1: Commonly used applications and products that are produced using lactic acid bacteria.

Product/application	Reference
Bacteriocin production	[141, 142]
Probiotics in livestock production	[143]
Control of pathogenic biofilms	[144]
Reduce exposure to food contaminants	[145]
Reduction of bioaccessibility of mercury	[146]
Treatment of gastrointestinal inflammation	[147]
Food production	[148, 149, 150]
Reduction of methane production in ruminants	[151]
Lactic acid production	[152]

### 2.12.1 Proposed mechanism of action for DMSO-melanin pH sensitivity

As an Arrhenius acid dissolves in  $\text{H}_2\text{O}$ , a  $\text{H}^+$  ion is transferred from the Arrhenius acid to the surrounding  $\text{H}_2\text{O}$  molecules forming hydronium cations ( $\text{H}_3\text{O}^+$ ). The pH of a solution is determined by the ratio of hydronium to hydroxide ions. The molecules in  $\text{H}_2\text{O}$  disassociate into  $\text{OH}^-$  and  $\text{H}_3\text{O}^+$  in the following equilibrium:



Melanin contains structural features that make it a possible candidate for application in a pH sensing semiconductor. These features consist of a large number of potential proton binding sites: the two hydroxyl groups in the

aromatic ring, the hydroxyl group of the carboxylic acid and the quinone imine (Figure 2.2).

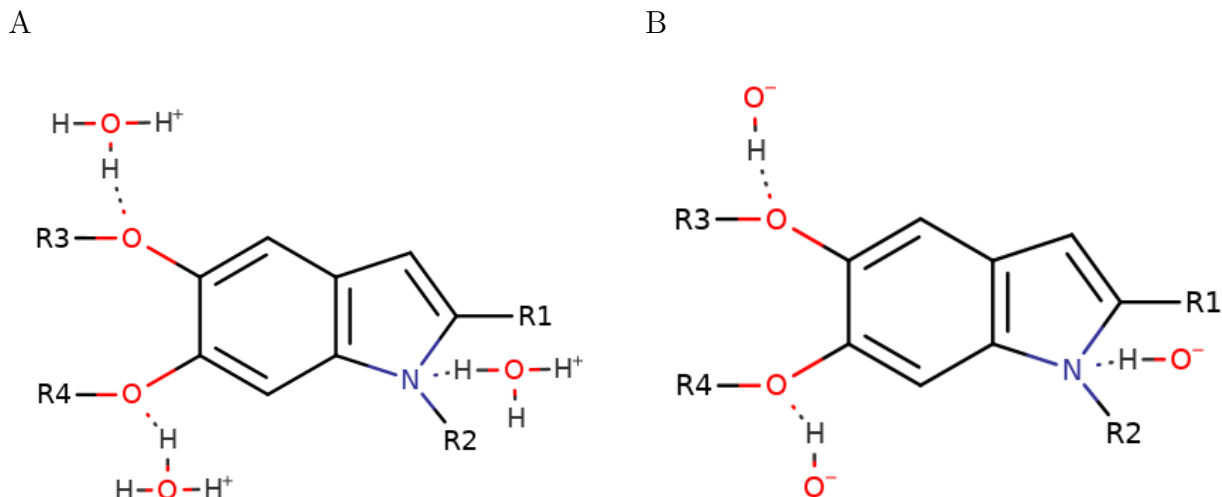


Figure 2.2: Hydrogen acceptor sites on the DMSO-melanin molecule allow interactions to take place between the DMSO-melanin and the charged hydronium (H<sub>3</sub>O<sup>+</sup>) and hydroxyl (OH<sup>-</sup>) molecules. Image produced using MarvinJS.

The following describes the potential mechanism that underpins the operation of the DMSO-melanin based pH sensor. The recorded sensitivity is consistent with previously published data regarding standard melanin [153, 91]. Such an observation is initially surprising as DMSO-melanin contains additional sulphonated moieties that are not present in standard melanin. However recent research [154] has indicated that the pH sensitive properties are caused by the reduction potentials of the one electron redox reactions that yield the comproportionation reactions for the quinone/semiquinone semiquinone/hydro quinone pairs. These reactions produce a theoretical pH sensitivity of approximately 60mV/pH which is consistent with the sensitivity reported here.



### 2.12.2 Overview of lactic acid bacteria

The taxonomic classification of microbes into the genera lactic acid bacteria (LAB) is based upon mechanisms of glucose fermentation, morphology, sugar utilisation and optimal growth temperatures [155]. LAB share similarities in these properties as well as phylogenetic similarities. LAB generally have the following attributes; Gram positive cocci or bacilli that are non spore forming and non respiring, they produce lactic acid via the fermentation of carbohydrates. The bacterial genera that compose the LAB group are shown in Table 2.2.

Table 2.2: Genera of lactic acid bacteria.

Genus name	Reference
<i>Abiotrophia</i>	[156]
<i>Aerococcus</i>	[157]
<i>Carnobacterium</i>	[158]
<i>Enterococcus</i>	[159]
<i>Lactobacillus</i>	[160]
<i>Lactococcus</i>	[161]
<i>Leuconostoc</i>	[162]
<i>Oenococcus</i>	[163]
<i>Pediococcus</i>	[164]
<i>Streptococcus</i>	[165]
<i>Tetragenococcus</i>	[166]
<i>Vagococcus</i>	[167]
<i>Weissella</i>	[168]

### **2.12.3 Industrial uses**

#### **2.12.3.1 Food production**

LAB have a beneficial influence on the shelf life, nutritional and organoleptic characteristics of fermented foods [169, 170]. This is due to their ability to cause the rapid acidification of the environment which occurs predominantly as a result of lactic acid production. Traditional methods of food fermentation using LAB are reliant on spontaneous fermentation whereas modern industrial methods rely upon the deliberate addition of LAB starter culture to the raw material which has allowed the final products to become standardised due to an increased control over the fermentation process [171]. The use of starter cultures has also led to the development of new generations of starter cultures that confer benefits to the food production process other than acidification [170, 172, 173]. These benefits include antimicrobial properties that increase food preservation. In addition to lactic acid, some LAB strains are known to also produce acetic acid, formic acid, reutericyclin, hydrogen peroxide, ethanol, reuterin and fatty acids [174, 175, 176, 177, 178, 179, 174].

#### **2.12.3.2 Antimicrobial products**

Many LAB strains produce bacteriocins which have antimicrobial activity [180]. *Lactococcus plantarum* produces organic acids that have antifungal properties. In the modern age where the prevalence of resistance to antimicrobial products including both antibiotics and commercially available chemical biocides is both high and increasing, the potential to identify and produce new products which is extremely important.

### **2.12.3.3 Lactic acid production**

Lactic acid (2-hydroxypropionic acid) is an organic compound that is characterised by containing both carboxylic acid and hydroxyl groups [181]. This compound has been used within industry for a long period of time, having been first isolated in 1780 from sour milk and first commercially produced in 1881 [182, 183].

### **2.12.4 The importance of pH in healthcare**

There are potential applications for a pH sensor in healthcare as pH is an important factor in different health situations including dental where changes in pH are associated with the formation of dental plaque and the development of caries [184]. pH is also important in skincare as healthy skin has a lower pH and increased skin pH is associated with infection and chronic skin disorders [185]. As part of homeostasis blood pH is tightly regulated and is slightly alkaline and deviating outside a narrow window between pH7.35 and pH7.45 results in the onset of acidosis or alkalaosis [186, 187]. Cellular organelles and enzymes need to be at optimal pH levels in order to function as such changes in pH result in the disruption of cellular processes leading to cellular death [188].

## **2.13 Current gaps in research**

While the production and properties of DMSO-melanin have been thoroughly documented [189, 136, 190, 138, 98, 134], prior to this work there has been no reports of this molecule being utilised and tested in an application in a real world setting. Prior to this work there have been no reports of a screen printed pH sensor being successfully tested in applications where there are

live bacterial cultures where there is a potential application for monitoring the pH of culturing media in order to ensure optimal growth or detect possible contamination.

This work also aims to test whether a DMSO-melanin pH sensor is suitable for use in a disposable point of care platform that could be used as a test for lactic acidosis. While there have been reports of biosensors that are able to detect lactic acid for example in breath [191] there have been no reports of a working screen printed pH sensor that is able to aid in the diagnosis lactic acidosis by measuring the pH of blood samples that may be useful in a point of care setting.

There have been reports of biosensors that are able to detect bacteria in solutions where there are potential applications for detecting food spoilage or contamination these sensors rely upon the working electrode being functionalised in order to cause them to become sensitive to the bacteria [192, 193, 194, 195, 196, 197]. Such functionalisation typically involves attaching biomolecules to the working electrode that are specific to a target analyte that is part of the microorganism of interest. This functionalisation step increases the cost of the sensors as the biomolecules (such as antibodies) can be expensive themselves. Functionalisation also results in a higher cost as it introduces complexity to the manufacturing process where electrochemical steps are needed in order to modify the surface of the working electrode and cause the biomolecules to bond to it. Part of this work seeks to see whether it is possible to eliminate this functionalisation step by testing sensors with plain printed carbon electrodes using different electrochemical techniques in order to see whether the signal generated correlates with relevant environmental changes (such as bacterial concentration within a solution) with the intention of producing useful sensors that are easier and

therefore cheaper to manufacture.

The next chapter will detail how the SPEs that are used as the base for the DMSO-melanin are pH sensor fabricated along with the techniques and methods that are used to assess their quality.

## Chapter 3

# Sensor fabrication and characterisation

This chapter details the fabrication of the SPEs that were used as the base of the DMSO-melanin pH sensor (Chapter 5) and in the electrochemical testing of media and bacteria (Chapter 8). Screen printing, the process by which these sensors were fabricated is introduced and the materials used for the sensors are described. The apparatus and techniques that were used to characterise the sensors are also covered here along with the settings used.

### 3.1 Introduction

Screen printing technology has allowed for the mass production of screen printed electrodes (SPEs) that perform consistently without the need of a centralised laboratory [198]. SPEs have properties that make them appropriate for *in situ* electrochemical analysis. Such properties include a low power requirement, repeatable output, an ability to operate at room temperature, rapid response and high sensitivity [199, 200, 201].

Commercially available sources of SPEs exist, such as Dropsense by Methrohm. It is also convenient to fabricate custom made SPEs via the use of screen printing machines as this allows for a high volume of sensors to be produced at a lower cost than purchasing them from an external supplier [198]. SPE formats are changeable with regards to specific requirements that are necessary for different analytes. The surface of the SPE can also be modified to suit different purposes and improve the performance of the sensor. Modifications for SPEs include inorganic nanomaterials, enzymes, DNA sequences and noble metals [198].

### **3.1.1 Principles of screen printing**

The technique of screen printing is extremely old, first being introduced over a thousand years ago, initially in the field of art. Since its introduction screen printing has primarily been used in the production of art and within the textiles industry. More recently, researchers have used the screen printing technique to produce electrode devices upon various substrates. The production of SPEs fulfils the demand for reproducible electrode devices that are stable and suitable for mass production. This has resulted in the attraction of wide interest in related SPEs [202, 203].

#### **3.1.1.1 Screen printing process**

Screen printing relies upon using a woven mesh that supports a stencil which blocks the ink. A squeegee is then moved across the screen stencil forcing the ink past the threads of the woven mesh in the open areas [198] this process is shown in Figure 3.1. A series of such woven meshes is required in order to print the different parts of the electrode. After each layer of ink has been printed onto a substrate, it must undergo thermal treatment that

solidifies the ink. Once all the required layers of conductive ink have been printed, a layer of protective ink is printed onto the electrode that insulates the conductive track from the electrodes.

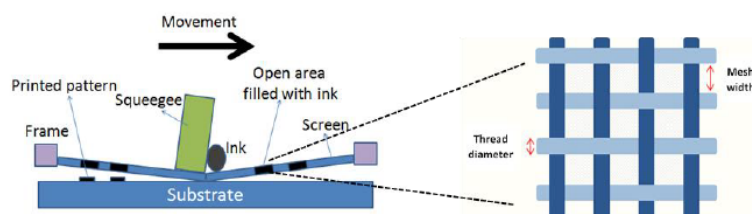


Figure 3.1: Diagram overviewing the general process of screen printing.

### 3.1.2 SPE designs

The design of the SPEs used for this research include a disk shaped working electrode surrounded by a ring and a small Ag/AgCl reference present towards the bottom of the ring. The designs that were used for each of the layers that compose the SPEs that were used in this work are shown in Figures 3.2 and 3.3 and photographs of the screen are shown in Figure 3.4.



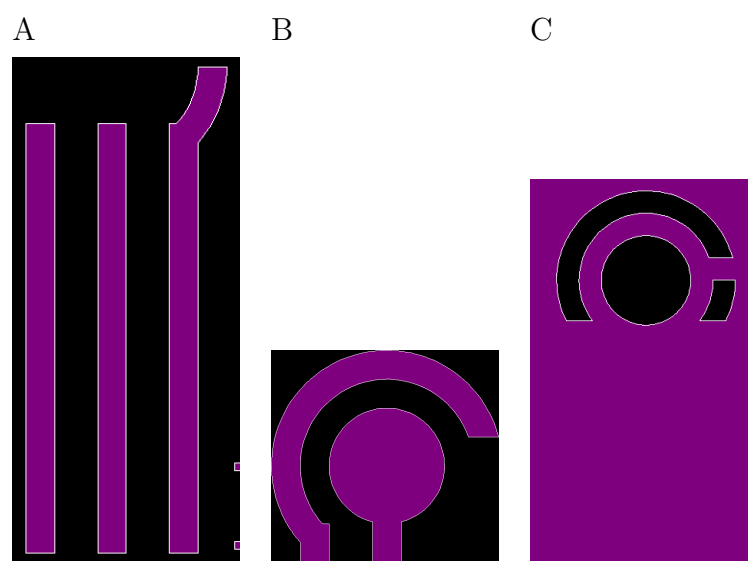


Figure 3.2: Designs for each layer of the screen printed electrode shown in purple in the order that they were printed. A. Silver or silver/silver chloride ink conductive tracks and reference electrode. B. Carbon/graphene working electrode. C. Insulator layer.

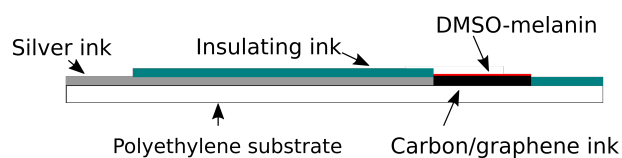


Figure 3.3: Side view showing the layers of a SPE that has been functionalised with DMSO-melanin.

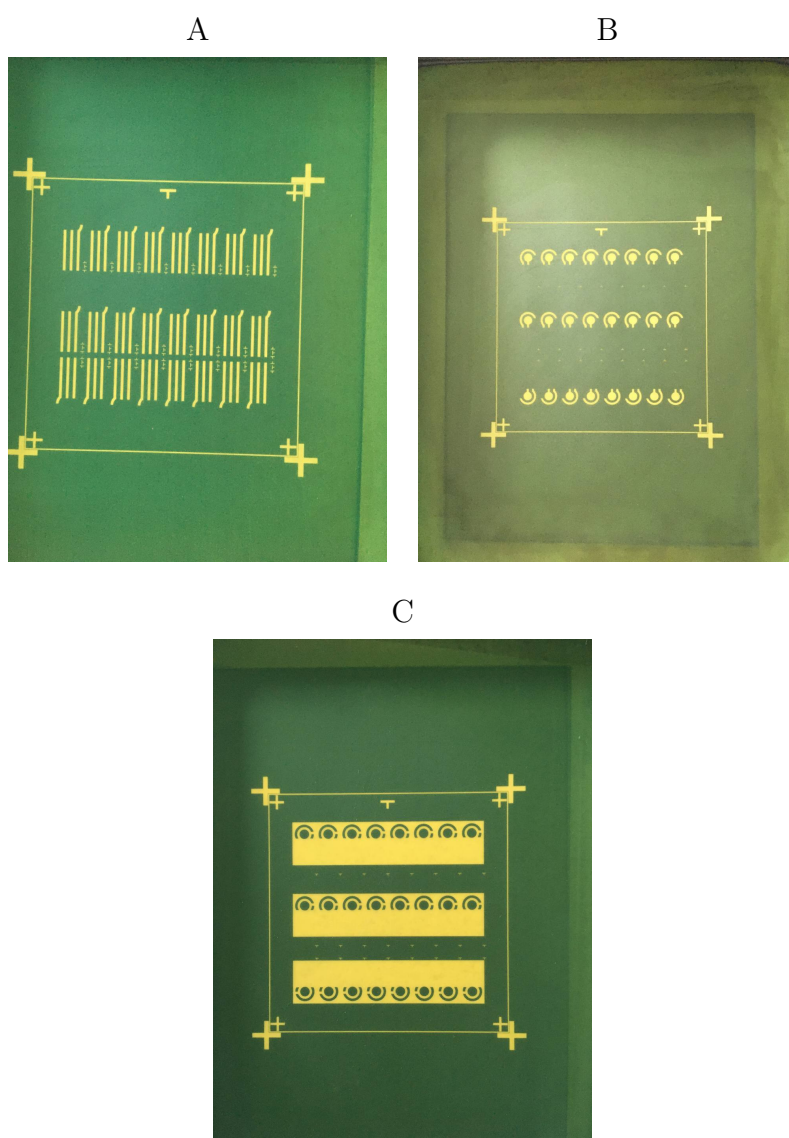


Figure 3.4: Photographs of the screens that were used in the fabrication of the SPEs. A. Silver or silver/silver chloride connection tracks/reference electrode. B. Carbon/graphene working and counter electrodes. C. Insulating layer. These screens are capable of producing a total of 24 SPEs.

### 3.1.2.1 Printing materials

The inks that are most commonly used in the production of SPEs are carbon ink and silver ink. Silver ink is usually printed as a conductive track while the working electrodes are often printed either using carbon ink or gold ink [204]. These inks exist in the form of pastes. Carbon paste is commonly used as it is chemically inert and easy to modify whilst also being a relatively inexpensive material. The increased cost of gold paste over carbon contributes to it being a less popular choice in SPEs than carbon. However interest in gold is increasing due to generation of self assembled monolayers (SAMs) that occur through strong Au-S bonds [205, 206]. Applications of gold sensors are focused upon electrochemical biosensors such as immune, enzymatic and genosensors [207, 208, 209, 210].

The printing inks that are used to fabricate SPEs contain polymers that hold the ink film together. Such polymers may shelter electrochemically active carbon in the ink, increasing electron transfer resistance which would cause slower kinetics of heterogeneous reaction and irreversible or quasi reversible redox processes may occur at the SPEs [211]. The printing paste can be modified to improve the slow electron transfer of bare SPEs. The greatest improvements in overall catalytic performance are seen with the addition of noble metals, however these are associated with a high cost that limits their potential for usage in commercial applications. To address this, less expensive materials are used to replace the noble metals, an example material being manganese oxide ( $\text{MnO}_x$ ). Commercial grade  $\text{MnO}_x$  have been mixed into carbon ink prior to screen printing and the resulting electrode was reported to have a good performance with sensing nitrite ions and ascorbic acid [212]. Bismuth oxide and bismuth nanoparticles have also been mixed with the carbon ink to successfully produce SPEs [213, 214, 215].

**3.1.2.1.1 Inks used in sensor fabrication** The sensors were fabricated using a commercially available carbon based ink composed of graphene, graphite and carbon black (Gwent C2171023D1 conductive carbon:BG04) for the working and counter electrodes. The connective tracks and the reference electrode were produced using either conductive silver (SunTronic AST6025) or silver/silver chloride ink (Gwent C2130809D5). In order to protect the connective tracks a layer of dielectric paste (Gwent D2140114D5) was printed as a top layer.

## **3.2 SPE fabrication**

### **3.2.1 Screen printer operation**

The R29 screen printer is operated by first activating the pressure pump (Figure 3.5) as the machine is driven by compressed air. The stencil must then be released (Figure 3.6) and the screen needs to be attached and secured using the screws and washers (Figure 3.7) ensuring that the screen is level. The printer settings (Figure 3.8) that need to be modified include the print parameters which are detailed in Section as well as the “print limits”, “PCB on-contact calibration” and “squeegee zero pressure calibration” (Figure 3.9). The “print limits” refer to the positions on the screen where the squeegee applies pressure. “PCB on-contact calibration” refers to the contact point between the print table and the screen and this must be assessed manually. “Squeegee zero pressure” refers to the pressure applied to the screen by the squeegee.

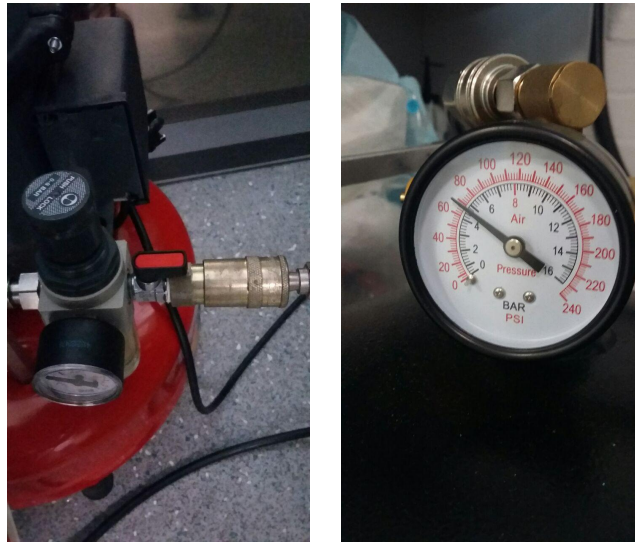


Figure 3.5: The pressure pump must be activated prior to operating the screen printer as the machine runs on compressed air.

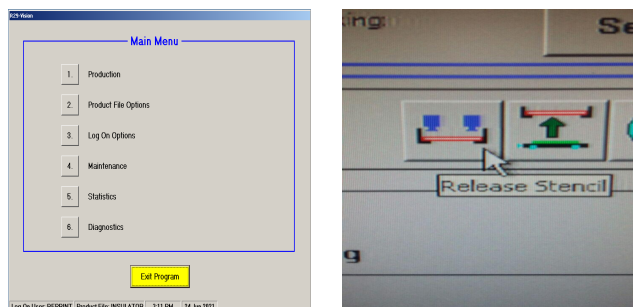


Figure 3.6: The main menu screen that is displayed to users when opening the “Shuttle29” software that drives the screen printer. The frame must be removed from the screen printer so that the screen can be loaded onto it. To do this the “release stencil” button should be pressed.



Figure 3.7: The screen must be fixed securely in place using screws and washers. Once in place it is important to ensure that the screen is level before printing.

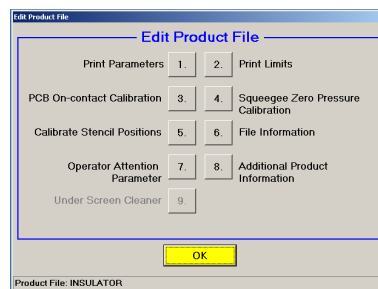


Figure 3.8: Menu displaying the various settings that can be edited, only options 1 to 4 were edited.

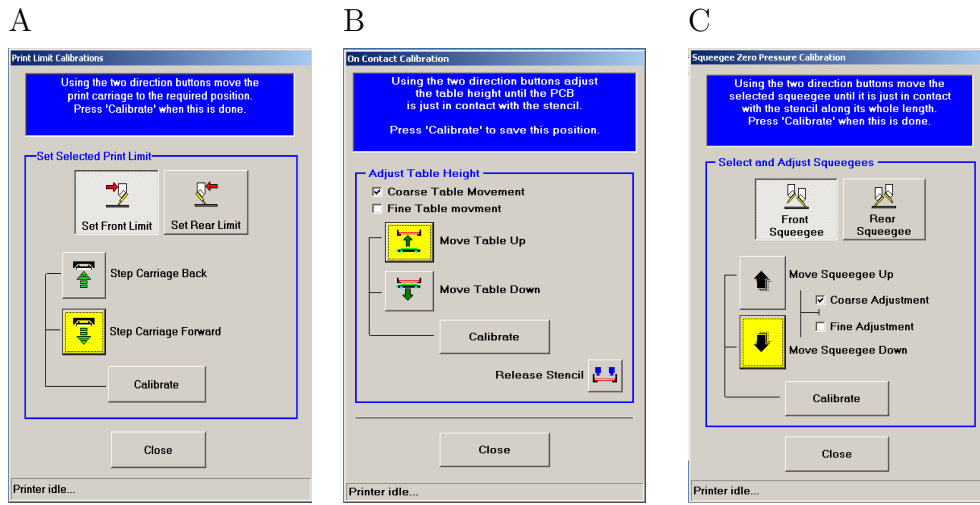


Figure 3.9: Menus displaying the print limits (A), the contact pressure of the table to the screen (B) and the pressure calibration settings for the squeegees (C).

### 3.2.2 Printing settings

The SPEs were fabricated using a R29 series screen printer (Reprint UK) using the parameters shown in Table 3.1. These settings were chosen as a result of previous screen printing optimisation work that was not a part of this study.

Table 3.1: Printing parameters that were used during the fabrication of the screen printed electrodes.

<b>Print pressures</b>	
Front squeegee	6kg
Rear squeegee	0kg
<b>Print speeds</b>	
Forward	50mm/s
Reverse	10mm/s
<b>Print deposits</b>	1
<b>Print cycle</b>	flood - print
<b>Table details</b>	
Print gap	2mm
Snap off distance	0mm
Snap off speed	0.3mm/s
Down speed	25mm/s
Down delay	0s

### 3.3 Characterisation techniques

Various characterisation techniques were employed to investigate the surface morphology and the surface chemistry of the printed electrodes in order to understand the properties of the SPEs and ensure that there is uniformity between them as inconsistencies between the SPEs could lead to less reliable results impacting the potential usefulness of the SPEs in applications.



### 3.3.1 Scanning electron microscopy

The wavelength of visible light limits the magnification that is achievable with traditional optical microscopes. The wavelength of electrons is smaller and as such they have been utilised in microscope technology such as scanning electron microscopy (SEM) and thus have achieved significantly greater magnifications than that which is possible with a light microscope ( $>100,000$  as opposed to  $\approx 400$ ). The underlying principle of how SEM works is well documented [216]. Within the context of this work SEM is used to characterise the surface topography of the electrode. This provides insights into the materials that are in the ink as well as an indication as to the roughness of the electrode surface which impacts on the surface area of the electrode. Such characterisation with SEM is also useful for assessing uniformity between sensors and seeing whether there have been any morphological changes to the electrode after the sensors have been used with a sample. An example of the output that is produced using SEM is shown in Figure 3.10. A disadvantage of SEM is that it only provides a two dimensional image of the electrode surface. To overcome this white light interferometry (WLI) and atomic force microscopy (AFM) were used to gain insight into the three dimensional properties of the electrode surface. WLI covers a greater area of the electrode surface than AFM however AFM has a greater resolution therefore using a combination of these techniques provides the most complete insight into the surface topology of the electrode.

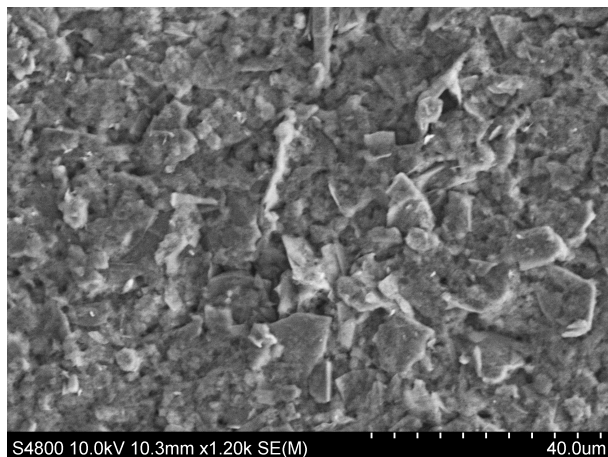


Figure 3.10: An example of an image produced using SEM of a carbon/graphene working electrode from an SPE.

#### 3.3.1.1 SEM settings

SEM images were generated using a Hitachi S4800 scanning electron microscope using the settings shown in Table 3.2. However some settings such as the voltage and current of the electron beam as well as magnification were varied in an effort to increase the quality of each image. Generally lower voltages were used as these are better for imaging the surface of the carbon electrode as higher voltages are too penetrating [217].

Table 3.2: Scanning electron microscopy settings used when visualising the electrode surface.

Setting	Variable used
Probe current	High
Working distance	11.6mm
Cond lens 1	5
Cond lens 2	1
Column condenser	1

### 3.3.2 Surface roughness and thickness of the printed working electrodes

#### 3.3.2.1 White light interferometry

WLI is based upon the superposition of light waves and is a method for measuring vertical changes across the surface of a sample optically. Similarly to AFM, WLI is used to measure the three dimensional properties of the electrode topology. There are advantages and disadvantages to both techniques for example AFM is able to measure at a higher resolution than WLI however WLI has a higher range of heights that it is able to measure as well as being better for characterising angles which makes it more suited for measuring thickness [218]. It has been reported that using a combination of both AFM and WLI is useful for correct surface characterisation [219]. WLI produces graphical output as shown in Figure 3.11 as well as numerical data that describes the surface roughness. These are the mean roughness ( $R_a$ ), the sum of the maximum peak height and maximum valley depth averaged over sampling lengths ( $R_z$ ), the sum of the maximum peak height and max-

imum valley depth over the evaluation length and the root mean square of the roughness ( $R_q$ ). The difference between the  $R_a$  and the  $R_q$  indicates how uniform the surface is and the difference between  $R_t$  and  $R_z$  suggests whether there may be a scratch (indicated by a high difference) where the difference between the peaks and valleys is larger than the typical surface features [220].

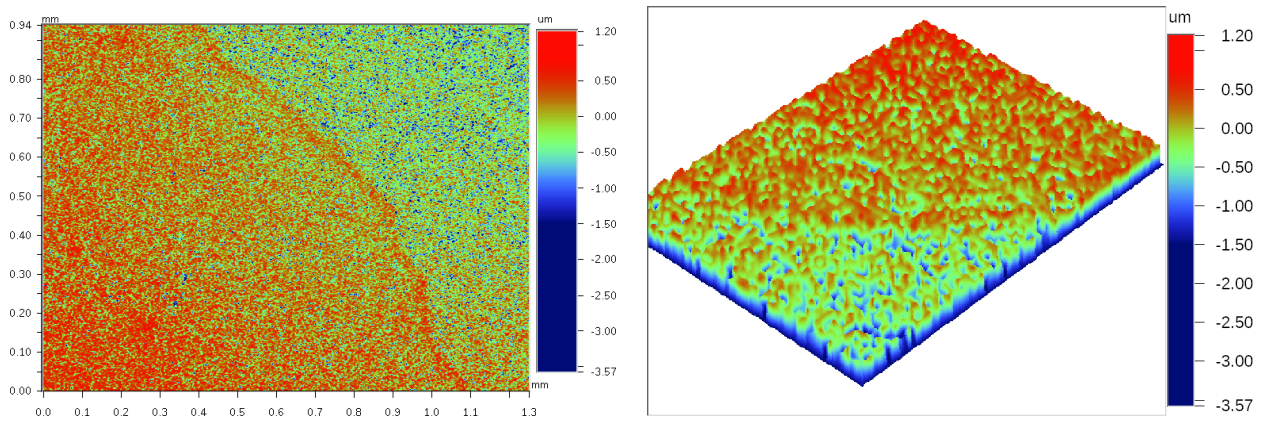


Figure 3.11: Example of the graphical output produced by WLI of printed carbon ink on a PET substrate. The left image shows a top down image of the surface where the height is represented by a colour spectrum ranging from blue (lowest) to red (highest). The right image shows a three dimensional representation of the measured surface.

### 3.3.2.2 White light interferometry settings

WLI was carried out using the Veeco Wyko NT9300 optical profiling system using the vertical shift interferometry mode. Primary scan was set with a backscan of  $45\mu\text{m}$  and length of  $50\mu\text{m}$ . The area measured was  $1.3 \times 0.94\text{mm}$  at a resolution of  $640 \times 480$  with a magnification of 5x.

### 3.3.3 Raman spectroscopy

Raman spectroscopy is an optical technique that is used to investigate the molecular vibrational energy levels. This spectroscopic technique can give specific molecular and chemical information regarding a sample due to it yielding spectrally narrow bands which occurs as a result of Raman scattering being an inelastic scattering process that occurs when light and matter interact. Further details of the principles that underlie Raman spectroscopy may be found here [221]. Raman spectroscopy is an important technique for detailing the chemical composition of the electrode surface. This is also useful for assessing any chemical changes that occur on the surface of the electrode following functionalisation. An example of the output generated using Raman spectroscopy is shown in Figure 3.12.

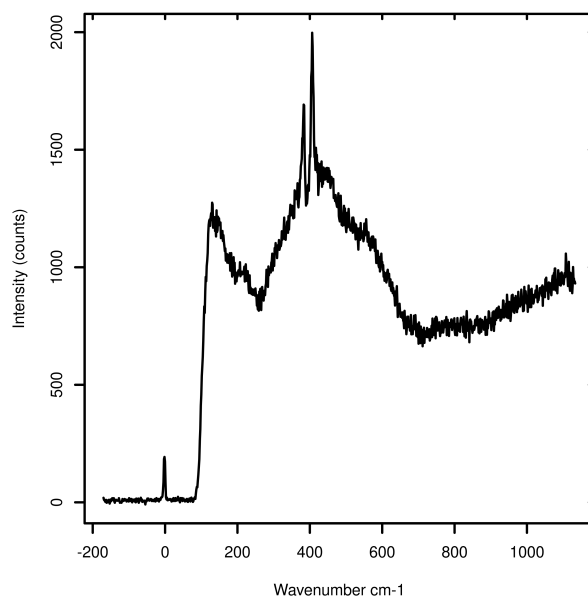


Figure 3.12: Raman spectra obtained from a sample of molybdenum disulfide. The peaks in the spectra correspond with the absorption of infra red light at various different wavelengths. These provide a fingerprint that is associated with groups of atoms or functional groups thereby elucidating the chemical structure of the material that is undergoing analysis.

Measurements were carried out using a laser at a wavelength of 532nm using a Renishaw inVia system.

### 3.3.4 Fourier-transform infrared spectroscopy

Fourier-transform infrared spectroscopy (FTIR) is a surface characterisation method that uses infra red to analyse the composition of a sample, it is based on the interference of radiation between two beams [222]. This is functionally similar to other forms of spectroscopy where the amount of light absorbed at a particular wavelength corresponds with specific atom or bond types. The use case of FTIR is similar to that of Raman, as both techniques have

their own advantages and limitations using a combination of both techniques allows for better characterisation of the sensor. The advantages of FTIR include that it is able to produce spectra quickly due to a high signal to noise ratio [223] however Raman spectroscopy has a higher resolution than FTIR and is also capable of producing 3D images [224].

FTIR measurements were conducted between wavelengths of 400 and  $4000\text{cm}^{-1}$ .

### **3.3.5 Resistance of the printed carbon working electrodes**

A current is applied to the electrode surface through one wire and the voltage is measured using the other wire in order to measure the conductivity of the electrode surface using the settings shown in Table 3.3. Where current is applied from the outer two wires and the voltage difference is detected between the inner two wires. Ohm's law is applied to take a ratio of the measured voltage difference to the applied current to determine the four wire resistance. It is also possible to get the four wire resistance by applying a known voltage and measuring the resulting current and taking the ratio of the difference. Being able to assess the conductivity/resistance of the electrode allows for the quality of the electrodes to be assessed as well as to check for consistency between different sensors. Higher conductivity is also associated with increased sensor sensitivity and improved limits of detection [3]. A photograph of the 4 wire configuration is shown in Figure 3.13 and the measurements are shown in Figure 3.14.

### 3.3.5.1 Settings

Table 3.3: Settings used on the Keithley multimeter for resistance/conductivity measurements.

Setting	Option
Assignment Type	Sweep
Source Function	voltage
Source Mode	Normal
Measure Function	current
Sense Mode	Four-Wire
Asymptote	Not Applicable
Source Limit	10.0 mA
Source Range	200 mV
Bias Source Value	Not Applicable
Step/Sweep Start Level	-10.0 mV
Step/Sweep Stop Level	10.0 mV
Step/Sweep Style	LIN
Number of steps / sweep points	101
Measure Range	10 mA
Step-to-Sweep delay	Not Applicable
Custom Sweep?	No
Sweep time/point	200.06 ms
Pulse Sweep?	No



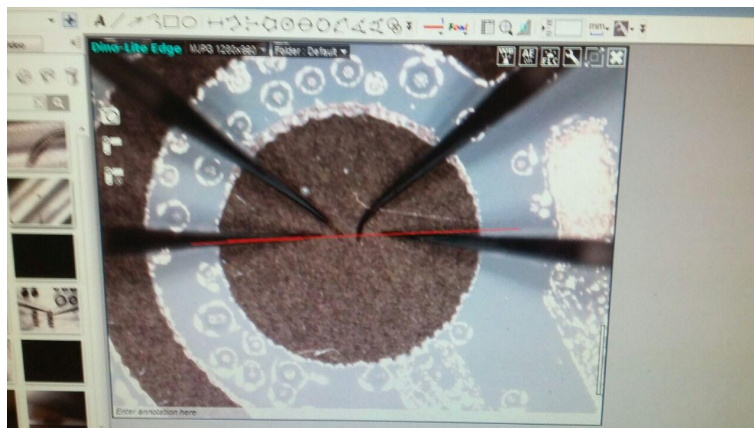


Figure 3.13: Layout of probe position for testing the working electrode of the SPEs for four point IV testing. This setup was maintained and applied to different areas on the working electrode in order to measure the consistency of resistance across the electrode surface.

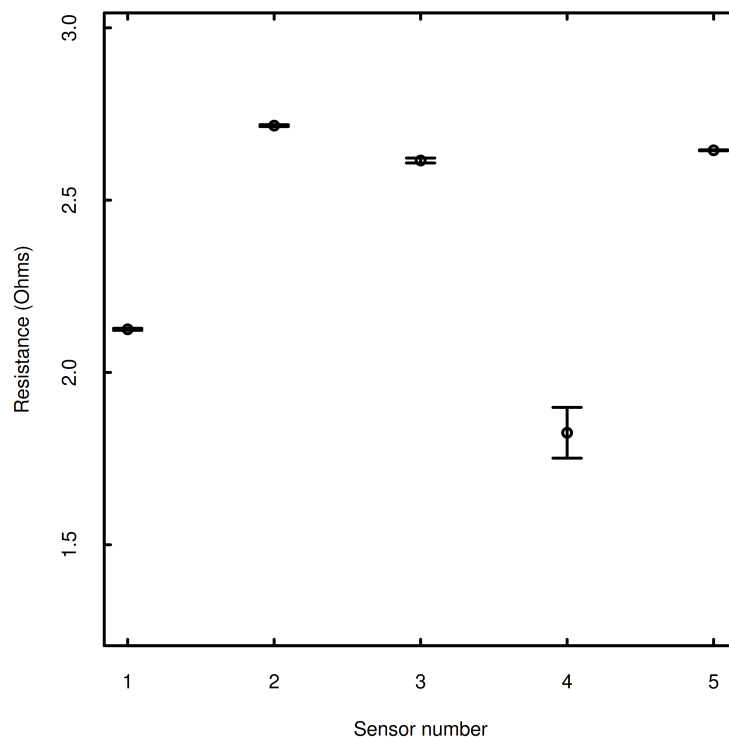


Figure 3.14: Contact resistance for the working electrode measured using four point IV in the configuration shown in Figure 3.13. The error bars represent the standard error times 1.96 of the resistance that was measured on each sensor ( $n=5$ ). The distance between the probes was kept constant between measurements. These results indicate that the sensors are consistent as there is little variation between the measured resistance.

### 3.3.5.2 AFM settings

AFM was performed using a tip radius of resonant frequency of 320 kHz, a spring constant of 40 N/m and a 8 nm tip radius. The instrument used was a JPK NanoWizards II (Dimension-3100 Multimode, Bruker, Billerica, MA, USA).

### 3.4 Testing consistency between printed electrodes

It is important to assess the quality of the sensors in order to ensure repeatability by making sure that there is little variation between the sensors as inconsistent sensors may lead to a variation in measurements. The printed sensors were numbered by row and column (Figure 3.15) so that the sensors at different locations could be compared in order to assess their consistency. This was achieved using electrochemistry where SWV and EIS produced similar outputs when performed on the sensors using 5 mM  $\text{K}_3[\text{Fe}(\text{CN})_6]/\text{K}_4[\text{Fe}(\text{CN})_6]$  as electrolyte (Figures 3.16 and 3.17). The consistency between the electrochemical results indicates that there is consistency between the sensors. The thickness of printed ink was measured using WLI (Figure 3.18). These thicknesses were similar and consistent across all the tested sensors with an average thickness of  $10.625\mu\text{m}$  with a standard deviation of 0.861 for the silver track and an average thickness of  $8.61\mu\text{m}$  with a standard deviation of 0.87 for the carbon/graphite electrodes (Figure 3.19).

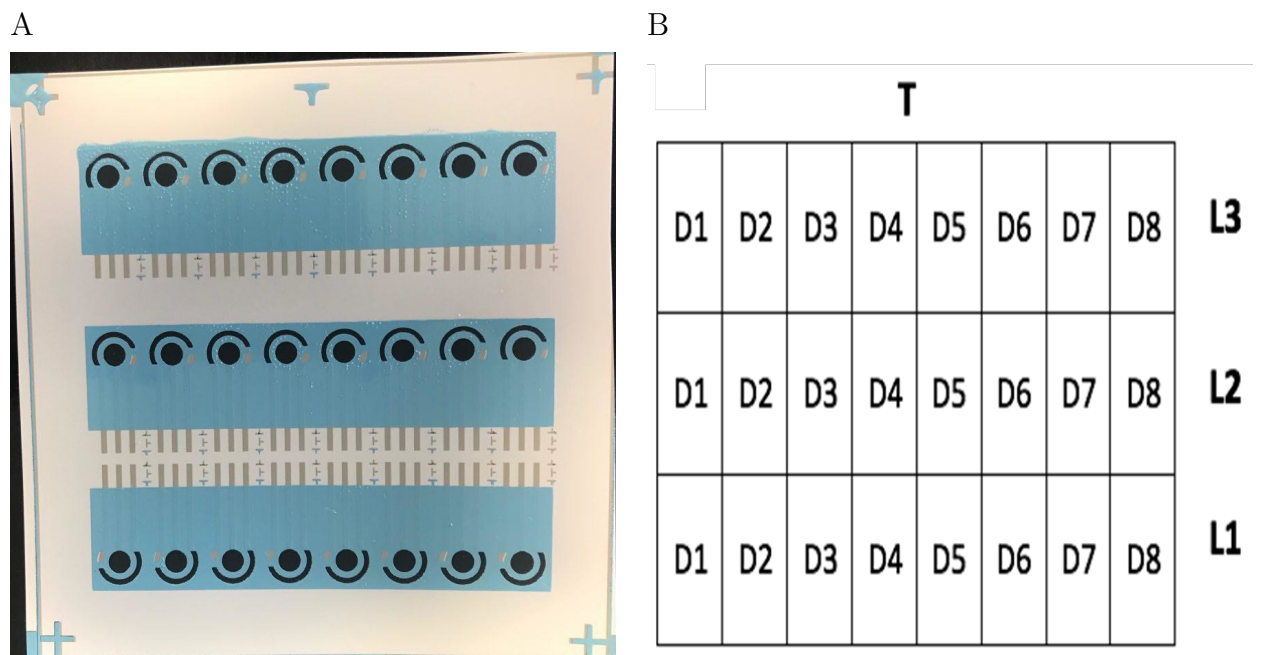


Figure 3.15: A: Photograph showing a completed sheet of SPEs that are ready to be cut into individual units. B: Identification of each sensor on the sheet for use in subsequent testing.

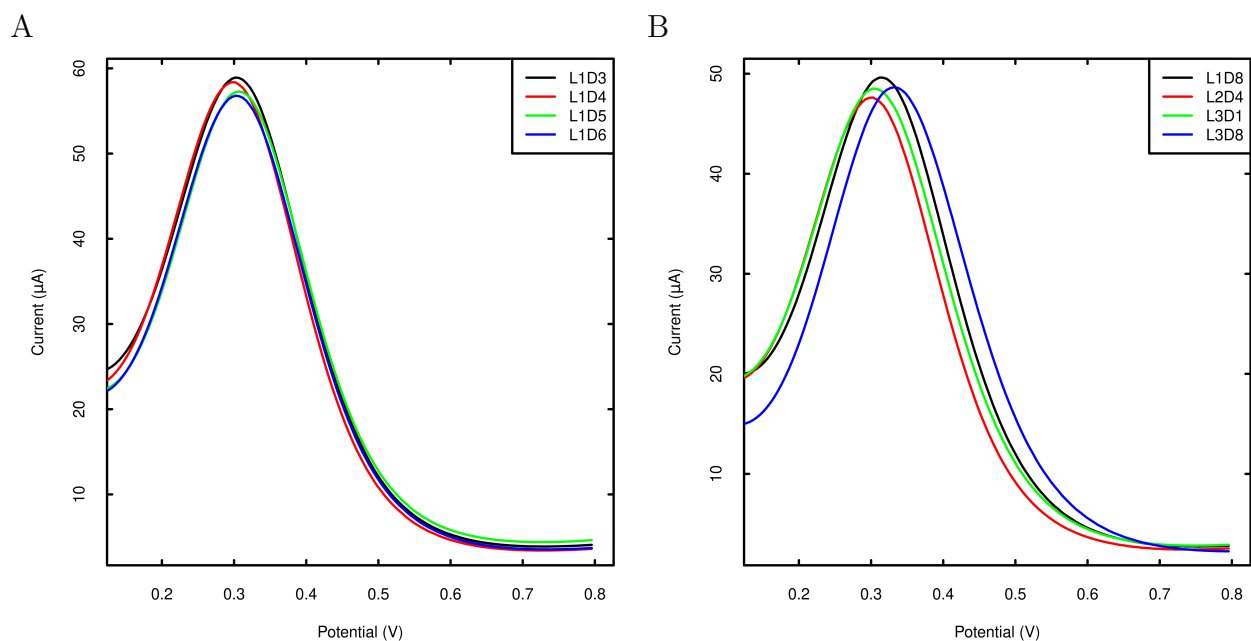


Figure 3.16: Square wave voltammetry carried out on screen printed electrodes from positions along A: a row of the printed sheet and B: Across the rows of the printed sheet. From sheet number 22. The consistency appears to be greater within a row and less consistent between the different rows. This could possibly be due to the age and condition of the screen printer.

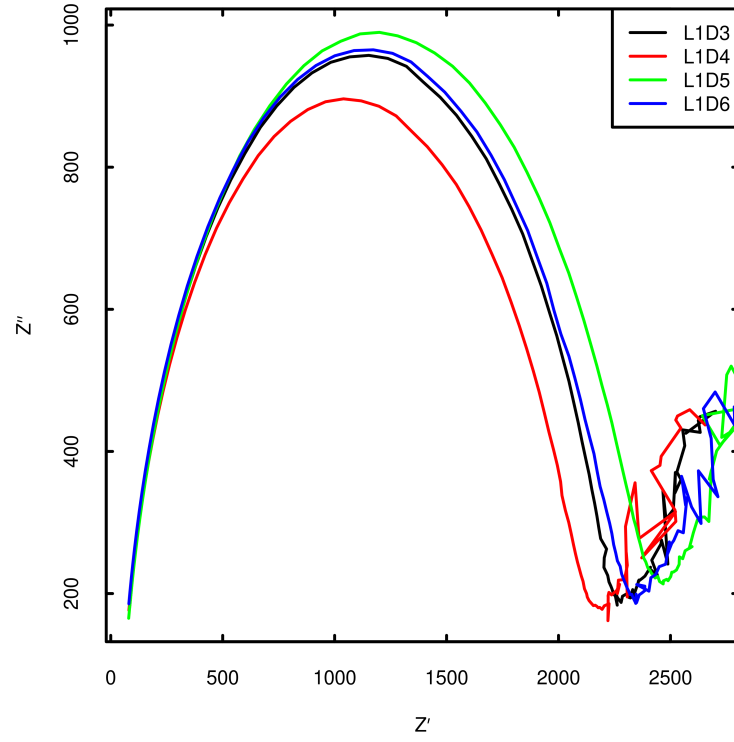


Figure 3.17: Impedance spectroscopy of the different screen printed electrodes from sheet number 3. The impedance measured from the SPEs taken from different locations on the sheet is similar indicating that the electrodes are consistent.

#### 3.4.0.1 Surface thickness and roughness

Both the thickness and the roughness were measured using white light interferometry as is described in Section 3.3.2.1.

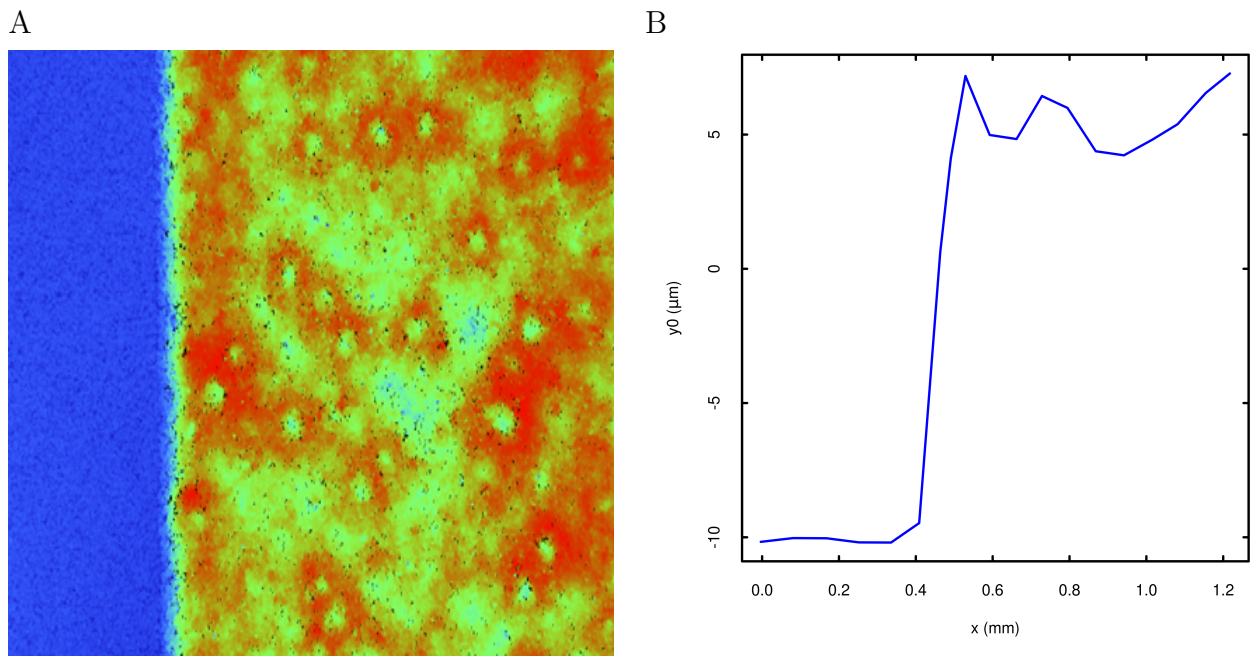
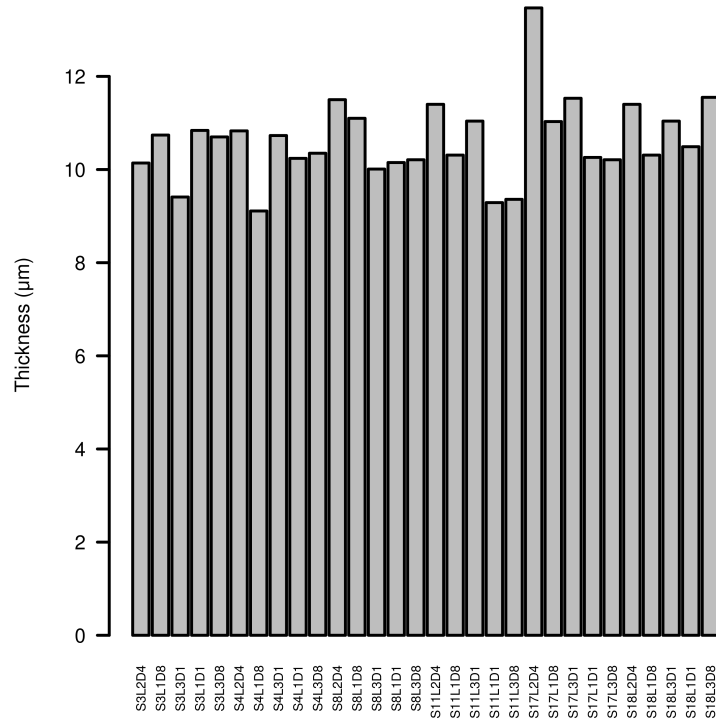


Figure 3.18: A. Image of the silver track under white light interferometry and B. the associated graph measuring the thickness.

A



B

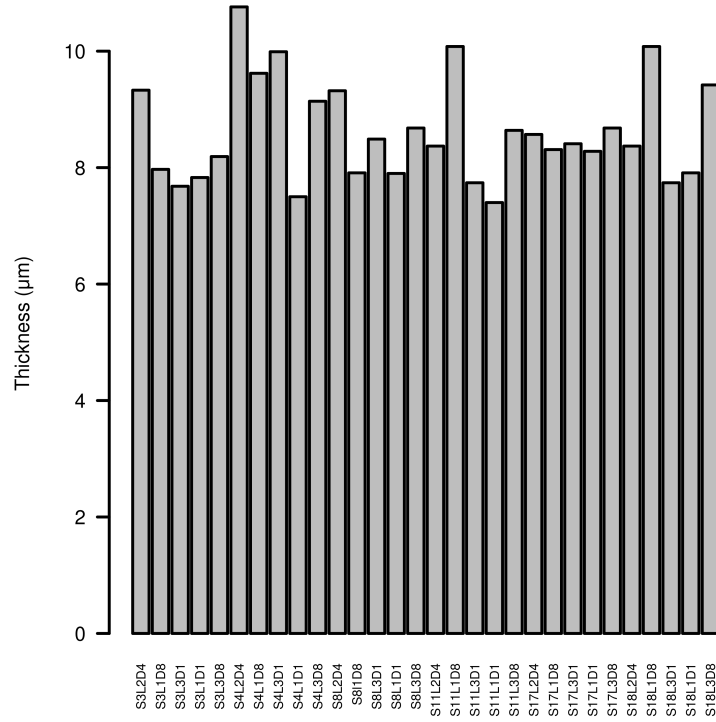


Figure 3.19: A. The thickness of the silver ink screen printed onto the PET substrate that composes the conductive tracks and the reference electrode of the sensor. B. The thickness of the working electrode printed with the carbon/carbon graphite ink measured with white light interferometry as described in section 3.3.2.2. The average thickness of the silver reference electrode is 10.63 with a standard deviation of 0.86 and the average thickness of the carbon working electrode is 8.61 with a standard deviation of 0.87 indicating that the thickness of both electrodes is consistent.



### 3.4.1 Electrode surface

The surface of the electrode was examined visually using a light microscope (Figure 3.20).

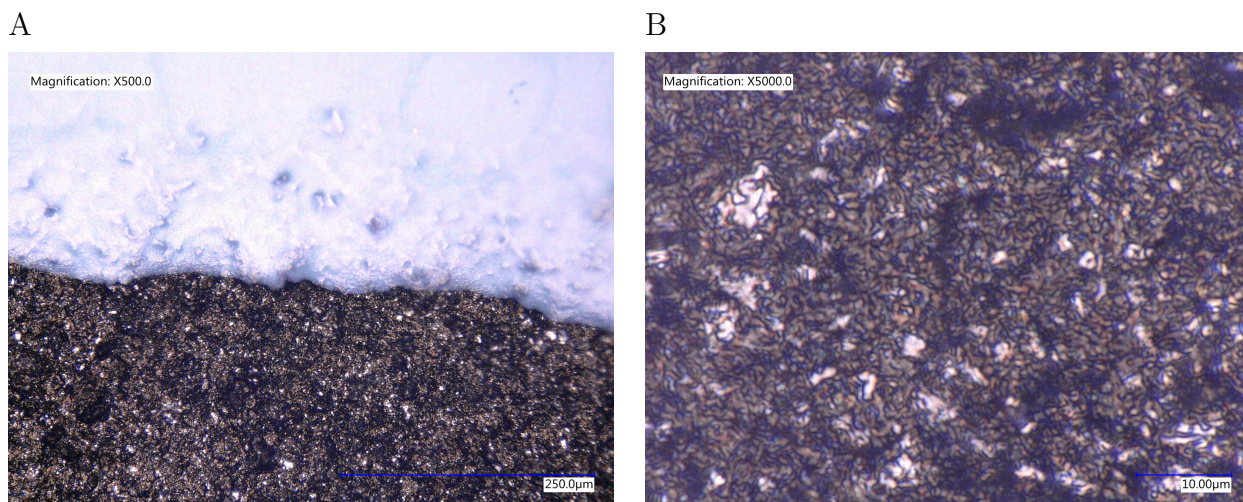


Figure 3.20: The working electrode of the sensor through a light microscope. A. Boundary where working electrode (black) and insulator layer (blue) meet. B. Working electrode.

The morphology of the electrode surface appeared to consist of flake like structures and much smaller spheres as can be seen in the SEM generated images 3.21. These flakes are morphologically consistent with graphene/graphite and the small spheres are morphologically consistent with carbon black suggesting that the carbon/graphene based ink that is used to print the working and counter electrodes contains a mixture of these substances.

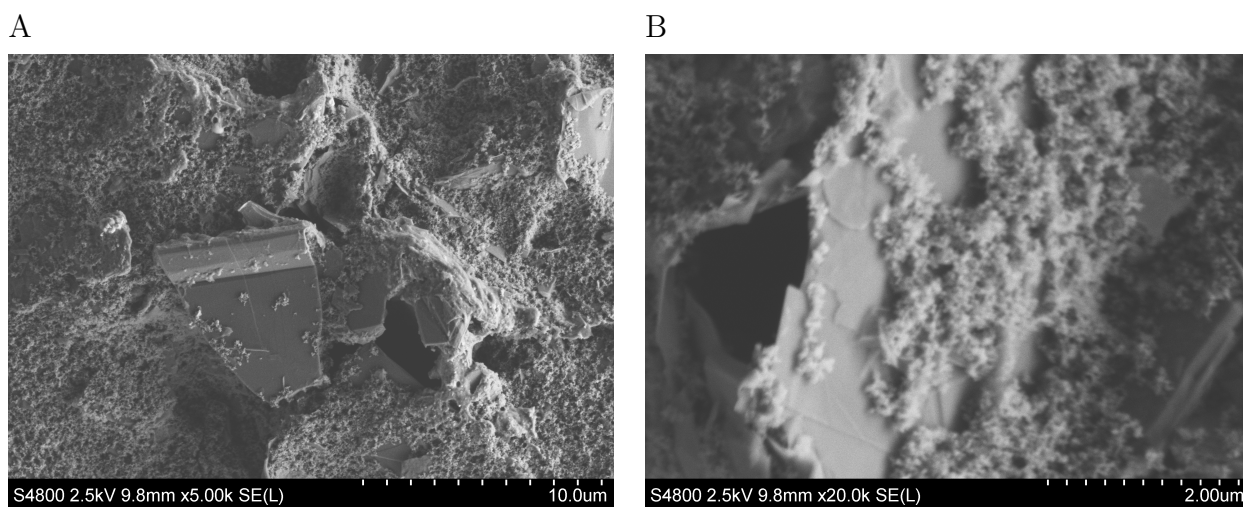


Figure 3.21: SEM images of the printed working electrode of the sensor.

### 3.5 Summary

This chapter has covered the fabrication process by which the SPEs were produced. The techniques that were used to characterise and assess the quality of the sensors have been described along with the appropriate settings. The output from Raman spectroscopy and conductivity testing are presented later in Chapter 5 as they are compared with working electrodes that have been functionalised with DMSO melanin. The next chapter will describe the electrochemical processes that were used to characterise the sensors as well as being the underlying mechanism behind generating the signal used to perform measurements using the sensors.

# Chapter 4

## Electrochemistry

### 4.0.1 Overview and theory

Electrochemistry refers to the study of charge transfer involving electrons/ions across the interface between a solution and an electrode. When an electrode is inserted into a solution then electrons may be transferred between the electrode and the solution until electrochemical equilibrium occurs. This leads to a potential difference resulting from a charge separation between the metal electrode and the solution. This potential difference is denoted as  $\phi_M - \phi_S$ .

### 4.0.2 The Nernst equation and pH

pH is a logarithmic scale that is used to measure the potential of hydrogen in a solution. Acidic solutions contain a greater concentration of hydrogen ions and the scale is inverse to the activity of hydrogen with more acidic solutions measuring lower on the scale. This is shown in equation 4.1 where  $[H^+]$  is the equilibrium molar concentration of hydrogen ions in the solution.

$$\text{pH} = -\log(\alpha_{H^+}) \approx -\log([H^+]) \quad (4.1)$$

The Nernst equation is well established for relating potential to the activities of reactants and products based upon three parameters, these are the standard electrode potential, the temperature, and the ratio of the concentrations of the oxidized and reduced species [225, 226, 227] and it is derived from Gibbs free energy ( $\Delta G$ ) under standard conditions (equation 4.2).

$$E^0 = E_{red}^0 - E_{ox}^0 \quad (4.2)$$

The potential difference is also related to  $\Delta G$  under general conditions (equation 4.3) where  $n$  is the number of electrons transferred,  $E$  is the potential difference and  $F$  is the Faraday constant.

$$\Delta G = -nFE \quad (4.3)$$

The Nernst equation is used to express the oxidation/reduction reactions that occur as a reversible process and allows for the calculation of the concentrations of the oxidised and reduced species at equilibrium. In the case of the following oxidation/reduction reaction:



In this instance the Nernst equation is expressed as:

$$E = E^0 - \frac{RT}{F} \ln \left( \frac{A_{Red}^b}{A_{Ox}^a} \right) \quad (4.5)$$

where  $E$  is the reduction potential (V),  $E^0$  is the standard reduction potential (V),  $R$  is the gas constant (8.314J/molK),  $T$  is temperature (K)  $n$  is the stoichiometric number of electrons in the reaction,  $F$  is the Faraday constant

(96485C/mol),  $a$  is the stoichiometric coefficient of the oxidised species,  $b$  is the stoichiometric coefficient of the reduced species,  $A_{Red}$  is the activity of the reduced species and  $A_{Ox}$  is the activity of the oxidised species.

The potential of the electrode is dependant on species reactivity, the potential in the Nernst equation is the potential at the equilibrium. The concentration of the species is used to calculate their activities based upon:

$$A_i = f_i C_i \quad (4.6)$$

where  $f$  represents the species coefficient of the species  $i$ , with this accounted for the Nernst equation is expressed as:

$$E_{Ox/Red} = E_{Ox/Red}^{0'} - \frac{RT}{nF} \ln \left( \frac{C_{Red}^b}{C_{Ox}^a} \right) \quad (4.7)$$

here  $E^{0'}$  represents a potential that is under non-standard conditions. This potential is dependant upon the composition of the system and it contains the standard potential value in addition to the species activity coefficient value.

### 4.0.3 Open circuit potentiometry

OCP involves the passive measuring of a solutions potential using two electrodes. In this system the potential of the working electrode changes along with the composition of the solution while the potential of the reference electrode remains constant. The working electrode may be composed of or coated with a material that allows for selectivity to the desired ion of interest, such is the role of the DMSO-melanin in the pH sensor that is presented in this work. This mechanism is described in greater detail in section 2.12.1.

#### 4.0.4 Electrochemical impedance spectroscopy

EIS functions by inducing alternating electrical signals at different frequencies into a system and subsequently measuring the signals that occur in response in order to analyze and characterise the electrical properties of materials within the system. In EIS the impedance of the cell or electrode is plotted vs frequency, this is measured using frequency response analysers or lock in amplifiers. These measurements can be used to interpret the theoretical capacitance, inductance and resistance of electrodes and electrolyte under varying conditions. This technique is capable of high precision and various different potentials can be used via the preparation of solutions that contain varying concentration ratios [228]. EIS typically uses low amplitude excitation signals and as such is dependant upon the virtually linear relationship between current and overpotential that exists at low overpotentials. Excitation at frequency  $\omega$  within a linear system provides a current that is also at frequency  $\omega$ . Conversely, if the relationship between current and overpotential is nonlinear then the response is not purely sinusoidal and distorted however it remains periodic and may be represented as a superposition of signals at  $\omega$ ,  $2\omega$  and  $\omega$  etc. [228]. The nonlinear relationship between current and overpotential that exists over moderate overpotential ranges results in effects that can be measured in order to characterise the electrochemical system. EIS can be applied to both simple electrochemical systems that involve solutions where a heterogeneous electron transfer reaction takes place as well as more complicated systems where there are adsorbed intermediates or coupled homogeneous reactions. Data generated with EIS can be fitted to equivalent circuit models represent the theoretical system reactions where the extracted results may be attached to a variable however analysis by fitting to an equivalent circuit can be

problematic as they present an ideal electrical response that might not represent a complicated electrochemical system [229].

#### **4.0.5 Relationship between $Z'$ and $Z''$**

Impedance is composed of a real number and an imaginary number, the real component is typically represented as  $Z'$  whereas the imaginary component is represented as  $Z''$ . EIS measurements are often expressed as a Nyquist plot though they may also be expressed as a bode or 3D plot. Nyquist plots are produced by plotting both the imaginary and real components of the measurement and frequently produce a distinctive semicircular shape.  $Z'$  represents the resistive part of the impedance, while  $Z''$  represents the reactive part of the impedance. The relationship between  $Z'$  and  $Z''$  is dependent on the frequency of the applied signal and the characteristics of the system thereby providing information about the electrochemical system under investigation [230].

#### **4.0.6 Fitting Nyquist plots to an equivalent circuit**

The shape that is produced is what allows the impedance to be fitted to an equivalent circuit. The equivalent circuit consists of electrical components including resistor, inductors, capacitors and memristors. The equivalent circuit refers to the presence and arrangement of these electrical components in such a manner that the impedance and the shape of the Nyquist plot resemble that of the electrochemical system that is being tested therefore providing some insight into the characteristics of the electrochemical system. An example of a Nyquist plot is shown in Figure 4.1.

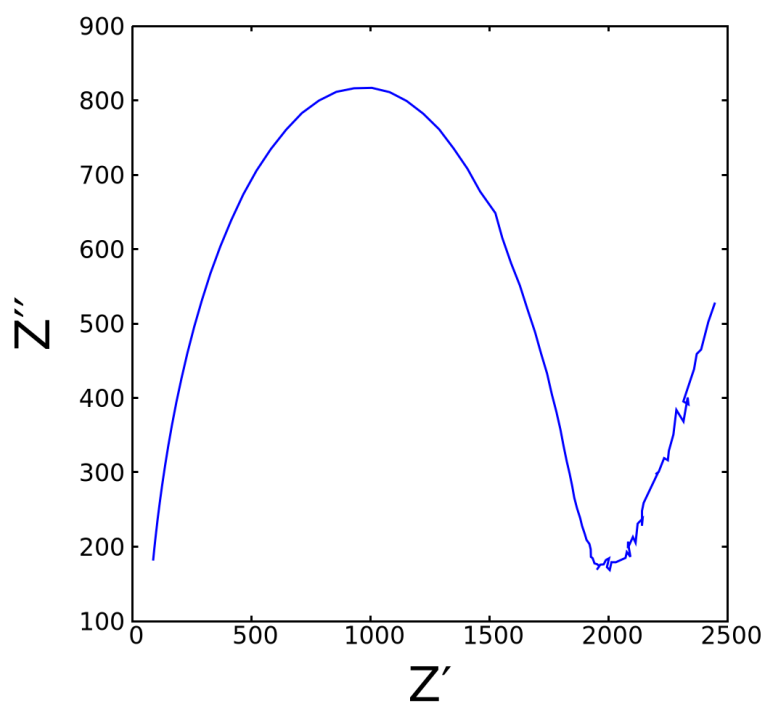


Figure 4.1: Nyquist plot generated by performing EIS on a SPE using the raw data output by the Metrohm Autolab potentiostat and K3/K4 solution.

### 4.0.7 Equivalent circuit elements

The equivalent circuit may contain various electrical elements. By monitoring the current response while an AC voltage is applied to an electrochemical cell EIS is able to measure the resistance, capacitance and inductance [231].

#### 4.0.7.1 Resistance

The resistance represents the charge transfer resistance or the solution resistance and is represented by the symbol shown in Figure 4.2. The impedance



of resistance is provided by Equation 4.8 where  $Z$  is impedance and  $R$  is resistance [232].

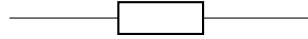


Figure 4.2: Electrical symbol that represents a resistor.

$$Z_R = R \quad (4.8)$$

#### 4.0.7.2 Capacitance

Capacitance represents the double layer capacitance of the electrochemical interface and is represented by the symbol in Figure 4.3. The impedance of capacitance is provided by Equation 4.9 where  $Z$  is impedance,  $C$  is capacitance, and  $j$  is the imaginary unit [232, 233].

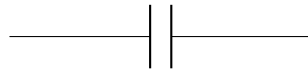


Figure 4.3: Electrical symbol that represents a capacitor.

$$Z_C = \frac{-j}{\omega C} \quad (4.9)$$

#### 4.0.7.3 Constant phase element

The constant phase element (CPE) represents the behaviour of an imperfect capacitor [234]. The CPE is represented by the symbol in Figure 4.4 and is provided by Equation 4.10 where  $Z$  is impedance,  $Q$  is 4.4,  $\omega$  is angular frequency,  $j$  is the imaginary unit,  $n$  is the CPE exponent that characterises the deviation from ideal capacitor behaviour and  $Y_0$  is the pre exponential

parameter that is directly proportional to the double layer capacitance of a pure capacitor. [235, 236, 237].

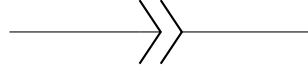


Figure 4.4: Electrical symbol that represents a CPE.

$$Z_Q = \frac{1}{Y_0(j\omega)^n} \quad (4.10)$$

#### 4.0.7.4 Inductor

Within an equivalent circuit an inductor represents the adsorption process on the electrochemical interface and is represented by the symbol in Figure 4.5 and the impedance of the inductance is provided by Equation 4.11 where  $Z$  is impedance  $L$  is inductance  $j$  is the imaginary unit and  $\omega$  is the angular frequency [231].



Figure 4.5: Electrical symbol that represents an inductor.

$$Z_L = j\omega L \quad (4.11)$$

The Nyquist plot in Figure 4.1 was fitted into an equivalent circuit using Nova (Metrohm) software (Figure 4.6). This equivalent circuit contains two resistors and one CPE.

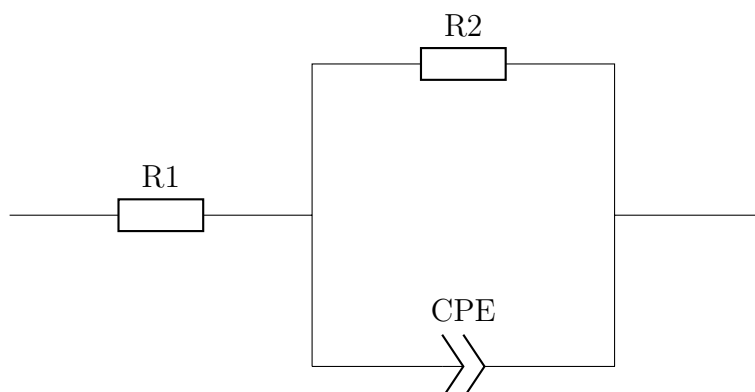


Figure 4.6: Equivalent circuit generated from the Nyquist plot shown in Figure 4.1.  $R1=36.1\Omega$ ,  $R2=1.95\text{ k}\Omega$ , CPE:  $Y_0 = 1.0026 \times 10^{-6}$ ,  $n = 0.998$ .

#### 4.0.8 Cyclic voltammetry

CV is an electrochemical technique that is frequently used in the investigation of oxidation and reduction processes as well as chemical reactions that are initiated by electron transfer [238]. The fundamental principle of CV involves applying a potential to an electrode while it is immersed in an electrolyte solution, this is the working electrode. The potential of the working electrode is cycled and controlled versus a reference electrode that is composed of a material that maintains a constant potential such as silver silver/chloride [239]. In CV this applied potential acts as an excitation signal occurs as a linear scan with a triangular waveform. The scan occurs between two potentials and begins negatively towards one potential before the direction is reversed and the scan proceeds positively towards the original potential, an example graph showing these potentials along with the classic shape associated with CV is shown in Figure 4.7A. The scan rate, number of cycles and the range of potentials used can be variable [239]. This triangular waveform is represented mathematically in equation 4.12 [240] where oxidation and re-

duction are represented by  $\pm$  and  $\mp$  respectively,  $t$  is time and  $E$  is potential a schematic diagram representing the triangular wave is illustrated in Figure 4.7B.

$$E(t) = \begin{cases} \pm vt + E(t = 0) & \text{for } t < t_{1/2} \\ \mp v(t - t_{1/2}) + E(t = t_{1/2}) & \text{for } t \geq t_{1/2} \end{cases} \quad (4.12)$$

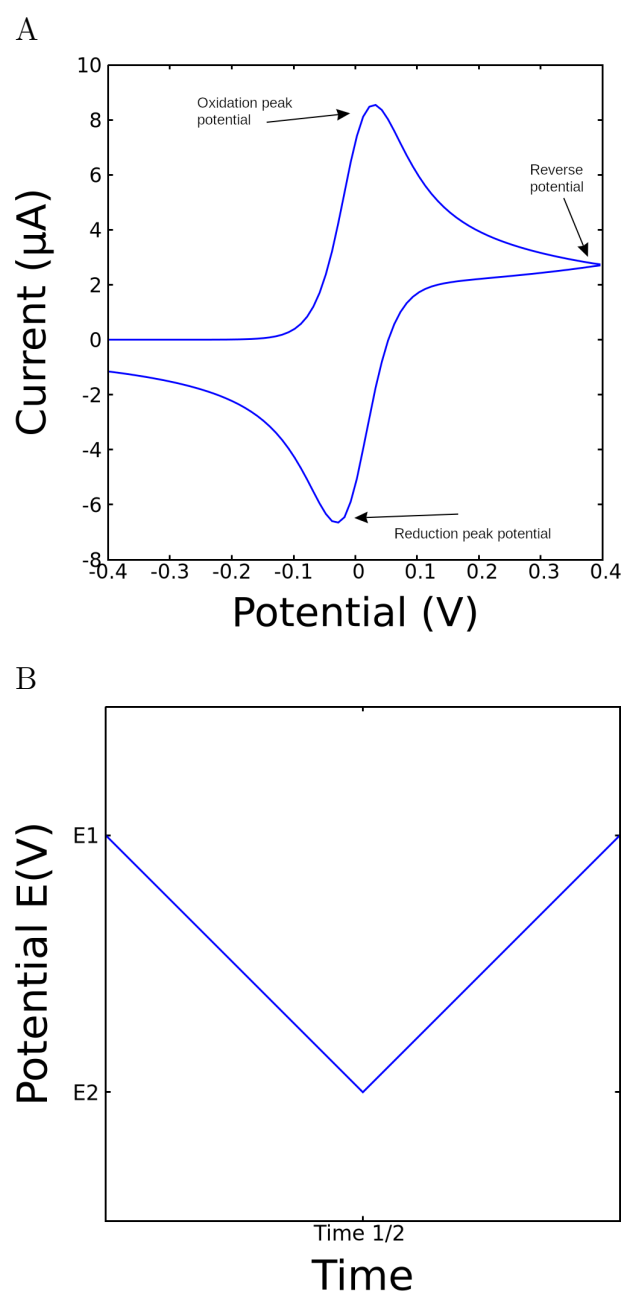


Figure 4.7: A. Example of a classically shaped cyclic voltammetry plot with the oxidation, reduction and reverse potentials annotated. B. Schematic representing a triangular potential wave as it is used in CV.

## 4.1 Square wave voltammetry

The electrochemical technique of SWV is derived from Barker's square wave polarography [241] and the Kalousek communicator [242], it employs a periodic square shaped potential function that is applied at a stationary electrode along with a staircase potential modulation [243]. The square shaped staircase potential is shown in Figure 4.8A. Two oppositely directed potential pulses are imposed at each step of the staircase. The pulses complete a potential cycle that is repeated at each step along the staircase. The potential pulses which have an odd serial number are assigned as forward pulses while those with an even serial number are considered reverse pulses. The electrode reaction takes place in both directions during a potential cycle which provides insight into the electrode mechanism [244, 245].

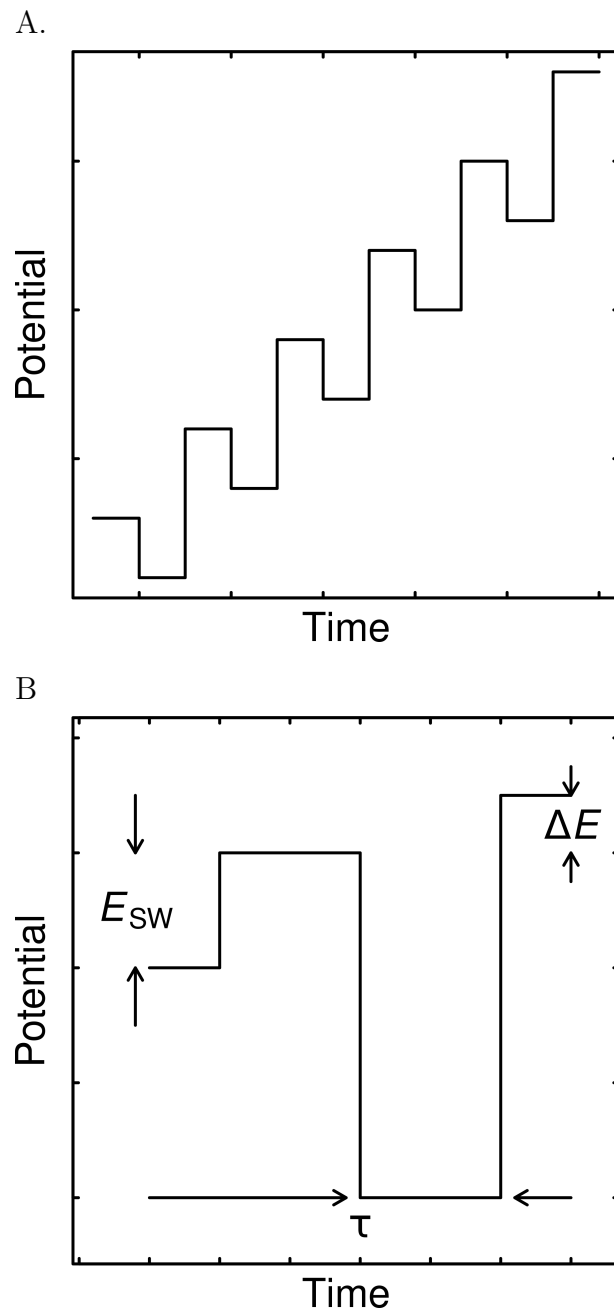


Figure 4.8: A. Example of the shape of the potential waveform of the staircase. B. Plot representing a single potential cycle that takes place at each step of the staircase ramp.

The scan rate can be defined as  $v = f\Delta E$  with  $\Delta E$  as the step of the staircase potential, this is also known as the pulse amplitude (Figure 4.8B). The duration of a single potential is defined as  $\tau$  (Figure 4.8B), the duration of a single potential pulse is  $t_p = \tau/2$  and the frequency ( $f$ ) is  $f = 1/\tau$ . Interpretation of the voltammetric signal can be performed based on  $t_p$ ,  $\tau$  or  $f$ .

## 4.2 Summary

The electrochemical measurement techniques that have been described in this chapter are used throughout this research focus on how the techniques are used to measure the key attributes of the sensors as well as being the mechanisms by which the sensors sense their target analytes.

CV and EIS are used during characterisation, OCP is used to detect pH changes by the DMSO-melanin pH sensor in Chapters 5, 6 and 7. SWV is used to detect the presence of microorganisms using the non functionalised electrode in Chapter 8. The next chapter describes the development, characterisation and initial testing of the screen printed pH sensor.



## Chapter 5

# Development and fabrication of a pH sensor utilising DMSO-melanin

### 5.1 Introduction

This chapter details the development of a pH sensor with the intention of developing applications for the sensor within biological environments. The motivation for this and a review of the existing pH sensors is presented in Chapter 2. Different approaches and materials were tested. The candidate pH sensors included a commercially available SPE where the working electrode had been coated with PANI (Dropsens 110PANI), a graphene device that had been deposited with aluminium oxide and in house produced using the SPEs that were described in Chapter 3. The chapter is arranged by first investigating different pH sensor candidates seeing whether they had appropriate sensitivity to pH as well as how consistent and stable the measurements were. Once the candidate that gave the best performance had

been established that material was taken forward for further analysis and characterisation (DMSO-melanin). The pH was determined by measuring the voltage of buffer solutions of a known pH via OCP using an ANA-POT potentiostat (Zimmer & Peacock). A calibration curve was produced using the mean signal vs pH that was measured over a 10 minute period to allow the signal to settle. While there are other pH sensors that exist that utilise other electrochemical techniques to measure pH such as CV [246] or SWV [247]. OCP was selected here because it allows for the signal to be measured in real time. This could lead to potential benefits in applications where the pH of a solution such as microbiological culturing where changes in pH can indicate contamination or indicate how much product has been produced in the case of a bioreactor. This could also be useful in clinical applications such as monitoring the wounds of patients for infection onset as higher pH levels of fluid from wounds is associated with infection risk therefore potentially providing an early warning sign of infection [248].

## 5.2 DMSO-melanin synthesis

The DMSO-melanin used to functionalise the working electrode was synthesised by PhD student João Vitor Paulin according to the following method [249]: 1.5g of DL-DOPA and 0.93g of benzoyl peroxide (Vetec, 75.0–80.0%) were combined in 200ml of DMSO (PA, Vetec, 99.9%). This mixture was kept at room temperature for 58 days whilst undergoing constant stirring. This took place in a flask with a reflux condenser attached. To purify the mixture the reaction solution was first concentrated to 25% of the initial volume after which 150ml of acetonitrile (Synth, 99.5%) was added to it. This combined solution was left to stand for two days before undergoing centrifugation.

gation at 2500 rpm for 15 minutes. The precipitate was collected and dried at 90°C for two days.

### **5.2.1 Application of DMSO-melanin to working electrode**

The DMSO-melanin pH sensor consisted of an SPE that was fabricated in house as described in Chapter 3. Sensitivity to pH was achieved by coating the working electrode with DMSO-melanin. A thin film of DMSO-melanin was applied to the working electrode of the SPE via a two step process. For the first step the electrode was spin coated at 1000 rpm for 60 seconds followed by a second step of 4000 rpm for 30 seconds using a Laurell WS-650MZ-8NPP Spin Coater. During this process the working and reference electrodes were protected by covering them with kapton tape in order to prevent them from also being coated with the DMSO-melanin. The coating integrity of the DMSO-melanin on the graphene/carbon working electrode was explored and is discussed later in this chapter in Sections 5.6.4 and 5.6.5.

## **5.3 Response of sensors to reference buffer solutions**

In this initial test for pH sensitivity the DMSO-melanin, PANI and  $\text{Al}_2\text{O}_3$  pH sensors were first exposed to pH4 reference buffer solution followed by pH7 and pH10 (HANNA Instruments, HI-7004L, HI-7007L, HI-7010L) for 10 minute periods while the OCP was recorded. The initial testing of the candidate sensors with these buffer solutions showed a clear distinction between the voltage that was measured and the pH of the solution with lower voltages

correlating with higher pH levels in the case of all of the sensors implying that they all likely had some degree of pH sensitivity (Figures 5.1, 5.2, 5.3 for PANI,  $\text{Al}_2\text{O}_3$  and DMSO-melanin respectively).

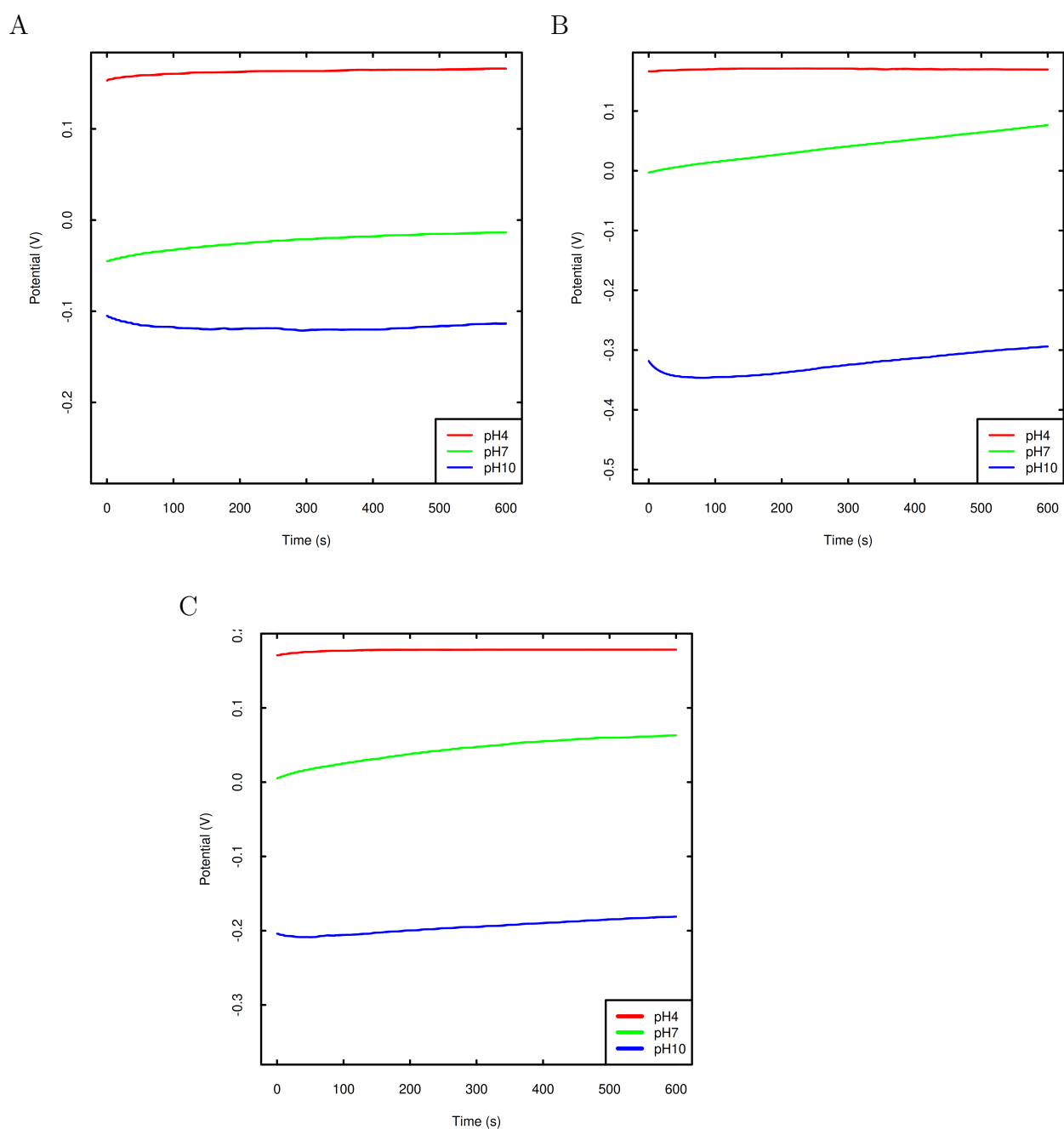


Figure 5.1: Potential measured using the PANI coated electrodes over a 10 minute period in reference buffer solutions of known pH where red = pH4, green = pH4 and blue = pH10. A, B and C are replicates. While the signal that is measured appears to be stable across the replicates there is variability between them.

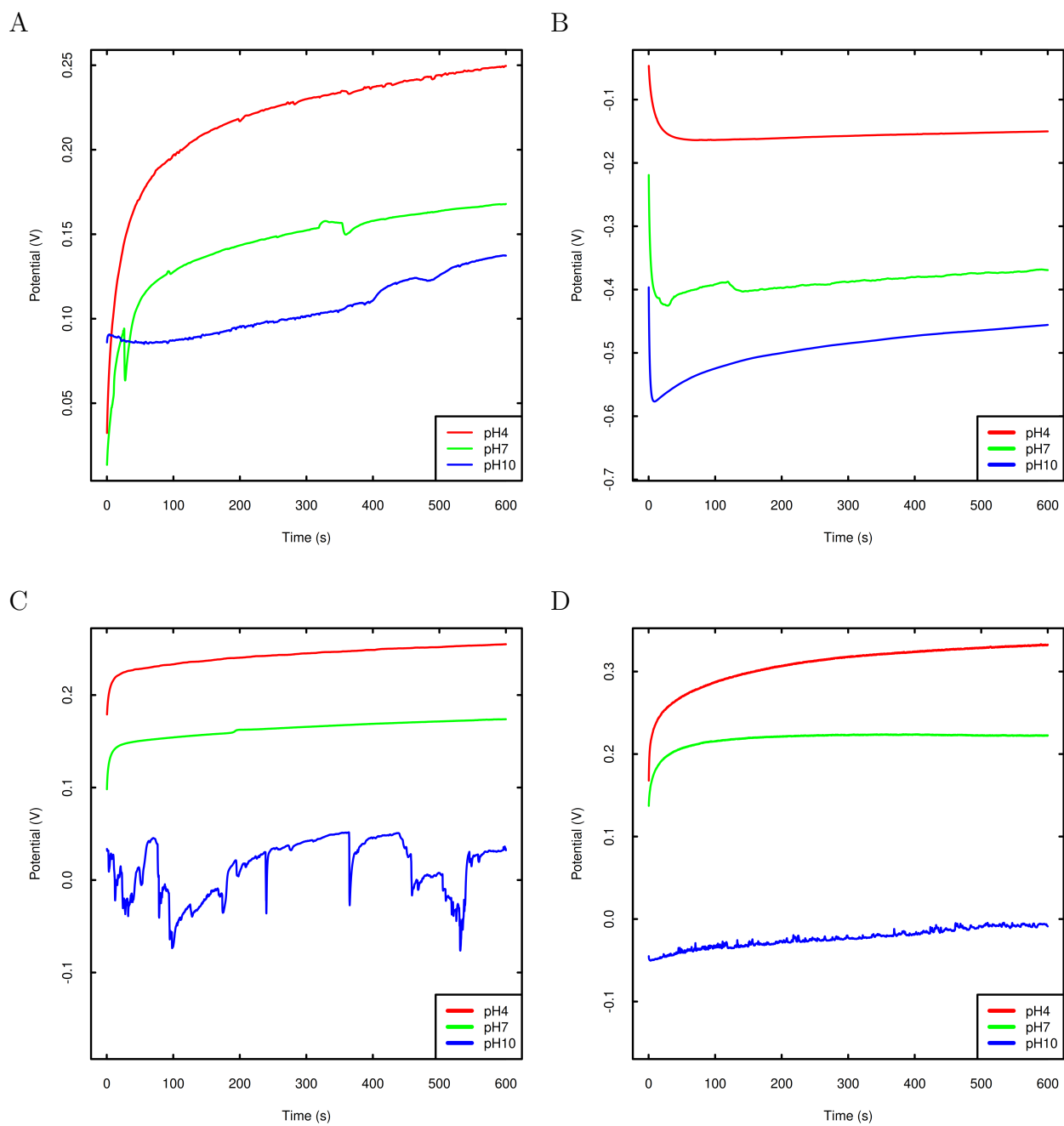


Figure 5.2: Potential measured using  $\text{Al}_2\text{O}_3$  coated sensors in solutions of known pH for 10 minutes. Red = pH4, green = pH7 and blue = pH10. A, B, C and D are replicates.

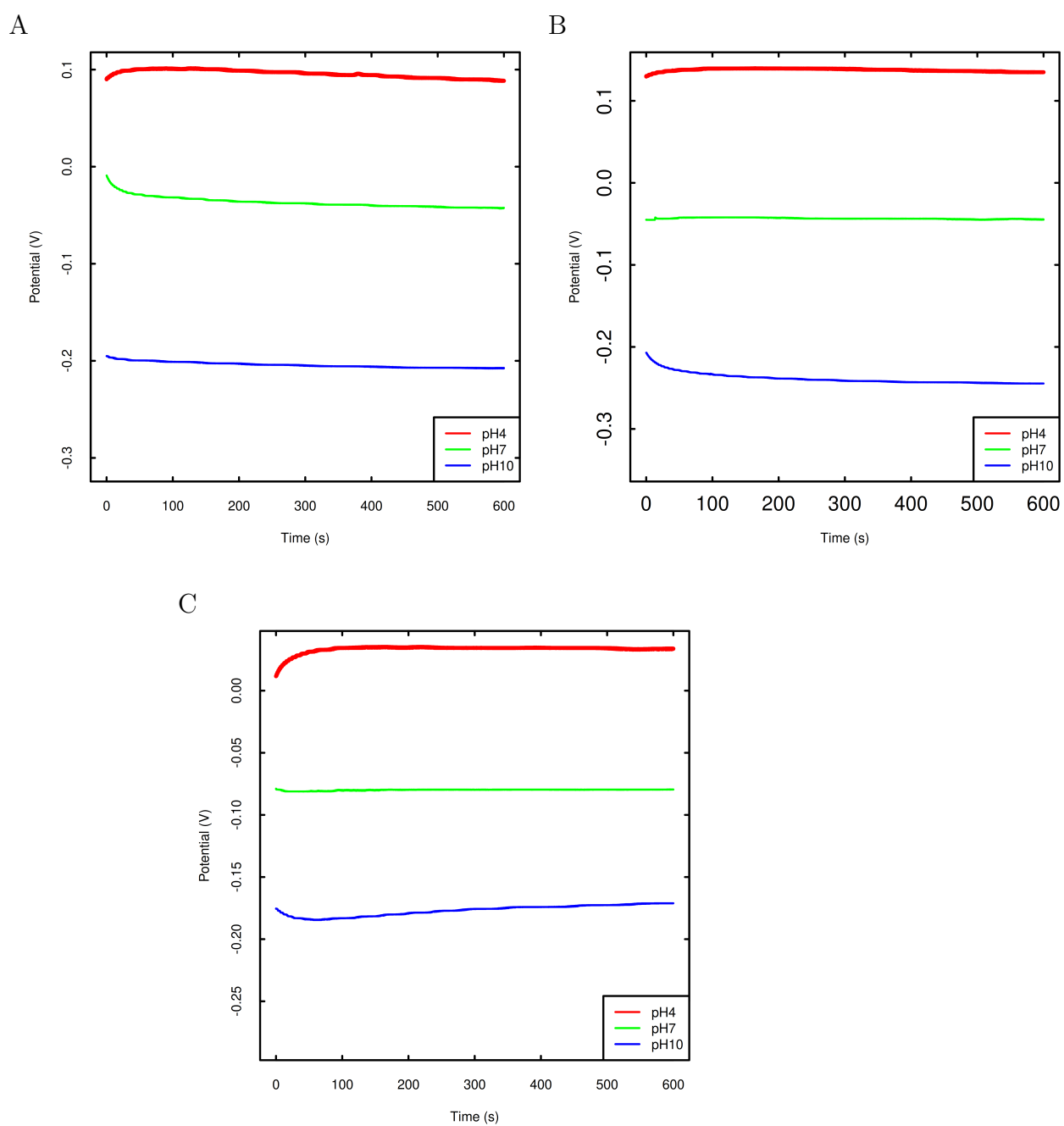


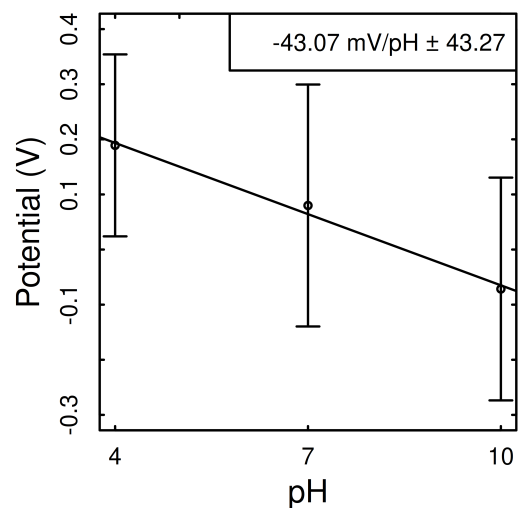
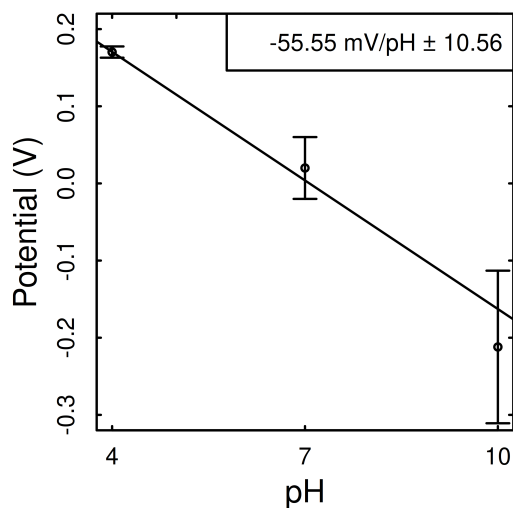
Figure 5.3: Potential voltage measured using DMSO-melanin coated sensors in solutions of known pH for 10 minutes. Red = pH4, green = pH7 and blue = pH10. A, B, and C are replicates.

The raw data signal presented in Figures 5.1, 5.2 and 5.3 has been summarised in Figure 5.4 in order to show the average, standard error and the slope of how the pH of the solution relates to the signal that was measured by the sensor. The PANI sensor appeared to be less consistent at higher pH levels (Figure 5.4A). The DMSO-melanin sensors also appeared to perform well with a slightly lower sensitivity than the PANI sensors but they also had less error and performed more consistently at higher pH levels (Figure 5.4B). Aluminium oxide did display some pH sensitivity as there was a noticeable drop in the voltage recorded as the sensor was exposed to reference buffer solutions of increasing pH (Figure 5.2) however the voltage to pH relationship was not consistent between different sensors (Figure 5.4C). The  $\text{Al}_3\text{O}_2$  based sensors however were less stable and more variable, although a linear relationship between the signal and pH was observed, it was inconsistent and much less stable than in the case of both the DMSO-melanin and PANI based sensors. Therefore the  $\text{Al}_3\text{O}_2$  sensor was excluded from further testing and the DMSO-melanin and PANI sensors were taken forward to assess whether they could recover after being exposed to solutions of different extreme pH ranges in order to assess whether they are suitable for multiple uses. It is important to determine this as whether the sensor is limited to a single use impacts upon the type of real world applications where it may be useful.



PANI

$\text{Al}_2\text{O}_3$



DMSO-melanin

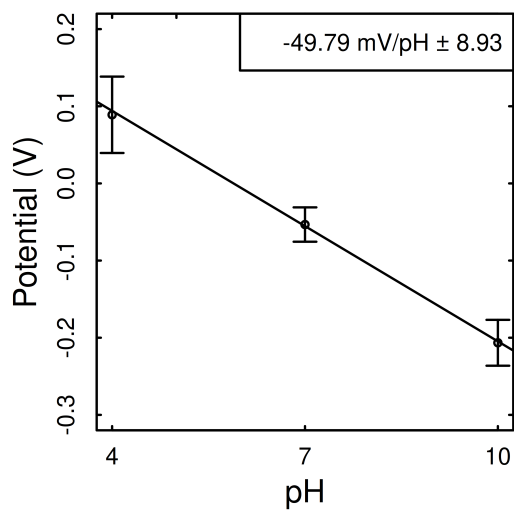


Figure 5.4: The mean signal that was measured using the sensors over a 10 minute period in reference buffer solutions at known pH levels (pH4, pH7 and pH10). PANI (n=3),  $\text{Al}_2\text{O}_3$  (n=4), DMSO-melanin (n=3). Error bars represent the standard error times 1.96.

## 5.4 Sensor recovery and reusability

The ability for the sensor to recover from exposure to different pH levels can impact its usefulness in applications. Here recovery refers to whether the sensor is still sensitive to pH after it has been exposed to different pH levels. For example the sensors have already shown that they are sensitive to pH10 after being exposed to pH4 and pH7 during the initial sensitivity testing but it is unknown whether they remain sensitive to low pH solutions after being exposed to pH10. That is what is investigated here.

The signal that was measured using the sensors that utilised DMSO-melanin or PANI as their pH sensitive functional layer had a clear linear relationship with the pH of the buffer solution that the sensor was exposed to. The signal also appeared to be stable in both cases.

How the sensors recovered following exposure to extreme pH was assessed by exposing each sensor first to pH4 buffer solution and recording the potential over a 10 minute period. Following this the sensor was rinsed with DI water and the process was repeated with pH7 and pH10 reference buffer solutions. Once this sequence had been completed it continued in reverse by exposing the sensor to pH7 buffer and finally pH4 buffer (Figure 5.5). The PANI sensors remained sensitive to pH as they were exposed to solutions of increasing pH but they lost sensitivity after pH10 exposure and the potential measured was far lower while exposed to the pH4 and pH7 buffers than it had been on the initial measurements in these solutions. The DMSO-melanin based sensor recovered after being exposed to each buffer solution and did not appear to degrade in the same way that the PANI based sensor did. These results therefore indicate that while both sensors show strong sensitivity to pH the DMSO-melanin sensor is more recoverable and has the potential be used more than once. This advantage makes the DMSO-melanin sensor more

versatile for use in real world applications so therefore this sensor was taken forward for further development and characterisation.

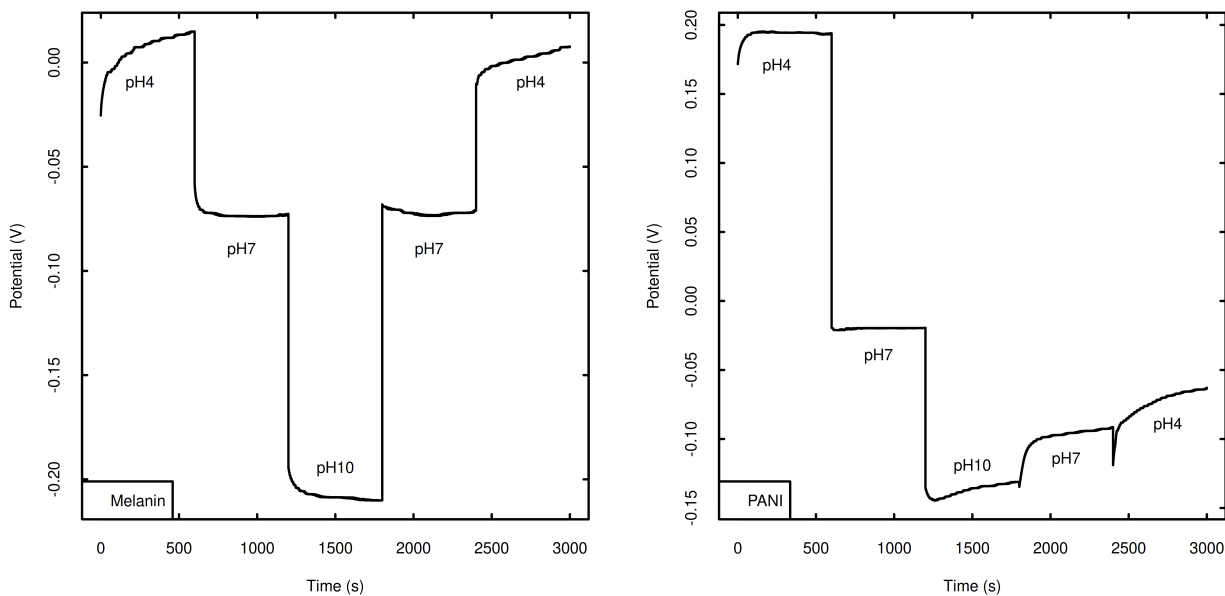


Figure 5.5: Potential recorded using both DMSO-melanin (left) and PANI (right) functionalised sensors in buffer solutions of known pH. While both types of sensor showed a strong sensitivity to pH as they were exposed to buffers of increasing pH, the PANI based sensor was unable to recover after being exposed to a high pH buffer.

## 5.5 Comparison with pH sensors reported in the literature

The sensitivity of the DMSO-melanin based screen printed pH sensor presented in this work of  $-49.79 \pm 8.93 \text{ mV/pH}$  with a drift of 5.9mv over 10 minutes (Figure 5.4C) over a range of pH4 to pH10 and  $-63 \pm 4.79 \text{ mV/pH}$  (Figure 6.4) over pH levels between 5 and 8 is superior to the pH sensors

reviewed in Table 5.1 with the exception of the three dimensional graphene on copper foam sensor that is described by [81]. However while this sensor is highly sensitive it is fabricated via a process that is far more elaborate than the simple screen printing and spin coating fabrication process that is used to produce the DMSO-melanin pH sensors and it requires multiple steps using cleanroom techniques and specialist equipment. Another sensor which showed promise was a PANI based screen printed sensor reported by [77] which was tested for biocompatibility with eukaryotic cells however this pH sensor was not tested for the prolonged periods of time that are required for applications that involve the continuous monitoring of microbial culturing. Based on the observations carried out during this research there are potential concerns whether that sensor would be stable for 24 hours as palette paper is used as the substrate so whether this is able to maintain structural integrity while submerged would need to be assessed. As the DMSO-melanin pH sensors use polyethylene (PET) as a substrate which is more flexible and durable than palette paper these sensors are better suited for applications that require longer periods of measurements being taken.

Table 5.1: pH sensors that have been reported in the literature, along with the pH range of solutions that they have each been tested with along with their observed sensitivity.

Sensor material	Reported sensitivity	Range (pH)	Reference
IrO <sub>2</sub>	-51.1mV/pH	1.5-12	[76]
SM <sub>2</sub> O <sub>3</sub>	56.2mV/pH	2-12	[250]
C coated with PANI	-50mV/pH	4-10	[77]
RuO <sub>2</sub> -SnO <sub>2</sub>	56.5mV/pH	2-12	[78]
GO	31.8mV/pH	4-10	[80]
IrO <sub>2</sub> -RGO nanohybrid	-62mV/pH	2-12	[61]
3D graphene coated with HfO <sub>2</sub>	71±7mV/pH	3-9	[81]
RGO	40±5mV/pH	4-10	[82]
SnO <sub>2</sub>	56-58/mV/pH	2-12	[251]
DMSO-melanin	63±4.79mV/pH	5-8	This study

## 5.6 Characterisation studies

The methods and settings used to perform these characterisation studies are described in detail in Chapter 3 where the in house SPE is characterised. Once the DMSO-melanin had been selected as the final material to take forwards for further development, the characteristics of the sensors were measured using a variety of experimental techniques that are described in Section 3.3. The purpose of such characterisation studies is to observe whether there are any differences in the characteristics of the sensor after

functionalisation with DMSO-melanin had been completed. Such differences provide evidence that the DMSO-melanin layer has been deposited successfully and may also provide additional insight into the mechanisms by which the sensor functions. For example an increase in contact resistance following functionalisation suggests that a layer of material has been applied to the surface of the electrode. Further investigation with FTIR and X-ray photoelectron spectroscopy (XPS) provides evidence that this layer of material is DMSO-melanin as the peaks within the spectra correspond to chemical bonds so the peaks can be compared to what is expected in DMSO-melanin. The surface of the electrode can also be characterised visually using SEM to see whether there are any optical differences in the electrode before and after functionalisation, AFM provides a three dimensional view of the surface topology. WLI and Raman spectroscopy allow the thickness of the deposited DMSO-melanin to be determined.

### **5.6.1 Contact resistance**

The contact resistance was measured by plotting current vs voltage as described in section 3.3.5, first on the blank working electrode after which DMSO-melanin was applied and the resistance was measured again. The resistance measured was higher in the sensors that had been functionalised with DMSO-melanin than the blank screen printed electrodes (Figures 5.6 and 5.7). The replicates were consistent within each individual sensor however there was some variation between different sensors and this variation increases following the application of DMSO-melanin. This could be due to how the DMSO-melanin is applied to the working electrode during the spin coating process and it may be possible to reduce or eliminate the variability by modifying the application process. However the sensitivity and reliability

of the sensors produced is sufficient for use in culturing applications as will be demonstrated in Chapter 6.

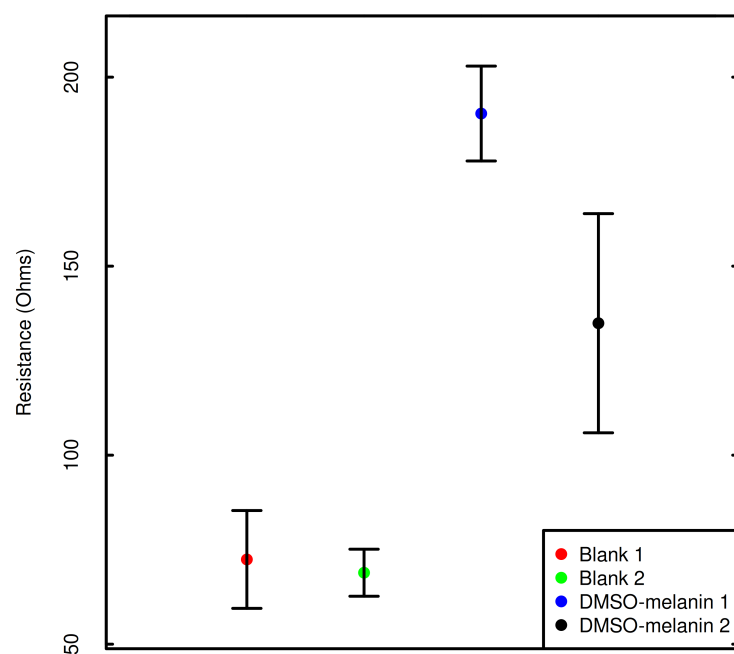


Figure 5.6: Average resistance that was measured with a two probe IV test (n=5).

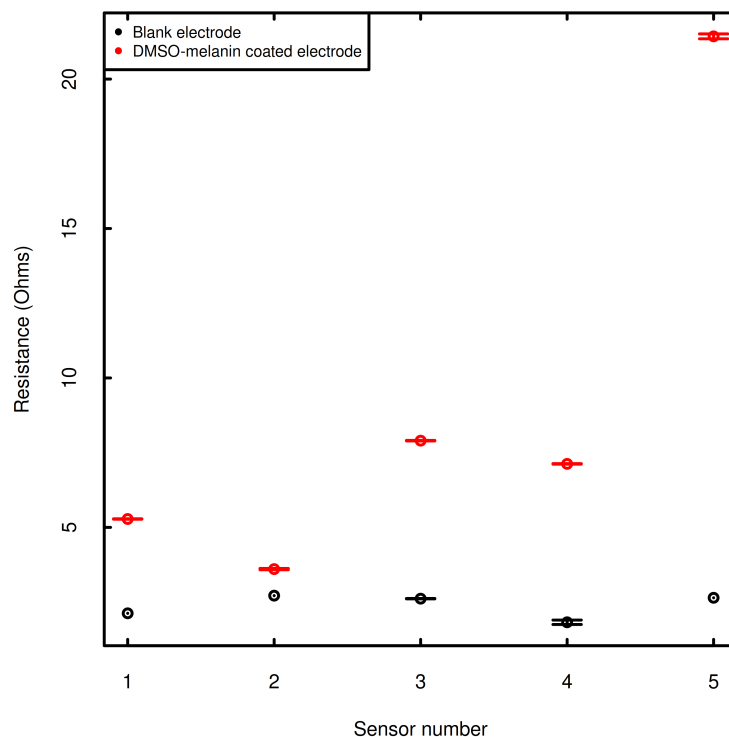


Figure 5.7: The resistance that was measured using four point IV testing for the working electrode surface of both a blank SPE and one that had been coated with DMSO-melanin. Five sensors were tested for both sets, and each sensor was tested five times with the probes in different positions on the electrode surface. The error bars represent the standard error times 1.96 of the resistance that was measured on each sensor ( $n=5$ ). The distance between the probes was kept constant between measurements.

### 5.6.2 Raman spectroscopy

Raman spectroscopy was carried out using a Renishaw inVia system using a 532nm laser both before and after the DMSO-melanin had been applied to the graphene working electrode. The intensity of the D-peak ( $1350\text{cm}^{-1}$ ) increases following the application of DMSO-melanin which is possibly due



to the presence of additional carbon on the electrode that is present in the melanin. The D-peak is only present in defected graphite and is not seen in pristine samples indicating that the working electrode contains materials other than graphite [252]. When additional carbon compounds are detected by the Raman system this results in an increased D-band signal [253]. This spectra suggests that the working electrode contains multiple layers of carbon due to the intensity ratio between the G peak and the 2D peak (Figure 5.8).

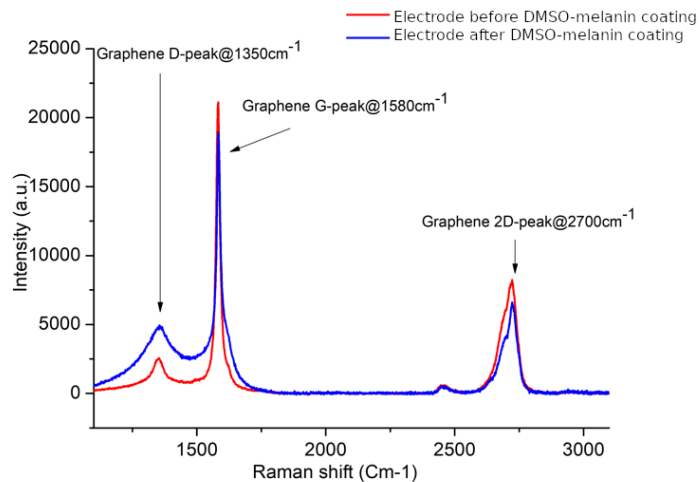


Figure 5.8: Raman spectra measured before (red) and after (blue) the graphene electrode had been coated with DMSO-melanin.

In the case of single layer graphene the intensity of the G peak is lower than that of the 2D peak and the reverse is the case in graphite (Figure 5.9). Raman spectra of 5 layers of graphene is indistinguishable from bulk graphite so it is not possible to determine how many layers of carbon the working electrode is composed of suggesting that the ink is primarily graphite.

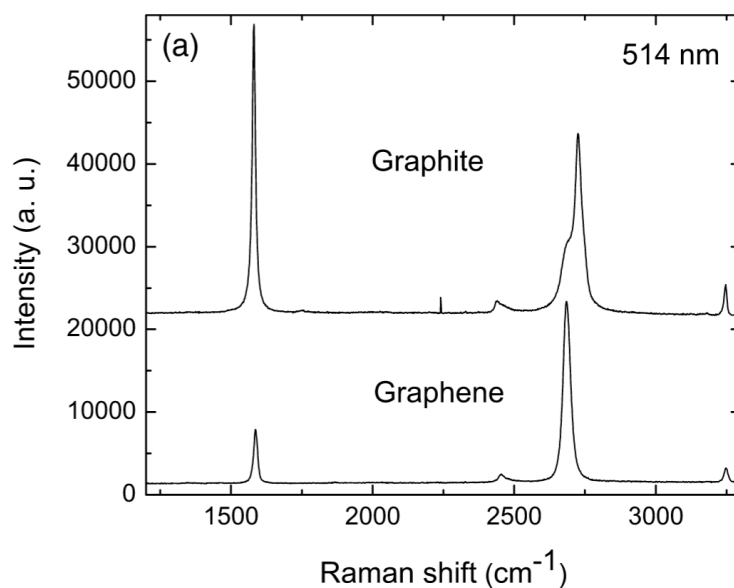


Figure 5.9: Raman spectra of bulk graphite and graphene [252].

### 5.6.3 Scanning electron microscopy

The method and settings used during SEM are described in Section 3.3.1.1. The surface morphology of the working electrode of the DMSO-melanin pH sensors was imaged using SEM. At lower magnifications the electrode surface appeared to be quite rough (Figure 5.10) WLI revealed that the roughness of the working electrode coated with DMSO-melanin is  $282.66 \pm 0.019$ .

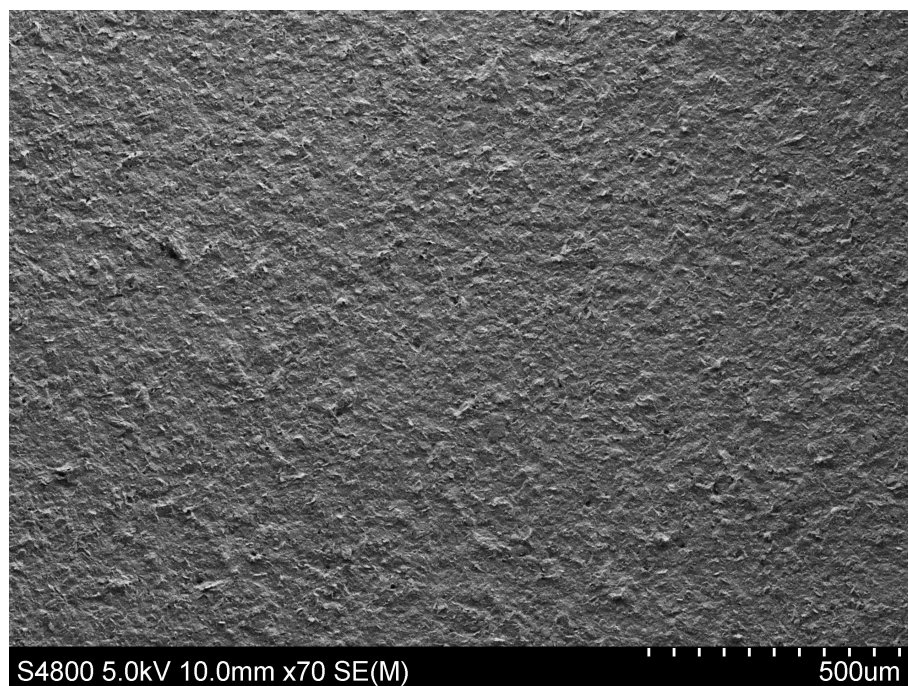
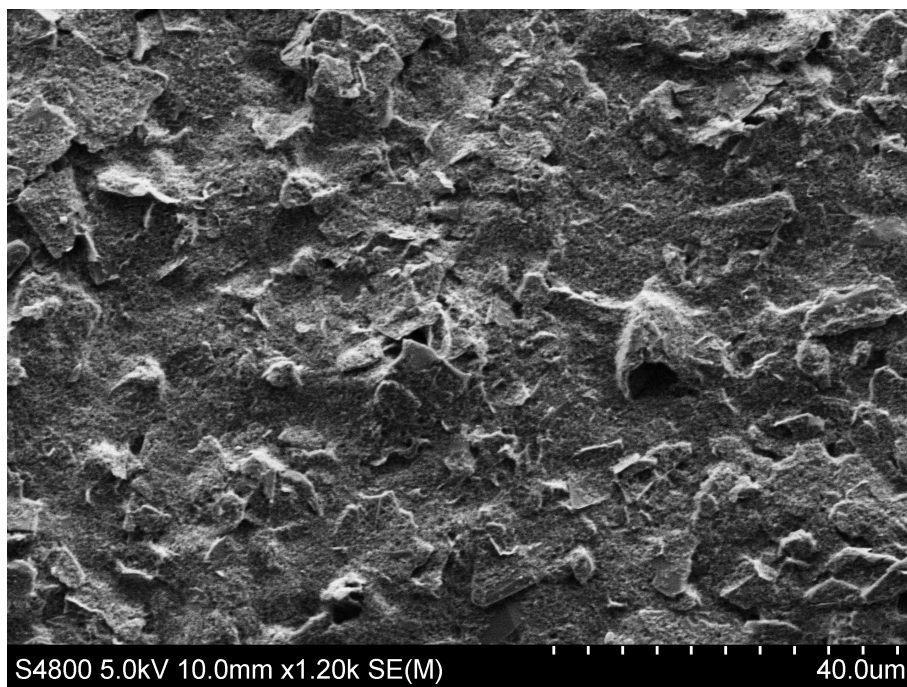


Figure 5.10: SEM image of the surface of the working electrode of a DMSO-melanin pH sensor, at this magnification the surface of the electrode appears relatively rough.

An increase in image magnification revealed that this roughness was a result of flake like structures that were present across the surface of the DMSO-melanin working electrode (Figures 5.11A and B). As the magnification was increased further there appeared to be two morphologically distinct structures within the working electrode, these included the larger flake like structures as described above and smaller structures that appeared as aggregates on the surface of the flakes (Figure 5.12). These structures are morphologically similar to previously published TEM and SEM images of carbon black (Figure 5.13A) with regards to the aggregates and graphite (Figure 5.13B) with regards to the flakes. Therefore it is possible that these structures (Figure 5.13C) are carbon black and graphite. The ink is described as

“carbon graphite ink” by the manufacturer however the exact formulation is unknown as it is proprietary. This description is consistent with what has been observed with the SEM as “carbon” may refer to the carbon black and “graphene” may refer to the observed flakes. The DMSO-melanin coating on the working electrode was not visible under SEM.

A



B

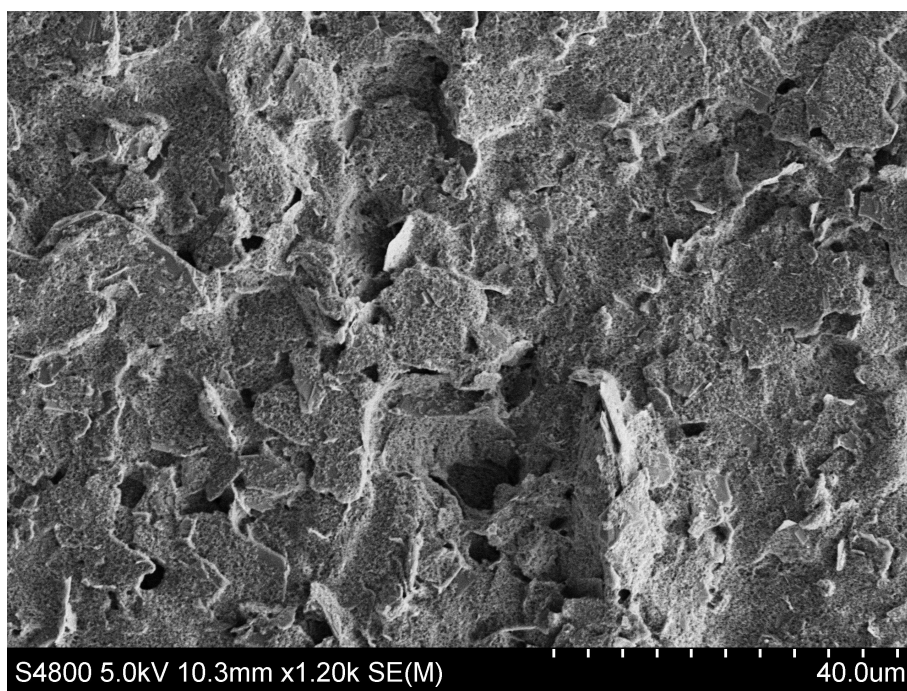


Figure 5.11: Higher magnification SEM images of the working electrode of a DMSO-melanin pH sensor. These images were taken at different positions on the surface of the working electrode showing that it is consistent.

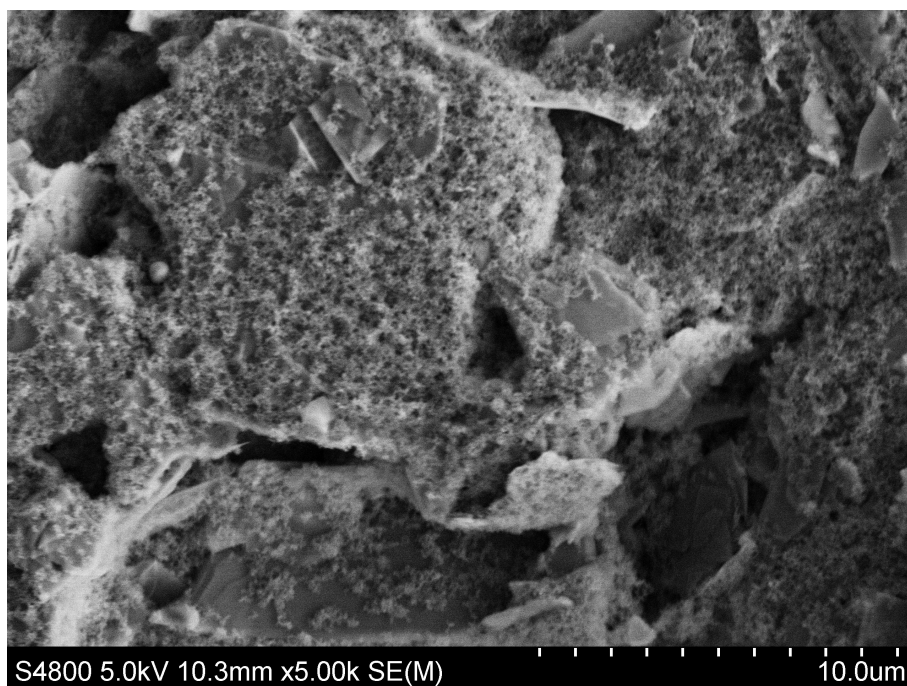


Figure 5.12: SEM at further magnifications reveal that the surface of the DMSO-melanin working electrode is not simply rough, there are two distinct surface morphologies here, graphite appears as smooth flakes of as well carbon black which appears as clumps. The DMSO-melanin is not visible under SEM.

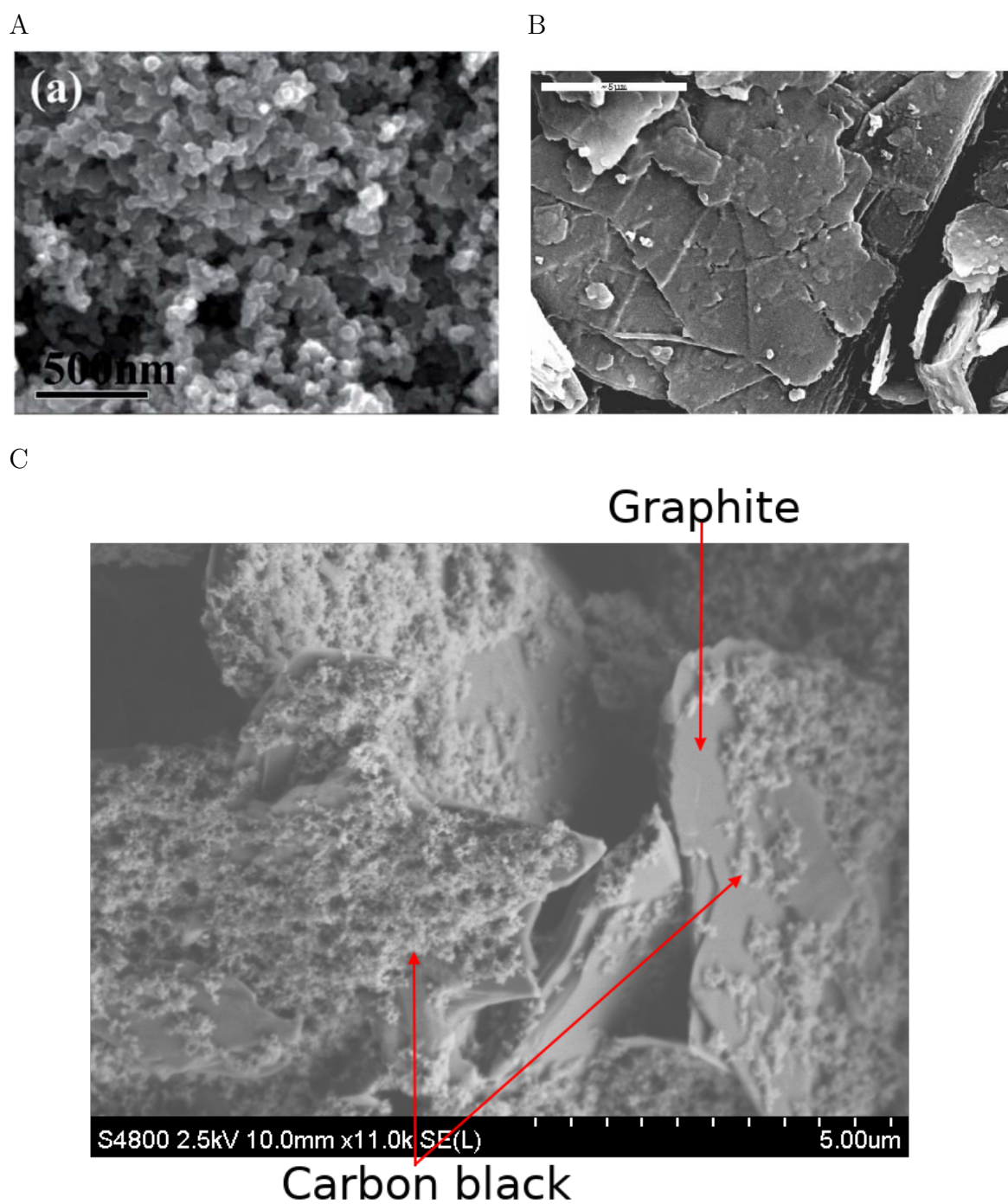


Figure 5.13: Comparison of SEM images of carbon black from [254] (A), graphite [255] (B) and the working electrode of a DMSO-melanin pH sensor (C) [256]. The SEM image of the DMSO-melanin pH sensor appears to contain both carbon black and graphite/graphene fragments however the DMSO-melanin itself is not visible under SEM.

#### 5.6.4 X-ray photoelectron spectroscopy

XPS is a useful characterisation tool for the surface analysis of the electrode as it is able to identify both chemical and elemental characteristics including bond types and functional groups [257, 258]. This is particularly useful in comparing an electrode before and after functionalisation has been carried out in order to assess whether the surface composition of the electrode has changed in line with what is expected. XPS measurements were taken with a monochromatic Al K $\alpha$  X-Ray source, with an emission current of 15 mA using a with a Kratos Axis Supra XPS system.

XPS was used to characterise the surface of the working electrode before and after DMSO-melanin deposition (Figure 5.14). The procedure is described in more detail in Section 5.6.4.



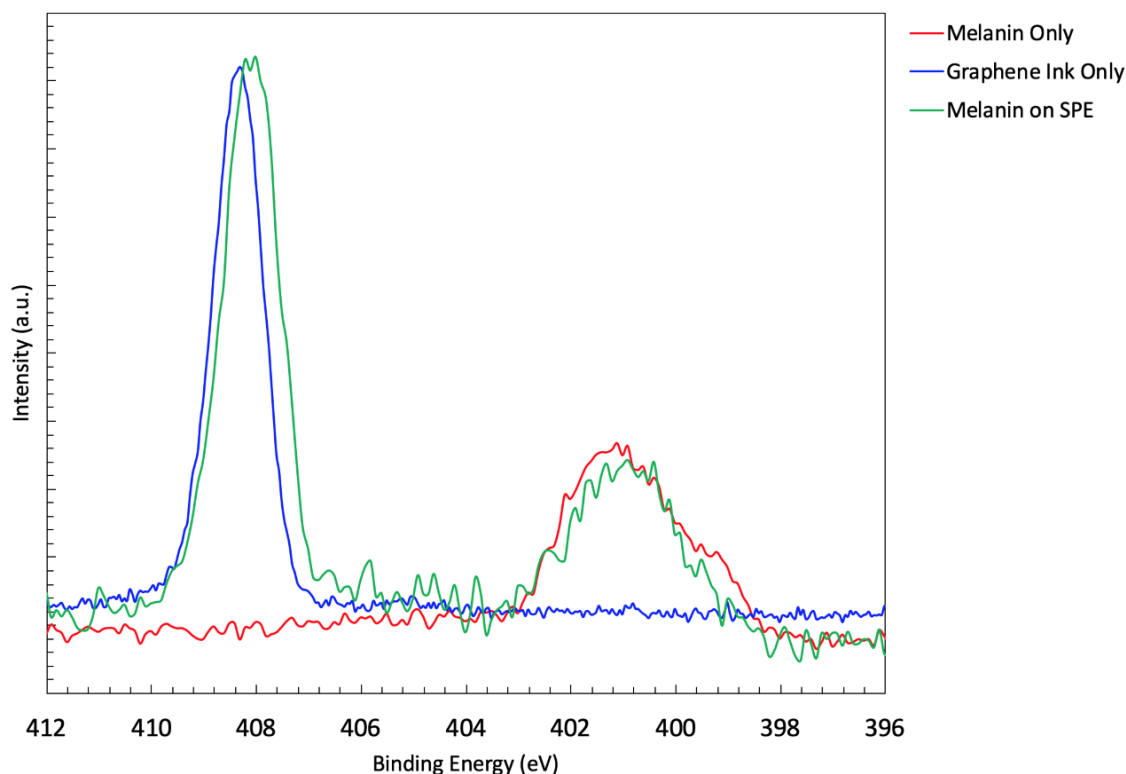


Figure 5.14: XPS spectra where the DMSO-melanin coated electrode contains peaks that match with both DMSO-melanin alone and an uncoated electrode indicating that the DMSO-melanin coat has been successfully applied to the working electrode of the pH sensor. The melanin ink is shown in red, the carbon/graphene electrode is shown in blue and the carbon/graphene electrode coated in DMSO-melanin is shown in green.

### 5.6.5 Fourier-transform infrared spectroscopy

FTIR was used to characterise the elements and bonds on the working electrodes of the sensors, this technique is described in more detail in Section 3.3.4. The FTIR spectra (Figure 5.16) contained peaks that correspond with the presence of elements and bonds that are within the structure of DMSO-melanin (Figure 5.15).

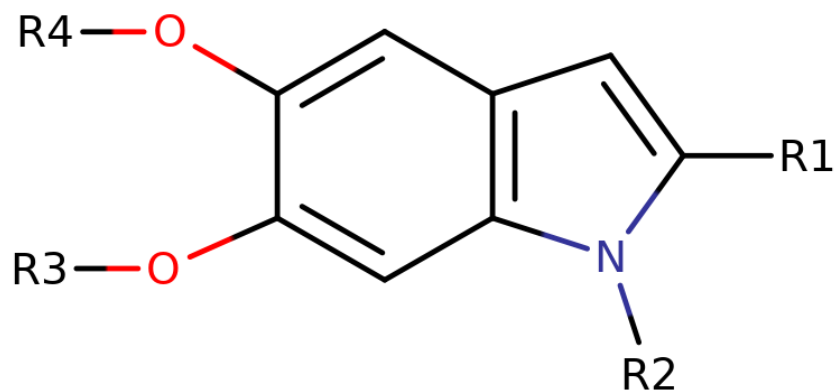


Figure 5.15: Basic monomer proposed for DMSO-melanin, R1 = H or COOH, R2 = H or SO<sub>2</sub>CH<sub>3</sub>, R3 = H or SO<sub>2</sub>CH<sub>3</sub>, R4 = H or SO<sub>2</sub>CH<sub>3</sub>. Image produced using MarvinJS.

These peaks were absent on the unfunctionalised working electrode. This suggests that the spin coating process has been successful in coating the working electrode with DMSO-melanin.

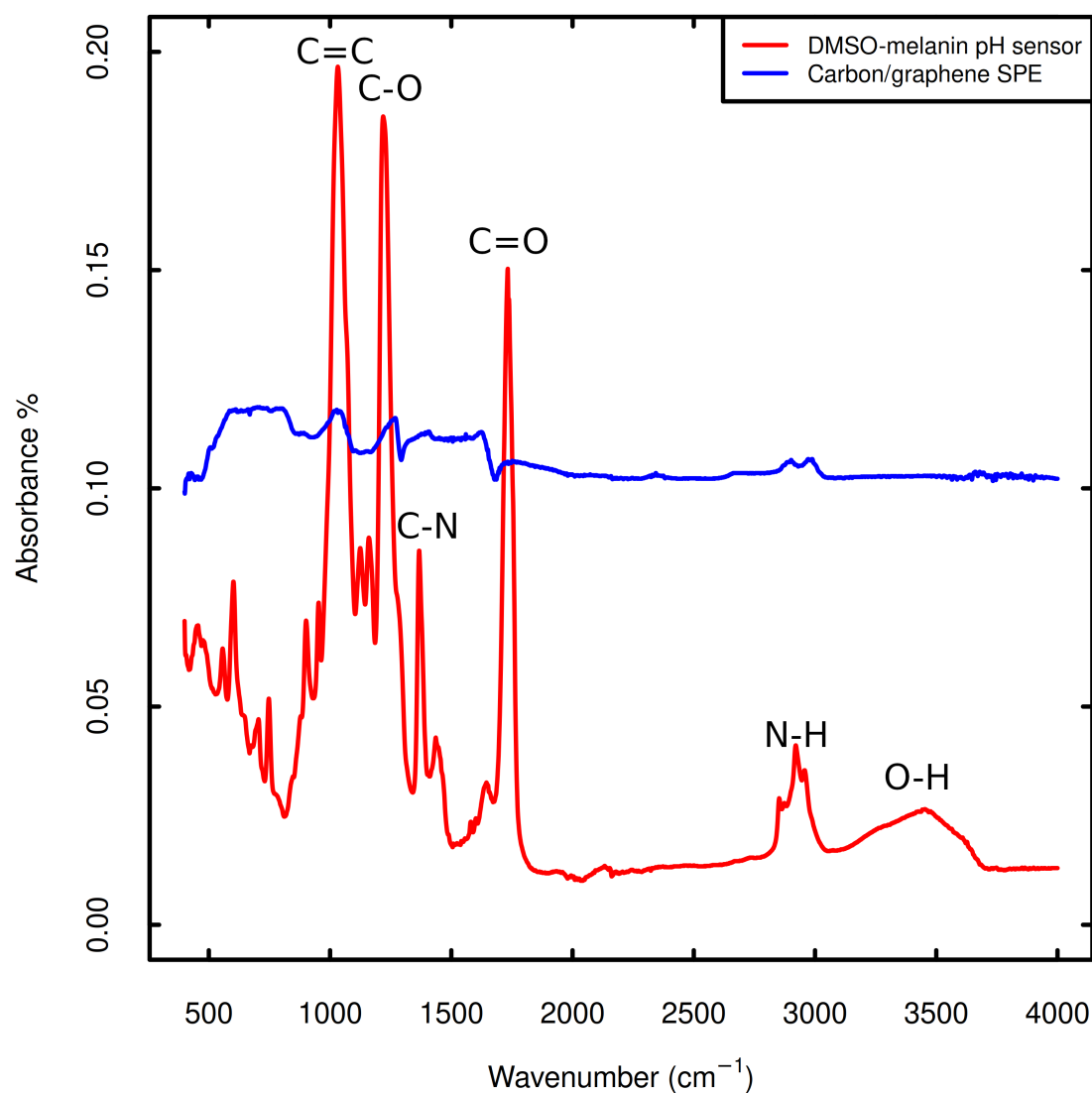


Figure 5.16: Annotated FTIR spectra of a working electrode that had been coated with DMSO-melanin and an electrode that had not. Clear differences in the spectra are present with the presence of additional peaks in the spectra from the melanin coated electrode that are consistent with the elemental bonds that are present in the proposed structure of DMSO-melanin, with the addition of a C=O bond.

### **5.6.6 Atomic force microscopy**

AFM consists of a cantilever that has a sharp tip. The surface of the sample is measured based on the forces that are between this tip and the surface. As a well established technique the principles of AFM have been documented previously [259]. AFM is another technique that is used to characterise the surface morphology of the electrode. The particular advantage that AFM offers over other characterisation techniques is it's ability to measure the three dimensional morphology of the electrode. AFM is therefore useful in understanding what the surface area of the electrode is taking into account the three dimensional structure.

#### **5.6.6.1 AFM settings**

AFM was performed using a tip radius of resonant frequency of 320 kHz, a spring constant of 40 N/m and a 8 nm tip radius. The instrument used was a JPK NanoWizards II (Dimension-3100 Multimode, Bruker, Billerica, MA, USA).

#### **5.6.6.2 AFM results**

The surface of the working electrode was analysed using AFM to examine the surface roughness before and after DMSO-melanin deposition (Figure 5.17). Following the deposition of DMSO-melanin onto the electrode surface the root mean square of the roughness increases from 102.1nm to 292.5nm. The dimension of DMSO-melanin particles ranges between 5nm to 200nm [134]. An increase in roughness results in an increased surface area on the electrode surface which allows for more electrochemical reactions to take place which should lead to better sensitivity [260].

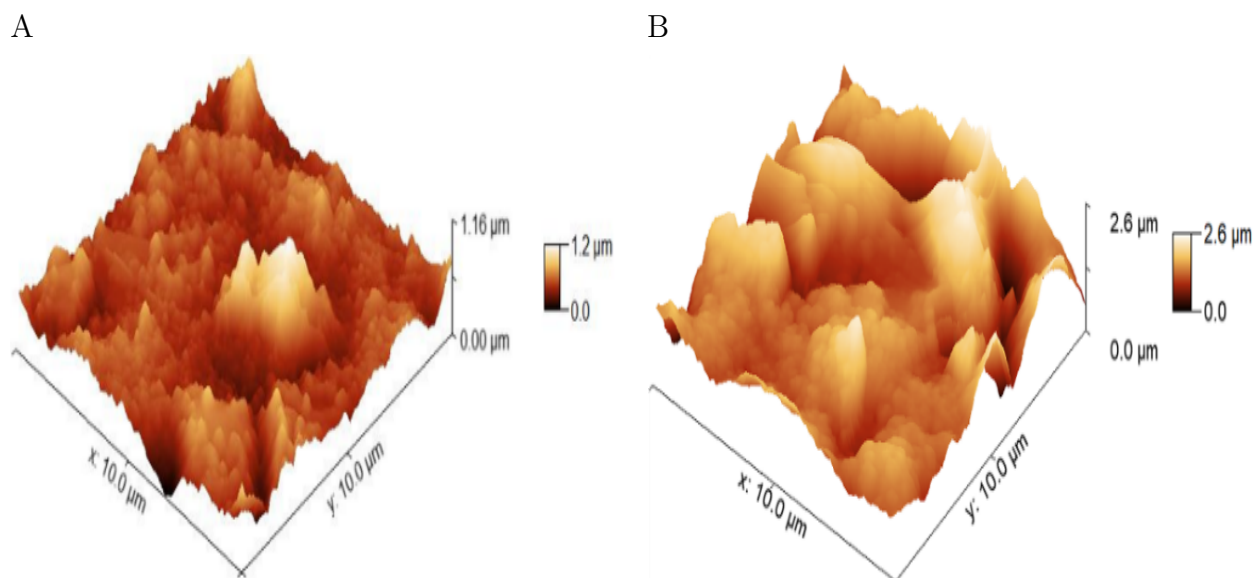


Figure 5.17: (A) Morphology of the surface of the working electrode before and after (B) the layer of DMSO-melanin has been applied.

### 5.6.7 Thickness and roughness of the DMSO-melanin pH sensor

The thickness and roughness of the DMSO-melanin pH sensor was measured using WLI using the settings shown in Chapter 3.3.2.2. The thickness of the DMSO-melanin was  $0.268 \pm 0.03$  and the roughness was  $282.66 \pm 0.019$ .

## 5.7 Discussion

The various candidate materials for a pH sensor all showed some degree of pH sensitivity however depositing DMSO-melanin on the working electrode of a SPE that had been produced in house appeared to generate the most reliable signal that correlated with changes in pH of a solution. The DMSO-melanin pH sensor also had advantages associated with being produced in house as

this allowed for the SPEs to be mass produced easily at a lower cost than relying on SPEs that had been purchased from an external manufacturer. Characterisation studies revealed that the functionalisation of the working electrode via spin coating with DMSO-melanin was associated with an increased surface resistance of the working electrode as well as an increase in the variation of the resistance that was measured between different sensors suggesting that the spin coating process may not be as reproducible as screen printing which may be an area for future optimisation. WLI and AFM show that the layer of DMSO-melanin is thin while XPS and FTIR spectra show evidence that the layer of DMSO-melanin has successfully adhered to the working electrode surface as in the case of XPS both the peak associated with the carbon working electrode and the DMSO-melanin peak are only present in the spectra that was measured from the functionalised working electrode. FTIR spectra contained peaks that are associated with chemical bonds that are present within the structure of DMSO-melanin providing further evidence that the surface of the working electrode has been modified as intended.

## 5.8 Summary

In this chapter a novel working pH sensor has been produced and characterised that consists of a screen printed electrode containing a silver reference electrode and carbon/graphene counter and working electrodes where the pH sensitivity is achieved by functionalising the working electrode by applying a thin layer of DMSO-melanin. The DMSO-melanin pH sensor has demonstrated that is able to effectively measure the pH of reference buffer solutions in a manner that is repeatable and stable over a 10 minute period. This

suggests that this sensor may be useful in applications where pH measurement is necessary. Such applications include biological applications such as monitoring the pH of solutions of culture media where the pH is important for optimal productivity and where changes in pH may also indicate contamination. Such sensors may also be useful in clinical applications as well and the feasibility of such applications is investigated over the next chapters. A microfluidic sample delivery system that covers the working electrode protecting it from damage whilst using capillary flow to deliver the sample to the working electrode, is presented in Appendix A.

## Chapter 6

# Suitability of the DMSO-melanin pH sensor for pH monitoring of bacterial cultures

### 6.1 Introduction

The development and functionality of the DMSO-melanin pH sensor has been outlined in Chapter 5 however there it was only so far demonstrated to work successfully in reference buffer solutions of known pH values. The sensor has been demonstrated to be particularly accurate in the range of pH5 to pH8. This range covers pH levels that allow for optimal growth of a number of different bacteria [261, 140]. Examples of different microbial species and their optimal pH requirements for culturing are shown in Table 6.1.

As the bacterial cells in culturing media replicate, various metabolites are produced that may alter the pH of the surrounding environment [262]. The



internal pH of bacterial cells is close to neutral and this must remain consistent in order for the maintenance of metabolic capacity and cellular integrity [263]. As the bacteria grow the pH of the media changes over time however how the pH changes depends upon the source of carbon in the media and the species of bacteria that is being cultured [264].

Table 6.1: Various species of microorganisms and the pH level that is optimal for culturing.

Microorganism	Optimal pH	Reference
<i>E. coli</i>	7.3	[265]
<i>S. cerevisiae</i>	4-6	[266]
<i>L. casei</i>	6.5	[267]
<i>S. thermophilus</i>	6.5	[268]
<i>L. bulgaricus</i>	5.8-6	[269]
<i>L. lactis</i>	6.3-6.9	[270]
<i>T. aquaticus</i>	7.5-7.8	[271]

Hydrogen transfer is a fundamental feature of biological metabolic processes. An example of this is the metabolism of glucose generating  $\text{NADPH} + \text{H}^+$  due to oxidation by glucose-6-phosphate [272]. The Entner-Doudoroff pathway is an important metabolic pathway in bacteria that is involved with facilitating the metabolism of glucose. Two steps of this pathway result in the release of hydrogen ions as shown in Figures 6.1 and 6.2. In addition to glucose, bacterial culturing media contains additional sources of hydrogen including tryptone and peptone which are derivatives of the protein casein.

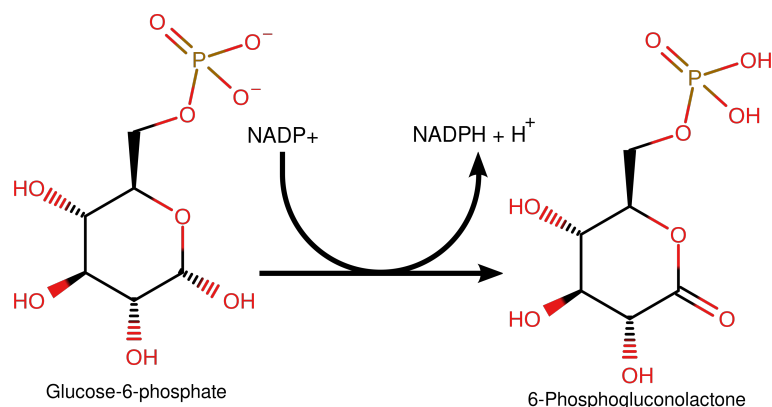


Figure 6.1: The conversion of glucose-6-phosphate to 6-phosphogluconolactone in the Entner–Doudoroff pathway - an important metabolic pathway for bacteria for the metabolism of glucose.

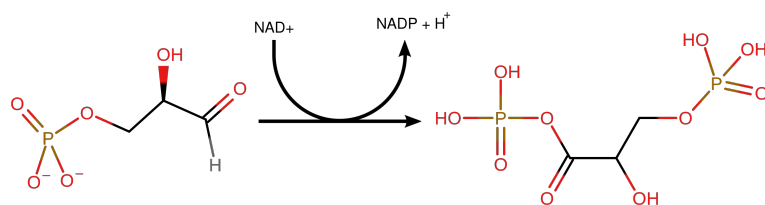


Figure 6.2: Another step in the Entner-Doudoroff pathway where  $\text{H}^+$  is released is during the conversion of glyceraldehyde 3-phosphate to 1,3-Bisphosphoglyceric acid.

## 6.2 Methods

The pH sensors used were functionalised with DMSO-melanin and were produced as described in Chapter 5. Three commonly used formulations of culturing media were selected for testing. These include LB (Sigma L3022-250G), brain heart infusion (BHI) (ThermoFisher CM1135B) and nutrient broth (NB) (Thermofisher CM0001B). These types of culturing media were selected because they are frequently used in molecular biology and microbiology and they are made of different components which allows for the deter-

mination of whether these different components impact upon the signal that is measured by the pH sensor. The components of these different culturing media are shown in Table 6.2. Each of the media used were prepared by first weighing out the mass according to the manufacturers instructions, after which distilled deionised water was added to the powder which was then thoroughly mixed by inversion and sterilised by using an autoclave. Four pH points were produced (pH5, pH6, pH7 and pH8) by modifying each of the media solutions using the pH4, pH7 and pH10 reference buffer solutions. This was achieved by measuring the pH of the culturing media with a standard glass electrode pH meter (Hanna Instruments pH20) and adding drops of the reference buffer solutions to the culturing media until the desired pH level had been reached. These pH levels were selected due to their relevance in optimal microbiological culturing as described in section 6.1. Solutions containing only reference buffers and no culturing media were also prepared at these same pH levels in order to compare just buffer solutions to the buffer and media mixture.

Table 6.2: The types of culturing media that were tested in this study and their components.

Media Type	Components (g/l)	Reference
Lysogeny broth	NaCl, tryptone, yeast extract, NaCl	[273, 274]
Brain heart infusion	Glucose, proteose, peptose, NaCl, Na <sub>2</sub> HPO <sub>4</sub> , brain and heart infusion solids	[275, 276]
Nutrient broth	"Lab-Lemco" powder, yeast extract, peptone, NaCl	[277]

## 6.3 Testing the DMSO-melanin pH sensors with media and bacteria

The pH of the culturing media was tested both with sterile media and with media that had been inoculated with *L. casei* bacteria that had been cultured until reaching the stationary phase of growth. This strain was selected because it is commonly available and is used within bioreactors [278, 279, 280]. More details with regards to lactic acid bacteria, their usefulness and how a pH sensor may be useful with regards to culturing them are described in Section 2.12.

### 6.3.1 Calibrating sterile media

Once the media solutions had been produced to the desired pH value as described in Table 6.2 measurements were carried out by OCP on the DMSO-melanin pH sensors while they were in contact with the solutions. The raw signal of these measurements is shown in Figure 6.3.

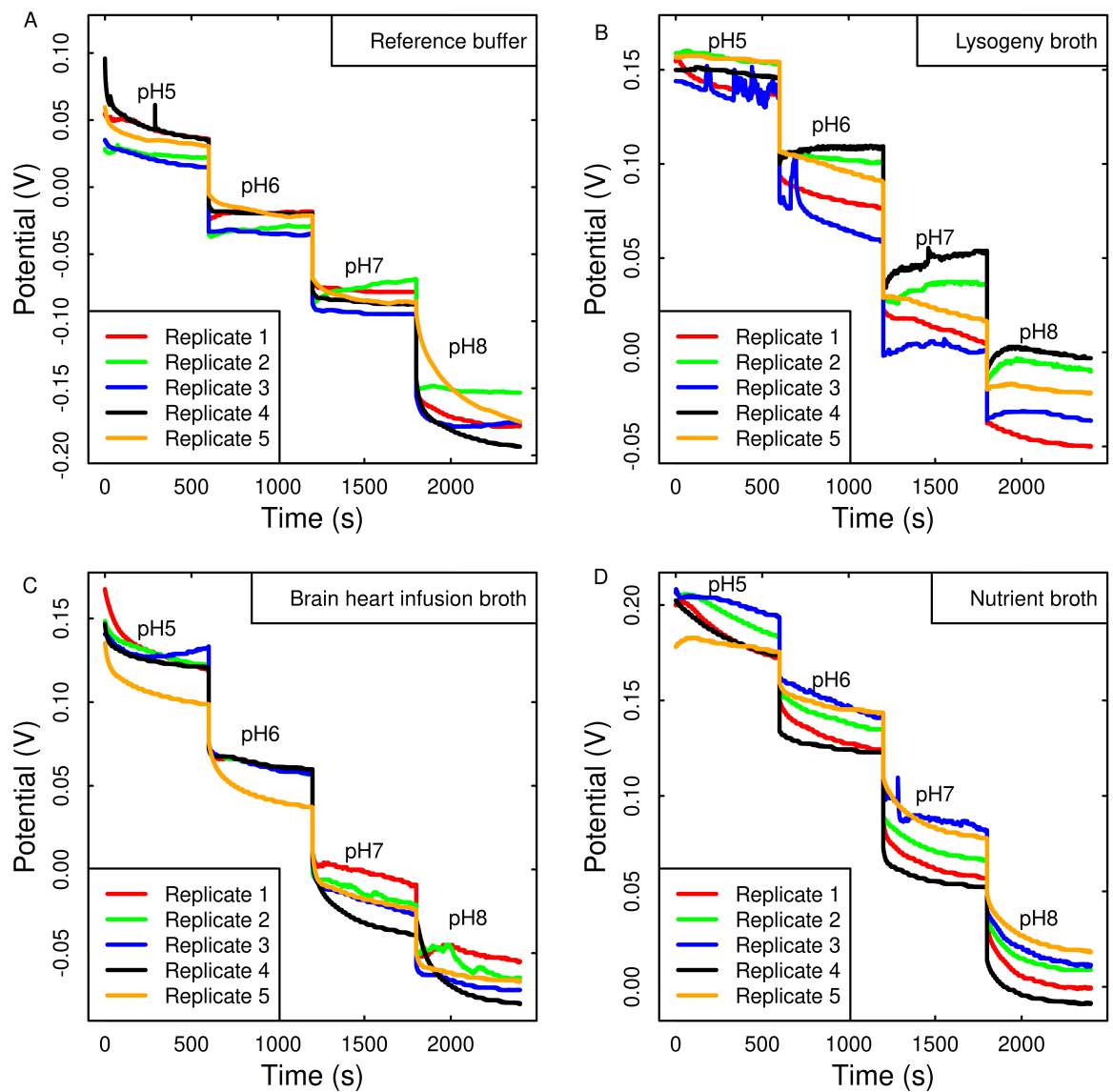


Figure 6.3: Voltage measured in the four different solutions tested with the DMSO melanin pH sensor. (A) reference buffer, (B) lysogeny broth, (C) brain heart infusion broth, (D) nutrient broth. In addition to measuring the stability of the signal, the mean value from these measurements was taken to produce a calibration curve that was used to estimate changes in pH to each media sample following bacterial inoculation.

This signal was processed to produce a standard curve which could then be used to predict the pH of an unknown solution of each media type (Figure 6.4).

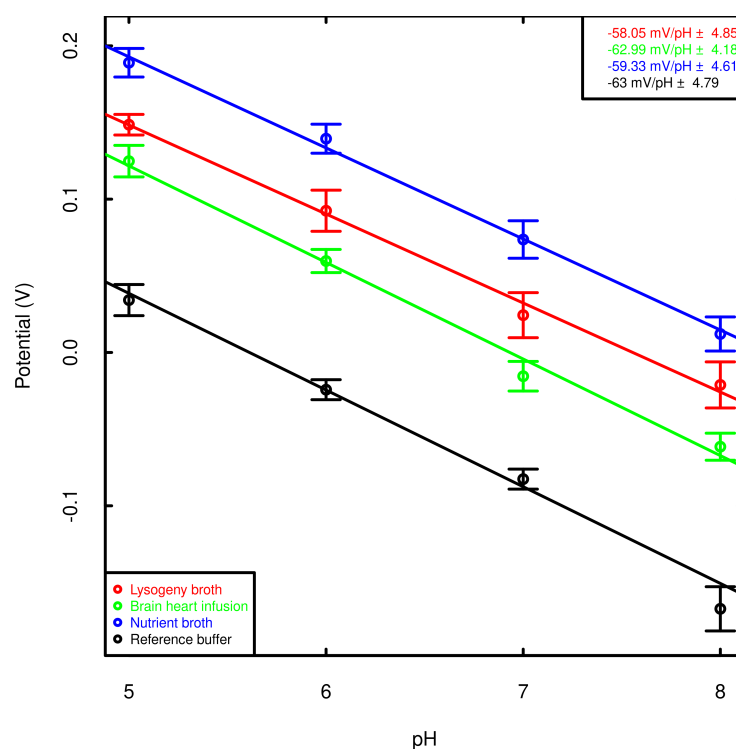


Figure 6.4: The slopes calculated from the data shown in Figure 6.3 showing the relationship between the pH of each solution to the voltage that was recorded during OCP measurements that were carried out using each pH sensor. The gradient of each slope suggests that the relationship between voltage and pH is a similar sensitivity across all of the solutions that were tested, the absolute voltage signal that was measured is variable. The slopes were generated by weighted least squares regression with error bars representing the standard error of the mean multiplied by two (n=5).

### 6.3.2 Testing in inoculated media

The purpose of this testing is to see whether the pH sensor was still able to accurately determine the pH of the media in the presence of live bacteria and their metabolites. Each of the media types were inoculated with *L. casei* and incubated at 25°C for 48 hours until they reached the stationary phase, following this they were tested by measuring the OCP using the DMSO-melanin pH sensor. The voltage measured in each of the inoculated culturing media samples was compared with the standard curve in Figure 6.4 in order to predict the pH of the sample. The pH of each sample was also measured using a standard glass electrode pH meter in order to verify whether the pH prediction based on the DMSO-melanin pH sensor and the generated standard curve was accurate. The results suggested that the pH value obtained using the DMSO-melanin pH sensor are accurate in each media type as they are similar to those that were measured using the glass electrode (Table 6.3).

Table 6.3: The culturing media pH calculated from the OCP signal that was measured in the DMSO-melanin based pH sensor following *L. casei* inoculation and incubation to stationary phase. The accuracy of this predicted value was verified by measuring the pH of each sample using a standard commercial glass electrode pH meter which confirmed that accuracy of the sensor is good enough for laboratory practice.

Media type	Sensor calculated (pH)	Glass electrode (pH)	Difference (pH)
LB	4.97	5.06	-0.09
BHI	4.63	4.65	-0.02
NB	6.31	6.3	0.01

### **6.3.2.1 Measuring pH at different bacterial loads**

As the number of bacteria in the culturing media changes over time due to cellular replication it was necessary to ensure that the signal that is measured using the sensor is not subject to interference by the presence of varying numbers of bacterial cells. In order to achieve this a serial dilution of the bacterial culture was carried out which was then measured using OCP and the DMSO-melanin pH sensor which was correlated to the LB standard curve in order to predict the pH values (Figure 6.5). The measurements were once again verified using a glass electrode pH meter. Measuring the pH of the different serial dilutions functions to simulate bacterial multiplication during the culturing process. As with the previous results the DMSO-melanin pH sensor performed well in the presence of the different bacterial dilutions and did not appear to be impacted by various levels of bacteria suggesting that it is reliable enough to be used in such an environment (Table 6.4). The reason why the pH levels were between pH5 and pH6 are due to the lactic acid being the major metabolite produced by the bacteria which results in a lowering of the pH of the media.



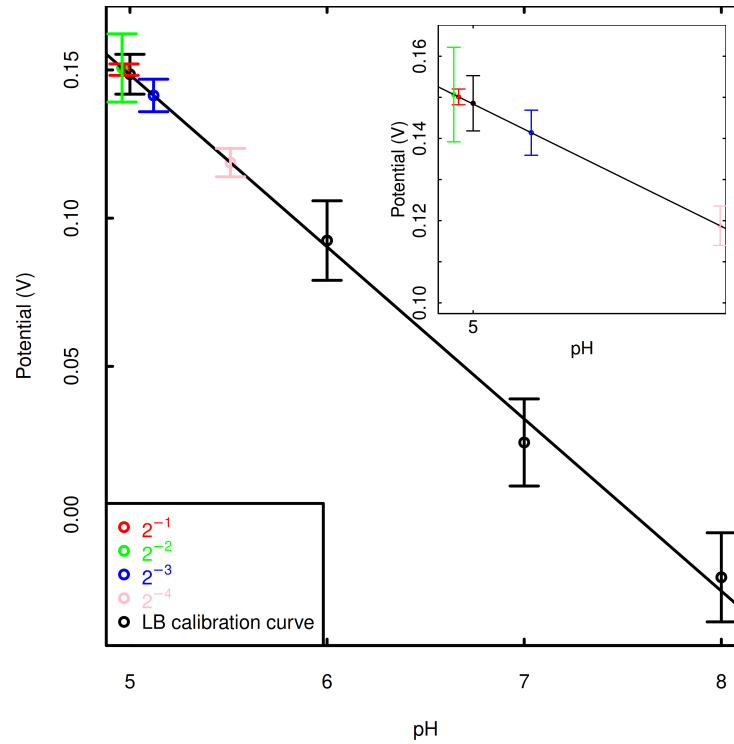


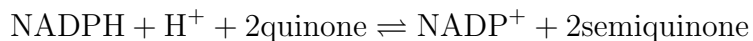
Figure 6.5: The LB calibration curve was used to predict the pH of the serial dilutions of cultured *L. casei* in LB. The inset shows the same graph zoomed in on the region where the dilutions are.

Table 6.4: The predicted pH values according to where the measured OCP values correlate with the LB calibration curve as shown in Figure 6.5 compared to the pH measured using a standard glass electrode pH meter.

Dilution	Sensor calculated (pH)	Glass electrode (pH)	Difference (pH)
$2^{-1}$	5.15	4.97	0.18
$2^{-2}$	5.02	4.96	0.06
$2^{-3}$	5.26	5.21	0.14
$2^{-4}$	6.02	5.51	0.51

## 6.4 Discussion

As with previous results measured in reference buffer solutions there was a strong linear relationship observed between the different pH of culturing media and the voltage that was measured using the DMSO-melanin pH sensors. These results suggest that the redox processes between the hydroquinone and quinone moieties that are responsible for the pH sensitivity of DMSO-melanin are not disrupted by the presence of either bacterial cultures or the components of the media solutions that were tested here. *L. casei* is one of many species of bacteria which produces the enzyme quinone reductase [281]. There was a possibility that this enzyme would impact on the pH sensitive DMSO-melanin aspect of the sensors as it acts upon three substrates including quinone, NADPH and  $H^+$  in the following reaction:



There was also potential interference in the signal from the presence of bacteria as they multiplied within the media due to their negatively charged components such as the bacterial cell walls, membranes as well as biomolecules such as DNA and proteins. That accurate pH levels were able to be determined using the sensor in the presence of bacterial cultures suggests that the sensor is robust enough in order to be used in environments with bacteria for pH monitoring purposes. However it is important to note that while the signal that was measured using the sensor had a strong relationship to the pH level of each media, the absolute potential that was measured in each sample of culturing media was different which suggests that there are components within the culturing media which affect the base signal that is measured using the sensor.

## 6.5 Summary

The results presented in this chapter provide evidence that the DMSO-melanin pH sensor is capable of accurately measuring the pH of the types of culturing media that have been tested provided that it is calibrated beforehand. This is the first time that a screen printed pH sensor has been used for this application. It has also been demonstrated as being robust enough to be able to accurately generate pH data in culturing samples that have bacterial cultures present in them. This requires that this pH sensor which is disposable in nature might have useful applications where it is bundled with a disposable bioreactor in order to continuously monitor the pH of the media. This would allow checking for the development of suboptimal culturing conditions or possibly identify contamination from an undesirable species. However it should also be noted that the absolute voltage that was measured in each of the media types was different which suggests that a calibration curve needs to be performed on each type of culturing media before it's pH can be measured using the DMSO-melanin sensors. The difference in absolute voltage is likely to be due to the different culturing medias being composed of different substances that interact with the reference electrode, it may be possible to improve this by changing the material used for the reference electrode. This is investigated in Chapter 7. Prototype software has been written that is able to calculate the pH of the different culturing media based on the slopes in this chapter, these are presented in Appendix B.1.

# Chapter 7

## Potential clinical applications for the pH sensor.

### 7.1 Rationale

Biological processes are extremely sensitive to changes in pH. Disposable sensors have the potential to be used in clinical monitoring applications. Other sensors have been developed for monitoring wounds in the form of smart bandages [77] however these pH sensors have not been reported as having been tested with blood samples [282]. This is possibly due to blood being a difficult material to work with. Despite this difficulty, testing with blood is worthy of pursuit as a disposable inexpensive pH sensor that is able to accurately and reliably measure pH has the potential to be used for life saving point of care applications. A life threatening condition associated with blood pH is lactic acidosis due to sepsis, this chapter outlines testing the pH sensors against a preclinical model for lactic acidosis with the intention of developing an inexpensive point of care test that can detect this condition quickly thus allowing for treatment to commence as early as possible.

## 7.2 Point of care testing

### 7.2.1 Background

Diagnostic testing that is performed outside of the hospital or laboratory setting at the same location as the patient is referred to as POC testing. The primary purpose of POC is the rapid generation of results so that the appropriate treatment can be implemented as quickly as possible in an effort to maximise clinical outcome [283]. Some examples of these improved clinical outcomes and associated conditions are listed in Table 7.1. POC tests can take place in a variety of different settings including a general practitioners office, the hospital bedside, emergency medical incidents (involving paramedics) as well as for the monitoring of chronic conditions in the home [284]. POC devices are used with body fluids such as blood and saliva and they react to analytical targets including proteins, ion, nucleic acids and metabolites [285].

Table 7.1: Examples of improved clinical outcomes that arise when POC testing is used. Adapted from [283].

Outcome	Example
Faster decision making	Chest pain, drug overdose
Earlier treatment onset	Drug overdose
Improved patient compliance	Diabetes
Reduced complications	Diabetes
Faster treatment optimisation	Anticoagulation
Reduction of readmissions	Parathyroidectomy
Patient satisfaction	Less hospital visits

## 7.2.2 Carbon based point of care devices

Carbon based sensors are good candidates for point of care devices due to the sensitivity of graphene to changes in its environment [286, 287, 288] due to high surface area to volume ratio [289, 290, 291]. The ability to functionalise graphene sensors makes them highly specific to the point that they are able to identify single nucleotide polymorphism (SNP)'s [292]. Carbon based POC devices may be employed to detect a variety of different biomarkers therefore impacting upon the treatment of different diseases.

### 7.2.2.1 Detection of nucleic acids

The identification of specific nucleic acid sequences is of significant clinical interest when identifying an infectious agent is crucial when considering the necessary course of patient care. Historically this was performed (in the case of bacteria or yeasts) by culturing a swab taken from the site of infection and subsequently analysing the morphological and biochemical traits of the microorganism such as its Gram type, what sugars it is able to ferment, what treatment it may be resistant to as well as general microscopic analysis. This process can take several days during which the patients condition may deteriorate while results are being waited upon. Furthermore relying on culturing based processes has limitations when working with species that are difficult to culture (For example *Chlostridium difficile*, where “difficile” translates to “difficult” [293]) or viruses. The time taken to generate results has been greatly impacted since the invention of PCR in 1985 [294] and its improvement to real time PCR [295] which has allowed results to be generated within a few hours. Utilising graphene based POC devices has the potential to improve the time to generate results further therefore providing a rapid screening test where positive results can be confirmed via PCR testing

allowing for a more targeted approach that improves efficiency [296, 297].

#### **7.2.2.2 Detection of proteins**

Proteins are useful biomarkers for several disease states [298] but for biosensors to be able to detect such biomarkers in a useful manner they must be highly sensitive with limits of detection that operate within the femtomolar and picomolar range of concentrations [299, 300]. POC devices based on graphene have been developed to detect cancer by sensing proteins that are either released directly by cancer cells or by other cells in response to the development of cancer [301, 302]. Graphene POC platforms have also been developed that are able to detect viral infections [303] by sensing viral proteins [304]. Such low limits of detection are also required for the detection of biomarkers for cancer [305].

#### **7.2.3 Point of care tests for sepsis**

Due to the nature of sepsis requiring early treatment in order to maximise the potential for successful treatment it is a desirable candidate for a POC device [284]. Traditional methods for the determination of sepsis are laborious and slow processes which include blood culture which can take between one to five days to grow the bacteria and PCR which can take several hours to generate a result [306]. A POC device would therefore have the potential to increase the speed of the diagnostic process allowing for the correct treatment to be administered more rapidly thereby maximizing prognostic outcomes. Currently suspected sepsis is treated by a course of antibiotics therefore a POC test would be useful in ruling out suspected sepsis in order to prevent the inappropriate administering of antibiotic usage which may compromise future treatment [307].

## 7.3 Lactic acidosis

The levels of lactate in the blood are dependent upon the production of lactate and its uptake into tissues [308]. Lactate is produced from pyruvate during anaerobic glycolysis and is converted to pyruvate via the action of the enzyme nicotinamide adenine dinucleotide (NAD)-dependent lactate dehydrogenase (LHD) this is subsequently oxidised to  $\text{CO}_2$  and  $\text{H}_2\text{O}$  by the mitochondria [309]. Due to the complex nature of cellular metabolism lactate is a waste product produced by some types of cells while also being a substrate for another. The recycling rate for lactate in intermediary metabolism is therefore high [310]. While red blood cells (RBC)s and muscles are the primary source of lactate under normal physiological conditions, it may be produced by any organ within the body [311] and the kidneys and liver are responsible for the removal of lactate at rates of 30% and 60% respectively [312, 313]. Lactic acid is almost completely ionised to lactate at normal physiological pH levels  $(\text{CH}_3\text{CH}(\text{OH})\text{COOH}) \rightleftharpoons \text{CH}_3\text{CH}(\text{OH})\text{COO}^- + \text{H}^+$  [314, 315]. Lactate blood concentration ranges between 0.5 mmol/l and 1.8 mmol/l with abnormal levels being associated with mortality [316, 317, 318]. Lactic acidosis presents a clinical problem either as a result of impaired lactate metabolism or due to excessive lactate production [319, 320] and depending on the mechanism that is causing it lactic acidosis is characterised into types A and B [321, 322]. Type A and type B lactic acidosis can coexist. Type A is the most common of the two and typically occurs as a result of reduced oxygen carrying and delivery, increased glycolysis and/or hypoperfusion which causes tissue hypoxia [323, 324]. In type B lactic acidosis there is no evidence of tissue hypoxia however there may be occult hypoperfusion [325], with hypoperfusion referring to the inadequate supply of nutrients and oxygen as a result of reduced blood flow [326].



### **7.3.1 Lactic acidosis and sepsis**

Sepsis can lead to both types of lactic acidosis [327]. Sepsis refers to acute circulatory failure that is associated with infection [328, 329], the consensus definitions for sepsis and septic shock were updated in 2016 to state that septic shock is a subset of sepsis that is associated with a greater degree of mortality that results from underlying circulatory, cellular and metabolic abnormalities [330]. Elevated lactate levels are common in critically ill patients [331] and elevated levels upon hospital admission are associated with an increase in 30 day mortality [332]. According to the World Health Organisation the annual mortality rate is approximately 6 million, with the majority of these being preventable [333]. The severity of the condition has led to research into its epidemiology [334] and improving diagnosis, as part of this process over 200 biomarkers have been investigated as being potentially useful in sepsis diagnosis [335]. Lactate has been identified as a biomarker for septic shock, a subset of sepsis where underlying circulatory and cellular metabolism abnormalities increase mortality substantially. In septic shock serum lactate levels are greater than 2mmol/l [336].

### **7.3.2 Lactate directed therapy**

The evidence of lactate being a useful prognostic marker led to research that investigated whether therapy that aims to reduce the concentration of lactate in the blood was associated with a positive clinical outcome. One such study initially measured patient lactate levels upon their admission to intensive care unit (ICU). Those patients that presented with elevated lactate levels were split into two groups, a control group and a group where the lactate levels were monitored and treatment aimed to reduce lactate levels by

20% every two hours. The study concluded that the lactate directed therapy significantly lowered hospital mortality and that the initial monitoring of lactate levels was associated with an improved patient outcome [337]. Another randomised trial however did not find any significant difference in mortality between patients that had undergone lactate directed therapy and those who had not, it is important to note though that in this study lactate levels were only reduced by 10% which is significantly less than in the study mentioned above [338]. Blood pH level is a biomarker for lactic acidosis along with elevated levels of the enzyme lactate dehydrogenase, blood pH levels are also used to determine whether emergency treatment with bicarbonate is required [339, 340]. Therefore measuring blood pH could be beneficial for the early screening of patients that are demonstrating potential signs of septic shock.

## **7.4 Materials and methods**

The DMSO-melanin sensors were prepared as is described in Chapter 5. Plasma was prepared via centrifugation of citrated blood for 15 minutes at 3153 RPM. Blood was prepared by mixing it with either sodium citrate or lithium heparin in order to prevent coagulation. The samples were tested by pipetting 120 $\mu$ l of plasma or blood onto the electrodes that compose the sensor and recording the open circuit potentiometry for a 10 minute period in the same fashion that is described in Chapter 5.

## **7.5 Results**

### **7.5.1 Initial sensitivity testing**

Before testing whether the sensor can effectively operate in blood samples it was important to first determine whether the sensor was capable of operating at the required sensitivity range that is necessary for the detection of lactic acidosis (Figure 7.1). This was tested by preparing buffer samples that had a pH of 7.4 and pH7.3 and subsequently measuring the OCP using the sensors and determining whether there was a consistent difference in the potential signal that was measured (Figure 7.1A). While there was some drift and variation in the signal there appeared to be a sufficient difference at this initial stage (Figure 7.1B) to warrant further investigation into the viability of using these sensors in the development of a point of care diagnostic platform for lactic acidosis.

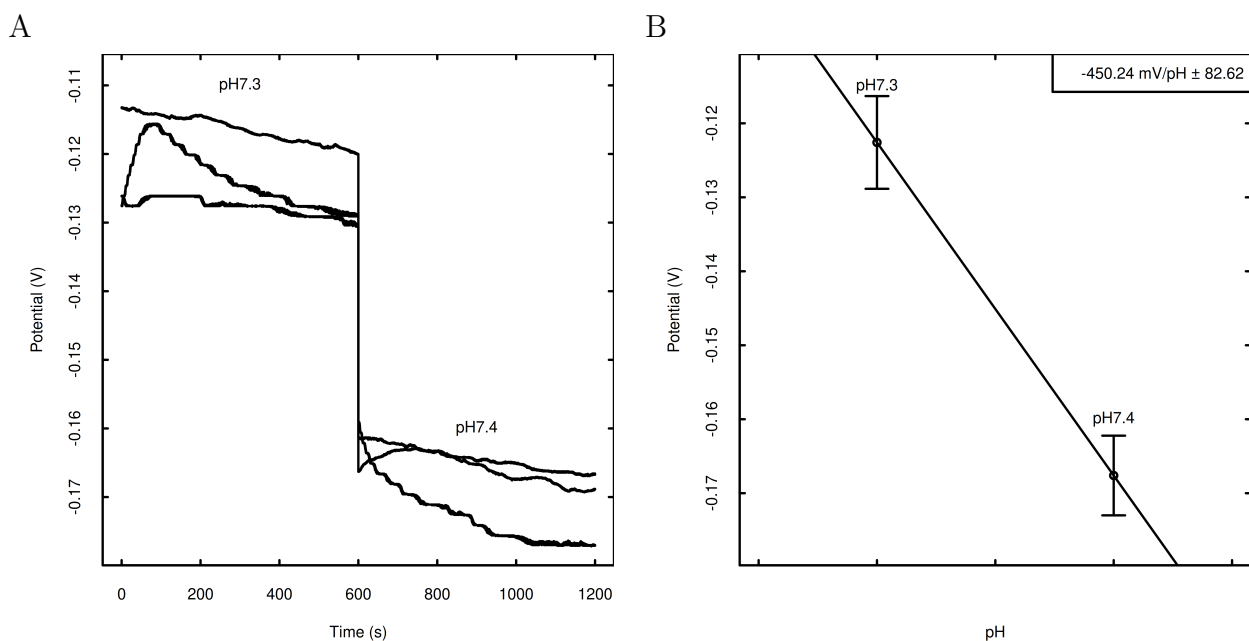


Figure 7.1: (A) Potential measured in modified reference buffers that had a clinically relevant pH range (7.3 - 7.4) for the detection of acidosis. (B) Potential plotted against pH. Error bars represent the standard error multiplied by two (n=3).

### 7.5.2 Investigation into alternative anticoagulants

Due to the nature of blood clotting as soon as it leaves the body it is necessary to perform these experiments in blood that has been mixed with an anticoagulant in order to prevent clot formation. Lithium heparin and sodium citrate are routinely used as anticoagulants in blood samples that undergo clinical biochemical analysis [341, 342, 343]. These anticoagulants function via different mechanisms with lithium heparin binding to the plasma protein antithrombin III. This proteins physiological function is to prevent the onset of coagulation and it's efficacy is increased over 1000 times when it is com-

plexed with lithium heparin [344, 345] which accounts for the anticoagulant effect of this compound. Sodium citrate functions via chelating calcium ions, this inhibits clotting as calcium ions are responsible for activating platelets as well as multiple coagulation factors involved with the clotting cascade [346]. An investigation into how blood samples that had been treated with these two different anticoagulants was necessary because the type of anticoagulant used could impact on the measured result. Lithium heparin is acidic and has been reported as to having a statistically significant effect on the pH of blood samples that it has been mixed with [347]. Sodium citrate is alkaline with a pH that ranges between 7.5 and 9 which may also affect the results [348]. Therefore blood samples that had been prepared using both of these anticoagulants were tested using the DMSO-melanin pH sensors. When tested both the blood samples prepared with sodium citrate and lithium heparin displayed a decay in the signal that was measured over a 10 minute period suggesting that this decay is not due to the type of anticoagulant used as they both function via different mechanisms (Figure 7.2, 7.3).

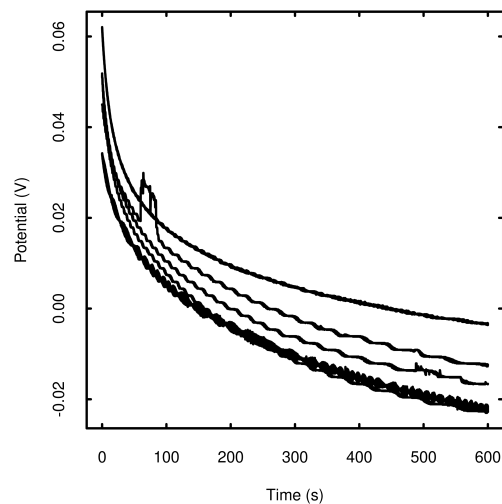


Figure 7.2: Signal measured by a DMSO-melanin pH sensor in a citrated blood sample. As with the plasma sample there was a sharp drop in the potential that was measured at the start of the test. Each line represents the potential measured in a replicate.

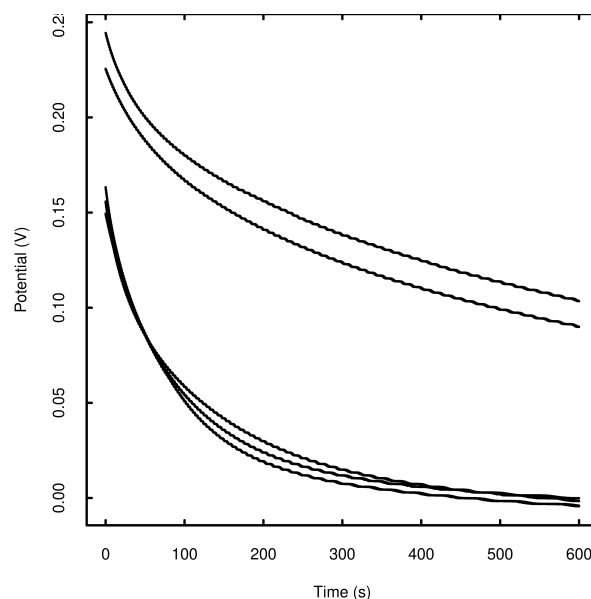


Figure 7.3: Signal measured in blood where lithium heparin has been used as the anticoagulative agent. Each line represents the potential measured in a replicate.

### 7.5.3 Initial testing on blood

The first step involved testing whether the sensor is capable of detecting pH changes in a blood sample. To achieve this the potential of a citrated blood sample was measured using the sensors. Once the measurements had been completed then the citrated blood sample was spiked with lactic acid and the process was repeated. The pH of the sample was measured using a glass electrode pH meter so that it could be compared with the potential that was measured using the sensor. There was a pH dependent difference in the signal (Figure 7.4) however the pH of the spiked sample was outside the clinically relevant range. This indicates that the sensor does respond to pH changes in blood but further testing was needed to verify whether the sensor could operate at a resolution that is high enough to detect the slight changes in blood pH that are clinically significant. The slopes representing

the relationship between the measured voltage and pH also varied between tests suggesting repeatability problems when using the sensors to measure the pH of blood.

#### 7.5.4 Expected pH change

In the blood lactic acid is buffered almost entirely by the bicarbonate buffering system [349]. The concentration of bicarbonate in the blood of healthy individuals ranges from 22mmol/l to 29mmol/l. The  $pK_a$  of lactic acid is 3.86 [350]. Using the Henderson–Hasselbalch equation (Equation 7.1) increasing the concentration of lactic acid by increments of 0.01mmol/l should theoretically cause the pH to decrease by 0.3 for the first increment and 0.2 for second increment assuming that the concentration of bicarbonate in the blood is 25.5mmol/l.

$$pH = pK_a + \log_{10} \left( \frac{[Base]}{[Acid]} \right) \quad (7.1)$$



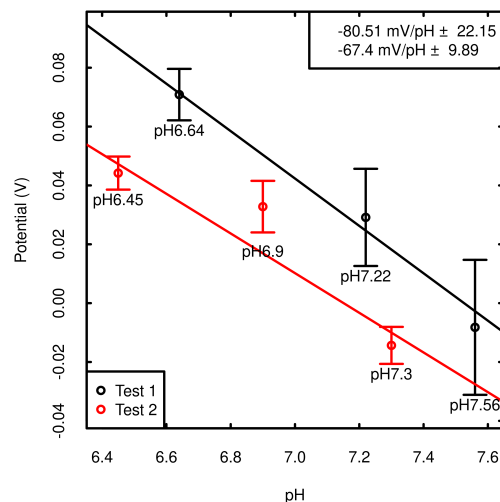


Figure 7.4: Average signal taken from the final 100 seconds of a 10 minute measurement of citrated blood samples ( $n=5$ ) that had been spiked with  $10\mu\text{l}$  lactic acid in order to alter their pH. A gradual decrease in pH upon further additions of lactic acid in increments of  $0.01\text{mmol/l}$  was observed as expected however it was slightly greater than what was predicted theoretically in Section 7.5.4. The pH of the samples were confirmed using a glass electrode pH meter. This was repeated across two different samples where the relationship between the pH and the signal varied between the different samples.

### 7.5.5 Comparison with sensors in the literature

This is the first time that a screen printed pH sensor has been tested using blood samples. While there are other screen printed pH sensors that have been reported in there literature there are currently no reports of them being used to measure the pH of blood accurately. Although some mention that using SPE pH sensors in blood is useful for applications they do not report the results of any such tests themselves [351, 247]. The majority of reports

detailing screen printed pH sensors do not mention blood at all [352, 353, 246, 354, 355, 356, 357, 358, 359]. The closest application to blood measurements reported is the usage of screen printed pH sensors to measure the pH of wound exudate [77, 80, 63]. This suggests that there are challenges associated with measuring blood pH using screen printed pH sensors as the measuring of blood pH is an important biomarker and therefore an attractive application for these sensors.

#### **7.5.6 Initial testing of the DMSO-melanin pH sensors with plasma**

Due to the possibility that the some of the constituents of blood such as red blood cells might be responsible for the repeatability problems described above (Figure 7.3), some of these components were removed via centrifugation in an attempt to increase the stability and repeatability of the test. While an extra centrifugation step would limit the sensors application as a point of care test, it still may be useful for applications in a small research laboratory or at a general practitioners clinic. Unfortunately this approach did not solve either the problem of the signal taking a long time to settle or the lack of consistent repeatability between the replicates (Figure 7.5).

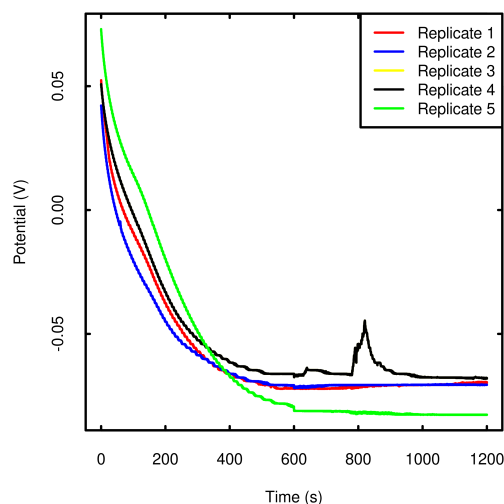


Figure 7.5: The potential measured using 5 DMSO-melanin pH sensors over a 20 minute period. The sensor took almost 10 minutes for the signal to become stable. Once stable the measured potential was not consistent enough between the sensors to indicate that they are repeatable enough to detect lactic acidosis in a clinical setting.

## 7.6 Investigation into alternative inks for the reference electrode

As the signal measured in both blood and plasma samples appears to vary significantly between the same sample when measured with different sensors the ink that was used to print the reference electrode was switched to observe whether this had any impact or improvement on the signal being measured as one of the possible causes of the variation could be due to components within the blood and plasma reacting with the reference electrode. Whilst these results were interesting as they showed that there was little difference

between the signal profile of the sensors that contained silver and silver/silver chloride reference electrodes - both of which show an initial sharp drop in the potential measured until it eventually stabilises and the signal flattens (though at levels that are variable between replicates indicating a lack of repeatability when measuring the potential of blood). The profile of the sensors that use carbon/graphene reference electrodes was different in that it showed a stable signal from the beginning of the measurement (Figure 7.6). However there was still a lack of repeatability in the signal that was measured between different replicates which suggests that while the drop in signal that was seen in the sensors with silver and silver chloride reference electrodes could possibly be due to an interaction between components of the blood/plasma and the silver in the reference electrode which can be overcome by substituting this reference electrode with one made from carbon, a carbon reference electrode is still not able to produce a repeatable signal that can be used to determine the pH of a blood or plasma sample.

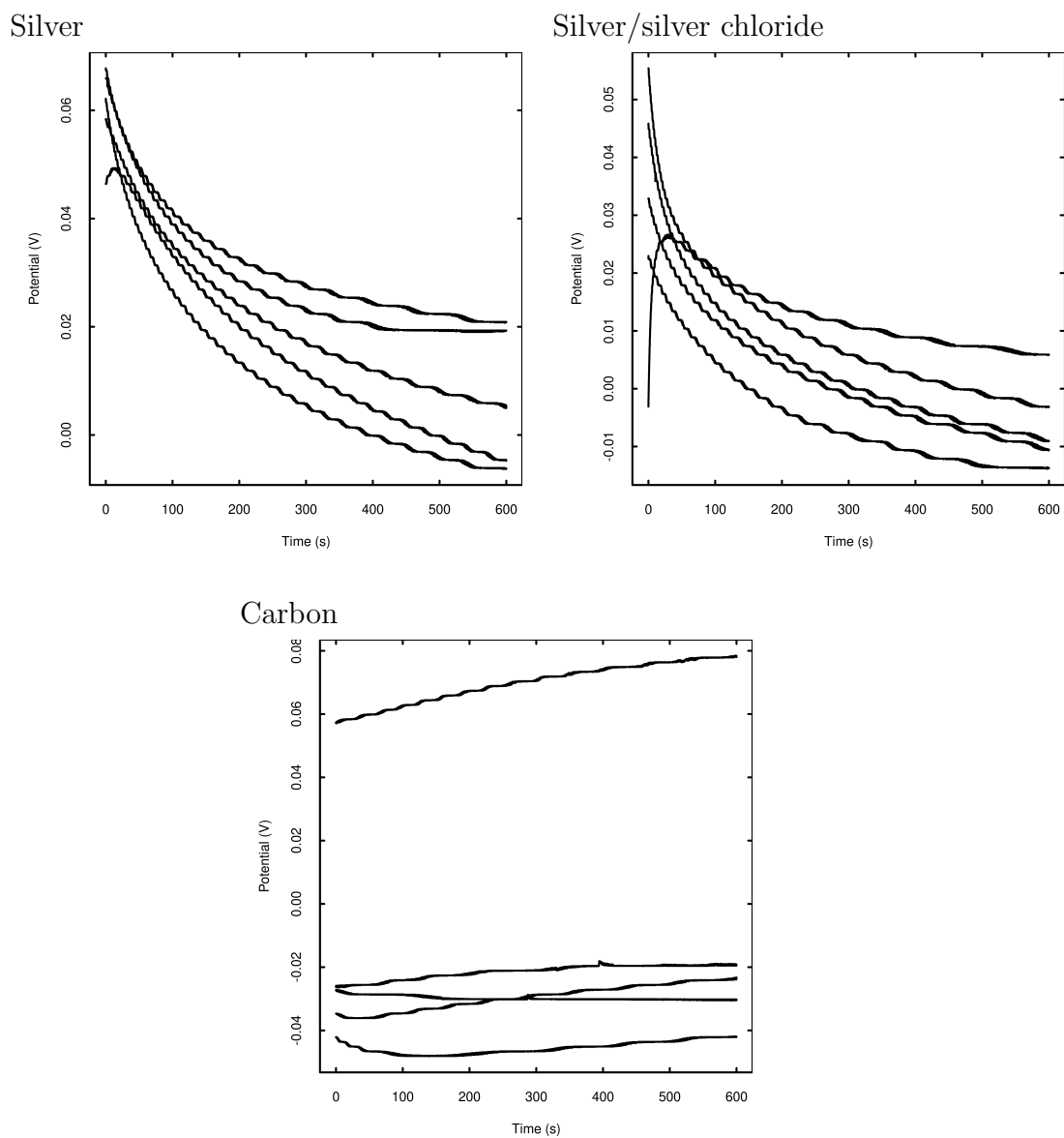


Figure 7.6: Signal measured in blood samples using DMSO-melanin pH sensors that utilised different inks for the reference electrode. Both sensors with the silver and silver silver chloride reference electrodes showed a similar decay in signal over time. This was not the case in the sensors that utilised a carbon/graphene reference electrode however the measurements did not show good repeatability.

## 7.7 Investigation into interfering substances

Due to being unable to obtain repeatable results an investigation into the substances in blood that might be affecting the results was carried out. Blood is a solution that contains many components which have the potential to interfere with the signal that is measured with the sensor. The changes in pH level that are being monitored in the blood are also very small which presents a challenge as a high degree of both accuracy and precision are important for detecting such a small but clinically significant change in pH level.

### 7.7.1 Spiked pH7 buffer

In order to test whether substances that are present in blood affect the signal that is measured by the DMSO-melanin pH sensor pH7 reference buffer solution was spiked with these substances at concentrations that are normal in blood (Table 7.2). OCP was then measured as usual. The buffer was spiked with bovine serum albumin (BSA) to represent albumin - a protein found in blood, glucose and sodium chloride. Of these substances BSA and glucose did not have a large effect on the measured signal whereas with sodium chloride there was a large decay in the measured signal that was observed similar to what had taken place in the plasma and blood samples (Figure 7.7) that had been tested previously suggesting that the sodium and/or the chloride could be responsible for the problems that occur when attempting to use the DMSO-melanin sensors to measure the pH of blood.

Table 7.2: Substances were tested at both the top and bottom ends of the clinical reference ranges. Sodium and chloride reference ranges were added together for a NaCl solution as working individually with sodium and chlorine is difficult. These substances were selected for investigation as they are typical components of blood and understanding which (if any) of these substances interferes with the sensor may lead to a better understanding of how to fix or compensate for the interference in future work.

Substance	[Low]	[High]	Reference
Bovine serum albumin (BSA)	35mg/ml	55mg/ml	[360]
Glucose	0.6mg/ml	1.4mg/ml	[361]
Sodium	3.1mg/ml	3.4mg/ml	[362]
Chloride	3.4 mg/ml	3.7mg/ml	[363]

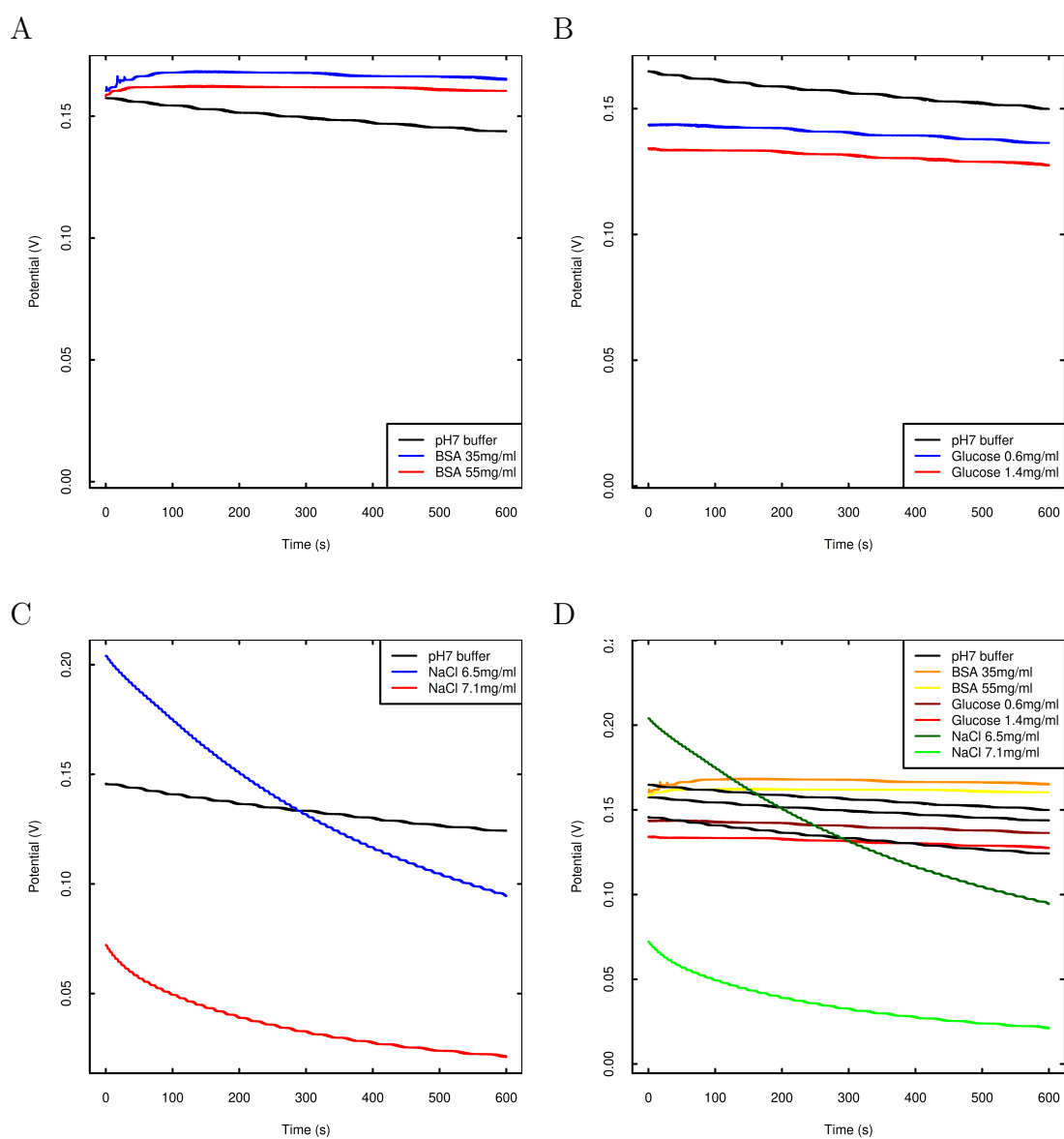


Figure 7.7: pH7 reference buffer that had been spiked with clinically relevant concentrations of substances present in blood which may interfere with the signal including (A) BSA (as a substitute for human albumin), (B) glucose and (C) sodium chloride. (D) Shows all of these signals plotted together on the same axis showing clearly that sodium chloride has the greatest effect on the signal measured.



### 7.7.2 Clinical intravenous solutions

In order to further investigate what substances in blood might be responsible for the interference that prevents using the pH sensors to measure blood pH intravenous (IV) solutions that are administered by drip to patients. These solutions were saline solution (Baxter Healthcare FKE1322) and Ringer's solution (Terumo BCT Limited 19-09-115) (Table 7.3). This allowed for the sensor to be assessed with different concentrations of electrolytes found in blood.

Table 7.3: Composition of the solutions that were tested.

Solution	Composition	pH (glass electrode)
Saline	0.9% sodium chloride	5.5
Ringer's	0.3% potassium chloride, 0.45% sodium chloride, 5% glucose	6.1

The signal measured (Figure 7.8) is in agreement with what has previously been reported suggesting that sodium chloride is likely to be one of interfering components within blood. The solution which contained a higher concentration of sodium chloride showed the same pattern of gradual potential decrease and large variation in the potential measured as to what has been observed previously in blood and plasma.

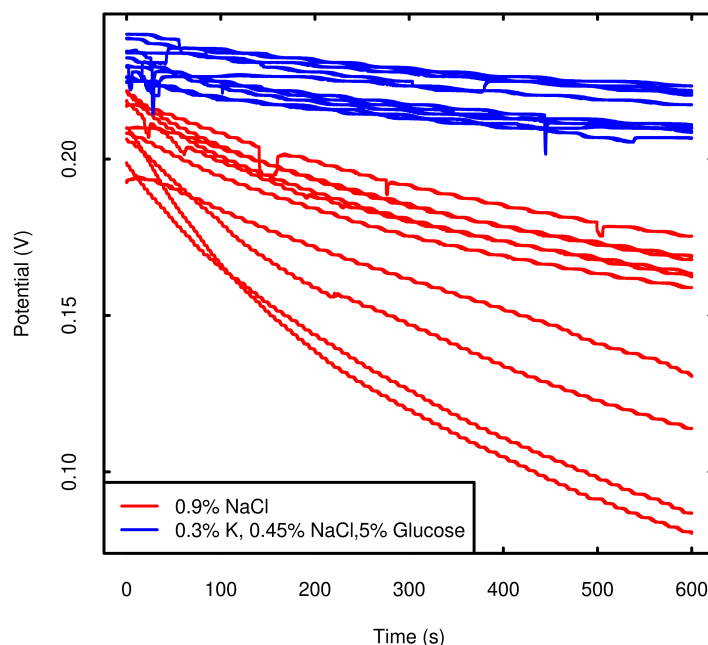


Figure 7.8: Signal measured using DMSO-melanin sensors in the two IV solutions provided by Morrision where red = saline and blue = Ringer's. Each line represents the signal recorded by a previously unused pH sensor ( $n=10$ ).

As the previous test indicated that sodium chloride is likely to be interfering with the voltage being measured by the pH sensor a further investigation was carried out where the pH sensor exposed to a sodium chloride solution for 10 minute intervals of gradually increasing the concentration of sodium chloride in order to determine where the concentration begins to interfere with the sensor. The concentrations ranged between 1mg/ml and 10mg/ml and the concentration was increased by 1mg/ml after each 10 minute interval (Figure 7.9).

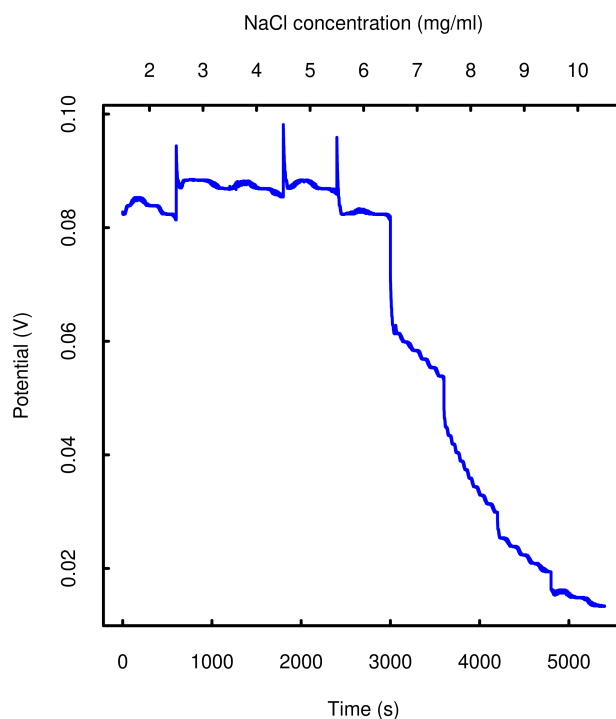


Figure 7.9: pH sensor exposed to increasing concentrations of NaCl over 10 minute periods.

As the previous graph shows that solutions that have a concentration of sodium chloride that is higher than 6mg/ml begin to have an impact on the signal measured by the sensor. A further test was performed in order to gain an understanding of whether it is the sodium, the chloride or both ions that are causing the interference. This was carried out by repeating the test described above with solutions containing other sodium and chloride salts (Figure 7.10).

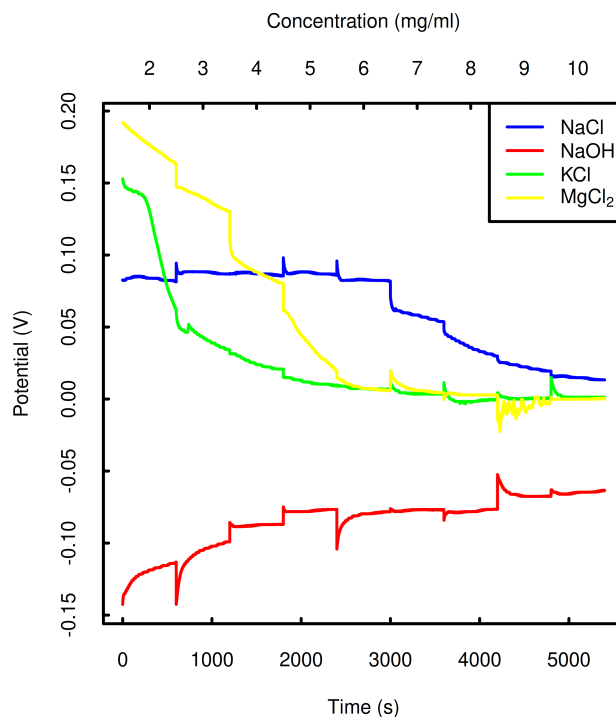


Figure 7.10: pH sensor exposed to increasing concentrations of Sodium and Chloride solutions over 10 minute periods.

These results suggest that the chloride is responsible for having the most impact on the signal measured by the pH sensor. Since chloride is a component of blood it may be necessary to change the material of the reference electrode to something that is less reactive.

### 7.7.3 Gold ink reference electrode

It is possible that the repeatability and signal disruption that is observed when the pH sensors are used in solutions that contain sodium and chloride compounds (such as blood) is due to these compounds reacting with the silver based reference electrode. Should this be the case then it might be

possible to address this issue by replacing the silver reference electrode with gold due to gold being less reactive than silver.

#### **7.7.3.1 New prototype design for the pH sensor with a gold reference electrode**

Due to the long and expensive process that is associated with designing a screen for screen printing and having that screen manufactured externally these sensors were produced using a stencil cutter.

A stencil cutter was used to produce the sensors to reduce fabrication time. This process is not as accurate or reproducible as screen printing however it has both cost and time advantages which allows for a prototype sensor to be produced quickly therefore allowing for a quick assessment as to whether or not this approach of replacing the silver reference electrode with gold is likely to be effective. The layers that make up the prototype design is presented in Figure 7.11 and the combined design is presented in Figure 7.12. A photograph of the prototype sensors produced by bar coating is shown in Figure 7.13.

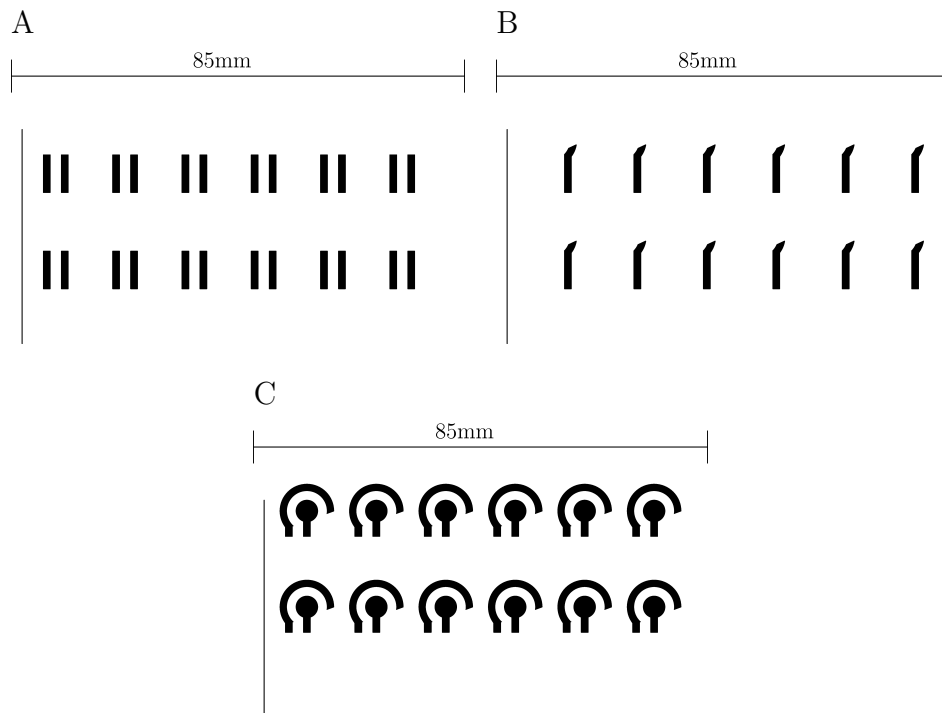


Figure 7.11: The designs for the individual layers to be cut using the stencil cutter to compose the sensor. The primary difference between this design and that which was used for the screen printed electrodes is that the silver tracks and reference electrode layer has been split into two layers in order to facilitate having a separate gold reference electrode. (A) silver layer (B) gold layer (C) carbon/graphene layer. Designs were created using the Asymptote vector graphics language.

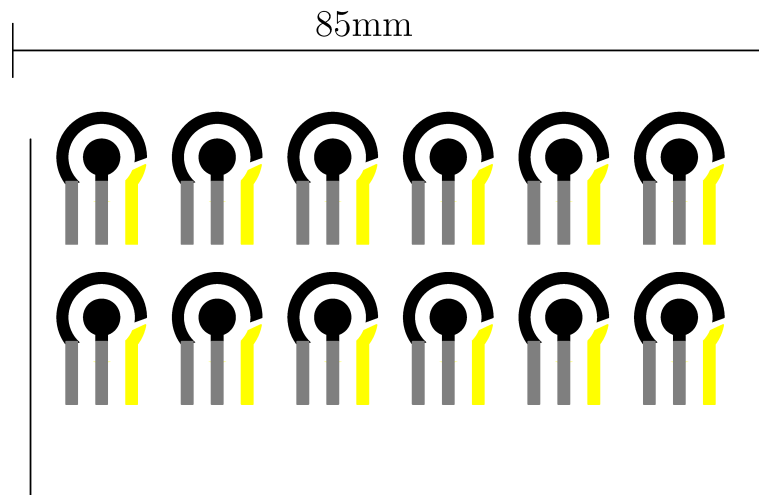


Figure 7.12: The stencil design layers from Figure 7.11 combined to show the full sensor design.



Figure 7.13: The final sensors that were produced using bar coating and the silver, gold and carbon/graphene ink.

#### 7.7.4 Results

The prototype gold reference electrode DMSO-melanin pH sensors were first tested with the pH4, pH7 and pH10 reference buffers in order to determine whether they were sensitive to pH. The measured signal was stable with the pH4 and pH7 reference buffers however there was a signal decay over time

when the pH10 reference buffer was used (Figure 7.14). Although the signal did not appear as stable as had been measured previously with the DMSO-melanin pH sensors with silver reference electrodes the prototype sensors did show sensitivity to different pH levels, however it was less sensitive than the pH sensor that utilised a silver reference electrode. Therefore the sensor was taken forward for further testing with a blood sample.

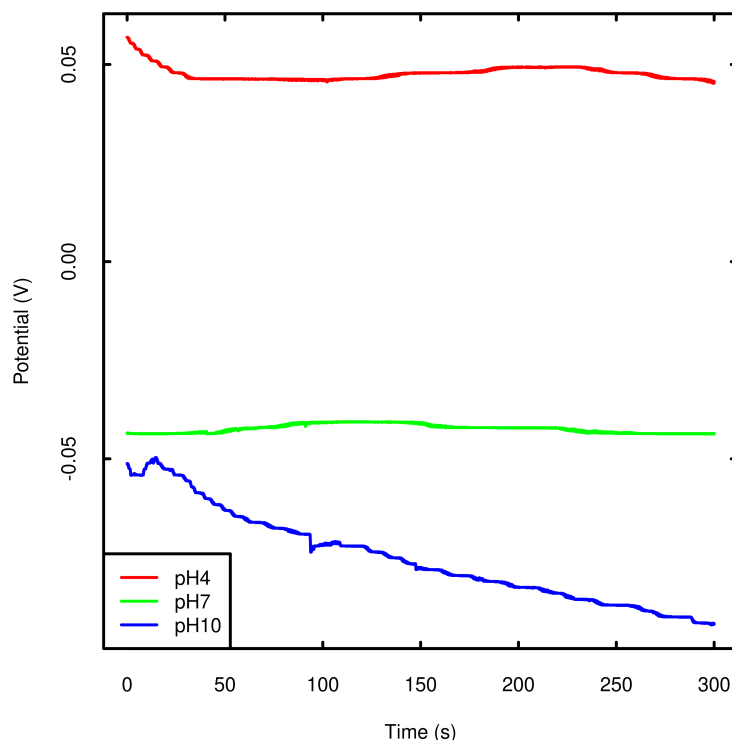


Figure 7.14: Prototype DMSO-melanin pH sensors utilising a gold reference electrode were tested with reference buffers of a known pH (red = pH4, green = pH7, blue = pH10) in order to ensure that they were sensitive to difference pH levels.

The substituting of the silver reference electrode with gold did appear to improve the stability of the signal as the signal decay (in blood but not buffer) that had been observed with the sensors with a silver reference electrode (Figure 7.5) was not present with the prototype sensors with a gold reference



electrode (Figure 7.15). However the signal that was measured using four prototype sensors with the same blood sample was not consistent. It is possible that this consistency is related to the nature of these prototype electrodes being visibly more variable (Figure 7.13) than the SPEs as they were produced using a stencil cutter and manual alignment as opposed to an automated screen printer making them inherently less consistent as is clear from the photograph (Figure 7.13). Therefore it might be worthwhile to explore SPEs with a gold reference electrode during future work.

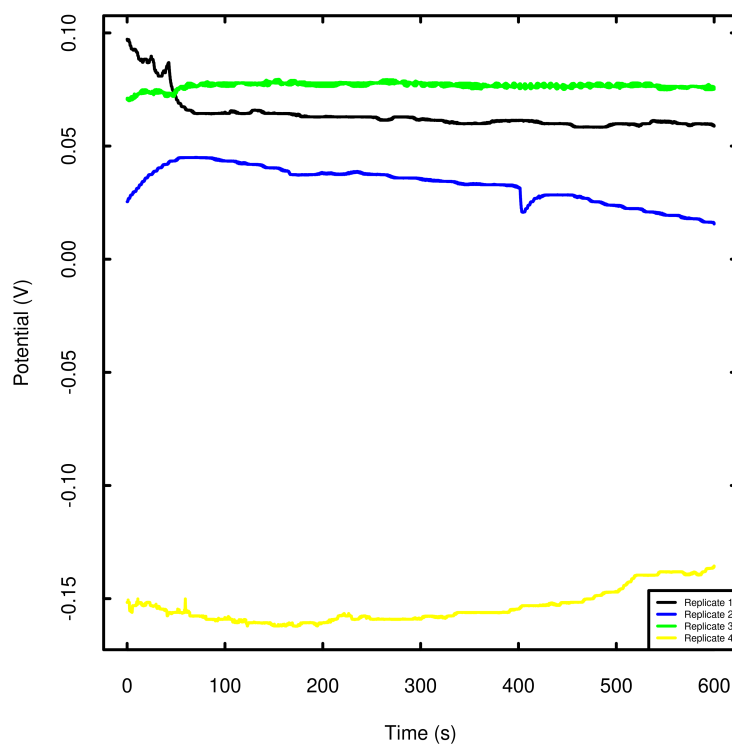


Figure 7.15: The prototype pH sensors were run with a blood sample to see whether the same problems involving repeatability and signal decay were present as they were with the silver reference electrode.

## 7.8 Discussion

While the previous success of testing the pH sensor in reference buffers and microbiological culturing media justified attempting to utilise the DMSO-melanin pH sensors in point of care applications where the detection of changes to blood pH is a useful diagnostic marker, the results suggest that this sensor is not well suited for these applications. The signal that was measured in both whole blood and plasma consistently showed a decay before eventually stabilising after approximately 500 seconds however there was significant variability between repeat blood and plasma measurements from the same sample. This inconsistency means that it is not possible to determine the pH from the signal since the signal that is generated appears to vary in a manner that is not related to pH suggesting that there is some component within the blood that is impacting upon the measured signal that is not present in the case of either reference buffers or microbiological cultures. Components within the blood appear to be interacting with the silver or silver/silver chloride reference electrodes since measurements that were taken with DMSO-melanin pH sensors that had either silver or silver/silver chloride both showed the same decay in signal after being exposed to blood however the DMSO-melanin pH sensors with a carbon/graphene reference electrode and the prototype stencil pH sensors with a gold reference electrode did not show this decay in signal however the voltage that was measured was highly variable between replicate tests of the same sample meaning that these were not suitable for measuring the pH of blood either. An investigation into substances within blood that could potentially interact with the suggested that chloride in particular is interacting with the sensor as NaCl, KCl and MgCl<sub>2</sub> all produce a decay in signal that is similar to what has been observed with the blood and plasma samples. This is likely due to the silver reference

electrode being subject to oxidation.

### **7.8.1 Potential solutions and future work**

Although it has not yet been possible to use the sensors in their current form to determine the pH level of blood, the success of the sensors in measuring other things suggests that it may be possible to modify the sensor in order to improve its performance in blood. Such changes that might be worth investigating include using different materials for the electrodes that make up the sensor as replacing the reference electrode with either gold or carbon/graphene eliminated the signal decay that was seen with the silver and silver/silver chloride reference electrodes. Another aspect to investigate would be to use a SPE that has multiple electrodes similar to that in Figure 7.16, this electrode would take 8 measurements simultaneously that could then be used to generate an average. Using these averages might help reduce the inconsistency in the measured signal that has been observed in blood samples.



Figure 7.16: A DropSens brand SPE produced by Metrohm that contains 8 working electrodes. This SPE or a similar design that incorporates multiple working electrodes could be used to measure an average signal in blood which might improve signal consistency.

## 7.9 Summary

This is the first time that a screen printed pH sensor has been tested using blood samples in a preclinical model. This pH sensing platform has been demonstrated to be able to accurately measure the pH of environments where there are microorganisms being cultured such as within a bioreactor or standard laboratory microbial culturing conditions. However as shown in the different media types analysed in Chapter 6 the baseline voltage is different depending upon the constituents of the media. This was easily overcome in media by producing a calibration curve of known pH values for each specific media type. While effective in situations where the components of the solution that is being measured (such as in media where the constituents of the

media are known as the media is either prepared in house or it's components are given by the manufacturer). This does appear to present a problem when measuring blood as the constituents of blood vary between samples (RBC, WBC, platelet, protein, urea, creatine etc) and this appears to influence baseline voltage that is measured. This means that in order to reliably measure the pH of blood solution a calibration curve would need to be carried out on each blood sample before it is run. However despite this limitation there are still potential uses this sensor in a clinical setting. While it is not possible to calculate the absolute pH due to the variable consistency of blood impacting upon the baseline voltage, the sensor still displays sensitivity to changes of pH in blood and therefore might be useful for measuring any relative changes. For example the sensor could detect a relative lowering of pH thus potentially indicating the onset of acidosis and allowing for the early intervening treatment by alerting clinical staff.

## Chapter 8

# Investigation into using electrochemical techniques to assess microbial growth

### 8.1 Introduction

Determining the quantity of bacteria within a solution is a process that is essential across many distinct disciplines [14, 15]. Since the initial discovery of bacteria in the mid 1600s [364], they along with other microorganisms have been associated with a variety of different fields and applications within industry. The most notable being the ancient process of fermentation which is essentially a bioreactor as well as within medicine following the establishment of germ theory [365]. This work proposes to investigate whether the SPEs described in Chapter 3 and electrochemical techniques can be used to measure the quantity of bacterial growth in culturing media by immersing the SPE in media containing different concentrations of bacteria then applying SWV and analyzing any relationship between bacterial concentration and the measured

voltammogram.

## **8.2 Culturing microorganisms**

Although microorganisms including bacteria and yeast had been identified and visualised via microscopy, the discovery of culturing media and the development of associated culturing protocols has enabled the field of microbiology to grow which has in turn lead to the development of biotechnology.

### **8.2.1 Monitoring bacterial growth**

Monitoring the growth of cultured microorganisms is an important aspect of biology with regards to optimising the growth kinetics, metabolite production and biomass [366]. The classical techniques employed in monitoring these cultures include counting the total number of cells visually or through a technique such as flow cytometry, assessing the viable number of cells through culturing diluted media on plates or estimating the number of cells present through the turbidity of the culturing media in the form of measuring the optical density using a UV spectrophotometer [367, 368]. The non destructive nature of optical methods has rendered them the most popular method to measure bacterial growth [366].

### **8.2.2 Growth curves**

Bacteria are frequently cultured in a well mixed liquid suspension when grown in laboratory settings, such as in a flask or a 96 well plate when working with smaller volumes. Growth in these environments produces characteristic growth curves similar to the sample shown in Figure 8.1. Such growth curves

are typically measured by optically measuring the media's turbidity via optical density using equipment such as a UV spectrophotometer or a plate reader. The initial segment of the growth curve is the “lag phase”, during this period the number of bacterial cells present in the media is so few that no growth is able to be detected using optical density, furthermore it is assumed that the cells need to adjust to their new environment having been previously under different conditions for storage. Following the “lag phase” is the “log phase” which is also referred to as the “exponential phase” due to the exponential or logarithmic growth that is measured over the course of this period. As bacteria continue to replicate and the growth media becomes more crowded the required nutrients become scarce and waste products accumulate, this causes the number of cells to plateau which is referred to the “stationary phase” of the growth curve. Bacterial population dynamics can be described as

$$\frac{dN(t)}{dt} = rN(t) \quad (8.1)$$

$$N(t) = e^{rt}N(0) = 2^{t/T}N(0) \quad (8.2)$$

where  $N(t)$  is bacteria at time  $t$  and  $r$  is the rate of bacterial replication [369].

### 8.2.3 Applications

Measuring or monitoring bacterial growth is desirable in various industrial, medical and research applications. In industry the microorganisms that reside within a chemostat bioreactor should be monitored to ensure that the bioreactor is operating efficiently and to alert personnel if the growth rate



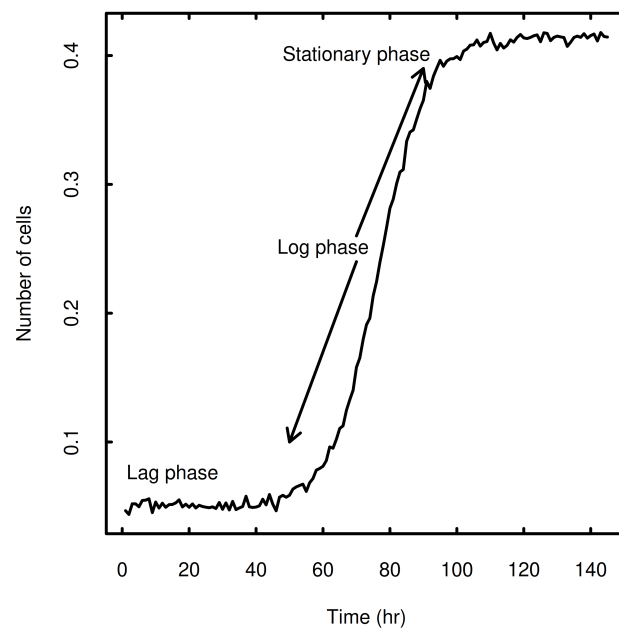


Figure 8.1: An example of a typical bacterial growth curve which is composed of a lag phase immediately after inoculation has taken place followed by exponential growth over the course of the log phase before a growth plateau is reached at the stationary phase.

changes in such a way that potentially impacts upon the bioreactor [370]. In medicine and research assessing the growth rate can indicate whether a bacterial strain is resistant to or partially resistant to specific antibiotics and suggest the type of antimicrobial resistance that is present [371, 372, 373].

#### **8.2.3.1 Sensitivity of bacteria to antimicrobials**

The emergence of pathogenic bacteria that are resistance to antimicrobial agents is recognised as one of the most serious contemporary health threats [374]. Infections with resistant strains are associated with higher levels of morbidity and mortality along with increased healthcare costs [375]. Treatment options for patients infected with resistant strains are limited and inappropriate treatment with broad spectrum antibiotics in these cases can further drive resistance [376]. Therefore the targeted treatment with appropriate antimicrobial agents is an important element in prognostic outcome [377, 378, 379]. As a result of this there is demand for techniques that are able to determine antibiotic susceptibility so that effective treatment can be administered.

Classical techniques for assessing susceptibility include disc diffusion [380] which involves spreading the bacterial culture over an agar plate before placing discs that are infused with on to the surface of the plate and incubating the plate for a period sufficient for the bacteria to grow. If the bacteria are sensitive then there is a gap between the bacterial lawn of the surface of the agar and the disc caused by the antibiotic in the disc diffusing into the agar thus preventing bacterial growth. This method is inexpensive and simple however it suffers from drawbacks such as taking a long time to generate a result as there are two culturing steps required each of which is at least 24 hours long, also analysing the results is a manual process which must be

carried out by a trained individual. As such assessing the bacteria on the plates takes more time and introduces the possibility of human error. The relative size of the discs and agar plates also creates efficiency problems.

Antimicrobial susceptibility testing can be improved by using spectrophotometry. The advantages to this approach include increased space efficiency if a 96 well plate reader is used to perform the measurements as well as the fact that the data measured in the form of absorbance is numerical and generated by an instrument which removes a step where human error may occur as well as enabling the automation of data processing. The disadvantage of this technique is that it is dependent upon expensive equipment that requires space and training to operate.

Sensors are an attractive platform for improving antimicrobial susceptibility testing. The aim of this section of research was to develop a technique based on screen printed sensors that may be used as an alternative to spectroscopy. The sensors can be incorporated into the design of the culturing vessel such as a multi well microtitre plate removing the need for a large expensive plate reader and facilitating high throughput measurements of the bacterial concentration in each well.

#### **8.2.3.2 Plasmid fitness cost**

Plasmids are extrachromosomal DNA elements that contain genes that confer traits which may be advantageous to their host cell. These traits include resistance to antimicrobials and biocides as well as heavy metal tolerance and factors that are associated with virulence [381]. Plasmids are interesting because they are a major mechanism by which antibiotic resistance is transferred horizontally between bacteria both within the same and different species [382, 383]. Research into elements that are associated with antimicro-

bial resistance involves the characterisation of fitness costs that are associated with maintaining plasmids and as such the sensors described here could be employed within a commercially produced assay where plasmid fitness cost is measured.

## **8.3 Electrochemical experimentation using screen printed electrodes and bacterial cultures**

### **8.3.1 Initial testing**

The aim of the initial testing was to test the viability of the concept of measuring bacterial growth with SPEs and the electrochemical technique square wave voltammetry. The culturing media 2YT was used, first sterile 2YT was measured followed by 2YT that had been inoculated with 1 $\mu$ l *L. casei* and incubated for 24 hours at 37°C. Measurements were carried out using the ANA-POT (Zimmer and Peacock) potentiostat by pipetting 100 $\mu$ l of culturing media onto the SPE and running the relevant test, the details of which are described below.

### **8.3.2 Square wave voltammetry**

The same SPE design described in Chapter 3 shown in Figure 3.2 was used however it was not functionalised with DMSO-melanin. The proof of concept for quantifying bacteria within a culturing media solution was first tested by measuring the signal current generated by square wave voltammetry that was applied to sterile culture media as well as media that had been inoculated

and reached the stationary phase of growth. As with the previous test using cyclic voltammetry, three different inks were tested for use as the reference electrode: silver, silver/silver chloride and carbon/graphite. There were clear and distinct differences within the patterns of the signal with all of the SPE types that were tested (Figure 8.2) however the signal measured using the carbon electrodes showed inconsistency. These results suggested that SPEs using silver and silver/silver chloride gave similar results and as such either reference electrode type would be suitable for further development.

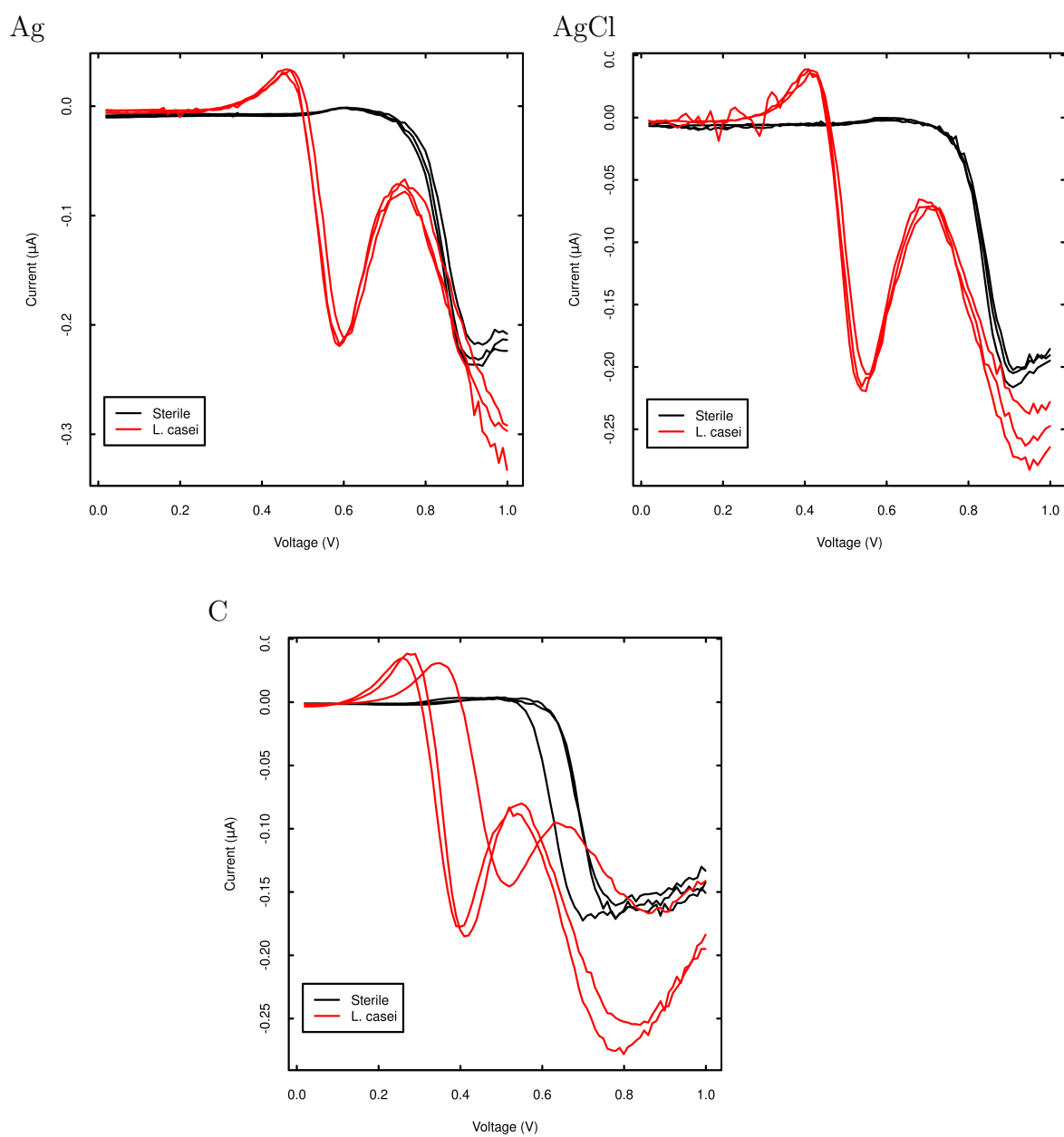


Figure 8.2: Square wave voltammogram of sterile and inoculated culturing media using screen printed electrodes with reference electrodes composed of either silver, silver/silver chloride or carbon/graphene ink.

#### **8.3.2.1 Voltammogram peaks and bacterial growth**

Having established that there is a clear distinct change in voltammogram measured utilising SPEs in sterile vs inoculated media, the next step was to determine whether these changes were dependent upon the yield of bacteria present within the media. A dose dependent signal would be useful because it would provide more information about how the bacteria are growing in the media such as whether they have partially grown which is useful for assays where growth rate is a point of interest such as when assessing antimicrobial resistance. Whether the signal varies based on dose was investigated by performing a serial dilution on the cultured media and repeating the test at each dilution point (Figure 8.3).

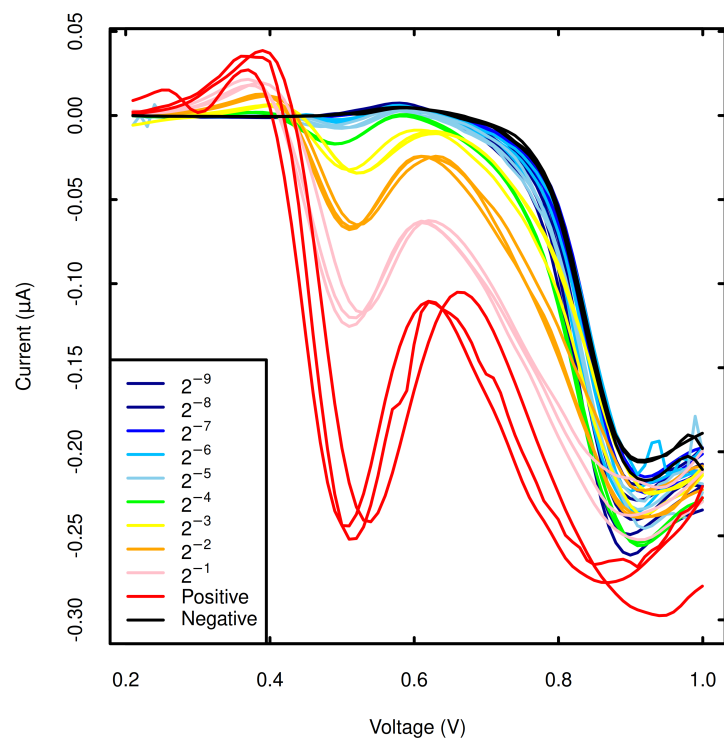


Figure 8.3: Square wave voltammogram obtained from each of the serially diluted culture media samples ranging from  $2^{-1}$  to  $2^{-9}$ . A fresh (previously unused) sensor was used for each measurement.

The positions of these peaks marked on the individual voltammograms is shown in Figure 8.4.



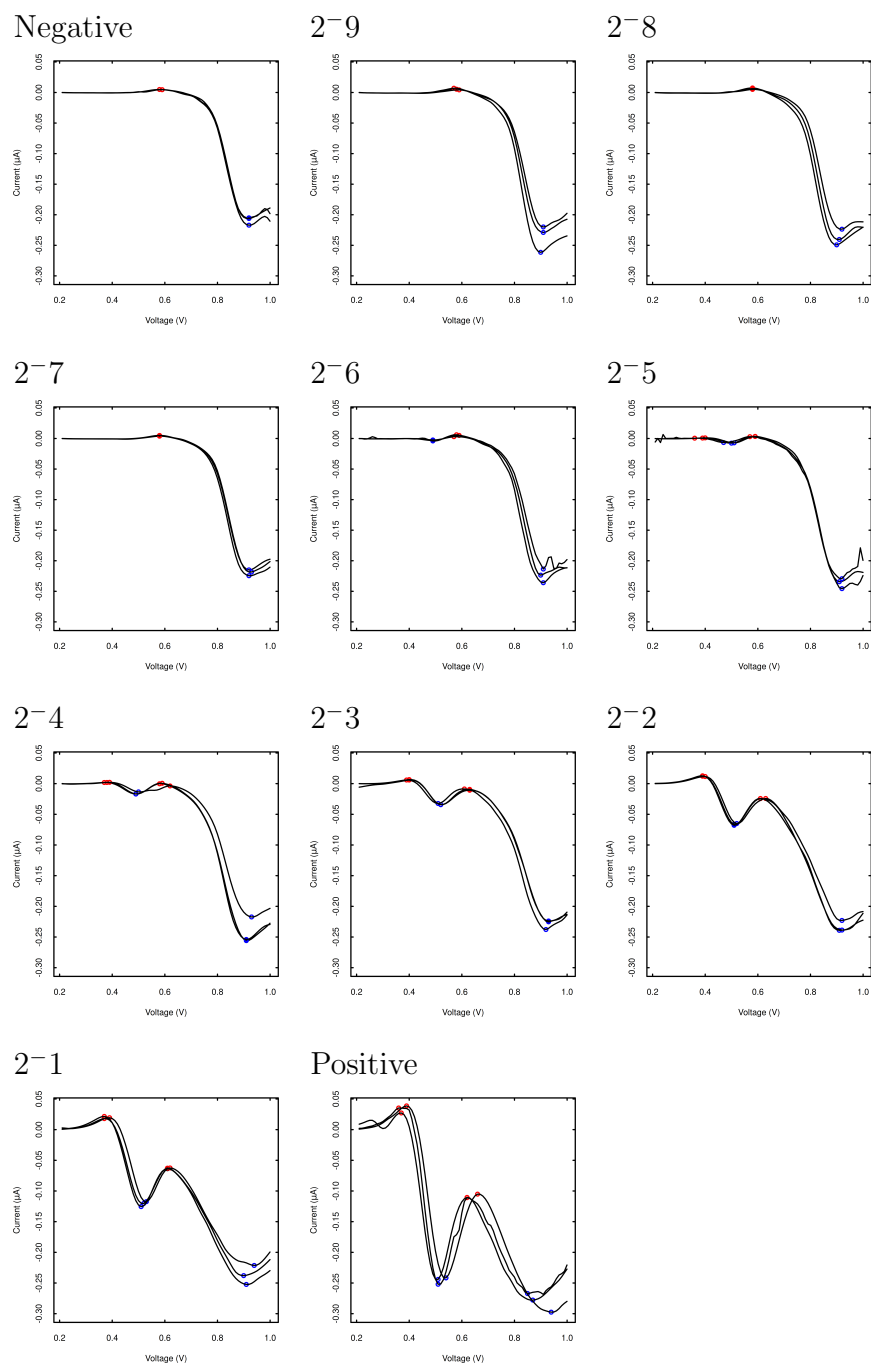


Figure 8.4: Individual peaks calculated for each of the serial dilutions. The maxima are shown in red and the minima are shown in blue. The difference between the peaks correlates with the concentration of *L. casei* in the media.

Analysis with polynomial regression showed a strong relationship between the peaks recorded in the voltammogram and the concentration of bacteria within the media (Figure 8.5). This suggests that the non functionalised SPEs can be used with CV to determine the number of bacteria within a culturing media solution by observing the size of the peaks on the voltammogram.

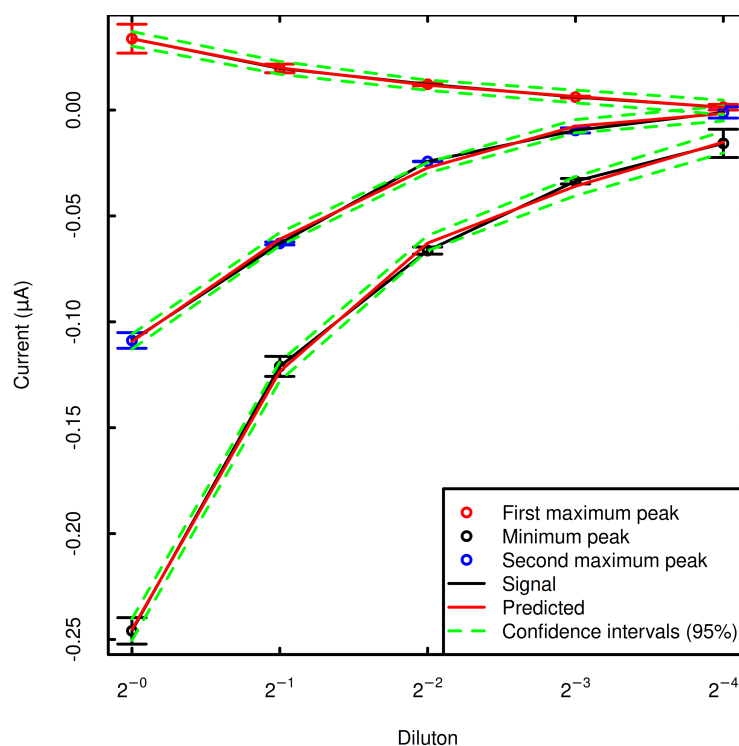


Figure 8.5: Maximum and minimum peaks plotted against bacterial dilution in media ranging from the media containing full growth to  $2^{-4}$ . Error bars represent the standard error times two. The predicted signal was obtained via polynomial regression. The  $R^2$  values for the first maximum peak, minimum peak and second maximum peak are 0.9599, 0.9964 and 0.9983 respectively.

The level of bacterial growth in each dilution was confirmed using UV spectroscopy (Figure 8.6).

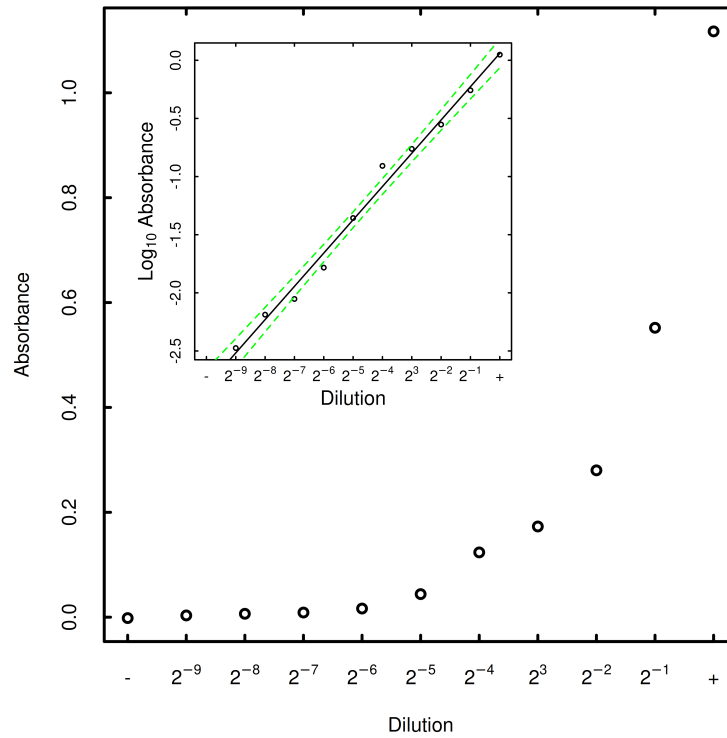


Figure 8.6: Absorbance of each *L. casei* serial dilution in LB measured using UV spectroscopy using a wavelength of 600nm. — represents sterile broth and + represents the undiluted bacterial culture. The inset graph shows the  $\log_{10}$  of the absorbance plotted against the dilution number. The  $R^2$  value is 0.9902.

## 8.4 Suitability of SPEs for taking repeat measurements

In order to assess whether the sensors are suitable for reuse the serial dilution test described above was repeated where each sensor was reused. The first reading was performed on the negative sterile sample followed by each of the incremental concentration increases through to the positive sample with full growth. The samples were measured in this order to simulate bacterial

growth where the number of bacteria that are present within the measured solution increases at each point of measurement. The results indicate that the sensors are not suitable to be reused as the clear pattern previously shown in Figure 8.3 was not longer observed and there were no obvious repeatable patterns in the voltammogram that correlated with bacterial concentration therefore suggesting that upon use something happens that degrades the sensor therefore making them only suitable to be used for one measurement before being discarded (Figure 8.7). It may be possible to refresh the sensor in order to allow it to be reused and avoid disposal however it is unknown whether this is possible and further research into this is required.

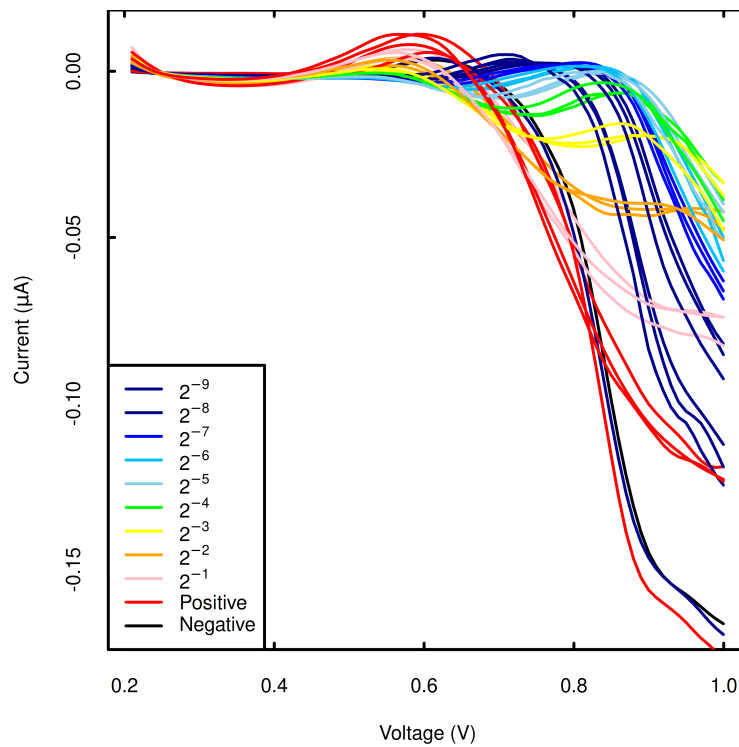


Figure 8.7: Square wave voltammogram from each of the serially diluted media run with reused sensors from negative to positive to simulate bacterial growth over time.

Characterisation techniques were employed in an attempt to understand what was happening at the electrode surface that causes the sensors to only be suitable for one usage.

#### **8.4.0.1 Impact of samples with growth vs without growth**

While it has been demonstrated above that applying square wave voltammetry to these sensors only produces a signal that has morphological characteristics that correlate with bacterial concentration if they have been previously unused, it was not clear whether the changes that impact upon the signal were predominantly a result of components within the media or the bacteria themselves. To investigate this a sensor was used to measure five sterile media samples concurrently (Figure 8.8), this was repeated using another sensor with media that contained bacterial cultures that had reached the stationary phase of growth (Figure 8.9).

These tests revealed that while running square wave voltammetry on both sterile media and media containing bacteria impacted upon the voltammogram obtained in subsequent measurements, they did not result in the same changes to the voltammogram.

In the case of the sterile media, presented in Figure 8.8, there was a clear shift in the voltage point where the measured current began to decrease where with each subsequent run this voltage point increased. Furthermore the reduction in the current measured decreased with each measurement. Despite these shifts the general morphology of the voltammogram remained consistent with that of a sterile media sample.

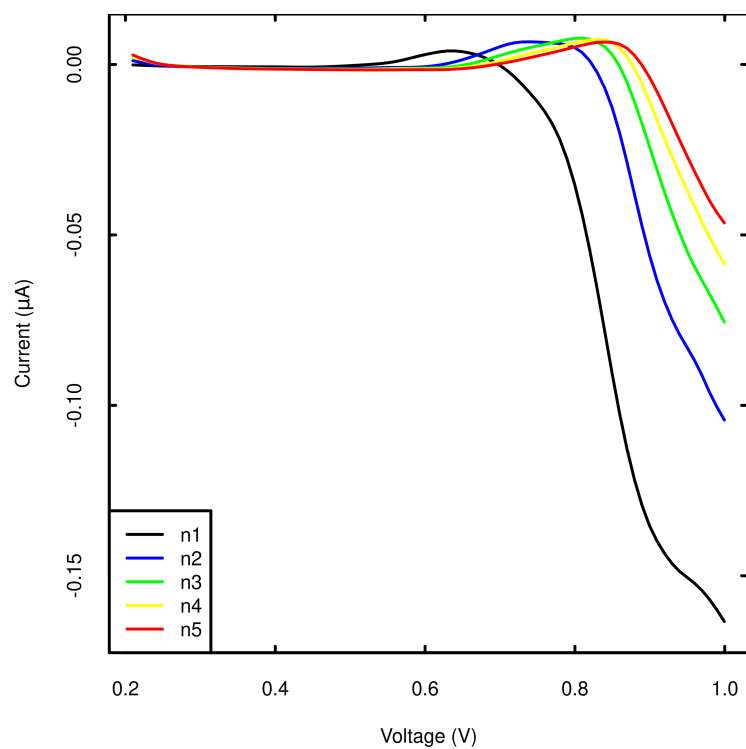


Figure 8.8: Voltammogram from a sensor that was used to measure five consecutive sterile media samples.

This contrasts with the voltammogram generated by repeatedly measuring media with bacterial growth shown in Figure 8.9.

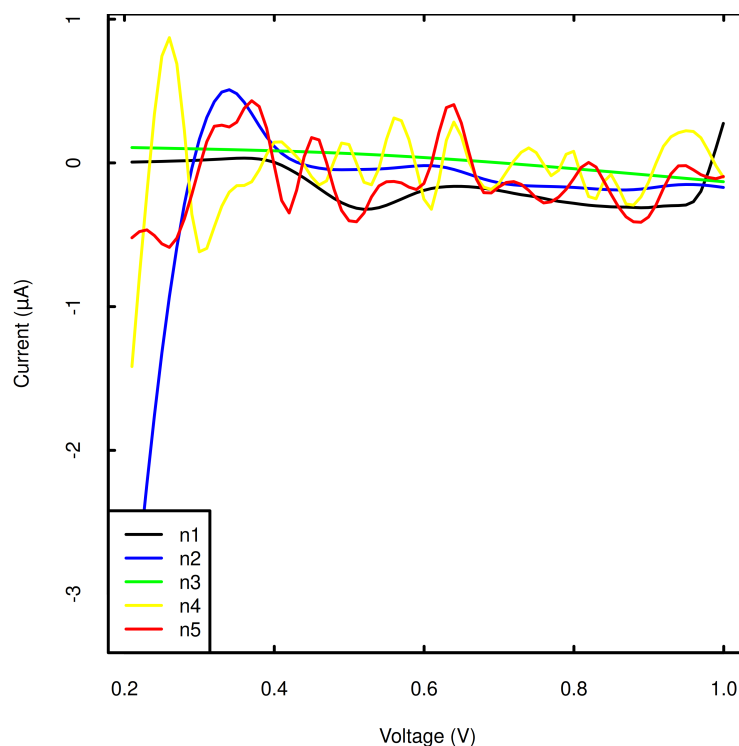


Figure 8.9: Voltammogram from a sensor that was used to measure five consecutive media samples that contained bacterial cultures that had reached the stationary phase of growth.

All voltammogram from the measurements that were carried out after the initial test appeared to show no consistent pattern. There was no incremental shift as had been the case when sterile media had been tested, the voltammogram appeared to be erratic noise that did not correlate with anything. These results suggest that the presence of bacteria within the media has the greatest impact upon the sensors and once square wave voltammetry has been carried out using media where there is bacterial growth present all further measurements will only produce noise. However while the sterile media alone did impact upon the voltammogram output following square wave voltammetry, it did so in the form of shifting the Voltage and current while

maintaining the general morphological characteristics of voltammogram generated when square wave voltammetry is carried out on sterile media. These results suggest that it might be possible to reuse the sensors provided that there has not been any prior bacterial growth however it is practically unlikely that the sensors will be exposed to sterile media given that this application involves bacterial culturing.

## **8.5 Investigation into effect of different culturing media on the signal generated**

Different microorganisms have a diverse range of nutritional requirements in order to grow. Therefore there are range of different culturing media with various components that have been optimised to facilitate the growth of certain species, or to inhibit the growth of undesirable species that may contaminate a batch. Therefore it is necessary to investigate whether the type of media that is used to culture the microorganism impacts upon the signal that is generated when using the sensor in order to have confidence that the signal that is measured is accurate.

### **8.5.1 Media tested**

The types of media that were tested included LB, BHI and 2YT. These are frequently used to culture bacteria in the fields of microbiology and molecular biology and as such are materials that it may be desirable to operate the sensors within. Because these media are used for the cultivation of different species with different requirements they contain different components. A summary of what composes these different media is presented on Table 8.1.



Table 8.1: The components that make up LB, 2YT and BHI culturing media.

Component	LB (g/l)	2YT (g/l)	BHI (g/l)
Tryptone	10	16	—
Peptone	—	—	10
NaCl	10	5l	5l
Yeast extract	5	10	—
Glucose	—	—	2
Disodium phosphate	—	—	2.5
Calf brain	—	—	200
Beef heart	—	—	250

The type of media that was used did appear to impact upon the morphology of the signal that was measured when square wave voltammetry was applied (Figure 8.10 and 8.11).

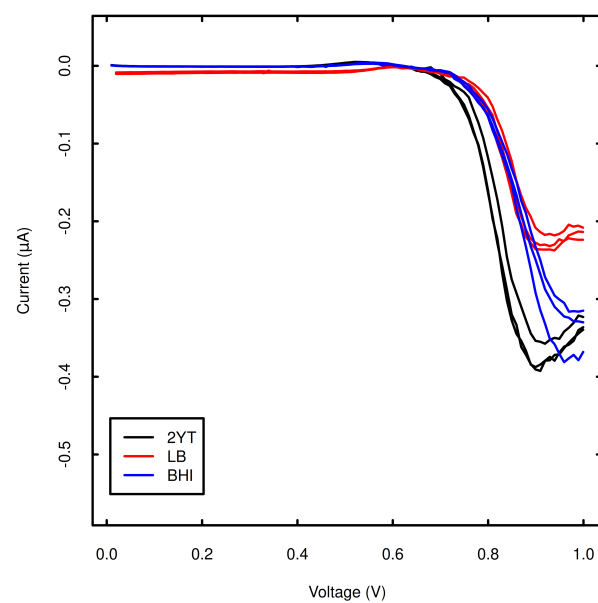


Figure 8.10: Voltammogram measured from square wave voltammetry applied to the SPE in different types of sterile (has not been inoculated) media.

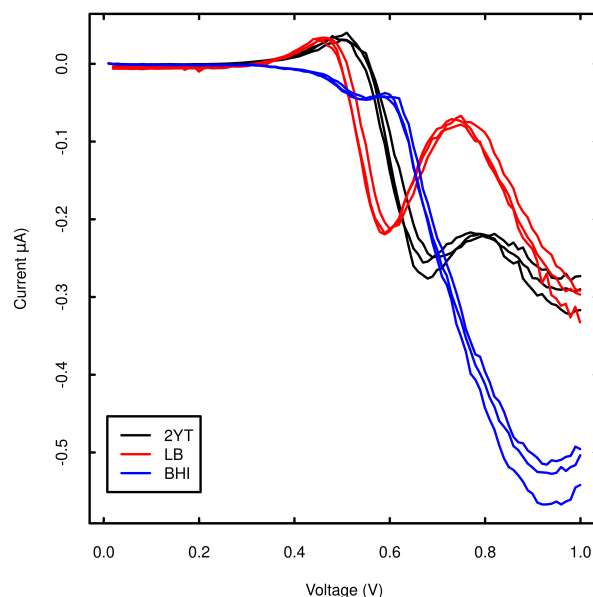


Figure 8.11: Different media types were inoculated with *L. casei* bacteria, the morphology of the voltammogram appears to be influenced by the type of media that the bacteria were grown in. This is possibly due to the media being composed of different substances as shown in Table 8.1.

## 8.6 Testing with different species of microorganisms

There are many different species of microorganisms which contain different components and as such may react differently to square wave voltammetry than the *L. casei* species of bacteria that had been tested previously. As *L. casei* is a Gram positive bacteria, *E. coli* a Gram negative bacteria and *Saccharomyces cerevisiae* a yeast were tested in the same manner in order to observe whether this technique is as effective for the quantification of microbial species that are structurally different from *L. casei*.

There were stark differences observed in the voltammograms that were mea-

sured when square wave voltammetry was applied to LB media that had different microorganisms being cultured in it (Figure 8.12). The voltammograms produced were repeatable and consistent (n=3). The strongest signal was observed when the procedure was carried out on *L. casei* bacteria however the signal produced when measuring the other microorganisms differed sufficiently from one another as well as the sterile LB which contained no microorganisms.

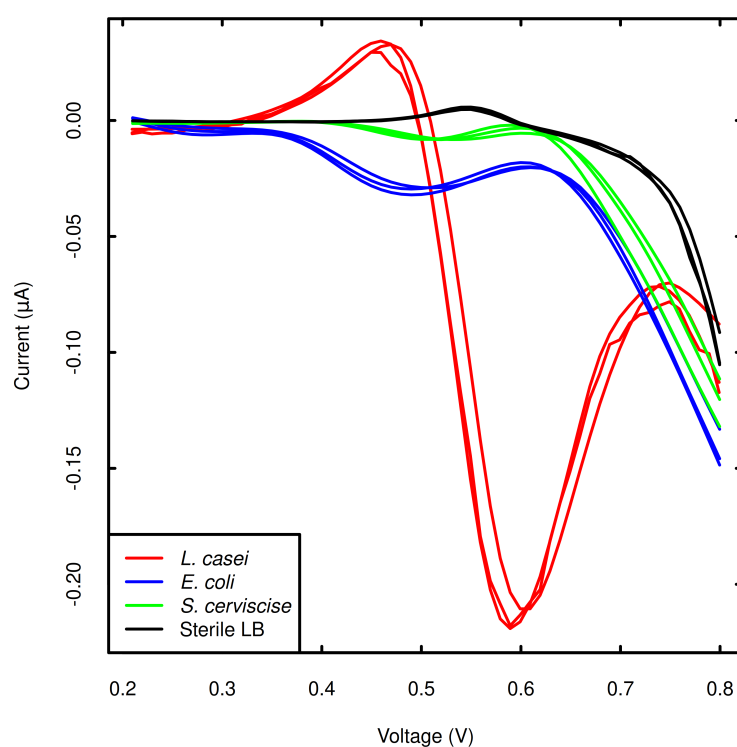


Figure 8.12: Square wave voltammogram of sterile LB media and media that has various microbial cultures growing in it.

## 8.7 Discussion

This chapter demonstrates the proof of concept that a non functionalised SPE and can be used in applications based on electrochemical techniques as well as the proof of concept that square wave voltammetry has the potential to be used in different applications that involve microorganisms. Reference electrodes that were composed of either silver or silver/silver chloride appeared to be more suitable than carbon/graphene. The square wave voltammograms that were obtained using the different species of microorganisms was consistently different depending upon what the microorganism being tested was. This phenomena might be a suitable base for developing a system that is able to rapidly identify an unknown microorganism by comparing the voltammogram of an unknown microoganmism to an established library in a database. Further work is needed in order to establish whether this is the case however the data presented in this chapter makes the case that further investigation is potentially worthwhile. The microbial species that were investigated over the course of this chapter were very different from one another. *L. casei* is a Gram positive bacteria, *E. coli* is a Gram negative bacteria and *S. cerevisiae* is a species of yeast. Due to this the structures of the cell walls of these microorganisms is very different and is comprised of different components. It is possible that it is these differences in cellular structure that are responsible for the differences in the voltammograms generated using the different species. An interesting study to investigate this further would be to expand on the testing presented in this chapter to include multiple species of each type (Gram positive, Gram negative and yeast) to see whether the differences in voltammogram are consistent according to type. Should this be the case then this method could be a replacement for the laborious and time consuming Gram staining test that was first developed in 1884 and is still

widely used in healthcare settings today [384].

The other aspect of this chapter demonstrated the proof of concept that when square wave voltammetry is applied to culturing media that contains different concentrations of *L. casei* bacteria the resulting voltammogram contains peaks that correlate with the concentration of bacteria in a dose dependent manner. This is an interesting observation that has the potential to be deployed in applications where the concentration of bacteria in a solution needs to be rapidly quantified. However there were some notable limitations associated with this method. One limitation is that the measurement can only be performed once before the electrode is “spent” and cannot be used for any further measurements. However the sensor still has the potential to be useful in situations where only one measurement is required. An example application would be the incorporation of these sensors within a 96 well microtitre plate that is used to culture bacteria in media that contains antibiotics where a single measurement is taken after an incubation period which assesses whether they are sensitive to the antibiotic. Further testing would need to investigate whether the presence of each antibiotic in the media impacts upon the morphology of the voltammograms that are produced.

## 8.8 Summary

This chapter details the development of a novel method for elucidating characteristics of microorganisms that are growing within a culturing media using nonfunctionalised carbon/graphene SPEs. The characteristics that were investigated include the type of microorganism growing in the media - further research may lead to useful applications involving the detection of contam-

ination where there may be undesired species growing. Another key characteristic investigated was determining the yield of bacteria growing in a media solution. Due to the testing environments being controlled where the only differing variable is whether the culturing media contains microorganisms or not it was hypothesised that the functionalisation of the working electrode may not be necessary since living cells and their components have electrochemical properties [385, 386, 387, 388, 389]. Therefore their presence or absence may be sufficient to change the voltammograms in a manner that could then be correlated with known characteristics (such as species or growth yield). This early novel work demonstrating that a combination of non-functionalised SPEs and square wave voltammetry may potentially be used together in methods that are useful in biological culturing applications. The results that are presented here are promising however they show an early proof of concept and further research is required in order to develop them into established methods and products. Such potential applications include measuring microbiological growth in a solution as well as possibly being able to identify information about what microorganism is growing by features that are associated with its voltammetric fingerprint. However there needs to be further research in order to determine whether this is possible and if so how much information can be determined from this fingerprint and what effect other factors such as culturing media have on it. At the time of writing, a literature search for applications using non functionalised sensors does not yield any studies that report this suggesting that the idea of finding applications for carbon based sensors that have not undergone any sort of functionalisation is under explored. The next chapter will outline a summary of the work that has been presented over the chapters of this thesis and provide an overall conclusion.

## Chapter 9

# Conclusion and future work

This work has focussed on the development of sensors that utilise carbon electrodes and are suitable for applications where there is a real world benefit. The primary objective was to implement nanomaterials such as carbon/graphene and DMSO-melanin in biosensing applications with a focus on applications that are useful in biotechnological and clinical settings. The proof of concept for such applications was investigated and demonstrated and the materials used were characterised. The processing techniques and the experimental procedures employed have been documented.

### 9.1 Novelty

This work includes the development of a novel screen printed DMSO-melanin pH sensor (Chapter 5). Other novel features include this being the first time that a screen printed pH sensor has been successfully demonstrated as being sensitive to pH in the presence of bacterial cultures (Chapter 6) as well as being the first time that a screen printed pH sensor has been tested in a preclinical model using blood samples (Chapter 7). This work is also the



first time that a nonfunctionalised SPE has been demonstrated in a useful application in determining the concentration of bacteria in culturing media as well as potentially being able to identify bacterial species electrochemically (Chapter 8).

## 9.2 Conclusion

Screen printed electrodes were produced and characterised. SEM analysis of the surface of the working electrode revealed that it consists of a mixture of carbon black and graphitic flakes. The SWV and EIS measurements were consistent between different SPEs indicating that the sensors have been produced to a consistent quality. Little variation in the contact resistance measurements further indicate that the sensors are consistent. Printed sensors from different positions on the screen were measured for thickness using WLI showed similar thickness across the tested sensors with the conductive silver ink having mean thickness of  $10.625\mu\text{m}$  with a standard deviation of 0.861 and the carbon/graphite ink had a mean thickness of  $8.61\mu\text{m}$  with a standard deviation of 0.87. These characterisation tests indicated that were of sufficient quality to take forward for the development of further applications and research.

The candidate materials for functionalisation that facilitate sensitivity to pH were assessed and a SPE produced in house and functionalised with by spin coating a layer of DMSO-melanin onto the working electrode was identified as being the best candidate material for producing the pH sensor over  $\text{Al}_2\text{O}_3$  and PANI. This is due to this sensor showing the most stability and the least variation across the three standard reference buffers at pH4, pH7 and pH10 with a sensitivity of  $-49.79\text{mV/pH} \pm 8.93$  and a drift of  $5.9\text{mV}$  over

10 minutes, this sensor is relatively easy to make as well as sensitive. The DMSO-melanin sensor also demonstrated that it could be reused as testing where the sensor was exposed to pH4 followed by pH7 and pH10 reference buffers then pH7 and pH4 again it showed consistent signal output. This was not the case with the commercially available SPEs that had been functionalised with PANI as while these sensors demonstrated a good sensitivity and good repeatability at low pH levels they showed a high variation at a high pH levels and they were also unable to recover after being exposed to a high pH as their sensitivity to pH7 and pH4 reference buffers was greatly reduced following exposure to the pH10 reference buffer. Characterisation studies showed that the application of DMSO-melanin to the surface of the working electrode demonstrated that the contact resistance of the electrode changed. The DMSO-melanin molecules were too small to visualise under the SEM however evidence that the DMSO-melanin was present on the surface of the working electrode following application was detected in the spectra generated by Raman spectroscopy, FTIR and AFM. This chapter demonstrates the initial proof of concept that an in house fabricated SPE with a working electrode functionalised with DMSO-melanin produces a pH sensor.

The DMSO-melanin pH sensor was tested under conditions that are relevant to applications involving measuring the pH of bacterial culturing media. The functional range of the pH sensor was shown to be effective in measuring changes in pH over a physiologically relevant range of pH5 to pH8 in reference buffers along with three relevant culturing media solutions. The pH sensor was also demonstrated as being effective in being able to accurately measure the pH of these media solutions following the inoculation and culturing of lactic acid bacteria to stationary phase within them thereby demonstrating a real world application where these sensors can be deployed. This chapter

demonstrates that the pH sensor is reliable and accurate enough to be used to measure the pH of culturing media and the presence of lactic acid bacteria in the media does not interfere with the measurement.

The suitability of the pH sensor for use in clinical applications measuring blood pH was investigated. As the pH sensor had been demonstrated to be successful in determining the pH of solutions of both reference buffers and biological culturing environments an investigation was carried out to determine whether the pH sensor would be able to measure the pH of blood. The data suggested that in its current form the pH sensor is unable to measure the pH of blood in an accurate or consistent manner. The potentiograms showed a decay in the voltage measured in both blood and plasma samples over the 10 minute measurement period. An investigation into using alternative materials for the reference electrode was carried out and while this did reduce the decay in measured potential over time there was still a significant variation in the potentiograms of replicates from the same samples meaning that the measured voltage cannot be used to infer the pH of the sample. Overall this chapter shows that the DMSO-melanin pH sensor is not suitable for measuring the pH of blood samples in its current format.

An investigation was carried out utilising non-functionalised screen printed electrodes to investigate whether they can be utilised alongside SWV to analyse microbes within culturing media. Three different microbes were tested with varying successes. Using the non functionalised SPEs with SWV on media with LB that had been serially diluted with *L. casei* cultures showed a large difference in voltamogram signal of the measured peaks, the relationship between the measured peaks and the concentration of bacteria in the solution was analysed via polynomial regression and the peaks on the voltammogram were able to predict the concentration of bacteria in the sample with a confi-

dence interval of 95% up to a concentration of  $2^{-3}$  after which the differences between the measured peak current are insufficient. Further investigation using the bacteria *E. coli* and fungi *S. cerevisiae* revealed differences in the signal of the voltammogram suggesting that there might be limitations on what species this technique is effective with however there is also the possibility that these differences in signal may be used to differentiate between different species or order, more research is required investigating this more thoroughly. Overall this chapter provides an interesting proof of concept with regards to utilising non functionalised SPEs and electrochemical processes to develop analytical techniques that are potentially useful.

### 9.2.1 Future work

The findings of this research can be used as a base for further research and development of these sensors and their potential applications. The pH sensor that was fabricated in Chapters 3 and 5 that was shown to measure pH in the presence of live bacterial cultures accurately in Chapter 6 could be integrated into a bioreactor or into the wells of a microtitre plate in order to provide continuous pH monitoring during culturing experiments or quality assurance data. It was also determined in Chapter 6 that the type of culturing media that was used to grow bacteria in changed the calibration slope, therefore future work could involve developing a library of data for each different type of culturing media for calculating the pH after growth has taken place.

Further work is needed to investigate the potential of the pH sensor being able to measure blood samples for clinical applications. Chapter 7 shows that the current design of DMSO-melanin pH sensors are unable to measure the pH of blood samples and that this is likely due to the presence of interfering components in the blood that exist in variable unknown concen-

trations. Work to remedy this situation could focus on modifying the sensor and testing its fabrication with different materials such as gold, changing the number of electrodes or by developing and incorporating other sensors that detect the levels of interfering substances to see whether this can be used to normalise the pH measurement.

The proof of concept work presented in Chapter 8 can be built upon by testing the application of SWV with different species of microbiota to establish whether the shape of the voltammograms produced can be used to identify specific characteristics such as whether the microorganism present is a yeast or bacteria or whether the bacteria present is Gram positive or Gram negative, it may even be possible to identify specific bacterial species by the shape of the voltammogram. This could lead to the development of rapid screening tests for environmental and medical applications.

### **9.2.2 Research goals outcome**

This research project set out to fabricate a DMSO-melanin pH sensor that is able to accurately measure the pH of real samples rather than just reference buffer solutions. This has been achieved as the sensor has demonstrated accuracy when measuring the pH of culturing media both when bacteria are present and absent. The project also aimed to investigate the suitability of this sensor for use in a point of care test for lactic acidosis and while progress has been made in this area in that the sensor appears to be sensitive enough to detect the small changes in pH necessary to screen for lactic acidosis, there appear to be variable components within the blood that interfere with the measurement so therefore more work is required if this is to be a successful application. This research also successfully identified a potential application for detecting characteristics of microorganisms in culturing media utilising

sensors that have not been functionalised. Prior to this work applications involving SPEs that had not undergone any functionalisation procedure was a gap in the research.

# References

- [1] Turner AP. Biosensors: sense and sensibility. Chemical Society Reviews. 2013;42(8):3184–3196.
- [2] Faridbod F, Gupta VK, Zamani HA. Electrochemical Sensors and Biosensors. International Journal of Electrochemistry. 2011;.
- [3] Karimi-Maleh H, Karimi F, Alizadeh M, Sanati AL. Electrochemical sensors, a bright future in the fabrication of portable kits in analytical systems. The Chemical Record. 2020;20(7):682–692.
- [4] Doughty J. The advantages of a soil paste for routine pH determination. Scientific Agriculture. 1941;22(3):135–138.
- [5] Lattanzio Jr FA. The effects of pH and temperature on fluorescent calcium indicators as determined with Chelex-100 and EDTA buffer systems. Biochemical and biophysical research communications. 1990;171(1):102–108.
- [6] Válek T, Pohanka M. The Determination of Lipase Activity by Measuring pH Using ion-Sensitive Field-effect Transistor. biosensors. 2021;16:17.
- [7] Dickson AG. The measurement of sea water pH. Marine Chemistry. 1993;44(2-4):131–142.

- [8] Glasoe PK, Long F. Use of glass electrodes to measure acidities in deuterium oxide1, 2. *The Journal of Physical Chemistry*. 1960;64(1):188–190.
- [9] Baishya N, Mamouei M, Budidha K, Qassem M, Vadgama P, Kyriacou P. In-vitro spectrometric analysis of hyperlactatemia and lactic acidosis in buffer relating to sepsis. *Journal of Near Infrared Spectroscopy*. 2021;29(1):53–59.
- [10] Bijapur MB, Kudligi NA, Asma S. Central venous blood gas analysis: an alternative to arterial blood gas analysis for pH, PCO<sub>2</sub>, bicarbonate, sodium, potassium and chloride in the Intensive Care Unit patients. *Indian Journal of Critical Care Medicine: Peer-reviewed, Official Publication of Indian Society of Critical Care Medicine*. 2019;23(6):258.
- [11] Uysal O, Sevimli T, Sevimli M, Gunes S, Sariboyaci AE. Cell and tissue culture: the base of biotechnology. In: *Omics technologies and bio-engineering*. Elsevier; 2018. p. 391–429.
- [12] Ferrari AGM, Rowley-Neale SJ, Banks CE. Screen-printed electrodes: Transitioning the laboratory in-to-the field. *Talanta Open*. 2021;3:100032.
- [13] Ono S, Imai R, Ida Y, Shibata D, Komiya T, Matsumura H. Increased wound pH as an indicator of local wound infection in second degree burns. *Burns*. 2015;41(4):820–824.
- [14] Kim DH, Park JC, Jeon GE, Kim CS, Seo JH. Effect of the size and shape of silver nanoparticles on bacterial growth and metabolism by monitoring optical density and fluorescence intensity. *Biotechnology and Bioprocess Engineering*. 2017;22(2):210–217.



- [15] Wu M, Hu X, Zhang Q, Xue D, Zhao Y. Growth environment optimization for inducing bacterial mineralization and its application in concrete healing. *Construction and Building Materials*. 2019;209:631–643.
- [16] Brogan DM, Mossialos E. A critical analysis of the review on antimicrobial resistance report and the infectious disease financing facility. *Globalization and health*. 2016;12(1):1–7.
- [17] for Microbiology Investigations US. Test procedures. *Public Health England*. 2019;39:13–15.
- [18] St-Louis P. Status of point-of-care testing: promise, realities, and possibilities. *Clinical biochemistry*. 2000;33(6):427–440.
- [19] Shaw JL. Practical challenges related to point of care testing. *Practical laboratory medicine*. 2016;4:22–29.
- [20] Mitra P, Sharma P. POCT in developing countries. *EJIFCC*. 2021;32(2):195.
- [21] Prattis I, Hui E, Gubeljak P, Schierle GSK, Lombardo A, Occhipinti LG. Graphene for biosensing applications in point-of-care testing. *Trends in Biotechnology*. 2021;39(10):1065–1077.
- [22] Gethin G, et al. The significance of surface pH in chronic wounds. *Wounds uk*. 2007;3(3):52.
- [23] Nischwitz S, de Mattos IB, Hofmann E, Groeber-Becker F, Funk M, Mohr G, et al. Continuous pH monitoring in wounds using a composite indicator dressing—a feasibility study. *Burns*. 2019;45(6):1336–1341.

- [24] Novoselov KS, Geim AK, Morozov SV, Jiang D, Zhang Y, Dubonos SV, et al. Electric field effect in atomically thin carbon films. *science*. 2004;306(5696):666–669.
- [25] Neto AC, Guinea F, Peres NM, Novoselov KS, Geim AK. The electronic properties of graphene. *Reviews of modern physics*. 2009;81(1):109.
- [26] Ergun S. Structure of graphite. *Nature physical science*. 1973;241(107):65–67.
- [27] Gui G, Li J, Zhong J. Band structure engineering of graphene by strain: First-principles calculations. *Physical Review B*. 2008;78(7):075435.
- [28] Meyer JC, Geim AK, Katsnelson MI, Novoselov KS, Booth TJ, Roth S. The structure of suspended graphene sheets. *Nature*. 2007;446(7131):60–63.
- [29] Hass J, De Heer W, Conrad E. The growth and morphology of epitaxial multilayer graphene. *Journal of Physics: Condensed Matter*. 2008;20(32):323202.
- [30] Sutter PW, Flege JI, Sutter EA. Epitaxial graphene on ruthenium. *Nature materials*. 2008;7(5):406–411.
- [31] Sarma SD, Adam S, Hwang E, Rossi E. Electronic transport in two-dimensional graphene. *Reviews of modern physics*. 2011;83(2):407.
- [32] Shao Y, Wang J, Wu H, Liu J, Aksay IA, Lin Y. Graphene based electrochemical sensors and biosensors: a review. *Electroanalysis: An International Journal Devoted to Fundamental and Practical Aspects of Electroanalysis*. 2010;22(10):1027–1036.

- [33] Han T, Mattinen U, Bobacka J. Improving the sensitivity of solid-contact ion-selective electrodes by using coulometric signal transduction. *ACS sensors*. 2019;4(4):900–906.
- [34] Salmanpour S, Khalilzadeh MA, Karimi-Maleh H, Zareyeea D. An electrochemical sensitive sensor for determining sulfamethoxazole using a modified electrode based on biosynthesized NiO nanoparticles paste electrode. *Int J Electrochem Sci*. 2019;14:9552–9561.
- [35] Jiwanti PK, Natsui K, Einaga Y. The Utilization of Boron-doped Diamond Electrodes for the Electrochemical Reduction of CO<sub>2</sub>: Toward the production compounds with a high number of carbon atoms. *Electrochemistry*. 2019;87(2):109–113.
- [36] Altintas Z, Akgun M, Kokturk G, Uludag Y. A fully automated microfluidic-based electrochemical sensor for real-time bacteria detection. *Biosensors and Bioelectronics*. 2018;100:541–548.
- [37] Castle LM, Schuh DA, Reynolds EE, Furst AL. Electrochemical sensors to detect bacterial foodborne pathogens. *ACS sensors*. 2021;6(5):1717–1730.
- [38] Bai Y, Xu T, Zhang X. Graphene-based biosensors for detection of biomarkers. *Micromachines*. 2020;11(1):60.
- [39] Hao Z, Wang Z, Li Y, Zhu Y, Wang X, De Moraes CG, et al. Measurement of cytokine biomarkers using an aptamer-based affinity graphene nanosensor on a flexible substrate toward wearable applications. *Nanoscale*. 2018;10(46):21681–21688.
- [40] Kumar S, Kalkal A. Electrochemical detection: Cyclic voltammetry/differential pulse voltammetry/impedance spectroscopy. *Nanotechnol-*

ogy in Cancer Management: Precise Diagnostics toward Personalized Health Care. 2021;p. 43.

- [41] Tehrani Z, Burwell G, Azmi MM, Castaing A, Rickman R, Almarashi J, et al. Generic epitaxial graphene biosensors for ultrasensitive detection of cancer risk biomarker. *2D Materials*. 2014;1(2):025004.
- [42] Gorton L. Biosensors and modern biospecific analytical techniques. Elsevier; 2005.
- [43] Tenaillon O, Skurnik D, Picard B, Denamur E. The population genetics of commensal *Escherichia coli*. *Nature reviews microbiology*. 2010;8(3):207–217.
- [44] Pennington H. *Escherichia coli* O157. *The Lancet*. 2010;376(9750):1428–1435.
- [45] Valilis E, Ramsey A, Sidiq S, DuPont HL. Non-O157 Shiga toxin-producing *Escherichia coli*—a poorly appreciated enteric pathogen: systematic review. *International Journal of Infectious Diseases*. 2018;76:82–87.
- [46] Mathew FP, Alocilja EC. Porous silicon-based biosensor for pathogen detection. *Biosensors and bioelectronics*. 2005;20(8):1656–1661.
- [47] Giovanni M, Setyawati MI, Tay CY, Qian H, Kuan WS, Leong DT. Electrochemical quantification of *Escherichia coli* with DNA nanostructure. *Advanced Functional Materials*. 2015;25(25):3840–3846.
- [48] Sharma M, Goel A, Singh L, Rao V. Immunological biosensor for detection of *Vibrio cholerae* O1 in environmental water samples. *World Journal of Microbiology and Biotechnology*. 2006;22(11):1155–1159.

- [49] Antunez EE, Mahon CS, Tong Z, Voelcker NH, Mullner M. A regenerable biosensing platform for bacterial toxins. *Biomacromolecules*. 2020;22(2):441–453.
- [50] Manoharan H, Kalita P, Gupta S, Sai V. Plasmonic biosensors for bacterial endotoxin detection on biomimetic C-18 supported fiber optic probes. *Biosensors and Bioelectronics*. 2019;129:79–86.
- [51] Fuentes-Arderiu X. What is a biomarker? It's time for a renewed definition. *Clinical chemistry and laboratory medicine*. 2013;51(9):1689–1690.
- [52] Katan M, Elkind MS. Inflammatory and neuroendocrine biomarkers of prognosis after ischemic stroke. *Expert review of neurotherapeutics*. 2011;11(2):225–239.
- [53] Galvez-Contreras AY, Campos-Ordóñez T, Lopez-Virgen V, Gomez-Plascencia J, Ramos-Zuniga R, Gonzalez-Perez O. Growth factors as clinical biomarkers of prognosis and diagnosis in psychiatric disorders. *Cytokine & growth factor reviews*. 2016;32:85–96.
- [54] Kiebish MA, Cullen J, Mishra P, Ali A, Milliman E, Rodrigues LO, et al. Multi-omic serum biomarkers for prognosis of disease progression in prostate cancer. *Journal of translational medicine*. 2020;18(1):1–10.
- [55] Qiu FM, Yu JK, Chen YD, Jin QF, Sui MH, Huang J. Mining novel biomarkers for prognosis of gastric cancer with serum proteomics. *Journal of Experimental & Clinical Cancer Research*. 2009;28(1):1–7.
- [56] Mahmudunnabi RG, Farhana FZ, Kashaninejad N, Firoz SH, Shim YB, Shiddiky MJ. Nanozyme-based electrochemical biosensors for disease biomarker detection. *Analyst*. 2020;145(13):4398–4420.

- [57] Senf B, Yeo WH, Kim JH. Recent advances in portable biosensors for biomarker detection in body fluids. *Biosensors*. 2020;10(9):127.
- [58] Santotoribio JD, Cañavate-Solano C, Quintero-Prado R, González-Macías C, Soto-Pazos E, Vilar-Sanchez Á, et al. Neuroapoptosis in newborns with respiratory acidosis at birth. *Clinical biochemistry*. 2019;74:69–72.
- [59] Racinet C, Ouellet P, Muraskas J, Daboval T. Neonatal cord blood eucapnic pH: a potential biomarker predicting the need for transfer to the NICU. *Archives de Pédiatrie*. 2020;27(1):6–11.
- [60] Baliga S, Muglikar S, Kale R. Salivary pH: A diagnostic biomarker. *Journal of Indian Society of Periodontology*. 2013;17(4):461.
- [61] Yang J, Kwak TJ, Zhang X, McClain R, Chang WJ, Gunasekaran S. Iridium Oxide-reduced Graphene Oxide Nanohybrid Thin Film Modified Screen-printed Electrodes as Disposable Electrochemical Paper Microfluidic pH Sensors. *Journal of visualized experiments: JoVE*. 2016;53339(117).
- [62] Lemos SG, Nogueira ARA, Torre-Neto A, Parra A, Alonso J. Soil calcium and pH monitoring sensor system. *Journal of agricultural and food chemistry*. 2007;55(12):4658–4663.
- [63] Guinovart T, Valdés-Ramírez G, Windmiller JR, Andrade FJ, Wang J. Bandage-Based Wearable Potentiometric Sensor for Monitoring Wound pH. *Electroanalysis*. 2014;26(6):1345–1353.
- [64] Phulara SC, Chaturvedi P, Chaurasia D, Diwan B, Gupta P. Modulation of culture medium confers high-specificity production of isopen-

- tenol in *Bacillus subtilis*. *Journal of Bioscience and Bioengineering*. 2018;.
- [65] Abdel-Rahman MA, Tashiro Y, Sonomoto K. Recent advances in lactic acid production by microbial fermentation processes. *Biotechnology advances*. 2013;31(6):877–902.
  - [66] Badnjević A, Beganović E, Mušić O. Facts about solution based and cartridge based devices for blood gas analysis. In: 2011 18th International Conference on Systems, Signals and Image Processing. IEEE; 2011. p. 1–5.
  - [67] Yuqing M, Jianrong C, Keming F. New technology for the detection of pH. *Journal of biochemical and biophysical methods*. 2005;63(1):1–9.
  - [68] Baucke F. The glass electrode—applied electrochemistry of glass surfaces. *Journal of Non-Crystalline Solids*. 1985;73(1-3):215–231.
  - [69] Palleschi G, Volpe G, Compagnone D, La Notte E, Esti M. Bioelectrochemical determination of lactic and malic acids in wine. *Talanta*. 1994;41(6):917–923.
  - [70] Komaba S, Seyama M, Momma T, Osaka T. Potentiometric biosensor for urea based on electropolymerized electroinactive polypyrrole. *Electrochimica acta*. 1997;42(3):383–388.
  - [71] Janata J. Potentiometric microsensors. *Chemical Reviews*. 1990;90(5):691–703.
  - [72] Contractor A, Sureshkumar TN, Narayanan R, Sukeerthi S, Lal R, Srinivasa R. Conducting polymer-based biosensors. *Electrochimica Acta*. 1994;39(8-9):1321–1324.

- [73] Ben-David O, Shafir E, Gilath I, Prior Y, Avnir D. Simple Absorption Optical Fiber pH Sensor Based on Doped Sol- Gel Cladding Material. *Chemistry of materials*. 1997;9(11):2255–2257.
- [74] Wu MH, Lee CD, Pan TM. High dielectric constant  $\text{PrY}_x\text{O}_y$  sensing films electrolyte-insulator-semiconductor pH-sensor for the detection of urea. *Analytica chimica acta*. 2009;651(1):36–41.
- [75] Fog A, Buck RP. Electronic semiconducting oxides as pH sensors. *Sensors and Actuators*. 1984;5(2):137–146.
- [76] Huang WD, Cao H, Deb S, Chiao M, Chiao JC. A flexible pH sensor based on the iridium oxide sensing film. *Sensors and Actuators A: Physical*. 2011;169(1):1–11.
- [77] Rahimi R, Ochoa M, Parupudi T, Zhao X, Yazdi IK, Dokmeci MR, et al. A low-cost flexible pH sensor array for wound assessment. *Sensors and Actuators B: Chemical*. 2016;229:609–617.
- [78] Manjakkal L, Cvejic K, Kulawik J, Zaraska K, Szwagierczak D, Stojanovic G. Sensing mechanism of  $\text{RuO}_2\text{-SnO}_2$  thick film pH sensors studied by potentiometric method and electrochemical impedance spectroscopy. *Journal of Electroanalytical Chemistry*. 2015;759:82–90.
- [79] Hashimoto T, Miwa M, Nasu H, Ishihara A, Nishio Y. pH Sensors Using 3d-Block Metal Oxide-Coated Stainless Steel Electrodes. *Electrochimica Acta*. 2016;220:699–704.
- [80] Melai B, Salvo P, Calisi N, Moni L, Bonini A, Paoletti C, et al.; IEEE. A graphene oxide pH sensor for wound monitoring. 38th Annual International Conference of the IEEE Engineering in Medicine and Biology Society (EMBC). 2016;p. 1898–1901.



- [81] Ameri SK, Singh PK, Sonkusale SR. Three dimensional graphene transistor for ultra-sensitive pH sensing directly in biological media. *Analytica chimica acta*. 2016;934:212–217.
- [82] Salvo P, Calisi N, Melai B, Cortigiani B, Mannini M, Caneschi A, et al. Temperature and pH sensors based on graphenic materials. *Biosensors and Bioelectronics*. 2017;91:870–877.
- [83] Chen JL, Yan XP. Ionic strength and pH reversible response of visible and near-infrared fluorescence of graphene oxide nanosheets for monitoring the extracellular pH. *Chemical Communications*. 2011;47(11):3135–3137.
- [84] Bai H, Li C, Wang X, Shi G. A pH-sensitive graphene oxide composite hydrogel. *Chemical Communications*. 2010;46(14):2376–2378.
- [85] Ang PK, Chen W, Wee ATS, Loh KP. Solution-gated epitaxial graphene as pH sensor. *Journal of the American Chemical Society*. 2008;130(44):14392–14393.
- [86] Hu Y, Ruan M, Guo Z, Dong R, Palmer J, Hankinson J, et al. Structured epitaxial graphene: growth and properties. *Journal of Physics D: Applied Physics*. 2012;45(15):154010.
- [87] Ohno Y, Maehashi K, Yamashiro Y, Matsumoto K. Electrolyte-gated graphene field-effect transistors for detecting pH and protein adsorption. *Nano letters*. 2009;9(9):3318–3322.
- [88] Fu W, Nef C, Knopfmacher O, Tarasov A, Weiss M, Calame M, et al. Graphene transistors are insensitive to pH changes in solution. *Nano letters*. 2011;11(9):3597–3600.

- [89] Sun S, Wu P. A one-step strategy for thermal-and pH-responsive graphene oxide interpenetrating polymer hydrogel networks. *Journal of Materials Chemistry*. 2011;21(12):4095–4097.
- [90] Shih CJ, Lin S, Sharma R, Strano MS, Blankschtein D. Understanding the pH-dependent behavior of graphene oxide aqueous solutions: a comparative experimental and molecular dynamics simulation study. *Langmuir*. 2011;28(1):235–241.
- [91] Piacenti da Silva M, Fernandes JC, de Figueiredo NB, Congiu M, Mulato M, de Oliveira Graeff CF. Melanin as an active layer in biosensors. *Aip Advances*. 2014;4(3):037120.
- [92] Felix C, Hyde J, Sarna T, Sealy R. Interactions of melanin with metal ions. Electron spin resonance evidence for chelate complexes of metal ions with free radicals. *Journal of the American Chemical Society*. 1978;100(12):3922–3926.
- [93] Zajac G, Gallas J, Cheng J, Eisner M, Moss S, Alvarado-Swaigood A. The fundamental unit of synthetic melanin: a verification by tunneling microscopy of X-ray scattering results. *Biochimica et Biophysica Acta (BBA)-General Subjects*. 1994;1199(3):271–278.
- [94] Arzillo M, Mangiapia G, Pezzella A, Heenan RK, Radulescu A, Paduano L, et al. Eumelanin buildup on the nanoscale: aggregate growth/assembly and visible absorption development in biomimetic 5, 6-dihydroxyindole polymerization. *Biomacromolecules*. 2012;13(8):2379–2390.
- [95] Chen W, Rakhi R, Alshareef HN. Capacitance enhancement of polyani-

- line coated curved-graphene supercapacitors in a redox-active electrolyte. *Nanoscale*. 2013;5(10):4134–4138.
- [96] Bernsmann F, Frisch B, Ringwald C, Ball V. Protein adsorption on dopamine–melanin films: Role of electrostatic interactions inferred from  $\zeta$ -potential measurements versus chemisorption. *Journal of colloid and interface science*. 2010;344(1):54–60.
- [97] Abbas M, D’Amico F, Morresi L, Pinto N, Ficcadenti M, Natali R, et al. Structural, electrical, electronic and optical properties of melanin films. *The European Physical Journal E*. 2009;28(3):285–291.
- [98] Paulin JV, Veiga AG, Garcia-Basabe Y, Rocco MLM, Graeff CF. Structural and optical properties of soluble melanin analogues with enhanced photoluminescence quantum efficiency. *Polymer International*. 2018;67(5):550–556.
- [99] Lampel A, McPhee SA, Park HA, Scott GG, Humagain S, Hekstra DR, et al. Polymeric peptide pigments with sequence-encoded properties. *Science*. 2017;356(6342):1064–1068.
- [100] d’Ischia M, Wakamatsu K, Cicoira F, Di Mauro E, Garcia-Borron JC, Commo S, et al. Melanins and melanogenesis: from pigment cells to human health and technological applications. *Pigment cell & melanoma research*. 2015;28(5):520–544.
- [101] Liu Y, Ai K, Ji X, Askhatova D, Du R, Lu L, et al. Comprehensive insights into the multi-antioxidative mechanisms of melanin nanoparticles and their application to protect brain from injury in ischemic stroke. *Journal of the American Chemical Society*. 2017;139(2):856–862.

- [102] Burbulla LF, Song P, Mazzulli JR, Zampese E, Wong YC, Jeon S, et al. Dopamine oxidation mediates mitochondrial and lysosomal dysfunction in Parkinson’s disease. *Science*. 2017;357(6357):1255–1261.
- [103] Ju KY, Lee Y, Lee S, Park SB, Lee JK. Bioinspired polymerization of dopamine to generate melanin-like nanoparticles having an excellent free-radical-scavenging property. *Biomacromolecules*. 2011;12(3):625–632.
- [104] Panzella L, Gentile G, D’Errico G, Della Vecchia NF, Errico ME, Napolitano A, et al. Atypical structural and  $\pi$ -electron features of a melanin polymer that lead to superior free-radical-scavenging properties. *Angewandte Chemie International Edition*. 2013;52(48):12684–12687.
- [105] Lee H, Dellatore SM, Miller WM, Messersmith PB. Mussel-inspired surface chemistry for multifunctional coatings. *science*. 2007;318(5849):426–430.
- [106] Liu Y, Ai K, Lu L. Polydopamine and its derivative materials: synthesis and promising applications in energy, environmental, and biomedical fields. *Chemical reviews*. 2014;114(9):5057–5115.
- [107] Solano F. Melanin and melanin-related polymers as materials with biomedical and biotechnological applications—cuttlefish ink and mussel foot proteins as inspired biomolecules. *International journal of molecular sciences*. 2017;18(7):1561.
- [108] Rani RA, Sidek O; IEEE. ISFET pH sensor characterization: towards biosensor microchip application. 2004 IEEE Region 10 Conference TENCN 2004. 2004;500:660–663.

- [109] Hart JP, Wring SA. Recent developments in the design and application of screen-printed electrochemical sensors for biomedical, environmental and industrial analyses. *TrAC Trends in Analytical Chemistry*. 1997;16(2):89–103.
- [110] Cui G, Kim SJ, Choi SH, Nam H, Cha GS, Paeng KJ. A disposable amperometric sensor screen printed on a nitrocellulose strip: a glucose biosensor employing lead oxide as an interference-removing agent. *Analytical chemistry*. 2000;72(8):1925–1929.
- [111] Zhang Y, Zhu Y, Zheng S, Zhang L, Shi X, He J, et al. Ink formulation, scalable applications and challenging perspectives of screen printing for emerging printed microelectronics. *Journal of Energy Chemistry*. 2021;63:498–513.
- [112] Cao X, Chen H, Gu X, Liu B, Wang W, Cao Y, et al. Screen printing as a scalable and low-cost approach for rigid and flexible thin-film transistors using separated carbon nanotubes. *ACS nano*. 2014;8(12):12769–12776.
- [113] Kahlert H. Functionalized carbon electrodes for pH determination. *Journal of Solid State Electrochemistry*. 2008;12(10):1255–1266.
- [114] Mote C, Dowling DA, Zhou J. The power of an idea: the international impacts of the grand challenges for engineering. *Engineering*. 2016;2(1):4–7.
- [115] Baldé CP, Forti V, Gray V, Kuehr R, Stegmann P. The global e-waste monitor 2017: Quantities, flows and resources. United Nations University, International Telecommunication Union, and ...; 2017.

- [116] Meredith P, Bettinger C, Irimia-Vladu M, Mostert A, Schwenn PE. Electronic and optoelectronic materials and devices inspired by nature. *Reports on Progress in Physics*. 2013;76(3):034501.
- [117] d’Ischia M, Wakamatsu K, Napolitano A, Briganti S, Garcia-Borrón JC, Kovacs D, et al. Melanins and melanogenesis: methods, standards, protocols. *Pigment cell & melanoma research*. 2013;26(5):616–633.
- [118] Solano F. Melanins: skin pigments and much more—types, structural models, biological functions, and formation routes. *New Journal of Science*. 2014;2014.
- [119] Meredith P, Sarna T. The physical and chemical properties of eumelanin. *Pigment cell research*. 2006;19(6):572–594.
- [120] Bernardus Mostert A, Powell BJ, Gentle IR, Meredith P. On the origin of electrical conductivity in the bio-electronic material melanin. *Applied Physics Letters*. 2012;100(9):093701.
- [121] Palumbo A. Melanogenesis in the ink gland of *Sepia officinalis*. *Pigment Cell Research*. 2003;16(5):517–522.
- [122] Xie J, Li H, Che H, Dong X, Yang X, Xie W. Extraction, physico-chemical characterisation, and bioactive properties of ink melanin from cuttlefish (*Sepia esculenta*). *International Journal of Food Science & Technology*. 2021;56(7):3627–3640.
- [123] Hsieh PH, Lien TF. Study of the physico-chemical properties and antioxidant activity of extracted melanins. *Journal of Agricultural Science*. 2012;4(9):217.

- [124] Liu Y, Simon JD. The effect of preparation procedures on the morphology of melanin from the ink sac of *Sepia officinalis*. *Pigment cell research*. 2003;16(1):72–80.
- [125] Novellino L, Napolitano A, Prota G. Isolation and characterization of mammalian eumelanins from hair and irides. *Biochimica et Biophysica Acta (BBA)-General Subjects*. 2000;1475(3):295–306.
- [126] Jimbow K, Miyake Y, Homma K, Yasuda K, Izumi Y, Tsutsumi A, et al. Characterization of melanogenesis and morphogenesis of melanosomes by physicochemical properties of melanin and melanosomes in malignant melanoma. *Cancer Research*. 1984;44(3):1128–1134.
- [127] YíáLiu S, et al. Elucidation of the chemical composition of avian melanin. *RSC Advances*. 2014;4(76):40396–40399.
- [128] Tran-Ly AN, Reyes C, Schwarze FW, Ribera J. Microbial production of melanin and its various applications. *World Journal of Microbiology and Biotechnology*. 2020;36(11):1–9.
- [129] Bell AA, Wheeler MH. Biosynthesis and functions of fungal melanins. *Annual review of phytopathology*. 1986;24(1):411–451.
- [130] López-serrano D, SAnchez-Amat A, Solano F. Cloning and molecular characterization of a SDS-activated tyrosinase from *Marinomonas mediterranea*. *Pigment cell research*. 2002;15(2):104–111.
- [131] López-Serrano D, Solano F, Sanchez-Amat A. Identification of an operon involved in tyrosinase activity and melanin synthesis in *Mari-nomonas mediterranea*. *Gene*. 2004;342(1):179–187.

- [132] Ito S, Fujita K. Microanalysis of eumelanin and pheomelanin in hair and melanomas by chemical degradation and liquid chromatography. *Analytical biochemistry*. 1985;144(2):527–536.
- [133] Ito S. Reexamination of the structure of eumelanin. *Biochimica et Biophysica Acta (BBA)-General Subjects*. 1986;883(1):155–161.
- [134] Da Silva M, Dezidério S, Gonzalez J, Graeff C, Cotta M. Synthetic melanin thin films: Structural and electrical properties. *Journal of applied physics*. 2004;96(10):5803–5807.
- [135] Martin D, Weise A, Niclas HJ. The solvent dimethyl sulfoxide. *Ange wandte Chemie International Edition in English*. 1967;6(4):318–334.
- [136] Dezidério S, Brunello C, Da Silva M, Cotta M, Graeff C. Thin films of synthetic melanin. *Journal of non-crystalline solids*. 2004;338:634–638.
- [137] Albano LG, Di Mauro E, Kumar P, Cicoira F, Graeff CF, Santato C. Novel insights on the physicochemical properties of eumelanins and their DMSO derivatives. *Polymer International*. 2016;65(11):1315–1322.
- [138] Bronze-Uhle ES, Batagin-Neto A, Xavier PH, Fernandes NI, De Azevedo ER, Graeff CF. Synthesis and characterization of melanin in DMSO. *Journal of Molecular Structure*. 2013;1047:102–108.
- [139] Yang E, Fan L, Yan J, Jiang Y, Doucette C, Fillmore S, et al. Influence of culture media, pH and temperature on growth and bacteriocin production of bacteriocinogenic lactic acid bacteria. *AMB express*. 2018;8(1):1–14.



- [140] Adamberg K, Kask S, Laht TM, Paalme T. The effect of temperature and pH on the growth of lactic acid bacteria: a pH-auxostat study. *International journal of food microbiology*. 2003;85(1-2):171–183.
- [141] Klaenhammer TR. Bacteriocins of lactic acid bacteria. *Biochimie*. 1988;70(3):337–349.
- [142] Field D, Ross RP, Hill C. Developing bacteriocins of lactic acid bacteria into next generation biopreservatives. *Current Opinion in Food Science*. 2018;20:1–6.
- [143] García-Hernández Y, Pérez-Sánchez T, Boucourt R, Balcázar JL, Nicoli JR, Moreira-Silva J, et al. Isolation, characterization and evaluation of probiotic lactic acid bacteria for potential use in animal production. *Research in Veterinary Science*. 2016;108:125–132.
- [144] Gómez NC, Ramiro JM, Quecan BX, de Melo Franco BD. Use of potential probiotic lactic acid bacteria (LAB) biofilms for the control of *Listeria monocytogenes*, *Salmonella Typhimurium*, and *Escherichia coli* O157: H7 biofilms formation. *Frontiers in microbiology*. 2016;7:863.
- [145] Chiocchetti GM, Jadán-Piedra C, Monedero V, Zúñiga M, Vélez D, Devesa V. Use of lactic acid bacteria and yeasts to reduce exposure to chemical food contaminants and toxicity. *Critical reviews in food science and nutrition*. 2019;59(10):1534–1545.
- [146] Jadán-Piedra C, Alcántara C, Monedero V, Zúñiga M, Vélez D, Devesa V. The use of lactic acid bacteria to reduce mercury bioaccessibility. *Food chemistry*. 2017;228:158–166.
- [147] Carvalho RD, do Carmo FL, de Oliveira Junior A, Langella P, Chatel JM, Bermúdez-Humarán LG, et al. Use of wild type or recombinant

- lactic acid bacteria as an alternative treatment for gastrointestinal inflammatory diseases: a focus on inflammatory bowel diseases and mucositis. *Frontiers in microbiology*. 2017;8:800.
- [148] Fguiri I, Ziadi M, Atigui M, Ayeb N, Arroum S, Assadi M, et al. Isolation and characterisation of lactic acid bacteria strains from raw camel milk for potential use in the production of fermented Tunisian dairy products. *International Journal of Dairy Technology*. 2016;69(1):103–113.
- [149] Lorusso A, Coda R, Montemurro M, Rizzello CG. Use of selected lactic acid bacteria and quinoa flour for manufacturing novel yogurt-like beverages. *Foods*. 2018;7(4):51.
- [150] Kuda T, Kataoka M, Nemoto M, Kawahara M, Takahashi H, Kimura B. Isolation of lactic acid bacteria from plants of the coastal Satoumi regions for use as starter cultures in fermented milk and soymilk production. *LWT-Food Science and Technology*. 2016;68:202–207.
- [151] Leahy SC, Doyle N, Mbandlwa P, Attwood GT, Li Y, Ross P, et al. Use of lactic acid bacteria to reduce methane production in ruminants, a critical review. *Frontiers in Microbiology*. 2019;10:2207.
- [152] Marques S, Matos C, Gírio F, Roseiro J, Santos J. Lactic acid production from recycled paper sludge: Process intensification by running fed-batch into a membrane-recycle bioreactor. *Biochemical Engineering Journal*. 2017;120:63–72.
- [153] Horak V, Weeks G. Poly (5, 6-dihydroxyindole) melanin film electrode. *Bioorganic Chemistry*. 1993;21(1):24–33.

- [154] Motovilov K, Grinenko V, Savinov M, Gagkaeva Z, Kadyrov L, Pronin A, et al. Redox chemistry in the pigment eumelanin as a function of temperature using broadband dielectric spectroscopy. *RSC advances*. 2019;9(7):3857–3867.
- [155] Khalid K, et al. An overview of lactic acid bacteria. *Int J Biosci*. 2011;1(3):1–13.
- [156] Kawamura Y, Hou XG, Sultana F, Liu S, Yamamoto H, Ezaki T. Transfer of *Streptococcus adjacens* and *Streptococcus defectivus* to *Abiotrophia* gen. nov. as *Abiotrophia adiacens* comb. nov. and *Abiotrophia defectiva* comb. nov., respectively. *International Journal of Systematic and Evolutionary Microbiology*. 1995;45(4):798–803.
- [157] Williams R, Hirsch A, Cowan S. *Aerococcus*, a new bacterial genus. *Microbiology*. 1953;8(3):475–480.
- [158] Hammes WP, Hertel C. The genera *Lactobacillus* and *Carnobacterium*. *Prokaryotes*. 2006;4:320–403.
- [159] Loguercio C, Blanco CDV, Coltorti M. *Enterococcus* lactic acid bacteria strain SF68 and lactulose in hepatic encephalopathy: a controlled study. *Journal of international medical research*. 1987;15(6):335–343.
- [160] Zheng J, Wittouck S, Salvetti E, Franz CM, Harris HM, Mattarelli P, et al. A taxonomic note on the genus *Lactobacillus*: Description of 23 novel genera, emended description of the genus *Lactobacillus* Beijerinck 1901, and union of *Lactobacillaceae* and *Leuconostocaceae*. *International Journal of Systematic and Evolutionary Microbiology*. 2020;70(4):2782–2858.

- [161] Bolotin A, Wincker P, Mauger S, Jaillon O, Malarne K, Weissenbach J, et al. The complete genome sequence of the lactic acid bacterium *Lactococcus lactis* ssp. *lactis* IL1403. *Genome research*. 2001;11(5):731–753.
- [162] Kim B, Lee J, Jang J, Kim J, Han H. *Leuconostoc inhae* sp. nov., a lactic acid bacterium isolated from kimchi. *Journal of Medical Microbiology*. 2003;53(4):1123–1126.
- [163] Grimaldi A, McLean H, Jiranek V. Identification and partial characterization of glycosidic activities of commercial strains of the lactic acid bacterium, *Oenococcus oeni*. *American Journal of Enology and Viticulture*. 2000;51(4):362–369.
- [164] Dobson CM, Deneer H, Lee S, Hemmingsen S, Glaze S, Ziola B. Phylogenetic analysis of the genus *Pediococcus*, including *Pediococcus clausenii* sp. nov., a novel lactic acid bacterium isolated from beer. *International Journal of Systematic and Evolutionary Microbiology*. 2002;52(6):2003–2010.
- [165] Simova E, Beshkova D, Angelov A, Hristozova T, Frengova G, Spasov Z. Lactic acid bacteria and yeasts in kefir grains and kefir made from them. *Journal of Industrial Microbiology and Biotechnology*. 2002;28(1):1–6.
- [166] Baliarda A, Robert H, Jebbar M, Blanco C, Deschamps A, Le Marrec C. Potential osmoprotectants for the lactic acid bacteria *Pediococcus pentosaceus* and *Tetragenococcus halophila*. *International journal of food microbiology*. 2003;84(1):13–20.
- [167] Lawson PA, Falsen E, Cotta MA, Whitehead TR. *Vagococcus elongatus* sp. nov., isolated from a swine-manure storage pit. *International*

- journal of systematic and evolutionary microbiology. 2007;57(4):751–754.
- [168] Kwak SH, Cho YM, Noh GM, Om AS. Cancer preventive potential of kimchi lactic acid bacteria (*Weissella cibaria*, *Lactobacillus plantarum*). Journal of cancer prevention. 2014;19(4):253.
  - [169] Wood BJ, Holzapfel W. The genera of lactic acid bacteria. vol. 2. Springer Science & Business Media; 1992.
  - [170] Leroy F, De Vuyst L. Lactic acid bacteria as functional starter cultures for the food fermentation industry. Trends in Food Science & Technology. 2004;15(2):67–78.
  - [171] Sáez GD, Flomenbaum L, Zárate G. Lactic acid bacteria from argentinean fermented foods: isolation and characterization for their potential use as starters for fermentation of vegetables. Food technology and biotechnology. 2018;56(3):398.
  - [172] Leroy F, Verluyten J, De Vuyst L. Functional meat starter cultures for improved sausage fermentation. International journal of food microbiology. 2006;106(3):270–285.
  - [173] De Vuyst L, Avonts L, Makras L. Probiotics, prebiotics and gut health. Functional Foods, Ageing and Degenerative Disease Cambridge, Woodhead Publishing. 2004;p. 416–482.
  - [174] Özcelik S, Kuley E, Özogul F. Formation of lactic, acetic, succinic, propionic, formic and butyric acid by lactic acid bacteria. LWT. 2016;73:536–542.

- [175] Nakanishi K, Tokuda H, Ando T, Yajima M, Nakajima T, Tanaka O, et al. Screening of lactic acid bacteria having the ability to produce reuterin. *Japanese Journal of Lactic Acid Bacteria*. 2002;13(1):37–45.
- [176] Hölzel A, Gänzle MG, Nicholson GJ, Hammes WP, Jung G. The first low molecular weight antibiotic from lactic acid bacteria: reutericyclin, a new tetramic acid. *Angewandte Chemie International Edition*. 2000;39(15):2766–2768.
- [177] Ogawa J, Kishino S, Ando A, Sugimoto S, Mihara K, Shimizu S. Production of conjugated fatty acids by lactic acid bacteria. *Journal of bioscience and bioengineering*. 2005;100(4):355–364.
- [178] Elshaghabee FM, Bockelmann W, Meske D, De Vrese M, Walte HG, Schrezenmeir J, et al. Ethanol production by selected intestinal microorganisms and lactic acid bacteria growing under different nutritional conditions. *Frontiers in microbiology*. 2016;7:47.
- [179] Islam R, Hossain MN, Alam MK, Uddin ME, Rony MH, Imran MAS, et al. Antibacterial activity of lactic acid bacteria and extraction of bacteriocin protein. *Advances in Bioscience and Biotechnology*. 2020;11(2):49–59.
- [180] De Vuyst L, Vandamme EJ. *Bacteriocins of lactic acid bacteria: microbiology, genetics and applications*. Springer; 2012.
- [181] Vu DT, Kolah AK, Asthana NS, Peereboom L, Lira CT, Miller DJ. Oligomer distribution in concentrated lactic acid solutions. *Fluid phase equilibria*. 2005;236(1-2):125–135.
- [182] Datta R, Tsai SP, Bonsignore P, Moon SH, Frank JR. *Technological*

- and economic potential of poly (lactic acid) and lactic acid derivatives. *FEMS microbiology reviews*. 1995;16(2-3):221–231.
- [183] Martinez FAC, Balciunas EM, Salgado JM, González JMD, Converti A, de Souza Oliveira RP. Lactic acid properties, applications and production: a review. *Trends in food science & technology*. 2013;30(1):70–83.
  - [184] Marsh PD. Dental plaque as a biofilm: the significance of pH in health and caries. *Compendium of continuing education in dentistry (Jamesburg, NJ: 1995)*. 2009;30(2):76–8.
  - [185] Wallace LA, Gwynne L, Jenkins T. Challenges and opportunities of pH in chronic wounds. *Therapeutic delivery*. 2019;10(11):719–735.
  - [186] Kregenow DA, Rubenfeld GD, Hudson LD, Swenson ER. Hypercapnic acidosis and mortality in acute lung injury. *Critical care medicine*. 2006;34(1):1–7.
  - [187] La Bella S, Fiorentino R, Carabotta M, Lizzi M, Rosato T, Trotta D, et al. A difficult case of hyponatremic and hypokalemic metabolic alkalosis: Questions. *Pediatric Nephrology*. 2022;37(12):3063–3064.
  - [188] Demaurex N. pH Homeostasis of cellular organelles. *Physiology*. 2002;17(1):1–5.
  - [189] Piacenti-Silva M, Matos AA, Paulin JV, Alavarce RAdS, de Oliveira RC, Graeff CF. Biocompatibility investigations of synthetic melanin and melanin analogue for application in bioelectronics. *Polymer International*. 2016;65(11):1347–1354.
  - [190] Wünsche J, Cicoira F, Graeff CF, Santato C. Eumelanin thin films:

- solution-processing, growth, and charge transport properties. *Journal of Materials Chemistry B*. 2013;1(31):3836–3842.
- [191] Shimomura T, Sumiya T, Ono M, Itoh T, Hanaoka Ta. An electrochemical biosensor for the determination of lactic acid in expiration. *Procedia Chemistry*. 2012;6:46–51.
- [192] Khan S, Akrema, Qazi S, Ahmad R, Raza K, Rahisuddin. In Silico and electrochemical studies for a ZnO–CuO-based immunosensor for sensitive and selective detection of *E. coli*. *ACS omega*. 2021;6(24):16076–16085.
- [193] Xu M, Wang R, Li Y. An electrochemical biosensor for rapid detection of *E. coli* O157: H7 with highly efficient bi-functional glucose oxidase-polydopamine nanocomposites and Prussian blue modified screen-printed interdigitated electrodes. *Analyst*. 2016;141(18):5441–5449.
- [194] Viswanathan S, Rani C, Ho JaA. Electrochemical immunosensor for multiplexed detection of food-borne pathogens using nanocrystal bioconjugates and MWCNT screen-printed electrode. *Talanta*. 2012;94:315–319.
- [195] Martínez-Paredes G, González-García MB, Costa-García A. Genosensor for detection of four pneumoniae bacteria using gold nanostructured screen-printed carbon electrodes as transducers. *Sensors and Actuators B: Chemical*. 2010;149(2):329–335.
- [196] Chen J, Jiang Z, Ackerman JD, Yazdani M, Hou S, Nugen SR, et al. Electrochemical nanoparticle–enzyme sensors for screening bacterial contamination in drinking water. *Analyst*. 2015;140(15):4991–4996.



- [197] Miranda-Castro R, Sanchez-Salcedo R, Suarez-Alvarez B, de Los-Santos-Álvarez N, Miranda-Ordieres AJ, Lobo-Castañón MJ. Thioaromatic DNA monolayers for target-amplification-free electrochemical sensing of environmental pathogenic bacteria. *Biosensors and Bioelectronics*. 2017;92:162–170.
- [198] Li M, Li YT, Li DW, Long YT. Recent developments and applications of screen-printed electrodes in environmental assays—A review. *Analytica chimica acta*. 2012;734:31–44.
- [199] Hori Y, Takahashi R, Yoshinami Y, Murata A. Electrochemical reduction of CO at a copper electrode. *The Journal of Physical Chemistry B*. 1997;101(36):7075–7081.
- [200] Amatongchai M, Sitanurak J, Sroysee W, Sodanath S, Chairam S, Jarujamrus P, et al. Highly sensitive and selective electrochemical paper-based device using a graphite screen-printed electrode modified with molecularly imprinted polymers coated Fe<sub>3</sub>O<sub>4</sub>@ Au@ SiO<sub>2</sub> for serotonin determination. *Analytica chimica acta*. 2019;1077:255–265.
- [201] Lee J, Hussain G, Banks CE, Silvester DS. Screen-printed graphite electrodes as low-cost devices for oxygen gas detection in room-temperature ionic liquids. *Sensors*. 2017;17(12):2734.
- [202] Metters JP, Kadara RO, Banks CE. New directions in screen printed electroanalytical sensors: an overview of recent developments. *Analyst*. 2011;136(6):1067–1076.
- [203] De Faria RD, Messaddeq Y, Heneine G, Matencio T. Application of screen-printed carbon electrode as an electrochemical transducer in biosensors. *Int J Biosens Bioelectron*. 2019;5(1).

- [204] Tavares AP, de Sá MH, Sales MGF. Innovative screen-printed electrodes on cork composite substrates applied to sulfadiazine electrochemical sensing. *Journal of Electroanalytical Chemistry*. 2021;880:114922.
- [205] Bain CD, Troughton EB, Tao YT, Evall J, Whitesides GM, Nuzzo RG. Formation of monolayer films by the spontaneous assembly of organic thiols from solution onto gold. *Journal of the American Chemical Society*. 1989;111(1):321–335.
- [206] Kochana J, Starzec K, Wieczorek M, Knihnicki P, Góra M, Rokicińska A, et al. Study on self-assembled monolayer of functionalized thiol on gold electrode forming capacitive sensor for chromium (VI) determination. *Journal of Solid State Electrochemistry*. 2019;23(5):1463–1472.
- [207] Serafín V, Agüí L, Yáñez-Sedeño P, Pingarrón J. A novel hybrid platform for the preparation of disposable enzyme biosensors based on poly (3, 4-ethylenedioxythiophene) electrodeposition in an ionic liquid medium onto gold nanoparticles-modified screen-printed electrodes. *Journal of electroanalytical chemistry*. 2011;656(1-2):152–158.
- [208] Pereira SV, Bertolino FA, Fernández-Baldo MA, Messina GA, Salinas E, Sanz MI, et al. A microfluidic device based on a screen-printed carbon electrode with electrodeposited gold nanoparticles for the detection of IgG anti-*Trypanosoma cruzi* antibodies. *Analyst*. 2011;136(22):4745–4751.
- [209] Tondro G, Vais RD, Sattarahmady N. An optical genosensor for *Enterococcus faecalis* using conjugated gold nanoparticles-rRNA oligonucleotide. *Sensors and Actuators B: Chemical*. 2018;263:36–42.

- [210] Huang Y, Cui L, Xue Y, Zhang S, Zhu N, Liang J, et al. Ultrasensitive cholesterol biosensor based on enzymatic silver deposition on gold nanoparticles modified screen-printed carbon electrode. *Materials Science and Engineering: C*. 2017;77:1–8.
- [211] Cabaniss GE, Diamantis AA, Murphy Jr WR, Linton RW, Meyer TJ. Electrocatalysis of proton-coupled electron-transfer reactions at glassy carbon electrodes. *Journal of the American Chemical Society*. 1985;107(7):1845–1853.
- [212] Muthumariappan A, Govindasamy M, Chen SM, Sakthivel K, Mani V. Screen-printed electrode modified with a composite prepared from graphene oxide nanosheets and Mn<sub>3</sub>O<sub>4</sub> microcubes for ultrasensitive determination of nitrite. *Microchimica Acta*. 2017;184(9):3625–3634.
- [213] Hwang GH, Han WK, Park JS, Kang SG. An electrochemical sensor based on the reduction of screen-printed bismuth oxide for the determination of trace lead and cadmium. *Sensors and Actuators B: Chemical*. 2008;135(1):309–316.
- [214] Kokulnathan T, Vishnuraj R, Wang TJ, Kumar EA, Pullithadathil B. Heterostructured bismuth oxide/hexagonal-boron nitride nanocomposite: A disposable electrochemical sensor for detection of flutamide. *Ecotoxicology and Environmental Safety*. 2021;207:111276.
- [215] Liu X, Yao Y, Ying Y, Ping J. Recent advances in nanomaterial-enabled screen-printed electrochemical sensors for heavy metal detection. *TrAC Trends in Analytical Chemistry*. 2019;115:187–202.
- [216] Akhtar K, Khan SA, Khan SB, Asiri AM. Scanning electron mi-

- croscopy: Principle and applications in nanomaterials characterization. In: Handbook of materials characterization. Springer; 2018. p. 113–145.
- [217] Xie J, Spallas JP. Different contrast mechanisms in SEM imaging of graphene. *Agil Technol.* 2012;.
- [218] Maniscalco B, Kaminski P, Walls J. Thin film thickness measurements using scanning white light interferometry. *Thin Solid Films.* 2014;550:10–16.
- [219] Recknagel RJ, Feigl T, Duparre A, Notni G. Wide-scale surface measurement using white light interferometry and atomic force microscopy. *Laser Interferometry IX: Applications.* 1998;3479:36–42.
- [220] Lowe H, Spindloe C. White light interferometric profilometry of surface structured glass for high power laser microtargets. *Laser Sci Development.* 2006;2007.
- [221] Larkin P. *Infrared and Raman Spectroscopy: Principles and Spectral Interpretation.* Elsevier; 2011.
- [222] Kumar R, Singh H, Singh Y; AIP Publishing LLC. FTIR characterization of  $\text{Bi}_2\text{Sr}_2\text{Ca}_{n-1}(\text{Cu}_{1-x}\text{Fe}_x)\text{O}_{10+\delta}$  with ( $n=3$ ,  $x=0.01$ ) ceramic superconductor. *AIP Conference Proceedings.* 2018;1953(1):030001.
- [223] Taylor EA, Donnelly E. Raman and Fourier transform infrared imaging for characterization of bone material properties. *Bone.* 2020;139:115490.
- [224] Petibois C, Desbat B. Clinical application of FTIR imaging: new reasons for hope. *Trends in biotechnology.* 2010;28(10):495–500.

- [225] Feiner AS, McEvoy A. The nernst equation. *Journal of chemical education*. 1994;71(6):493.
- [226] Brown AM. Flowcharts to aid student comprehension of Nernst equation calculations. *Advances in physiology education*. 2018;42(2):260–262.
- [227] Walczak MM, Dryer DA, Jacobson MG, Flynn NT. pH-dependent redox couple: Illustrating the nernst equation using cyclic voltammetry. *Journal of chemical education*. 1997;74(10):1195–1197.
- [228] Grossi M, Parolin C, Vitali B, Riccò B. Electrical Impedance Spectroscopy (EIS) characterization of saline solutions with a low-cost portable measurement system. *Engineering Science and Technology, an International Journal*. 2019;22(1):102–108.
- [229] Macdonald JR, Barsoukov E. Impedance spectroscopy: theory, experiment, and applications. *History*. 2005;1(8):1–13.
- [230] Magar HS, Hassan RY, Mulchandani A. Electrochemical impedance spectroscopy (EIS): Principles, construction, and biosensing applications. *Sensors*. 2021;21(19):6578.
- [231] Choi W, Shin HC, Kim JM, Choi JY, Yoon WS. Modeling and applications of electrochemical impedance spectroscopy (EIS) for lithium-ion batteries. *Journal of Electrochemical Science and Technology*. 2020;11(1):1–13.
- [232] Lazanas AC, Prodromidis MI. Electrochemical Impedance Spectroscopy- A Tutorial. *ACS Measurement Science Au*. 2023;p. 162—193.

- [233] Metrohm. NOVA User Manual; 2017.
- [234] Mohammadi F, Nickchi T, Attar M, Alfantazi A. EIS study of potentiostatically formed passive film on 304 stainless steel. *Electrochimica Acta*. 2011;56(24):8727–8733.
- [235] Jorcin JB, Orazem ME, Pébère N, Tribollet B. CPE analysis by local electrochemical impedance spectroscopy. *Electrochimica Acta*. 2006;51(8-9):1473–1479.
- [236] Zoltowski P. On the electrical capacitance of interfaces exhibiting constant phase element behaviour. *Journal of Electroanalytical Chemistry*. 1998;443(1):149–154.
- [237] Neves RS, De Robertis E, Motheo AJ. Capacitance dispersion in EIS measurements of halides adsorption on Au (2 1 0). *Electrochimica acta*. 2006;51(7):1215–1224.
- [238] Elgrishi N, Rountree KJ, McCarthy BD, Rountree ES, Eisenhart TT, Dempsey JL. A practical beginner’s guide to cyclic voltammetry. *Journal of Chemical Education*. 2018;95(2):197–206.
- [239] Kissinger PT, Heineman WR. Cyclic voltammetry. *Journal of Chemical Education*. 1983;60(9):702.
- [240] Uchida Y. New Potential Waveforms for Cyclic and Linear-Sweep Voltammetry [DPhil thesis]. University of Oxford; 2019.
- [241] Barker GC, Jenkins IL. Square-wave polarography. *Analyst*. 1952;77(920):685–696.

- [242] Ruić I. On the theory of Kalousek commutator, square-wave and related techniques: I. Equations for current-potential curves. *Journal of Electroanalytical Chemistry and Interfacial Electrochemistry*. 1972;39(1):111–122.
- [243] Christie JH, Turner JA, Osteryoung R. Square wave voltammetry at the dropping mercury electrode: theory. *Analytical chemistry*. 1977;49(13):1899–1903.
- [244] Ramaley L, Krause MS. Theory of square wave voltammetry. *Analytical Chemistry*. 1969;41(11):1362–1365.
- [245] Krause MS, Ramaley L. Analytical application of square wave voltammetry. *Analytical Chemistry*. 1969;41(11):1365–1369.
- [246] Srinivas S, Ashokkumar K, Sriraghavan K, Senthil Kumar A. A prototype device of microliter volume voltammetric pH sensor based on carbazole–quinone redox-probe tethered MWCNT modified three-in-one screen-printed electrode. *Scientific Reports*. 2021;11(1):1–11.
- [247] Singh M, Patkar RS, Vinchurkar M, Baghini MS. Cost effective soil pH sensor using carbon-based screen-printed electrodes. *IEEE Sensors Journal*. 2019;20(1):47–54.
- [248] Metcalf DG, Haalboom M, Bowler PG, Gamerith C, Sigl E, Heinzle A, et al. Elevated wound fluid pH correlates with increased risk of wound infection. *Wound Medicine*. 2019;26(1):100166.
- [249] Paulin J, Coleone A, Batagin-Neto A, Burwell G, Meredith P, Graeff C, et al. Melanin thin-films: a perspective on optical and electrical properties. *Journal of Materials Chemistry C*. 2021;9(26):8345–8358.

- [250] Wu MH, Cheng CH, Lai CS, Pan TM. Structural properties and sensing performance of high-k Sm<sub>2</sub>O<sub>3</sub> membrane-based electrolyte–insulator–semiconductor for pH and urea detection. *Sensors and Actuators B: Chemical*. 2009;138(1):221–227.
- [251] Chi LL, Chou JC, Chung WY, Sun TP, Hsiung SK. Study on extended gate field effect transistor with tin oxide sensing membrane. *Materials Chemistry and Physics*. 2000;63(1):19–23.
- [252] Ferrari AC, Meyer J, Scardaci V, Casiraghi C, Lazzeri M, Mauri F, et al. Raman spectrum of graphene and graphene layers. *Physical review letters*. 2006;97(18):187401.
- [253] Taylor CE, Garvey SD, Pemberton JE. Carbon contamination at silver surfaces: surface preparation procedures evaluated by Raman spectroscopy and X-ray photoelectron spectroscopy. *Analytical chemistry*. 1996;68(14):2401–2408.
- [254] Zhang L, Zhang M, Wang Y, Zhang Z, Kan G, Wang C, et al. Graphitized porous carbon microspheres assembled with carbon black nanoparticles as improved anode materials in Li-ion batteries. *Journal of Materials Chemistry A*. 2014;2(26):10161–10168.
- [255] Markervich E, Salitra G, Levi M, Aurbach D. Capacity fading of lithiated graphite electrodes studied by a combination of electroanalytical methods, Raman spectroscopy and SEM. *Journal of power sources*. 2005;146(1-2):146–150.
- [256] Tehrani Z, Whelan S, Mostert A, Paulin J, Ali M, Ahmadi ED, et al. Printable and flexible graphene pH sensors utilising thin film melanin for physiological applications. *2D Materials*. 2020;7(2):024008.



- [257] McArthur SL. Applications of XPS in bioengineering. *Surface and Interface Analysis: An International Journal devoted to the development and application of techniques for the analysis of surfaces, interfaces and thin films.* 2006;38(11):1380–1385.
- [258] Mazzotta E, Rella S, Turco A, Malitesta C. XPS in development of chemical sensors. *RSC advances.* 2015;5(101):83164–83186.
- [259] Meyer E. Atomic force microscopy. *Progress in surface science.* 1992;41(1):3–49.
- [260] Coelho D, Luiz GM, Machado SA. Estimating the Electrochemically Active Area: Revisiting a Basic Concept in Electrochemistry. *Journal of the Brazilian Chemical Society.* 2021;32:1912–1917.
- [261] Couto MR, Rodrigues JL, Rodrigues LR. Optimization of fermentation conditions for the production of curcumin by engineered *Escherichia coli*. *Journal of the Royal Society Interface.* 2017;14(133):20170470.
- [262] Pierson LS, Pierson EA. Metabolism and function of phenazines in bacteria: impacts on the behavior of bacteria in the environment and biotechnological processes. *Applied microbiology and biotechnology.* 2010;86:1659–1670.
- [263] Krulwich TA, Sachs G, Padan E. Molecular aspects of bacterial pH sensing and homeostasis. *Nature Reviews Microbiology.* 2011;9(5):330–343.
- [264] Sánchez-Clemente R, Igeño MI, Población AG, Guijo MI, Merchán F, Blasco R. Study of pH changes in media during bacterial growth of several environmental strains. *Multidisciplinary Digital Publishing Institute Proceedings.* 2018;2(20):1297.

- [265] Reinikainen P, Olkku J, Markkanen P, Holmberg A. Determination of pH and temperature profiles for the growth of *Escherichia coli*. IFAC Proceedings Volumes. 1985;18(17):219–224.
- [266] Narendranath NV, Power R. Relationship between pH and medium dissolved solids in terms of growth and metabolism of lactobacilli and *Saccharomyces cerevisiae* during ethanol production. Applied and environmental microbiology. 2005;71(5):2239–2243.
- [267] Panesar PS, Kennedy JF, Knill CJ, Kosseva M. Production of L (+) lactic acid using *Lactobacillus casei* from whey. Brazilian archives of Biology and Technology. 2010;53(1):219–226.
- [268] Beal C, Louvet P, Corrieu G. Influence of controlled pH and temperature on the growth and acidification of pure cultures of *Streptococcus thermophilus* 404 and *Lactobacillus bulgaricus* 398. Applied microbiology and biotechnology. 1989;32(2):148–154.
- [269] Rhee S, Pack M. Effect of environmental pH on chain length of *Lactobacillus bulgaricus*. Journal of bacteriology. 1980;144(3):865–868.
- [270] Bibal B, Goma G, Vayssier Y, Pareilleux A. Influence of pH, lactose and lactic acid on the growth of *Streptococcus cremoris*: a kinetic study. Applied Microbiology and Biotechnology. 1988;28(4):340–344.
- [271] Brock TD, Freeze H. *Thermus aquaticus* gen. n. and sp. n., a nonsporulating extreme thermophile. Journal of bacteriology. 1969;98(1):289–297.
- [272] Hansen T, Schlichting B, Schönheit P. Glucose-6-phosphate dehydrogenase from the hyperthermophilic bacterium *Thermotoga maritima*:

- expression of the g6pd gene and characterization of an extremely thermophilic enzyme. *FEMS microbiology letters*. 2002;216(2):249–253.
- [273] Bertani G. Studies on lysogenesis I: the mode of phage liberation by lysogenic *Escherichia coli*. *Journal of bacteriology*. 1951;62(3):293–300.
- [274] Bertani G. Lysogeny at mid-twentieth century: P1, P2, and other experimental systems. *Journal of bacteriology*. 2004;186(3):595–600.
- [275] Rosenow EC. Studies on elective localization focal infection with special reference to oral sepsis'. *Journal of Dental Research*. 1919;1(3):205–267.
- [276] FOSTER JH, Hsieh P. The vital capacity of the Chinese: an occupational study. *Archives of Internal Medicine*. 1923;32(3):335–342.
- [277] Koch R. Untersuchungen über bakterien V. Die aetiologie der milzbrand-krankheit, begründet auf die entwicklungsgeschichte *Bacillus anthracis*. *Beiträge zur biologie der Pflanzen*. 1877;2(2):277–310.
- [278] Boudrant J, Menshutina N, Skorohodov A, Guseva E, Fick M. Mathematical modelling of cell suspension in high cell density conditions: application to L-lactic acid fermentation using *Lactobacillus casei* in membrane bioreactor. *Process Biochemistry*. 2005;40(5):1641–1647.
- [279] Hujanen M, Linko S, Linko YY, Leisola M. Optimisation of media and cultivation conditions for L (+)(S)-lactic acid production by *Lactobacillus casei* NRRL B-441. *Applied Microbiology and Biotechnology*. 2001;56(1):126–130.
- [280] Olmos-Dichara A, Ampe F, Uribe Larrea JL, Pareilleux A, Goma G. Growth and lactic acid production by *Lactobacillus casei* ssp. *rhamno-*

- sus in batch and membrane bioreactor: influence of yeast extract and tryptone enrichment. *Biotechnology Letters*. 1997;19(8):709–714.
- [281] Kim E, Yang SM, Cho EJ, Kim HY. Novel real-time PCR assay for *Lactobacillus casei* group species using comparative genomics. *Food Microbiology*. 2020;90:103485.
- [282] Rahimi R, Ochoa M, Tamayol A, Khalili S, Khademhosseini A, Ziaie B. Highly stretchable potentiometric pH sensor fabricated via laser carbonization and machining of Carbon- Polyaniline composite. *ACS applied materials & interfaces*. 2017;9(10):9015–9023.
- [283] Price CP. Point of care testing. *Bmj*. 2001;322(7297):1285–1288.
- [284] Yager P, Domingo GJ, Gerdes J. Point-of-care diagnostics for global health. *Annu Rev Biomed Eng*. 2008;10:107–144.
- [285] Gubala V, Harris LF, Ricco AJ, Tan MX, Williams DE. Point of care diagnostics: status and future. *Analytical chemistry*. 2012;84(2):487–515.
- [286] Hill EW, Vijayaraghavan A, Novoselov K. Graphene sensors. *IEEE Sensors Journal*. 2011;11(12):3161–3170.
- [287] Mali KS, Greenwood J, Adisoejoso J, Phillipson R, De Feyter S. Nanostructuring graphene for controlled and reproducible functionalization. *Nanoscale*. 2015;7(5):1566–1585.
- [288] Goniszewski S, Adabi M, Shaforost O, Hanham S, Hao L, Klein N. Correlation of p-doping in CVD Graphene with Substrate Surface Charges. *Scientific reports*. 2016;6(1):1–9.

- [289] Yafia M, Foudeh AM, Tabrizian M, Najjaran H. Low-cost graphene-based digital microfluidic system. *Micromachines*. 2020;11(9):880.
- [290] Piccinini E, Bliem C, Reiner-Rozman C, Battaglini F, Azzaroni O, Knoll W. Enzyme-polyelectrolyte multilayer assemblies on reduced graphene oxide field-effect transistors for biosensing applications. *Biosensors and Bioelectronics*. 2017;92:661–667.
- [291] Park SJ, Kwon OS, Lee SH, Song HS, Park TH, Jang J. Ultrasensitive flexible graphene based field-effect transistor (FET)-type bioelectronic nose. *Nano letters*. 2012;12(10):5082–5090.
- [292] Teipel S, Drzezga A, Grothe MJ, Barthel H, Chételat G, Schuff N, et al. Multimodal imaging in Alzheimer’s disease: validity and usefulness for early detection. *The Lancet Neurology*. 2015;14(10):1037–1053.
- [293] Hall IC, O’toole E. Intestinal flora in new-born infants: with a description of a new pathogenic anaerobe, *Bacillus difficilis*. *American journal of diseases of children*. 1935;49(2):390–402.
- [294] Saiki RK, Scharf S, Faloona F, Mullis KB, Horn GT, Erlich HA, et al. Enzymatic amplification of beta-globin genomic sequences and restriction site analysis for diagnosis of sickle cell anemia. *Science*. 1985;230(4732):1350–1354.
- [295] Lundeberg J, Wahlberg J, Uhlen M. Rapid colorimetric quantification of PCR-amplified DNA. *BioTechniques*. 1991;10(1):68–75.
- [296] Chen JY, Liu ZJ, Wang XW, Ye CL, Zheng YJ, Peng HP, et al. Ultrasensitive electrochemical biosensor developed by probe lengthening for detection of genomic DNA in human serum. *Analytical chemistry*. 2019;91(7):4552–4558.

- [297] Lu W, Chen Y, Liu Z, Tang W, Feng Q, Sun J, et al. Quantitative detection of microRNA in one step via next generation magnetic relaxation switch sensing. *Acs Nano*. 2016;10(7):6685–6692.
- [298] Bollella P, Fusco G, Tortolini C, Sanzò G, Favero G, Gorton L, et al. Beyond graphene: electrochemical sensors and biosensors for biomarkers detection. *Biosensors and Bioelectronics*. 2017;89:152–166.
- [299] Ray S, Senapati T, Sahu S, Bandyopadhyaya R, Anand R. Design of ultrasensitive protein biosensor strips for selective detection of aromatic contaminants in environmental wastewater. *Analytical chemistry*. 2018;90(15):8960–8968.
- [300] Zhurauski P, Arya SK, Jolly P, Tiede C, Tomlinson DC, Ferrigno PK, et al. Sensitive and selective Affimer-functionalised interdigitated electrode-based capacitive biosensor for Her4 protein tumour biomarker detection. *Biosensors and Bioelectronics*. 2018;108:1–8.
- [301] Rauf S, Mishra GK, Azhar J, Mishra RK, Goud KY, Nawaz MAH, et al. Carboxylic group riched graphene oxide based disposable electrochemical immunosensor for cancer biomarker detection. *Analytical biochemistry*. 2018;545:13–19.
- [302] Panikar SS, Banu N, Haramati J, Gutierrez-Silerio GY, Bastidas-Ramirez BE, Tellez-Bañuelos MC, et al. Anti-fouling SERS-based immunosensor for point-of-care detection of the B7–H6 tumor biomarker in cervical cancer patient serum. *Analytica Chimica Acta*. 2020;1138:110–122.
- [303] Vermisoglou E, Panáček D, Jayaramulu K, Pykal M, Frébort I, Kolář

- M, et al. Human virus detection with graphene-based materials. *Biosensors and Bioelectronics*. 2020;166:112436.
- [304] Afsahi S, Lerner MB, Goldstein JM, Lee J, Tang X, Bagarozzi Jr DA, et al. Novel graphene-based biosensor for early detection of Zika virus infection. *Biosensors and Bioelectronics*. 2018;100:85–88.
- [305] Andoy NM, Filipiak MS, Vetter D, Gutiérrez-Sanz Ó, Tarasov A. Graphene-Based Electronic Immunosensor with Femtomolar Detection Limit in Whole Serum. *Advanced Materials Technologies*. 2018;3(12):1800186.
- [306] Reddy B, Hassan U, Seymour C, Angus D, Isbell T, White K, et al. Point-of-care sensors for the management of sepsis. *Nature biomedical engineering*. 2018;2(9):640–648.
- [307] Winter A, Jones WS, Allen AJ, Price DA, Rostron A, Filieri R, et al. The Clinical Need for New Diagnostics in the Identification and Management of Patients with Suspected Sepsis in UK NHS Hospitals: A Survey of Healthcare Professionals. *Antibiotics*. 2020;9(11):737.
- [308] Seheult J, Fitzpatrick G, Boran G. Lactic acidosis: an update. *Clinical Chemistry and Laboratory Medicine (CCLM)*. 2017;55(3):322–333.
- [309] Leverve X, Mustafa I, Péronnet F. Pivotal role of lactate in aerobic energy metabolism. In: *Yearbook of Intensive Care and Emergency Medicine 1998*. Springer; 1998. p. 588–596.
- [310] Leverve XM. Energy metabolism in critically ill patients: lactate is a major oxidizable substrate. *Current Opinion in Clinical Nutrition & Metabolic Care*. 1999;2(2):165–169.

- [311] Sekine N, Cirulli V, Regazzi R, Brown LJ, Gine E, Tamarit-Rodriguez J, et al. Low lactate dehydrogenase and high mitochondrial glycerol phosphate dehydrogenase in pancreatic beta-cells. Potential role in nutrient sensing. *Journal of Biological Chemistry*. 1994;269(7):4895–4902.
- [312] Cano N. Bench-to-bedside review: glucose production from the kidney. *Critical care*. 2002;6(4):1–5.
- [313] Tayek JA, Katz J. Glucose production, recycling, Cori cycle, and gluconeogenesis in humans: relationship to serum cortisol. *American Journal of Physiology-Endocrinology And Metabolism*. 1997;272(3):E476–E484.
- [314] Brooks GA. Cell–cell and intracellular lactate shuttles. *The Journal of physiology*. 2009;587(23):5591–5600.
- [315] Brooks G. Lactate, A Phoenix Rising in Contemporary Biology. Preprints. 2020;.
- [316] Kruse O, Grunnet N, Barfod C. Blood lactate as a predictor for in-hospital mortality in patients admitted acutely to hospital: a systematic review. *Scandinavian journal of trauma, resuscitation and emergency medicine*. 2011;19(1):1–12.
- [317] Gjesdal G, Braun OÖ, Smith JG, Scherstén F, Tydén P. Blood lactate is a predictor of short-term mortality in patients with myocardial infarction complicated by heart failure but without cardiogenic shock. *BMC cardiovascular disorders*. 2018;18(1):1–8.
- [318] Martín-Rodríguez F, López-Izquierdo R, Villamor MAC, del Pozo Vegas C, Benito MdPD, Caballero CMM, et al. The prognostic value



- of prehospital blood lactate levels to predict early mortality in acute cardiovascular disease. *Shock*. 2020;53(2):164–170.
- [319] Suetrong B, Walley KR. Lactic acidosis in sepsis: it’s not all anaerobic: implications for diagnosis and management. *Chest*. 2016;149(1):252–261.
- [320] De Backer D. Lactic acidosis. *Intensive care medicine*. 2003;29:699–702.
- [321] Cohen RD, Woods HF, Krebs HA. Clinical and biochemical aspects of lactic acidosis. vol. 162. Blackwell Scientific Publications Oxford; 1976.
- [322] Redant S, Hussein H, Mugisha A, Attou R, De Bels D, Honore PM, et al. Differentiating hyperlactatemia type A from type B: How does the lactate/pyruvate ratio help? *Journal of translational internal medicine*. 2019;7(2):43–45.
- [323] Ivashkiv LB. The hypoxia–lactate axis tempers inflammation. *Nature Reviews Immunology*. 2020;20(2):85–86.
- [324] Dean RK, Subedi R, Gill D, Nat A. Consideration of alternative causes of lactic acidosis: thiamine deficiency in malignancy. *The American journal of emergency medicine*. 2017;35(8):1214–e5.
- [325] Masood U, Sharma A, Nijjar S, Sitaraman K. B-cell lymphoma, thiamine deficiency, and lactic acidosis. *Proceedings (Baylor University Medical Center)*. 2017;30(1):69.
- [326] Ferrucci M, Biagioni F, Ryskalin L, Limanaqi F, Gambardella S, Frati A, et al. Ambiguous effects of autophagy activation following hypoperfusion/ischemia. *International journal of molecular sciences*. 2018;19(9):2756.

- [327] Gutierrez G, Wulf M. Lactic acidosis in sepsis: a commentary. *Intensive care medicine*. 1996;22(1):6–16.
- [328] Bone RC, Balk RA, Cerra FB, Dellinger RP, Fein AM, Knaus WA, et al. Definitions for sepsis and organ failure and guidelines for the use of innovative therapies in sepsis. *Chest*. 1992;101(6):1644–1655.
- [329] Levy MM, Fink MP, Marshall JC, Abraham E, Angus D, Cook D, et al. 2001 sccm/esicm/accp/ats/sis international sepsis definitions conference. *Intensive care medicine*. 2003;29(4):530–538.
- [330] Shankar-Hari M, Phillips GS, Levy ML, Seymour CW, Liu VX, Deutschman CS, et al. Developing a new definition and assessing new clinical criteria for septic shock: for the Third International Consensus Definitions for Sepsis and Septic Shock (Sepsis-3). *Jama*. 2016;315(8):775–787.
- [331] Masyuk M, Wernly B, Lichtenauer M, Franz M, Kabisch B, Muessig JM, et al. Prognostic relevance of serum lactate kinetics in critically ill patients. *Intensive care medicine*. 2019;45(1):55–61.
- [332] Bernhard M, Döll S, Kramer A, Weidhase L, Hartwig T, Petros S, et al. Elevated admission lactate levels in the emergency department are associated with increased 30-day mortality in non-trauma critically ill patients. *Scandinavian journal of trauma, resuscitation and emergency medicine*. 2020;28(1):1–8.
- [333] Reinhart K, Daniels R, Kisson N, Machado FR, Schachter RD, Finfer S. Recognizing sepsis as a global health priority—a WHO resolution. *New England Journal of Medicine*. 2017;377(5):414–417.

- [334] Gotts JE, Matthay MA. Sepsis: pathophysiology and clinical management. *Bmj*. 2016;353.
- [335] Kustán P, Horváth-Szalai Z, Mühl D. Nonconventional markers of sepsis. *Ejifcc*. 2017;28(2):122.
- [336] Tegkert A, Datta H, Ali Z. Biomarkers for point-of-care diagnosis of sepsis. *Micromachines*. 2020;11(3):286.
- [337] Jansen TC, van Bommel J, Schoonderbeek FJ, Sleeswijk Visser SJ, van der Klooster JM, Lima AP, et al. Early lactate-guided therapy in intensive care unit patients: a multicenter, open-label, randomized controlled trial. *American journal of respiratory and critical care medicine*. 2010;182(6):752–761.
- [338] Jones AE, Shapiro NI, Trzeciak S, Arnold RC, Claremont HA, Kline JA, et al. Lactate clearance vs central venous oxygen saturation as goals of early sepsis therapy: a randomized clinical trial. *Jama*. 2010;303(8):739–746.
- [339] Watson NC, Heard SO. The use of lactate as a biomarker. *Journal of Intensive Care Medicine*. 2010;25(5):301–302.
- [340] Duman A, Akoz A, Kapci M, Ture M, Orun S, Karaman K, et al. Prognostic value of neglected biomarker in sepsis patients with the old and new criteria: predictive role of lactate dehydrogenase. *The American journal of emergency medicine*. 2016;34(11):2167–2171.
- [341] Reneke J, Etzell J, Leslie S, Ng VL, Gottfried EL. Prolonged prothrombin time and activated partial thromboplastin time due to underfilled specimen tubes with 109 mmol/L (3.2%) citrate anticoagulant. *American journal of clinical pathology*. 1998;109(6):754–757.

- [342] Gray E, Hogwood J, Mulloy B. The anticoagulant and antithrombotic mechanisms of heparin. *Heparin-A century of progress*. 2012;p. 43–61.
- [343] Dugan G, O'Donnell L, Hanbury DB, Cline JM, Caudell DL. Assessment of Multiplate platelet aggregometry using citrate, heparin or hirudin in Rhesus macaques. *Platelets*. 2015;26(8):730–735.
- [344] Hirsh J. Heparin. *New England Journal of Medicine*. 1991;324(22):1565–1574.
- [345] Lawson JH, Butenas S, Ribarik N, Mann K. Complex-dependent inhibition of factor VIIa by antithrombin III and heparin. *Journal of Biological Chemistry*. 1993;268(2):767–770.
- [346] Singh S, Dodt J, Volkers P, Hethershaw E, Philippou H, Ivaskevicius V, et al. Structure functional insights into calcium binding during the activation of coagulation factor XIII A. *Scientific reports*. 2019;9(1):11324.
- [347] Hamilton R, Crockett A, Alpers J. Arterial blood gas analysis: potential errors due to the addition of heparin. *Anaesthesia and Intensive Care*. 1978;6(3):251–255.
- [348] ThermoFisher Scientific. Trisodium citrate, anhydrous; 2009. 45556, Rev. 3.
- [349] Beaver WL, Wasserman K, Whipp BJ. Bicarbonate buffering of lactic acid generated during exercise. *Journal of Applied Physiology*. 1986;60(2):472–478.
- [350] Pradhan N, Rene ER, Lens PN, Dipasquale L, D'Ippolito G, Fontana A, et al. Adsorption behaviour of lactic acid on granular activated carbon

and anionic resins: thermodynamics, isotherms and kinetic studies. *Energies*. 2017;10(5):665.

- [351] Bao Q, Yang Z, Song Y, Fan M, Pan P, Liu J, et al. Printed flexible bifunctional electrochemical urea-pH sensor based on multiwalled carbon nanotube/polyaniline electronic ink. *Journal of Materials Science: Materials in Electronics*. 2019;30:1751–1759.
- [352] Manjakkal L, Vilouras A, Dahiya R. Screen printed thick film reference electrodes for electrochemical sensing. *IEEE Sensors Journal*. 2018;18(19):7779–7785.
- [353] Aliyana AK, Ganguly P, Beniwal A, Kumar SN, Dahiya R. Disposable pH sensor on paper using screen-printed graphene-carbon ink modified zinc oxide nanoparticles. *IEEE Sensors Journal*. 2022;22(21):21049–21056.
- [354] Park HJ, Yoon JH, Lee KG, Choi BG. Potentiometric performance of flexible pH sensor based on polyaniline nanofiber arrays. *Nano convergence*. 2019;6(1):1–7.
- [355] Manjakkal L, Sakthivel B, Gopalakrishnan N, Dahiya R. Printed flexible electrochemical pH sensors based on CuO nanorods. *Sensors and Actuators B: Chemical*. 2018;263:50–58.
- [356] Glanc-Gostkiewicz M, Sophocleous M, Atkinson JK, Garcia-Breijo E. Performance of miniaturised thick-film solid state pH sensors. *Sensors and Actuators A: Physical*. 2013;202:2–7.
- [357] Laffitte Y, Gray BL. Real-time potentiometric pH-sensor using a screen-printable polyaniline composite on textiles. In: 2021 IEEE In-

- ternational Conference on Flexible and Printable Sensors and Systems (FLEPS). IEEE; 2021. p. 1–4.
- [358] Lazouskaya M, Tamm M, Scheler O, Uppuluri K, Zaraska K. Nafion as a protective membrane for screen-printed pH-sensitive ruthenium oxide electrodes. In: 2020 17th Biennial Baltic Electronics Conference (BEC). IEEE; 2020. p. 1–4.
- [359] Kumar A, SK NK, Aniley AA, Fernandez RE, Bhansali S. Hydrothermal growth of zinc oxide (ZnO) nanorods (NRs) on screen printed IDEs for pH measurement application. *Journal of The Electrochemical Society*. 2019;166(9):B3264.
- [360] Nishihara R, Niwa K, Tomita T, Kurita R. Coelenterazine analogue with human serum albumin-specific bioluminescence. *Bioconjugate chemistry*. 2020;31(12):2679–2684.
- [361] Rizzo SA, Bartley O, Rosser AE, Newland B. Oxygen-glucose deprivation in neurons: implications for cell transplantation therapies. *Progress in Neurobiology*. 2021;205:102126.
- [362] Gao S, Cui X, Wang X, Burg MB, Dmitrieva NI. Cross-sectional positive association of serum lipids and blood pressure with serum sodium within the normal reference range of 135–145 mmol/L. *Arteriosclerosis, thrombosis, and vascular biology*. 2017;37(3):598–606.
- [363] Goh D, Hall S, Gornall P, Buick R, Green A, Corkery J. Plasma chloride and alkalaemia in pyloric stenosis. *British Journal of Surgery*. 1990;77(8):922–923.

- [364] Lane N. The unseen world: reflections on Leeuwenhoek (1677)‘Concerning little animals’. Philosophical Transactions of the Royal Society B: Biological Sciences. 2015;370(1666):20140344.
- [365] Pasteur L, Joubert J, Chamberland C. The germ theory of disease. CR Hebd Seances Acad Sci. 1878;86:1037–1052.
- [366] Loutfi H, Pellen F, Le Jeune B, Lteif R, Kallassy M, Le Brun G, et al. Real-time monitoring of bacterial growth kinetics in suspensions using laser speckle imaging. Scientific reports. 2020;10(1):1–10.
- [367] Gunasekera TS, Attfield PV, Veal DA. A flow cytometry method for rapid detection and enumeration of total bacteria in milk. Applied and environmental microbiology. 2000;66(3):1228–1232.
- [368] Siro MR. Monitoring microbial growth by bioluminescent ATP assay. In: Rapid Methods and Automation in Microbiology and Immunology. Springer; 1985. p. 438–447.
- [369] Allen RJ, Waclaw B. Bacterial growth: A statistical physicist’s guide. Reports on Progress in Physics. 2018;82(1):016601.
- [370] Lourenço N, Lopes J, Almeida C, Sarraguça M, Pinheiro H. Bioreactor monitoring with spectroscopy and chemometrics: a review. Analytical and bioanalytical chemistry. 2012;404:1211–1237.
- [371] Andersson DI, Patin SM, Nilsson AI, Kugelberg E. The biological cost of antibiotic resistance. Enzyme-Mediated Resistance to Antibiotics: Mechanisms, Dissemination, and Prospects for Inhibition. 2007;p. 339–348.

- [372] Van Belkum A, Dunne Jr WM. Next-generation antimicrobial susceptibility testing. *Journal of clinical microbiology*. 2013;51(7):2018–2024.
- [373] Bottery MJ, Pitchford JW, Friman VP. Ecology and evolution of antimicrobial resistance in bacterial communities. *The ISME Journal*. 2021;15(4):939–948.
- [374] Lagier JC, Hugon P, Khelaifia S, Fournier PE, La Scola B, Raoult D. The rebirth of culture in microbiology through the example of culturomics to study human gut microbiota. *Clinical microbiology reviews*. 2015;28(1):237–264.
- [375] Yu VL. *Serratia marcescens*: historical perspective and clinical review. *New England Journal of Medicine*. 1979;300(16):887–893.
- [376] Sandle T. History and development of microbiological culture media. *The Journal*. 2011;p. 10–14.
- [377] Lass-Flörl C, Kofler G, Kropshofer G, Hermans J, Kreczy A, Dierich M, et al. In-vitro testing of susceptibility to amphotericin B is a reliable predictor of clinical outcome in invasive aspergillosis. *The Journal of antimicrobial chemotherapy*. 1998;42(4):497–502.
- [378] Van de Beek D, De Gans J, Spanjaard L, Weisfelt M, Reitsma JB, Vermeulen M. Clinical features and prognostic factors in adults with bacterial meningitis. *New England Journal of Medicine*. 2004;351(18):1849–1859.
- [379] Fang CT, Chen YC, Chang SC, Sau WY, Luh KT. *Klebsiella pneumoniae* meningitis: timing of antimicrobial therapy and prognosis. *Qjm*. 2000;93(1):45–53.



- [380] Bonnet M, Lagier JC, Raoult D, Khelaifia S. Bacterial culture through selective and non-selective conditions: the evolution of culture media in clinical microbiology. *New microbes and new infections*. 2020;34:100622.
- [381] Carroll AC, Wong A. Plasmid persistence: costs, benefits, and the plasmid paradox. *Canadian journal of microbiology*. 2018;64(5):293–304.
- [382] San Millan A, Santos-Lopez A, Ortega-Huedo R, Bernabe-Balas C, Kennedy SP, Gonzalez-Zorn B. Small-plasmid-mediated antibiotic resistance is enhanced by increases in plasmid copy number and bacterial fitness. *Antimicrobial agents and chemotherapy*. 2015;59(6):3335–3341.
- [383] Prenskey H, Gomez-Simmonds A, Uhlemann AC, Lopatkin AJ. Conjugation dynamics depend on both the plasmid acquisition cost and the fitness cost. *Molecular systems biology*. 2021;17(3):e9913.
- [384] Mody P, Wada P, Bloch KC, Lionakis MS, White KD, Maris AS, et al. Gram stain to the rescue: a case report of cerebral phaeohyphomycosis by *Cladophialophora bantiana* in an immunocompetent 24-year-old. *BMC Infectious Diseases*. 2022;22(1):1–5.
- [385] Lay M, González I, Tarrés JA, Pellicer N, Bun KN, Vilaseca F. High electrical and electrochemical properties in bacterial cellulose/polypyrrole membranes. *European Polymer Journal*. 2017;91:1–9.
- [386] Manohar AK, Bretschger O, Nealson KH, Mansfeld F. The use of electrochemical impedance spectroscopy (EIS) in the evaluation of the electrochemical properties of a microbial fuel cell. *Bioelectrochemistry*. 2008;72(2):149–154.

- [387] Joseph S, Husson O, Graber ER, Van Zwieten L, Taherymoosavi S, Thomas T, et al. The electrochemical properties of biochars and how they affect soil redox properties and processes. *Agronomy*. 2015;5(3):322–340.
- [388] Santos HA, García-Morales V, Pereira CM. Electrochemical properties of phospholipid monolayers at liquid–liquid interfaces. *ChemPhysChem*. 2010;11(1):28–41.
- [389] Kobayashi H, Saito N, Fu Q, Kawaguchi H, Vilcaez J, Wakayama T, et al. Bio-electrochemical property and phylogenetic diversity of microbial communities associated with bioelectrodes of an electromethanogenic reactor. *Journal of bioscience and bioengineering*. 2013;116(1):114–117.

# Appendix

# Appendix A

## Microfluidic sample delivery system

A prototype microfluidic case to encompass the DMSO-melanin pH sensor has been designed. The purpose of this is to protect the electrodes that the sensor is composed of from physical damage whilst also keeping the sample in constant contact with the sensor. Designs were completed using OpenSCAD and produced via 3D printing with the Dolomite FluidicFactory.

### A.1 Dimensions

The top section of the protective case is 15mm x 12.5mm x 5mm, the sample loading well has a radius of 4mm and the microfluidic capillary has a radius of 0.8mm. The capillary is connected to a chamber composed of a partial sphere with a radius of 2mm and a cylinder with a radius of 4mm. The bottom section of the protective case is 15mm x 12.5mm x 3mm. It contains a 0.5mm deep slot of 10mm x 10mm to contain the SPE.

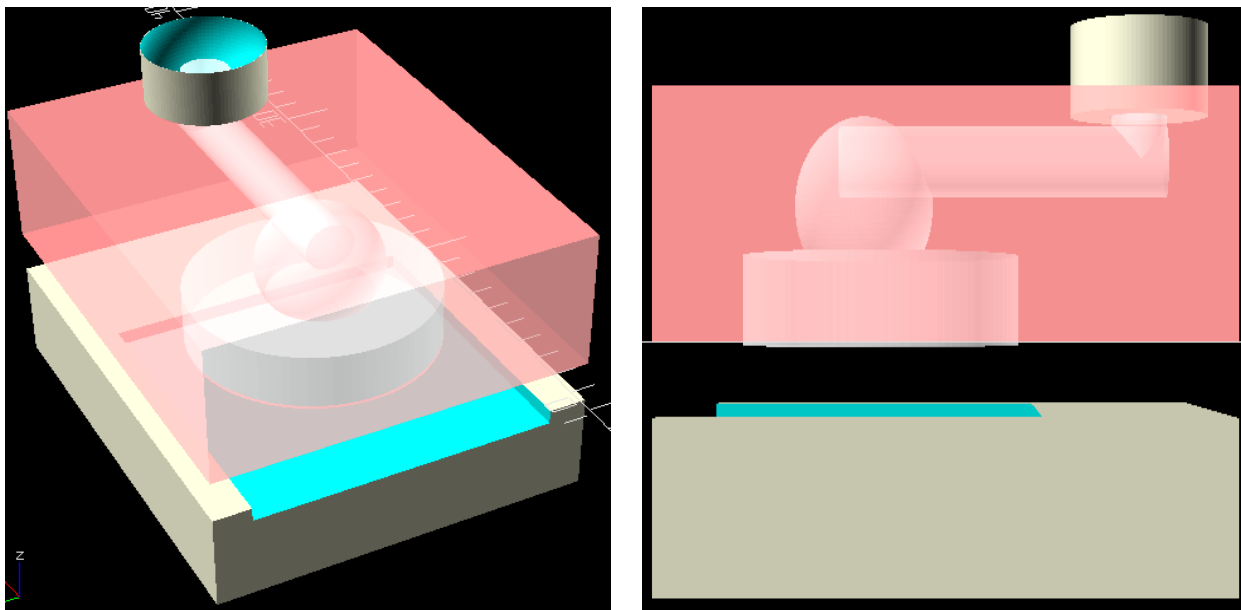


Figure A.1: Design of protective case for SPEs with a microfluidic sample delivery system that consists of two parts. A top section which contains the microfluidic capillary as well as a chamber where the sample is able to pool above the sensor and a bottom section which contains a groove that keeps the sensor in the correct position underneath the sample pooling chamber of the top section.



Figure A.2: Top and bottom sections of the protective case following 3D printing.

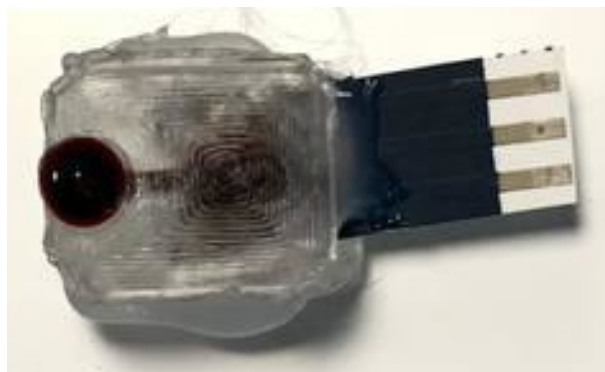


Figure A.3: The protective case assembled and glued together with an SPE.

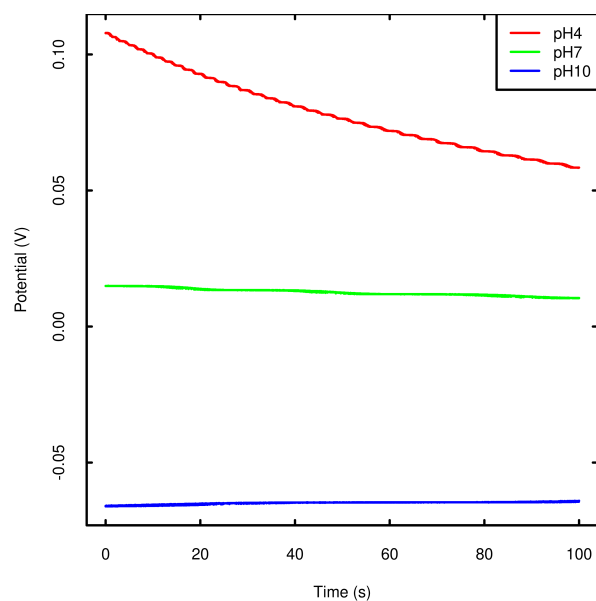


Figure A.4: The pH sensor sealed inside the microfluidic protective case as shown in Figure A.3 was tested with the standard pH4, pH7 and pH10 reference buffer solutions in order to determine whether sealing it inside the microfluidic system had any impact upon the functionality of the sensor.

## Appendix B

### Accompanying software application for pH sensor

This appendix details a software application that complements the DMSO-melanin pH sensors usage in bacterial culturing. This application allows for the automated calculation of a pH of culturing media based on the calibration curve that is specific for each type of media as is discussed in this chapter. The application allows the user to select the type of media being used from a drop down menu, the user also selects the relevant data file and the application is then able to calculate the pH of the solution using the appropriate standard curve. This provides an example of how the DMSO-melanin pH sensor may be used in an easy to use product.



## B.1 Interface and example usage

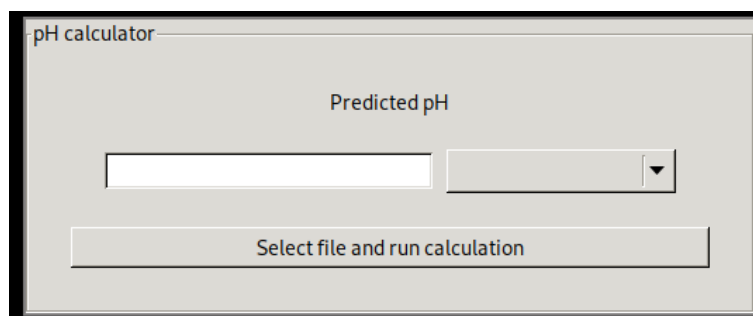


Figure B.1: The initial interface that the user is presented with, the white box on the left is the window in which the calculated pH will be displayed once the desired parameters have been set. The grey box on the right presents the user with a drop down menu when clicked, this menu contains a list of all of the solution types that are available for pH measurements.

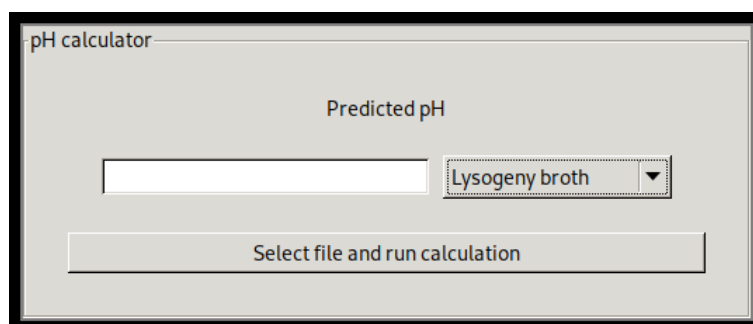


Figure B.2: This example shows that the user has selected “Lysogeny broth” from the drop down menu on the right.

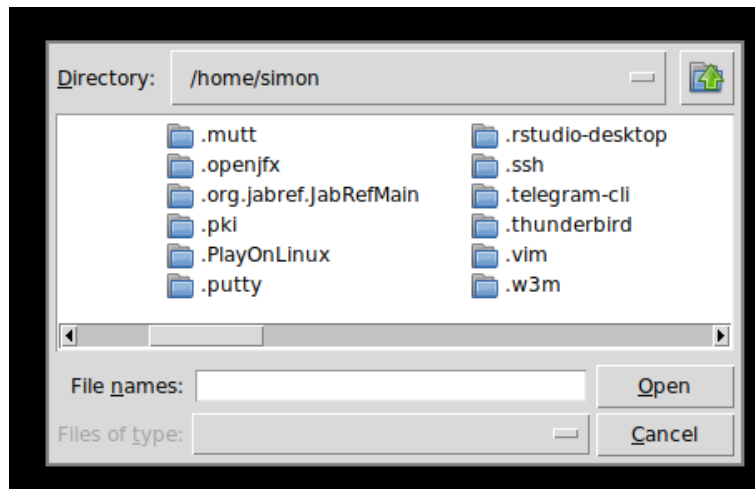


Figure B.3: This is the file selection menu that the user is presented with once “Select file and run calculation” has been clicked. The user is able to navigate through various directories and locate the file that contains the raw voltage data.

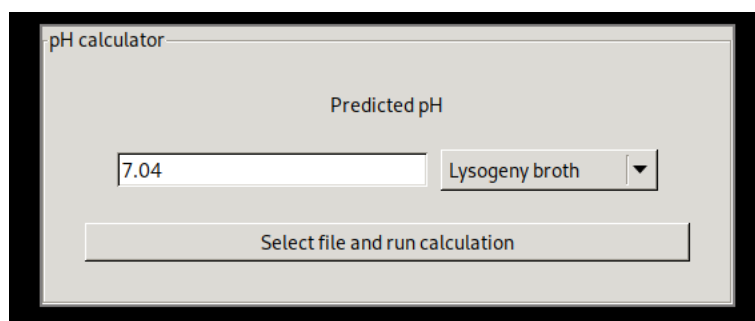


Figure B.4: Once the file has been selected the pH calculator automatically compares the mean voltage to the slope and predicts the pH of the measured solution. The predicted pH of the solution is displayed in the white box on the left.